Diastolic dysfunction in heart failure do repolarisation abnormalities play a role?

Anderson, Grace

Awarding institution:
King's College London

Diastolic Dysfunction in Heart Failure: Do Repolarisation Abnormalities Play a Role?

Grace Catherine Anderson

Thesis undertaken for the degree of Doctor of Philosophy in Cardiovascular Sciences

King's College London
Cardiovascular Division
The Rayne Institute
BHF Centre of Excellence
4th Floor Lambeth Wing
St Thomas' Hospital
London, SE1 7EH

ACKNOWLEDGEMENTS

There are many people to whom I am grateful for their support throughout my PhD:

- My supervisors Professor Michael Shattock and Dr James Winter for giving me the opportunity to undertake this PhD project, and for countless hours of training and guidance over the years. I feel very fortunate to have been given the opportunity to work on such an interesting and varied project with such excellent supervisors. Mike, I hope you've recovered from the expenses associated with this PhD, I know it's not what you bargained for with a Scottish student! It's been a pleasure to work with you both over the years and I've learned so much that I hope to take forward in my future career.
- The British Heart Foundation for their kind sponsorship of this work.
- Dr James Clark for his extensive support and training in various techniques including surgery, cardiac ultrasound and pressure-volume recordings, without which many of my experiments would not have been possible. I am very grateful for his technical expertise and scientific input throughout my PhD.
- Members of the Shattock lab group, particularly Dr Yujin Chung for her much-appreciated contribution of collecting and analysing the ^{23}Na NMR data and moral support in all things telemetry-related. I am also very grateful to Dr Lauren Albee for her western blotting expertise and David Sanchez for his laboratory support throughout my PhD.
- Dr Andrii Boguslavskyi for kindly offering his time to provide training in collecting cardiac ultrasound data.
- The Eaton lab group for use of the telemetry system equipment, and in particular Dr Olena Rudyk for her advice surrounding telemetry experiments.
- Louise Hesketh for sharing in the highs and lows of the perfusion lab and for being a sounding board for many a discussion about repolarisation and relaxation.
- Professor Michael Curtis for his sage advice surrounding experimental design and for providing amusing anecdotes during long days in the perfusion lab.
- To past and present colleagues at the Rayne Institute who have provided fresh insight into the findings from this project over the years.

- Members of the Biological Services Unit team for their kind support with animal husbandry.
- My awesome friends, who have been so understanding of my long periods of silence during the write-up process and supportive after bad days in the lab. Rachel, for truly understanding, sending much-needed support packages and for introducing me to Pitch Perfect when I needed it most. Nitsan, for always being there to keep me sane or share in my insanity, and for many a motivational 'Study Sunday'. Jordan, Takashi and Max, for the relentless mocking of my day job that never failed to raise a smile when I needed it, and for the planning of many impromptu weekend trips which are some of the highlights of my time as a PhD student. And of course, Jenny, for always being there over the years. I look forward to being able to plan our holidays with less of student budget in the future!
- My wonderful family, without whose support and guidance I wouldn't be where I am today. Thank you so much for all you've done over the years.
- Matt, for dealing with life for both of us while I've been writing up, and for always being a voice of reason and encouragement. I couldn't have asked for anyone more supportive and understanding and I promise to return the favour when you're writing up next year. Until then, I'm very excited to have free time for climbing and bikepacking trips!

ABSTRACT

Recent studies have revealed that around half of patients living with heart failure (HF) may present with heart failure with preserved ejection fraction (known as HFpEF). This is a condition of diastolic dysfunction in the absence of overt systolic dysfunction and is reported to have comparable clinical outcomes to systolic HF. These patients do not respond to existing therapies for HF, and HFpEF therefore represents a significant clinical burden. Clinical studies have recently highlighted a strong correlation between repolarisation abnormalities and diastolic dysfunction in HF patients, but it remains unclear whether this represents a causal relationship. It is possible that perturbations to ventricular repolarisation may act to disrupt normal intracellular calcium handling, thus contributing to diastolic dysfunction through impaired active ventricular relaxation.

The present study has aimed to address this question using a direct approach to determine the relationship between diastolic function and ventricular repolarisation in the whole heart, beginning in healthy Langendorff-perfused guinea pig hearts and progressing to isolated working hearts from a novel deoxycorticosterone acetate (DOCA)-salt guinea pig model of HFpEF. Action potential duration (APD) was prolonged via pharmacological blockade of repolarising currents I_{Kr} and I_{Ks} to replicate changes to QT interval seen in the clinic, while *ex vivo* cardiac function was measured with the use of an intraventricular balloon in Langendorff-perfused hearts and a pressure-volume admittance catheter in working hearts. *In vivo* cardiac function in the guinea pig DOCA-salt model was measured using cardiac ultrasound, while additional characterisation data was obtained from conscious radiotelemetry blood pressure and anaesthetised ECG recordings. *Ex vivo* characterisation included the assessment of intracellular sodium levels using ^{23}Na NMR spectroscopy in isolated Langendorff-perfused hearts and western blotting to examine the ventricular expression of proteins involved in intracellular calcium handling.

Initial experiments utilised whole-heart optical mapping to demonstrate that APD prolongation results in concomitant prolongation of the underlying calcium transient, providing proof-of-principle for the hypothesis. Cardiac function was then measured in the presence of APD prolongation in healthy hearts or in combination with the

pharmacological replication of other pathological changes commonly reported in HF. This was achieved using ouabain to elevate intracellular sodium and cyclopiazonic acid (CPA) to impair SERCA function, while QT interval was measured from ECG recordings and used as a surrogate of ventricular APD. These changes affect intracellular calcium handling and are therefore likely to be relevant to the proposed mechanism by which altered ventricular repolarisation could affect diastolic function. Data revealed mixed results, with APD prolongation resulting in mild diastolic impairment in healthy working hearts and Langendorff-perfused hearts under conditions of SERCA inhibition, but having no effect on diastolic function in working hearts in combination with ouabain and CPA treatment. These studies were followed by the development of a novel DOCA-salt guinea pig model of HFpEF, allowing the relationship between ventricular repolarisation and diastolic function to be assessed in a clinically relevant setting. Extensive characterisation data revealed this model to demonstrate many of the key characteristics of HF, including elevated intracellular sodium and reduced SERCA expression, which previous experiments had aimed to replicate. The presence of diastolic dysfunction *in vivo* was also confirmed, alongside hypertension and QT prolongation. However, APD prolongation in isolated working hearts from this model did not exacerbate diastolic dysfunction *ex vivo*.

Findings from the present study indicate that ventricular repolarisation abnormalities are likely not a major contributor to impaired diastolic function in the failing heart.

TABLE OF CONTENTS

LIST OF FIGURES

LIST OF TABLES

LIST OF ABBREVIATIONS

AP - action potential

APD - action potential duration

CaMKII - calcium/calmodulin-dependent protein kinase II

CaTD - calcium transient duration

CDI - calcium-dependent inactivation

CF - coronary flow

CO - cardiac output

CPA - cyclopiazonic acid

DD - diastolic duration

DOCA - deoxycorticosterone acetate

DMSO - dimethyl sulfoxide

DQF - double quantum filtered

EC - excitation-contraction

ECG - electrocardiogram

ECL - enhanced chemiluminescence

EDPVR - end diastolic pressure-volume relationship

ESPVR - end systolic pressure-volume relationship

HF - heart failure

HFpEF - heart failure with preserved ejection fraction

HFrEF - heart failure with reduced ejection fraction

HR - heart rate

$I_{Ca\text{-}L}$ - inward calcium current (via L-type channels)

I_K - delayed rectifier potassium current

$\mathbf{I_{K1}}$ - inward rectifier potassium current

I_{Kr} - rapidly activating component of the delayed rectifier potassium current

I_{Ks} - slowly activating component of the delayed rectifier potassium current

I_{Na} - inward sodium current

I_{to} - transient outward potassium current

IVB - intraventricular balloon

IVRT - isovolumic relaxation time

LA - left atrial

LAA - left atrial area

LQTS - long QT syndrome

LV - left ventricular

LVDP - left ventricular developed pressure

LVEDP - left ventricular end diastolic pressure

LVP - left ventricular pressure

MAP - mean arterial pressure

NCX - sodium-calcium exchanger

PKA - protein kinase A

PKC - protein kinase C

PKG - protein kinase G

PLB - phospholamban

RA - right atrial

RV - right ventricular

SD - systolic duration

SERCA - sarco(endo)plasmic reticulum calcium ATPase

SR - sarcoplasmic reticulum

TDR - transmural dispersion of repolarisation

TQF - triple quantum filtered

VDI - voltage-dependent inactivation

1 INTRODUCTION

1.1 Diastolic Dysfunction in Heart Failure

Heart failure (HF) represents a significant clinical burden, reportedly affecting 1-2% of the population in western nations.[1] A recent epidemiological study examining electronic medical records from the UK over the period from 2002-2014 revealed a 23% increase in the number of people living with HF during this time, representing an increase from approximately 750,000 - 921,000 individuals.[2] It has become increasingly recognised that, whilst HF is traditionally associated with pump failure and reduced ejection fraction (EF), it may also present as a disorder of primarily diastolic function where ejection fraction is preserved – typically known as heart failure with preserved ejection fraction (HFpEF). The prevalence of HFpEF amongst HF patients in more recent studies is reported at around 50%, with most studies reporting comparable clinical outcomes (i.e. mortality rate) in HFpEF patients compared to their counterparts with reduced ejection fraction.[3,4,5] Overall this makes HFpEF a significant global burden, in terms of both health (morbidity and mortality) and economic cost.

1.1.1 Defining Heart Failure with Preserved Ejection Fraction

Heart failure is defined as a loss of cardiac function, such that the heart can no longer fill with and/or eject an adequate volume of blood to meet metabolic demands or can only do so at the expense of raised filling pressures. Under such conditions cardiac output may be maintained at rest but cannot be increased to meet metabolic demand under exercise conditions. HFpEF has various definitions but for the purposes of recruiting patients for clinical trials has commonly been assigned to HF patients with an EF of ≥ 40-50%, whilst HF which is primarily associated with systolic dysfunction (heart failure with reduced EF (HFrEF)) is commonly assigned to patients with an EF of ≤ 35%. This lack of consistency has resulted in variation in the reported prevalence of HFpEF amongst HF patients, and risks obscuring the interpretation of trial data.

The official guidelines from the European Society of Cardiology state that in order for a diagnosis of HFpEF to be made, 4 criteria must be met: 1) symptoms typical of HF, 2)

signs typical of HF, 3) normal/mildly reduced EF, without left ventricular (LV) dilation and 4) relevant structural disease (e.g. LV hypertrophy, left atrial (LA) enlargement) and/or diastolic dysfunction (determined by echocardiography).[6] Direct assessment of LV relaxation is necessary to confirm diastolic dysfunction and can be performed using two different techniques. This is primarily carried out by non-invasive echocardiography (cardiac ultrasound), but studies have been performed using invasive cardiac catheterisation or a combination of the two techniques, which provides detailed physiological data on pressure-volume relationships in the heart and is considered to be a gold-standard measure of cardiac function. One such study recruited patients who met the Framingham criteria for congestive HF with a normal EF and showed that these patients demonstrated a shifted diastolic pressure-volume relationship alongside elevated passive stiffness.[7] This is consistent with diastolic failure and differs to what would typically be observed in systolic failure using this approach (Fig. 1.1).

Whilst there is some debate about the degree to which HFpEF and HFrEF may lie on a spectrum of HF, there is much evidence to support the separation of these two presentations of HF into distinct clinical conditions. One of the factors most indicative of the need to recognise two distinct clinical presentations of HF is the differing demographic between the two patient groups. Patients with HFpEF are more likely to be elderly females who present with comorbidities including diabetes, hypertension, chronic obstructive pulmonary disease, obesity, chronic kidney disease and atrial fibrillation than their counterparts with HFrEF.[8] These differences in co-morbidities are accompanied by differences in the pathophysiological changes to the myocardium, including type of LV hypertrophy displayed (concentric vs eccentric), increased LA diameter, differing passive stiffness of the myocardium (a possible reflection of titin phosphorylation and isoform expression) and the degree of fibrosis present.[9,10]

Given the broad spectrum of common comorbidities and characteristics of HFpEF, defining diagnostic and inclusion criteria for clinical trials remains challenging, and it may be that a single category for HFpEF patients is too simplistic. This has been the suggestion of more than one study and promotes the idea of subcategorising HFpEF patients according to large amounts of phenotypic data as a potential means of identifying patient groups who may benefit from specific therapies.[11,12]

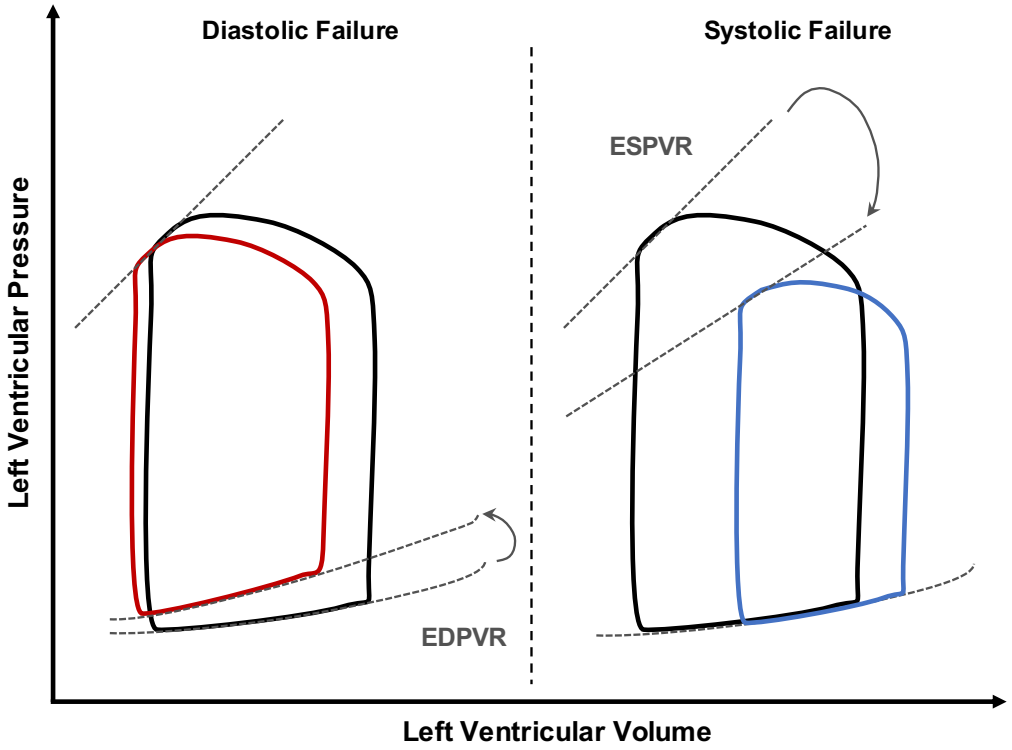

Figure 1.1 Pressure volume diagram representing diastolic vs systolic HF.

Pressure-volume (PV) loops are a well-accepted method of examining cardiac function, with the end diastolic and end systolic pressure-volume relationships (EDPVR and ESPVR) representing the gold standard in measuring diastolic and systolic function, respectively. In diastolic failure (red loop) there is an upwards shift in the EDPVR, indicating reduced compliance and therefore higher LVEDP for any given left ventricular volume. In systolic failure (blue loop) there is a downwards shift in the ESPVR, indicating reduced contractility and therefore a lower LVSP for a given left ventricular volume.

1.1.2 Current Therapies

To date, the treatments prescribed for HFpEF patients tend to revolve around the control of comorbidities, such as hypertension. Such studies will typically select HF patients with an EF greater than a defined cut-off point (e.g. ≥ 45%) and use cardiovascular-related hospital admissions or mortality as primary end points. One such study was the TOPCAT trial, which treated HFpEF patients with spironolactone; a potassium-sparing diuretic that also exerts anti-remodelling effects on the heart. The outcome of the trial was neutral,

with no beneficial effects observed in terms of hospital admissions or mortality relative to the placebo group.[13] The same outcome is true of studies which have targeted the renin-angiotensin system, including the I-PRESERVE trial, where the angiotensin-receptor blocker irbesartan was found to have no beneficial effect on outcomes in HFpEF patients.[14] Another study looked at the potential for the phosphodiesterase-5 inhibitor sildenafil to enhance cardiac function in HFpEF patients in the RELAX trial. However, results again revealed no benefit for patients when compared to placebo.[15]

Therefore, HFpEF represents a significant and growing clinical problem, which to date has no proven effective therapies available to patients. Consequently, further research is needed in order to better understand this condition and provide novel therapeutic strategies which can target the underlying causes of impaired ventricular relaxation. Repolarisation abnormalities are abundant in HF patients presenting with diastolic dysfunction and may represent such a target.

1.2 Cardiac Excitation-Contraction Coupling

Before it is possible to explain the potential role for myocardial repolarisation abnormalities in the development of diastolic dysfunction, is important to understand the principles of cardiac excitation-contraction (EC) coupling. This is the process which couples electrical excitation to physical contraction within the myocardium, and is central to the control of active contraction and relaxation in the heart.

1.2.1 The Ventricular Action Potential

Membrane potential is generated by imbalances in the distribution of charged ionic species across the sarcolemmal membrane, which flow through voltage-gated ion channels. Alterations in the permeability of the sarcolemmal membrane to different ions gives rise to the cardiac action potential (AP) waveform (Fig. 1.2).

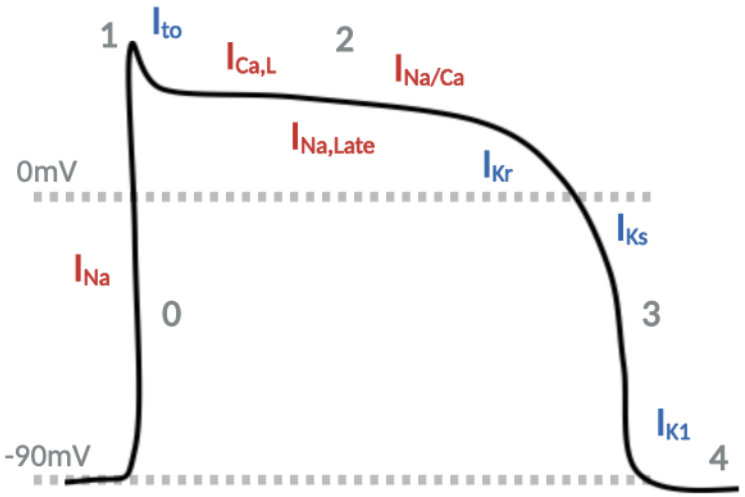

Figure 1.2 The ventricular action potential

Major currents contributing to the ventricular action potential. Depolarising currents are shown in red, while repolarising currents are shown in blue. Phases of the ventricular action potential shown in grey (0-4). Note that the sodium-calcium exchanger can function in forward or reverse mode, and as such $I_{Na/Ca}$ may produce a depolarising or repolarising current, respectively. However, under normal conditions in the healthy heart $I_{Na/Ca}$ will be depolarising during phase 2 and 3 of the action potential due to elevated intracellular calcium. Created with BioRender.com.

The ventricular AP displays a characteristic plateau phase, produced by an opposing balance of depolarising and repolarising currents during phase 2 of the action potential. This results in a long AP duration (APD) and is fundamental in producing a prolonged contraction, thus enabling the ventricles to contract slowly and act as an efficient pump. This also creates a long refractory period that prevents the ventricles from contracting again prematurely during the diastolic period and, by ensuring that each contraction is completed within the refractory period, prevents summation of contraction and tetany (as occurs in skeletal muscle).[16]

The upstroke of the ventricular AP (phase 0) is initiated by the rapid opening of voltage-gated sodium channels in response to the depolarisation of neighbouring cells. This results in a large inward sodium current (I_{Na}) which brings about rapid depolarisation of the cell. This depolarisation results in the activation of repolarising current I_{to}, which is responsible for the characteristic partial repolarisation that produces the 'notch' seen at

phase 1 of the AP (note that this characteristic may only be seen in some myocyte populations, with epicardial cells demonstrating a more pronounced notch than endocardial cells). This current is comprised primarily of the outward flow of potassium ions and demonstrates rapid inactivation.[16] Expression of the channels responsible for I_{to} varies widely between different cell types within the myocardium and species and contributes significantly to the APD by affecting the balance of depolarising and repolarising currents during the plateau.[17,18] Voltage-gated calcium channels carrying the depolarising current $I_{Ca,L}$ also rapidly activate upon depolarisation of the cell. This calcium current is responsible for bringing about contraction within cardiomyocytes (as discussed in section 1.2.2) and inactivates slowly, producing a prolonged inward flow of calcium ions during the AP plateau.[19,20,21] The late sodium current ($I_{Na,Late}$) is a small, sustained inward sodium current which persists after the inactivation of the majority of the fast sodium channels responsible for the AP upstroke, and contributes to the plateau phase and APD.[22] Another important player in the plateau phase of the AP is the sarcolemmal sodium calcium exchanger (NCX). This exchange of sodium and calcium is electrogenic, with 3 sodium ions being exchanged for every calcium ion.[23] However, the direction of exchange can be either forward (calcium extrusion) or reverse (calcium entry) depending on both the membrane potential and concentrations of intracellular sodium and calcium. During phase 2 of the ventricular AP, calcium concentration within the cell is elevated due to the influx of calcium via $I_{Ca,L}$ and so NCX functions in forward mode, extruding calcium from the cell and creating a net inward sodium current.[24] This current is a contributor to APD as it counteracts the outward potassium currents which become active later during the AP plateau.

As the AP progresses into late phase 2/early phase 3, the membrane potential drops below 0mV and allows for activation of the rapidly activating delayed rectifier current (I_{Kr}). The kinetics of the potassium channels that carry this current are such that repolarising currents do not overwhelm the depolarising currents during phase 2, thus allowing the plateau to be maintained. Whilst active at potentials positive to -40mV, the channels become largely inactivated at potentials greater than 0mV due to a more rapid development of channel inactivation relative to channel activation at positive potentials.[25] Similar characteristics are displayed by the channels responsible for inward-rectifier

potassium current (I_{K1}), which is the major contributing current to the resting membrane potential.[26] Another delayed rectifier (slowly-activating I_{Ks}) becomes active at the latter stages of phase 2 and during phase 3 in the AP. The channels responsible for this current are voltage-gated but activate very slowly upon depolarisation of the cell and may therefore contribute to the shape and duration of the latter phases of the AP.[16,27] However, the slow activation of these channels makes their contribution to repolarisation under basal conditions questionable, and some have proposed that the role of I_{Ks} may be limited to preventing excessively long APD under conditions of elevated heart rates or increased sympathetic tone, effectively providing 'spare' repolarisation capacity.[28] This may arise due to these channels demonstrating slow deactivation, which results in a greater I_{Ks} at higher heart rates as more channels will remain in the active state following subsequent depolarisations, as well as their sensitivity to β-adrenergic agonists which increase I_{Ks}.[29] This feature, combined with the fact that these channels demonstrate faster activation kinetics at higher heart rates, means that I_{Ks} may play a key role in rate adaptation of APD (i.e. shortening) at higher heart rates. This remains controversial, however, with some studies finding no significant I_{Ks} accumulation or contribution to APD at physiological cardiac cycle lengths.[30,31] At membrane potentials negative to -20mV, I_{K1} becomes active again and is largely responsible for the final stages of repolarisation, remaining active throughout phase 4 and providing the major determinant of the resting membrane potential in ventricular myocytes.[16,26]

Therefore, the ventricular AP arises as a result of carefully balanced depolarising and repolarising currents (Fig. 1.2), allowing for a sustained contraction and efficient ventricular pump. Underlying this is the carefully controlled entry and removal of calcium from the cell, which is fundamental to the process of ventricular contraction and relaxation.

1.2.2 Intracellular Calcium Handling During the Cardiac Cycle

Ventricular contraction and relaxation are active processes which depend upon the appropriate regulation of cytosolic calcium concentration within myocytes during EC-coupling. Subcellular microdomains are key to the process of triggering intracellular calcium transients, and it is important to note that the increases in calcium concentration

involved are localised in nature. Within cardiomyocytes, the SR forms a complex network of tubules which surround the myofibrils. The sarcolemmal membrane has characteristic invaginations called transverse (T) tubules which closely align with flattened regions of the SR called junctional SR cisternae, to form what are known as dyadic clefts. This region is composed of L-type calcium channels within the sarcolemmal membrane which closely appose clusters of ryanodine receptors. The formation of such microdomains restricts ion diffusion and so local changes in calcium concentration can occur very rapidly.[32] An approximation of this arrangement is shown in Fig. 1.3.

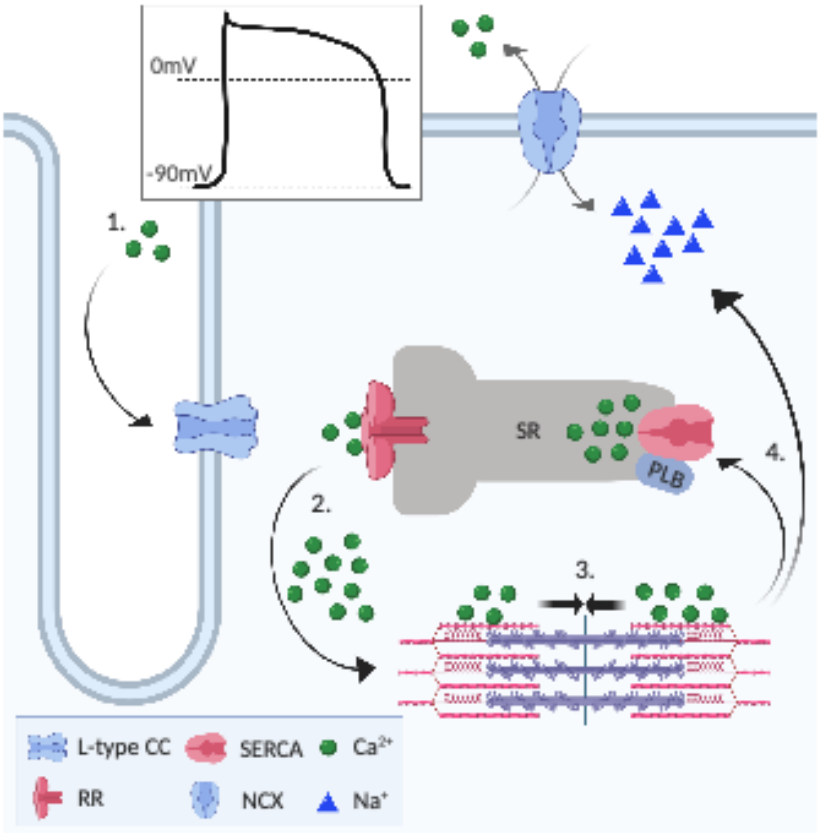

Figure 1.3 Cardiac excitation-contraction (EC) coupling

Major components of cardiac EC coupling cycle in the ventricular myocyte. 1) Following depolarisation of the sarcolemmal membrane, L-type calcium channels open, allowing a small amount of calcium to enter the dyadic cleft. 2) Calcium binds to ryanodine receptors, triggering a conformational change and resulting in a large release of calcium from SR stores. 3) Cytosolic calcium binds to troponin C resulting in a conformational change, allowing crossbridge cycling of the myofilaments to occur (i.e. contraction). 4) Calcium is removed from the cytosol by active return to SR stores by SERCA, and extrusion across the sarcolemmal membrane in exchange for sodium by NCX. Calcium dissociates from troponin C, inhibiting cross bridge cycling of myofilaments and enabling ventricular relaxation. Abbreviations: sarcoplasmic reticulum (SR), ryanodine receptor (RR), calcium channel (CC). Created with BioRender.com.

In EC-coupling, depolarisation of the sarcolemmal membrane causes the opening of L-type calcium channels, through which a small amount of calcium enters the cell (Section 1.2.1). The resultant increase in calcium levels in the dyadic cleft brings about a conformational change of the ligand-gated ryanodine receptors on the surface of the sarcoplasmic reticulum (SR), resulting in a larger efflux of calcium from intracellular stores into the cytosol - a process termed calcium-induced calcium release.[19] It is the resultant increase in cytosolic calcium concentration that is responsible for generating conformational changes in the contractile proteins by binding to troponin C and disinhibiting cross-bridge cycling of the myofilaments, allowing myocardial contraction to occur.[33]

Following contraction, it is necessary for the myocardium to relax in order to enable filling to occur before the next heartbeat. This process depends on the removal of calcium from the cytosol, thereby inhibiting cross-bridge cycling and resulting in a lengthening of the sarcomere. Calcium is extruded from the cytosol via two major mechanisms: i) via the sarco(endo)plasmic reticulum calcium ATPase (SERCA), which pumps calcium back into the SR at the expense of ATP and is responsible for the bulk of calcium removal, and ii) via NCX, which extrudes calcium from the cell in exchange for sodium, as previously discussed (Section 1.2.1).[34,35] This process is illustrated in Fig. 1.2. Intracellular calcium handling, specifically the rate-dependent removal of cytosolic calcium, is therefore fundamental to the process of active ventricular relaxation. Perturbations to this process could therefore lead to elevated cytosolic calcium levels during diastole and act to impair ventricular relaxation.

Given the importance of controlling intracellular calcium concentration, there are various ways in which calcium entry and removal from the cytoplasm are regulated. The L-type calcium current is responsible for triggering and maintaining the release of calcium from SR stores upon depolarisation of the cell, and as such must be tightly controlled. This is achieved by several mechanisms. Following depolarisation of the sarcolemmal membrane and resultant opening of L-type calcium channels, $I_{Ca,L}$ undergoes a slow inactivation during the plateau phase due to both voltage-dependant inactivation (VDI) and calcium-dependant inactivation (CDI) mechanisms. The contribution of VDI has been shown to be relatively small compared to CDI, which is thought to occur as a direct result of

calcium entry via L-type channels and due to release from SR stores.[21] Given that L-type channels are the mechanism by which calcium enters the cell and thus also contribute to SR calcium loading, this mechanism provides an effective negative-feedback loop that regulates intracellular calcium concentration on a beat-to-beat basis.[36] L-type calcium channels also contain phosphorylation sites, allowing $I_{Ca,L}$ to be modulated via the actions of calcium/calmodulin-dependent protein kinase II (CamK II), as well as via the G-protein cascade and protein kinase A (PKA).[37,38] PKA stimulation also affects other proteins important in the regulation of intracellular calcium handling, including ryanodine receptors (which contain phosphorylation sites and serve to increase calcium release from the SR when phosphorylated) and phospholamban (PLB).[39] PLB is a regulatory protein associated with SERCA, and under non-phosphorylated conditions acts to inhibit SERCA and reduce the rate of return of calcium to the SR. When phosphorylated, this inhibition by PLB is removed and rate of calcium removal is increased.[40]

Therefore, the intracellular calcium transient is the key driver of myofilament contraction and relaxation and must be tightly controlled to ensure that calcium levels are restored to normal following each depolarisation of the cell. Whilst this is regulated by inherent activation kinetics and phosphorylation status of ion channels and proteins involved in calcium handling, the duration of the AP itself can also influence intracellular calcium handling kinetics.

1.2.3 Action Potential Duration Modulates Intracellular Calcium Handling

Under normal circumstances ventricular APD changes in response to heart rate, with longer APs occurring at lower heart rates and shortening of the AP occurring at high rates. This effect is known as rate adaptation and enables the diastolic interval to be maintained at higher heart rates, ensuring adequate ventricular filling. This occurs through various mechanisms, one of which is a reduced availability of L-type calcium channels at higher heart rates due to the slow recovery of these channels, with the resultant reduction in $I_{Ca,L}$ causing APD to shorten.[41] Other mechanisms involve the elevation of subsarcolemmal sodium due to the relative increase of sodium influx at higher heart rates, which increases the activity of the Na^+,K^+-ATPase. This results in a faster rate of sodium extrusion across the sarcolemmal membrane, thus shortening APD.[42] As such, disproportionate

lengthening of APD for any given heart rate has the potential to disrupt normal intracellular calcium handling, owing to the mismatch between the period of time in which calcium is entering the cell and being released from the SR during depolarisation, and the amount of time available for calcium extrusion and ventricular relaxation. This disproportionate prolongation of APD is the reported situation in failing hearts and is the focus of the experimental hypothesis for the present study.[42] There are two major ways in which changes to APD may alter intracellular calcium handling in this setting: changes to the inward calcium current via L-type calcium channels and changes to NCX activity.

Changes to the duration of the cardiac AP influence the magnitude of $I_{Ca\text{-}L}$ due to the VDI and CDI mechanisms previously discussed (Section 1.2.2) and demonstrate a resultant impact on cardiac contraction and relaxation. Bouchard *et. al.* investigated the impact of alterations to AP duration on $I_{Ca\text{-}L}$, the intracellular calcium transient and contraction in isolated rat ventricular myocytes using whole-cell voltage clamping and application of short and long AP waveforms.[43] Data from this study revealed that prolonging APD resulted in a decreased maximal $I_{Ca\text{-}L}$ conductance, alongside a slowing of channel inactivation. The prolonged opening of L-type calcium channels during the AP resulted in an increase in the overall calcium influx, as well as the magnitude of cell shortening (a finding consistent with increased SR calcium loading). Interestingly, the rate of rise of intracellular calcium concentration was also closely linked with $I_{Ca\text{-}L}$, with peak cytosolic calcium concentration reached more slowly with prolonged APs. This was paralleled by a slowing of unloaded cell shortening and delayed peak contraction in isolated myocytes. Similarly, a slower rate of decay in the calcium transient was observed when APD was prolonged, which was reflected in a slowing of relaxation. This study by Bouchard *et. al.* therefore provides important evidence on the role of APD in modulating the process of EC-coupling in a single myocyte, and suggests that prolongation of the AP would result in three fundamental changes to EC-coupling: i) an increase in force, ii), a slower rate of contraction and delay to peak contraction, and iii) a slower rate of calcium removal and relaxation. In the whole heart, diastolic function is dependent upon the synchronous activity of many myocytes, and therefore AP prolongation may lead to dis-synchronous calcium handling. This would impact on both ventricular contraction and relaxation and would thereby impair normal diastolic function.

Another mechanism via which AP prolongation may serve to alter intracellular calcium handling is through altered NCX activity. As previously discussed (Section 1.2.1), ion exchange by NCX is electrogenic and may operate in either forward mode (calcium extrusion) or reverse mode (calcium entry), as determined by membrane potential and intracellular concentrations of calcium and sodium. Depolarised potentials result in a reduction in activity and therefore a reduction in calcium extrusion via this mechanism.[24] An increase in APD results in a greater amount of time spent at depolarised membrane potentials and may therefore result in a relative increase in intracellular calcium concentration during diastole, or a delay in the decay of the calcium transient. In addition, prolongation of APD at a constant heart rate results in a reduced diastolic period, which has the effect of decreasing the window for forward mode NCX function and thus calcium extrusion. However, the relationship between the AP and NCX activity is complex and will also be affected by the previously described effects of APD prolongation on the intracellular calcium transient (i.e. prolonged transient duration and increased calcium influx, see above). This will have an impact on NCX activity due to the prolonged increase in intracellular calcium concentration which occurs as a result, thereby increasing the driving force for forward-mode NCX function. The overall effects of NCX activity on calcium transient decay and diastolic calcium levels in HF will therefore depend on a combination of factors which include APD, as well as intracellular sodium concentration and the expression of relevant calcium handling proteins in ventricular myocytes.

In summary, APD represents an important mediator of EC-coupling and calcium influx/extrusion from the cell in isolated ventricular myocytes. Disproportionate changes to APD during HF therefore have the potential to disrupt normal diastolic function via alterations to intracellular calcium handling.

1.2.4 Changes to Intracellular Calcium Handling in Heart Failure

Whilst AP prolongation represents one mechanism by which calcium handling could be perturbed in HF, there are already several well-established causes of impaired calcium handling in patients and animal models of HF relating to the altered expression and/or function of calcium-handling proteins.

1.2.4.1 Alterations to SERCA Expression and Activity

Abnormalities in calcium handling are common in heart disease and contribute to the impairment of diastolic function. For example, dilated cardiomyopathy is associated with impaired LV relaxation, and experiments using myocardial tissue from patients with dilated cardiomyopathy have demonstrated abnormalities in intracellular calcium handling that result in a delay in the return to baseline calcium levels following contraction.[44,45] Similar findings have been demonstrated in studies using the fluorescent calcium indicator fura-2 in isolated cardiomyocytes from patients with HF, where results revealed a similar slow in the decay of the intracellular calcium transient.[46] Other studies have performed cardiac catheterization and echocardiography in patients presenting with diastolic HF and demonstrated abnormalities in active relaxation.[47] Given that the majority of cytosolic calcium is removed by SERCA during relaxation, it is perhaps not surprising that the abnormal calcium handling seen with HF has been linked to a reduction in the expression/activity of SERCA in cardiomyocytes.[48] In healthy hearts, removal of cytosolic calcium by SERCA has been reported to account for 70% of clearance in the rabbit, while NCX was responsible for 28%. This shifts to 92% and 7% contribution of SERCA and NCX, respectively, in the rat.[49,50] Guinea pigs and humans are reported to display similar relative contributions of SERCA and NCX to that seen in the rabbit.[51] However, this balance can shift in the presence of HF due to the changes in expression/activity of SERCA and/or NCX, reportedly resulting in a relatively equal contribution of SERCA and NCX to calcium clearance under such conditions.[49] The potential role for reduced cytosolic calcium clearance as a contributor to impaired diastolic function is supported by the findings of He *et. al*, who examined calcium handling in isolated mouse cardiomyocytes from transgenic animals overexpressing SERCA. Results demonstrated an increase in the rate of calcium clearance from the cytosol and a resultant increase in the rate of relaxation.[52] These findings were consistent with results obtained during additional experiments using isolated papillary muscles and *in vivo* investigations.

1.2.4.2 Alterations to Intracellular Sodium and NCX Activity

Another change frequently reported to occur within cardiomyocytes in the presence of HF is an increase in intracellular sodium concentration.[53, 54, 55, 56] This has been shown to have a major impact on intracellular calcium handling via alterations to NCX activity in muscle strips from failing human hearts, which demonstrate higher intracellular sodium concentrations relative to healthy hearts.[57] The authors proposed that this enabled cardiac contractility to be maintained at lower hearts rates by reducing calcium extrusion via forward-mode NCX activity and increasing calcium influx via reverse-mode NCX. Such conditions would result in greater calcium loading of the SR and act to maintain contractile function of the myocardium. However, it was proposed that this effect is only beneficial in the presence of a long diastolic period, allowing for diastolic calcium levels to return to normal between contractions despite the impaired functioning of SERCA commonly reported in HF.[48,49,58,59] At high heart rates, greater intracellular sodium concentrations were maintained in failing myocardial tissue, but the inotropic effect was lost. This occurred alongside the onset of diastolic dysfunction due to raised diastolic calcium levels and increased diastolic tension of the myocardium.

The function of NCX may also be impacted by the activity of Na^+,K^+-ATPase, with resultant effects on intracellular calcium handling. Na^+,K^+-ATPase plays a vital role in establishing the resting membrane potential by maintaining the sodium gradient across the sarcolemmal membrane. The pump is electrogenic and extrudes three sodium ions for every two potassium ions which are pumped into the cell. The activity/expression of Na^+,K^+-ATPase is often reported to be reduced in HF,[60,61,62,63] and this would be expected to result in an elevation of intracellular sodium concentration.[64] It is also known that inhibition of Na^+,K^+-ATPase (e.g. with ouabain) has a positively inotropic effect due to the resultant decrease in calcium efflux via NCX exchange in response to the reduced sodium gradient, thereby increasing intracellular stores.[60] Therefore, downregulation of Na^+,K^+-ATPase activity in HF may act to increase calcium influx via increased reverse mode/reduced forward mode NCX activity due to the altered sodium gradient across the sarcolemmal membrane. This is in line with the findings of a recent study which reported an increase in $I_{Na,late}$ alongside a decrease in the Na^+,K^+-ATPase current in a guinea pig model of HF.[63] The authors suggested that the resultant altered sodium gradient gave rise

to greater calcium influx via NCX, which was sufficient to maintain systolic function during the early stages of compensated hypertrophy but not following the progression to HF. Given that membrane potential also impacts on NCX activity (as previously discussed), the combination of reduced SERCA activity, increased intracellular sodium and prolonged APD seen with HF may serve to further alter intracellular calcium handling via effects on NCX, with the potential to result in elevated diastolic calcium levels and impaired ventricular relaxation.

In summary, abnormalities in intracellular calcium handling are commonly reported in patients with HF and may arise due to multiple factors including decreased expression/activity of SERCA, prolonged APD, and increased intracellular sodium with resultant effects on NXC activity. Such alterations to calcium handling, specifically the rate-dependent removal of cytosolic calcium, are likely to contribute to diastolic dysfunction. This effect may be heightened by the reported heterogeneous nature of these changes, which may act to disrupt synchronous activity of the myocardium.

1.3 Cardiac Repolarisation

As already discussed, there is a close link between repolarisation and active relaxation within the ventricular myocardium. The sequence and rate of ventricular repolarisation is therefore fundamental to the rate-dependant removal of calcium from the cytosol which, when rapid and coordinated, allows for the efficient relaxation and filling of the ventricles. Pathological changes to cardiac repolarisation therefore have the potential to impair diastolic function by disrupting normal intracellular calcium handling, however, this potential relationship has not been thoroughly investigated.

The sequence of depolarisation and repolarisation in the whole heart can be recorded in patients using electrocardiography. A typical electrocardiogram (ECG) displays three main features: the P wave, which reflects atrial depolarisation and contraction; the QRS complex, which reflects ventricular depolarisation and initiation of contraction; and the T wave, which reflects subsequent ventricular repolarisation and relaxation.[65,66] The ECG is therefore a useful tool for examining repolarisation, allowing parameters such QT interval (a measure of ventricular AP duration) and T-wave duration (a measure of

ventricular dispersion of repolarisation – typically measured as T_{peak} to T_{end} interval) to be determined. This relationship between APD and ECG parameters is shown in Fig. 1.4.

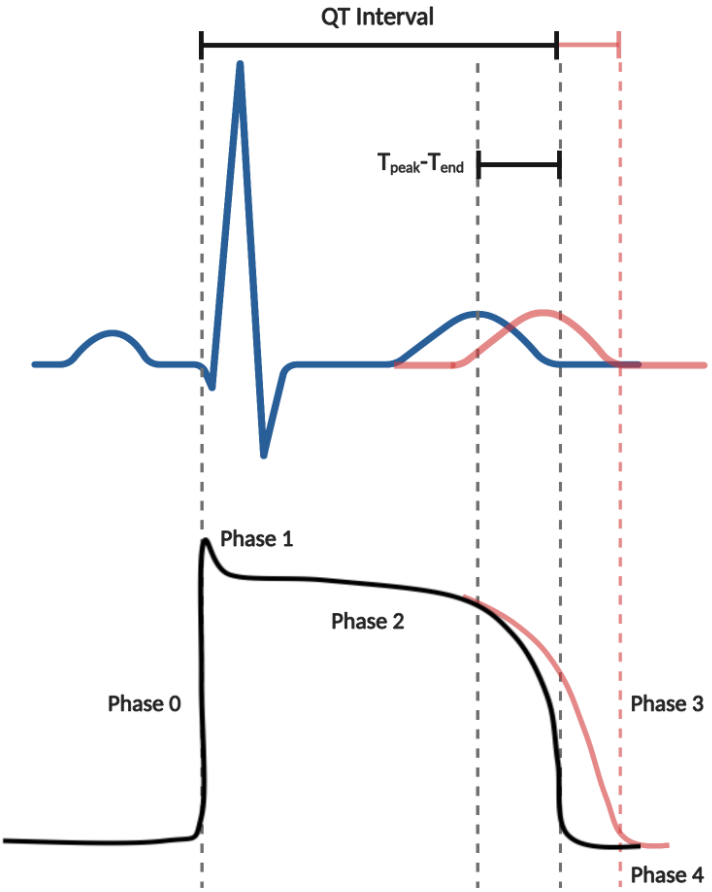

Figure 1.4 Relationship between ECG and ventricular AP parameters

Typical parameters reported as a measure of ventricular repolarisation time are QT interval and T_{peak}-T_{end} interval. As shown in the diagram, these parameters directly correspond to ventricular APD and phase 3 repolarisation. Prolongation of QT interval reflects prolongation of the ventricular AP (shown in red). Created with BioRender.com.

1.3.1 The Myocardial Repolarisation Sequence

In addition to tight control of intracellular calcium handling at the cellular level, global diastolic function is dependent upon synchronous activity across the whole of the myocardium to enable efficient relaxation and filling. There are several ion currents which play key roles in repolarisation of the human ventricular myocytes, as discussed in Section 1.2.1 (Fig. 1.2). Namely, these are: I_{to}, I_{Ks} and I_{Kr} and I_{K1}. Alterations to the

duration and/or magnitude of such currents (i.e. changes to the expression or activity of ion channels associated with these currents) can impact upon APD and repolarisation of the myocardium.

Under normal circumstances repolarisation of the myocardium begins first in the epicardium and travels through the myocardial wall with the endocardium repolarising last, and is opposite to the sequence that occurs upon depolarisation.[65] Heterogeneities in repolarisation have been observed since the work of Noble & Cohen, who first demonstrated differences in APD between ventricular slices taken from different regions of the sheep heart.[67] This dispersion of repolarisation occurs as a result of inherent regional variations in APD in cardiomyocytes across the ventricular wall and has been attributed to non-uniformity of ion channel expression.[67] One study examined apico-basal differences in the cardiac AP in canine cardiomyocytes.[17] The authors demonstrated that APD was shorter in myocytes isolated from the apex, and that this was as a result of a larger amplitude of I_{to} and I_{Ks}. Accordingly, the expression of the ion channels responsible for these currents was found to be higher in apical myocytes in tissue taken from both human and canine hearts. Such differences in APD and repolarising currents have also been described between the left and right ventricles.[68] Transmural differences in repolarisation are also present in the ventricular myocardium. The longest action potentials within contractile cells in the healthy heart have been reported to be found within M cells, which are present between the epicardial and endocardial cells within the ventricular wall.[69] This prolonged APD in M cells has been shown to be partly due to differences in the delayed rectifier potassium current (I_K) in these cells. Liu *et. al.* demonstrated that I_K was smaller in M cells when compared to that of epicardial and endocardial cells, and that this was due to a smaller flow of current via I_{Ks}. The contribution of I_{Kr} was similar in all three cell types.[70] In a separate study, Zygmunt *et. al.* found that the late I_{Na} was greater in M cells compared to epicardial and endocardial cells.[71] The authors concluded that this larger sodium current contributed to the prolonged APD in these cells. However, it should be noted that whilst the presence and characteristics of M cells have been extensively reported on ex *vivo,* their relevance to dispersion of APD/repolarisation in the human heart has been questioned. Some studies have suggested that the improved intercellular coupling seen in the whole heart

effectively abolishes the M cell characteristics seen in *ex vivo* experiments.[72] This may mean that the relative contribution of transmural dispersion of repolarisation is small compared to apico-basal gradients.

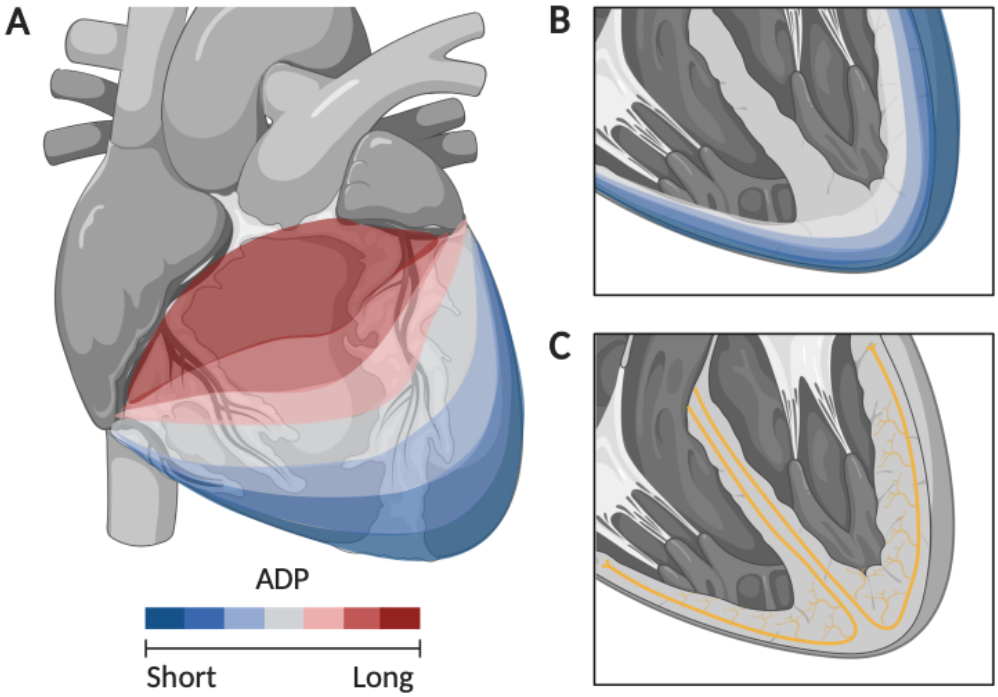

Figure 1.5 The myocardial repolarisation sequence

Representative depiction of the variation in APD across the ventricular myocardium and the pathway of ventricular conduction. A) Apico-basal gradient of APD across the ventricles, demonstrating shorter action potentials occurring at the apex of the heart relative to the base. B) Transmural gradient of APD across the ventricular wall, demonstrating shorter action potentials occurring at the epicardium relative to the endocardium. C) The ventricular conduction system. Following origin of the depolarising wave in the SA node and conduction through the AV node, the left and right bundle branches carry the signal through the ventricular septum before Purkinje fibres innervate the ventricular apex. Thus, depolarisation of the ventricular myocardium originates at the apex. This, combined with the APD gradient across the ventricles, allows for coordinated contraction and relaxation of the heart with efficient ejection and filling. Created with BioRender.com.

This sequence of repolarisation may play an important role in normal diastolic function, as demonstrated by the work from Zhu *et. al.* which used canine LV wedge preparations to investigate the relationship between ventricular repolarisation sequence and relaxation.[66] In this study, the interval between the peak and end of the T wave (TpTe)

was used as a measure of transmural dispersion of repolarisation (TDR), and the effect of switching between endo- and epicardial pacing on the transmural relaxation initiating time ($TR_{Epi–Endo}$) was examined. This parameter was measured by an isometric contraction loop and defined as the difference between onset of relaxation in the epicardium and endocardium, whereby the onset of relaxation referred to the point at which dT/dt (change in tension expressed as a function of time) became zero and proceeded to decrease continuously. It was demonstrated that changing from endocardial pacing (replicating the physiological activation sequence) to epicardial pacing resulted in an increase in both the TpTe and $TR_{Epi–Endo}$ in preparations isolated from the left and right ventricles. These data demonstrate the close association between repolarisation and initiation of relaxation. The authors also demonstrated that the polarity of the T wave could be reversed by cooling of the epicardial surface, resulting in prolonged epicardial APs and eventual reversal of the TDR sequence. The close link between repolarisation and relaxation was highlighted by the fact that the myocardial relaxation sequence was similarly reversed, with relaxation beginning in the endocardium.

In summary, myocardial repolarisation occurs in a specific sequence that ensures efficient myocardial relaxation and filling. It has been demonstrated that altering normal repolarisation has a negative impact on ventricular relaxation, and this may represent a mechanism through which regional differences in APD could result in altered intracellular calcium handling, thereby impacting negatively on global diastolic function.

1.3.2 Repolarisation Abnormalities: APD is Prolonged in Heart Failure

Having outlined why normal repolarisation is important for the efficient relaxation and filling of the ventricular myocardium, it is necessary to examine the changes to repolarisation which occur in a setting of cardiac dysfunction and HF.

Increases in APD are frequently reported in HF patients and are associated with delayed removal of cytosolic calcium. One study recorded APs from trabeculae carneae from patients with dilated cardiomyopathy and demonstrated increased APD in these patients compared to controls.[45] These findings were mirrored in a separate study which examined APD in isolated cardiomyocytes from patients with HF using current clamping techniques

and revealed a prolongation of APD in these patients compared to control.[46] Both groups also reported a delayed removal of cytosolic calcium in HF patients. Studies such as these show that the principles relating to APD and calcium transients demonstrated in the study by Bouchard *et. al.* (Section 1.2.3) are demonstrated in patients with HF, where diastolic function is known to be impaired.

Furthermore, HF has been demonstrated to induce cell type-dependent changes in APD with a resultant heterogeneous impact on calcium handling. One study examined these factors in rabbit epicardial, M and endocardial cells from animals with HF (induced by chronic coronary artery ligation) and control animals.[73] The data revealed that APD and intracellular calcium transient duration were prolonged in epicardial and M cells from animals with HF, but shortened in endocardial cells, when compared to control. Results also showed that end diastolic intracellular calcium concentration was reduced in epicardial cells but increased in endocardial cells compared with controls. Some of these findings relating to the heterogeneity of APD and calcium handling, are corroborated by another study, examining human ventricular wedge preparations from patients with and without HF prior to death.[74] Such heterogeneous alterations to APD could conceivably act to disrupt the ventricular repolarisation sequence and impair diastolic function.

In terms of the mechanism by which such prolongation of APD occurs in HF, there are several potential contributing factors. As may be expected, many depend upon alterations to the expression and/or activity of ion channels involved in the ventricular AP (see Section 1.2.1). In particular, changes to potassium current amplitudes are commonly reported as a cause APD prolongation in animal models of HF as well as in human patients. The delayed rectifier potassium current (I_K) has been reported to decrease in large and small animal models of experimental LV hypertrophy, with I_{Ks} and I_{Kr} displaying different prominence in different species.[75-78] However, the presence or absence of downregulation of I_{Ks} and/or I_{Kr} does appear to vary depending on the model used and there is a shortage of evidence for this type of remodelling in human HF.[79-81] The transient outward potassium current (I_{to}) is frequently reported to be reduced in small animal models of HF and is thought to arise predominantly through a reduction in the number of channels expressed, rather than due to altered channel kinetics.[77, 78, 82] In human HF, I_{to} has also been reported to be decreased, alongside a reduction in I_{K1} current

density.[83, 84] Downregulation of I_{to} appears to be a more consistent finding in HF, however, with other studies finding no change to I_{K1} in human HF or animal models of disease.[78, 79, 85] Therefore, there are various ways in which electrical remodelling can contribute to AP prolongation in HF, which the mechanism responsible likely to vary between different disease states and species.

In addition to the general association between AP prolongation and HF, there is now evidence to suggest a direct link between diastolic dysfunction in HF and repolarisation abnormalities. Two recent patient studies have demonstrated a correlation between abnormal repolarisation and diastolic dysfunction in HF patient cohorts. The first of these studies addressed whether electrocardiography could provide an effective means of demonstrating the presence of diastolic dysfunction, a condition more commonly determined with the use of echocardiography.[86] The authors examined the results from electrocardiography and echocardiography performed on patients referred to hospital with suspected HF. A first cohort of patients was used to statistically determine which ECG parameters most correlated with diastolic dysfunction. This was achieved by allocating patients into groups in order to grade their level of diastolic function, according to e' data obtained using tissue Doppler imaging. This parameter describes the early velocity of the mitral annulus and is widely accepted as a useful marker of diastolic function. Results revealed that a prolonged QTc interval (QT interval corrected using Bazett's formula) was most closely associated with reduced e', indicative of diastolic dysfunction. The QTc data was then compared to other echocardiographic parameters associated with diastolic function, and the same association was displayed. Phase two of the study involved gathering data from a second cohort of patients and revealed that QTc prolongation was indeed associated with reduced e'. A QTc interval of >435 ms and was found to be highly sensitive and specific in determining the presence of diastolic dysfunction when applied to patients with known or suspected HF. All electrocardiograms and echocardiograms in this study were analysed in a blinded fashion by a single individual (one for each diagnostic method), while potential confounding factors such as variations in patient age were also corrected for. Therefore, this study provides a robust example of the link between abnormal repolarisation and diastolic

dysfunction, and the potential usefulness of electrocardiography in assessing diastolic function.

The second of these studies, carried out by the same group, hypothesised that altered dispersion of repolarisation, as measured using the TpTe interval, may be associated with diastolic dysfunction.[87] This is a refinement on studies using QTc, since the TpTe interval is solely a measure of the magnitude of ventricular dispersion of repolarisation, whereas the QTc interval is influenced by the duration of the QRS complex (i.e. cardiac conduction), which can be delayed in HF and could also impact on diastolic function. The authors examined TpTe intervals in resting ECGs recorded from patients referred to hospital for exercise echocardiography, before assessing the diastolic function and ECGs obtained both at rest and at peak exercise stress. The results revealed that increased TpTe interval significantly correlated with a reduced septal e' velocity, as determined using tissue Doppler imaging. The authors also demonstrated that TpTe interval was still closely associated with diastolic dysfunction under exercise conditions, and that when this prolonged TpTe interval was taken into account, QTc was no longer associated with septal e' velocity. These findings led the authors to propose that the QTc prolongation previously reported was a manifestation of TpTe interval prolongation, and that this parameter provides a better measure of diastolic dysfunction and associated repolarisation abnormalities. The analysis of echocardiographic and electrocardiographic data used in this study was, again, carried out in a blinded fashion, while confounding factors such as patient age, QTc interval and left ventricular mass were accounted for.

Another clinical study by Shah *et. al.* was able demonstrate a link between delayed repolarisation/increased dispersion of repolarisation and increased severity of diastolic dysfunction.[12] The authors aimed to categorise patients with HFpEF according to various ECG, echocardiographic and haemodynamic parameters, in an attempt to better understand this heterogeneous condition. Results revealed that the group that had the highest number of patients with grade III (severe) diastolic dysfunction also demonstrated an increase in QTc interval as a measure of delayed repolarisation. This group also displayed a wider QRS-T angle, indicative of increased dispersion of repolarisation. Significantly, these findings suggest that repolarisation abnormalities may increase in severity in line with diastolic dysfunction.

Therefore, the above studies demonstrate in a clear and unbiased manner that a correlation exists between abnormal repolarisation and diastolic dysfunction in patients with HF, and that changes to APD are abundant in HF. However, it is not possible to conclude from such studies whether abnormal repolarisation represents a causal factor in the development of diastolic dysfunction, or if such abnormalities are merely a symptom of a diseased myocardium. Such a correlation is a recent finding and is worthy of further investigation, as if these abnormalities were found to be causative in the development of diastolic dysfunction in HF it would open the door to range of novel therapies which may prove effective in the treatment of diastolic HF.

1.3.3 Impact of Repolarisation Abnormalities on Diastolic Function

There appears to be a correlation between prolonged APD and abnormal intracellular calcium handling in HF, as well as between abnormal cardiac repolarisation and diastolic dysfunction. However, it is far from clear how such repolarisation abnormalities affect relaxation in the whole heart, and whether such abnormalities represent a primary causal factor for the impairment of diastolic function.

In the study by Zhu *et. al.* which demonstrated the effect of TDR on ventricular relaxation time, the authors also examined the role of this repolarisation sequence on ventricular diastolic function in isolated working rabbit hearts.[66] In these experiments hearts were bathed in ATX-II, an activator of I_{Na}, which had the effect of prolonging epicardial AP duration and consequently reversing the sequence of transmural repolarisation. This reversal of the transmural repolarisation sequence resulted in a significant increase in the isovolumic relaxation time within the LV, with a trend towards increased LV end diastolic pressure. Increases in these parameters are typical of diastolic dysfunction, suggesting a direct impact of abnormal dispersion of repolarisation on diastolic function in the whole heart.

Indeed, in addition to *ex vivo* studies, there is evidence to suggest a link between abnormal repolarisation and impaired cardiac function in patients with cardiac conditions other than HF. One such study examined the relationship between abnormal repolarisation and impaired diastolic function in patients with Behcet's disease.[88] Echocardiographic and

electrocardiographic data from Behcet's and control patients was gathered during exercise stress-testing, and the difference between maximal and minimum QT values obtained during 12-lead ECG recording used as a measure of dispersion of repolarisation (QTd). Results revealed that Behcet's patients displayed a significant increase in QTd compared to the control group and were also significantly more likely to present with diastolic dysfunction (as determined by prolonged isovolumic relaxation and mitral deceleration times). More significant, however, was the fact that those Behcet's patients with diastolic dysfunction displayed increased QTd compared to those without diastolic dysfunction. In fact, those without diastolic dysfunction did not have QTd levels that were significantly different when compared to controls. This finding ties dispersion of repolarisation to diastolic dysfunction, although still falls short of demonstrating a direct functional effect of abnormal repolarisation on ventricular relaxation.

However, the exact link between dispersion of repolarisation and diastolic dysfunction remains unclear. Another study looked at dispersion of repolarisation in patients with chronic HF and found that JTd in particular provided a good prognostic indicator of patients most at risk of sudden cardiac death or ventricular tachyarrhythmia.[89] Such patients displayed evidence of diastolic dysfunction in the form of increased LV end diastolic pressure (LVEDP) compared to control group and showed significantly increased dispersion of repolarisation. However, HF patients who did not go on to suffer from sudden cardiac death or ventricular tachyarrhythmia during follow up also displayed signs of diastolic dysfunction and did not demonstrate increased dispersion of repolarisation. The relationship between repolarisation abnormalities and diastolic dysfunction, therefore, may not be as simple as cause and effect.

Evidence from patients with congenital long QT syndrome (LQTS) may also be able to provide some insight into the mechanical impact of dispersion of repolarisation on the myocardium. Indeed, this may be an ideal setting to examine the effect of altered ventricular repolarisation on diastolic function, since this condition arises as a result of specific mutations to ion channels involved in the ventricular AP. As such, alterations to ventricular repolarisation occur in the absence of any of the confounding factors often present in HF which may also affect intracellular calcium handling (e.g. altered expression of SERCA/NCX). Long QT syndrome is characterised by repolarisation

abnormalities in affected individuals and it has been demonstrated that patients with congenital LQTS display increased spatial dispersion of repolarisation (measured both by TpTe, and the difference in QT intervals obtained between measurements from individual leads in a 12-lead ECG).[90] In the past LQTS had often been considered a purely electrical disease, with repolarisation abnormalities making affected individuals prone to life-threatening arrhythmias but not impacting on the mechanical function of the myocardium. However, more recently this has been demonstrated not to be the case. In a study using tissue Doppler imaging to assess the duration of contraction in six separate LV wall positions, the standard deviation of these measurements was used to determine the degree of dispersion of contraction.[91] This study examined data from two groups of LQTS single-mutation carriers; those with a history of relevant cardiac events, termed 'symptomatic', and those who were asymptomatic. Data revealed that the duration of contraction was longer in LQTS patients compared to control, as was the mechanical dispersion across the ventricular wall. Both parameters were also significantly greater in symptomatic patients compared to asymptomatic counterparts. Interestingly, the study also examined e' data for these patients, a parameter commonly used as a measure of diastolic function. The results demonstrated a significant decrease in e' velocity in symptomatic LQTS patients compared to control, and whilst asymptomatic patients were not significantly different to the control group, e' values for this group fell at the midpoint between the control and symptomatic group. This suggests that diastolic function is increasingly impaired in the presence of delayed and heterogeneous repolarisation (as indicated by increased duration and spatial dispersion of contraction). Such findings relating to the mechanical implications of LQTS have also been demonstrated by several other studies.[92,93,94]

Further evidence of a direct link between altered repolarisation and diastolic function was provided by a study looking into a phenomenon called 'cardiac memory', which describes changes in cardiac electrophysiology following prolonged periods of ventricular pacing.[95] This study examined myocardial repolarisation and relaxation parameters in patients with permanent pacemakers after varying lengths of pacing stimulus had been applied. Results demonstrated that all subjects showed changes in repolarisation following cessation of pacing, with prolongation of the QT interval appearing alongside increased isovolumic

relaxation time (a finding indicative of diastolic dysfunction in HF patients). The phenomenon of cardiac memory, as described in this study, has been reported to occur due to changes in the expression of ion channels involved in cardiac repolarisation following sustained pacing.[96]

Therefore, the direct impact of delayed repolarisation or increased dispersion of repolarisation on diastolic function remains unclear, since the majority of studies currently available can demonstrate only correlation. However, one study has demonstrated that reversal of the transmural repolarisation sequence directly impairs diastolic function in an isolated working heart preparation, and numerous clinical studies have evidenced increased dispersion of repolarisation as a risk factor in patients with various cardiac conditions. A potential physiological mechanism by which repolarisation abnormalities could impair diastolic function has also been demonstrated in studies assessing the impact of heart failure on APD and intracellular calcium handling. Therefore, evidence from existing studies suggests there is a strong association between diastolic dysfunction and repolarisation abnormalities which, if causal, may open the door to a novel class of therapy that could benefit patients suffering from HFpEF.

1.4 A Novel Treatment for Diastolic Dysfunction?

Conditions that are associated with prolongation of the AP, such as LQTS and HF, are commonly associated with repolarisation abnormalities.[12, 45, 46, 86, 87, 90, 91, 97] Given that there is a clear correlation between diastolic dysfunction and increased dispersion of repolarisation,[12, 86, 87] the possibility of correcting such an abnormality using pharmacological agents that shorten the AP represents a tempting novel therapy for diastolic HF. However, the regional differences in ionic conductance across the ventricular myocardium mean that care must be taken when selecting drugs to correct abnormal dispersion of repolarisation (which often act on such ion channels), since they may have a heterogeneous effect. It has been shown that the physiological sequence of transmural repolarisation must be maintained, as it is important to the efficient diastolic functioning of the heart.[66]

There are several potentially suitable ion currents which affect ventricular APD and repolarisation that could be targeted to correct repolarisation abnormalities. Late I_{Na} inhibitors would act to shorten APD and may provide a suitable pharmacological means of correcting abnormal repolarisation. Another class of drug which may be of interest are those which act to increase the I_{Ks} by increasing channel activation or slowing channel deactivation, thus reducing APD. Alternatively, increasing I_{Kr} may act to reduce the pathological delay of repolarisation seen with diastolic dysfunction and LQTS. The I_{Kr} may represent a more suitable target for correcting delayed repolarisation given that this current has been shown to have similar properties across the ventricular myocardium, and so there may be less risk of altering the natural transmural repolarisation sequence.[70] The I_{to}, which is the main contributor to phase 1 of the cardiac AP, may also represent a potential target for the treatment of HFpEF. A reduction in I_{to} has been reported in the diseased myocardium, and is associated with prolonged APD.[84, 98] Pharmacological agents which serve to increase this current may therefore be able to counteract pathological prolongation of the AP.

Therefore, although pharmacological correction of the prolonged repolarisation seen in patients with diastolic dysfunction represents a tempting novel therapy, it is associated with certain challenges owing to the intrinsic regional differences in ion currents found across the ventricular myocardium. Care must also be taken when aiming to shorten APD, since this has been found to be proarrhythmic.[99] However, if a causal link between repolarisation abnormalities and diastolic dysfunction can be demonstrated, it remains an interesting avenue of research given the current lack of successful therapies for patients with HFpEF.

1.5 Summary and Project Aims

Clinical studies have revealed a clear correlation between repolarisation abnormalities and diastolic dysfunction in patients with HFpEF, and it has been demonstrated using *ex vivo* preparations that repolarisation abnormalities have a negative impact on diastolic function. It is likely that abnormalities in intracellular calcium handling contribute to diastolic dysfunction, since this process is fundamental to active ventricular relaxation and studies have demonstrated abnormal calcium handling in patients with HF.

Alterations to APD associated with HFpEF may directly affect the inward calcium current and subsequent calcium handling. This is supported by studies in cardiac myocytes which show that prolonged APD acts to slow cytosolic calcium clearance and subsequent relaxation. Regional heterogeneity of APD and repolarisation seen in HFpEF may therefore lead to dis-synchronous relaxation of the myocardium, and impaired diastolic function. Such a mechanism would open the door to a range of novel therapies which may prove effective in the treatment of diastolic HF.

1.5.1 Hypothesis

That repolarisation abnormalities present in the failing heart may directly impair normal ventricular relaxation, leading to diastolic dysfunction. This would occur via perturbations to normal intracellular calcium handling as a result of altered ion exchange across the sarcolemma during the ventricular AP due to altered membrane potential. This may act in combination with other factors commonly present in HF, such as the altered expression of calcium handling proteins, to impair intracellular calcium handling and active ventricular relaxation, thereby contributing directly to diastolic dysfunction.

1.5.2 Specific Aims

1) To examine the relationship between APD and intracellular calcium handling in the healthy heart.
2) To determine the effect of prolonging APD on ventricular relaxation in the healthy heart, and in the presence of factors commonly associated with HF.
3) To establish and characterise an appropriate animal model of HF with diastolic dysfunction.
4) To determine the relationship between diastolic dysfunction and ventricular repolarisation in the failing heart.

2 METHODS AND MATERIALS

2.1 General Methods

This section will describe the general experimental setups and techniques used for the studies performed in this project. Specific protocols and conditions used for individual studies will be described in detail in the relevant results section.

2.1.1 Animal Housing and Husbandry

All animals used in studies were male Dunkin Hartley guinea pigs (Marshall BioResources) and ranged from 300-850g at the time at which experiments were carried out, as specified for individual studies. This variation in weight arose due to the rapid growth phase shown by young animals, resulting in a large weight gain during longitudinal *in vivo* studies. To allow for this, within any given study, animals were always age-matched. Animals were group housed where possible, and experienced standard 12-hour light-dark cycles with free access to food and drinking water at all times. Food consisted of standard guinea pig chow, hay and dried vegetables. All procedures were carried out according to the Animal (Scientific Procedures) Act (1986), under PPL 70/7491 and PPL PA527CE7C with ethical approval.

2.1.2 Isolation and Perfusion of Guinea Pig Hearts

Animals were anaesthetised by intraperitoneal injection of pentobarbitone sodium (approx. 160mg/kg) and heparin sodium (150 I.U.). A surgical level of anaesthesia was confirmed by checking for lack of pedal reflex before removal of the heart via thoracotomy and immediate submersion in ice-cold physiological buffer (composition given in Table 2.1) to prevent ischemic damage. The ascending aorta was then exposed, and the heart immediately mounted onto a cannula before commencing flow of buffer via a gravity fed/pump system, as specified in study protocols. This enabled retrograde coronary perfusion at a constant pressure of 60-70 mmHg. Physiological buffer was gassed throughout (95% O_2, 5% CO_2) to maintain correct oxygenation and pH (7.4), and reservoir temperature was maintained using a heated bath circulator (Thermo Scientific,

US) to give a heart temperature of 37.5°C ±0.5°C. All glassware was flushed with boiling, purified water (18.2MΩ.cm) after experiments to ensure that glassware remained clean and no contamination occurred between experiments.

2.1.2.1 Instrumentation of Langendorff-Perfused Hearts

The setup for Langendorff-perfusion of hearts is detailed in Fig 2.1 & 2.2. Following cannulation and commencement of coronary perfusion as described in Section 2.1.2, an incision was made in the left atrium, allowing for the insertion of a fluid-filled balloon coupled to a pressure transducer into the LV. Left ventricular end diastolic pressure (LVEDP) could then be adjusted by altering the volume of water inside the balloon and left ventricular pressure (LVP) measured throughout the contraction cycle. A pacing catheter (EP Technologies Inc., US) was then positioned at the right ventricular apex via an incision in the pulmonary artery, allowing endocardial pacing to be carried out during the experimental protocol using a DS3 Isolated Current Stimulator (Digitimer, UK). Pacing current was delivered at a value of 1.5 times the capture threshold. Finally, the heart was submerged in a warming chamber filled by coronary effluent, allowing a constant temperature to be maintained throughout the protocol. An ECG was also recorded throughout using a silver pellet electrode submerged in the buffer-filled warming chamber with negative/earth electrodes attached to the metal cannula above the aorta, allowing a modified lead II ECG to be recorded. Physiological data (LVP and ECG) was recorded using a PowerLab 8/30 with BioAmp and BridgeAmp, and LabChart 7 software (ADInstruments, Australia).

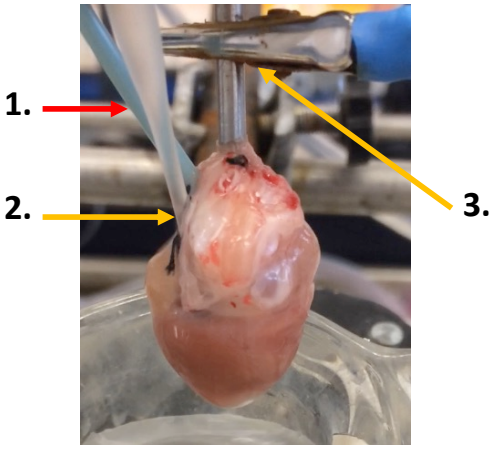

Figure 2.1 Langendorff heart instrumentation

Instrumented, Langendorff-perfused guinea pig heart. 1) Pacing catheter positioned at the endocardial right ventricular apex via the pulmonary artery. 2) Fluid-filled intraventricular balloon positioned within the left ventricle via the left atrium. 3) Negative and earth ECG leads positioned on the aortic cannula. (NB. Positive silver-pellet electrode positioned in the fluid-filled warming chamber while heart is submerged during experiments).

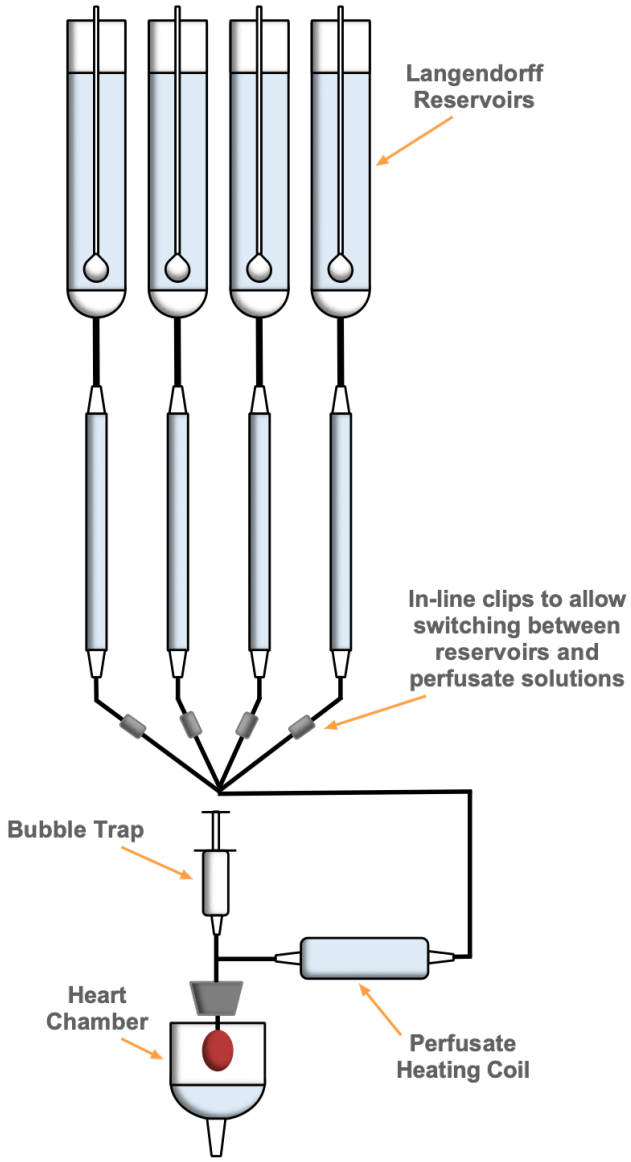

Figure 2.2 Langendorff heart setup

The heart is cannulated via the aorta to allow retrograde perfusion of the coronary arteries via either a gravity or constant-pressure pump system. Physiological buffer is maintained at 37.5℃ using water-jacketed glassware and a heated bath circulator, with a glass heating coil positioned immediately before the aortic cannula. Where a constant-pressure pump system was used, the pump was positioned before this glass heating coil. An air-filled syringe positioned above the aortic cannula acted as a compliance chamber and bubble-trap to prevent air entering the coronary circulation. The use of multiple reservoirs connected in parallel allowed for the switching between different concentrations of relevant pharmacological agents during studies.

2.1.2.2 Instrumentation of Isolated Working Hearts

Working hearts were initially cannulated to achieve retrograde perfusion in the same manner as described above and allowed to stabilise under these conditions. Subsequently, the pulmonary vein was identified and cannulated, allowing for filling of the left side of the heart. Perfusion was then switched from the aortic to the pulmonary vein cannula, allowing the left side of the heart to fill and eject physiological buffer via the aortic cannula against a set afterload of 55mmHg, which also served to maintain coronary perfusion. The working heart operated under a recirculating system within which the preload and afterload could be varied. This setup is described in detail in Fig. 2.4. Cardiac function was monitored via a pressure-volume catheter (Transonic, US) positioned within the left ventricle, and an ECG was recorded using silver wire electrodes positioned in a modified Lead II configuration. Where required, pacing was performed using a bipolar silver wire electrode positioned on the surface of the right atrium. (Fig. 2.3). Physiological data (LVP and ECG) was recorded using a PowerLab 8/30 with BioAmp and LabChart 7 software.

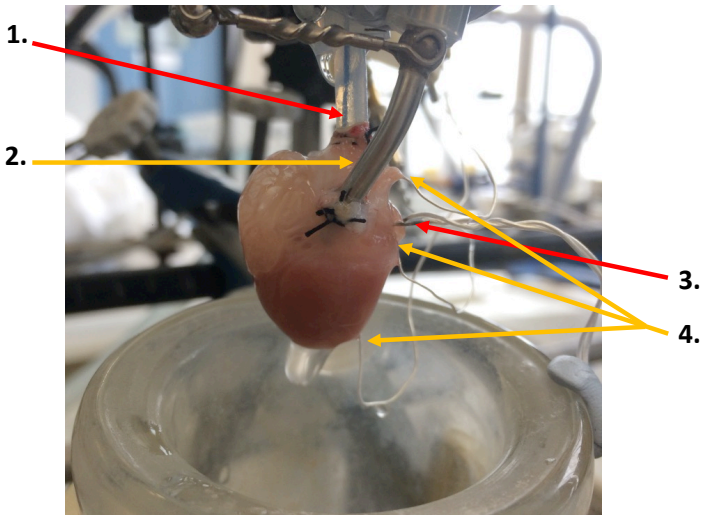

Figure 2.3 Working heart instrumentation

Instrumented, isolated working guinea pig heart. 1) Pressure-volume catheter within the aortic cannula. 2) Pulmonary vein cannula. 3) Bipolar pacing electrode positioned on the right atrium. 4) ECG wires positioned on the ventricular apex (positive), right atrium (negative) and connective tissue surrounding aorta (earth).

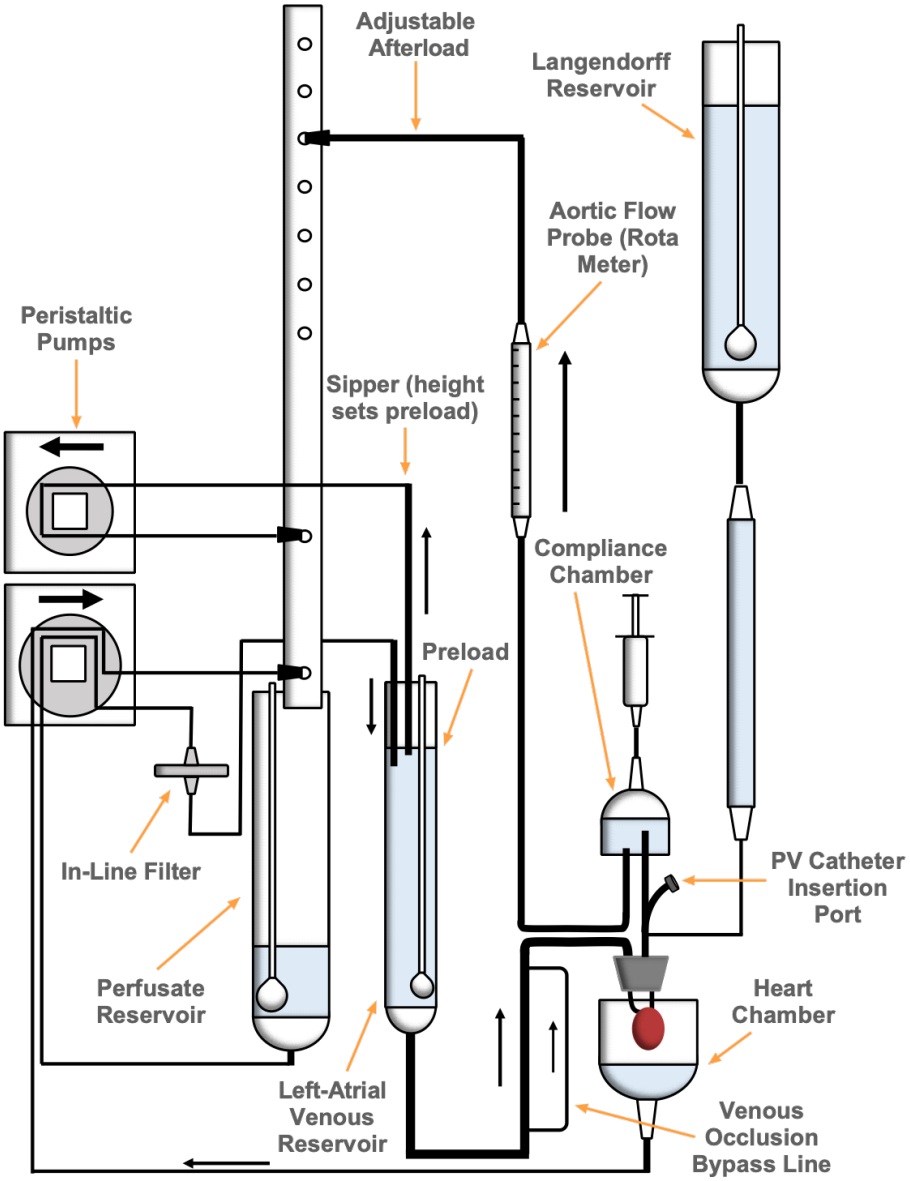

Figure 2.4 Working heart setup

Recirculating system allows for heart to be initially perfused in Langendorff mode, whilst a cannula is secured in the pulmonary vein (PV). This allows for the switch to working mode, whereby the left side of the heart is filled via the PV and the Langendorff reservoir closed off, allowing physiological buffer to be ejected via the aorta and recirculated. Buffer is then filtered before being reintroduced to the filling reservoir. Afterload is determined by the height of the outflow line, and preload is determined by setting a fixed height of solution within the filling reservoir. A catheter port off the aortic cannula allows for the introduction of a pressure-volume catheter into the left ventricle, and a double inflow line allows partial occlusions to be performed which mirror IVC occlusions performed *in vivo*.

2.1.2.3 Setup and Instrumentation of Langendorff Hearts for Optical Mapping

Although hearts used in optical mapping studies were also Langendorff-perfused, the requirement for the heart to be in a horizontal position necessitated isolating and cannulating the heart in a slightly different manner. Guinea pigs were anaesthetised as described above, and once surgical depth of anaesthesia was confirmed a thoracotomy was performed and the heart arrested using ice. The descending aorta was then identified and cannulated, and a small volume of ice-cold physiological buffer pushed through the coronary vessels using a syringe attached to the cannula. The subclavian arteries were then clamped to reduce loss of physiological buffer during perfusion, and the heart and surrounding ribcage removed leaving the spinal column intact. This allowed the heart to lie in a horizontal orientation during perfusion with the LV uppermost, allowing good exposure to the LEDs and camera. The spinal cord was destroyed using a wire prior to the start of the experiment to remove remaining sympathetic input during the protocol. Once in position, the heart was perfused with warmed physiological buffer via a constant pressure pump system, a catheter was positioned within the apex of the right ventricle to pace the heart and an ECG was recorded using silver wire electrodes. Physiological data (ECG) was recorded using a PowerLab 8/30 and LabChart 7 software.

2.1.2.4 Setup and Instrumentation of Hearts for NMR

Hearts used for ^{23}Na nuclear magnetic resonance (NMR) studies were isolated and Langendorff-perfused in the same manner as described in Section 2.2.1. However, owing to the necessity of having no metal within the magnet coil (this would create noise within the signal), slight modifications were made to the instrumentation (Fig 2.5). This included cannulating hearts onto a plastic cannula and using a fluid-filled plastic cannula coupled to a pressure transducer and positioned within the left ventricle as a crude method of monitoring function. Hearts were perfused using a constant-pressure pump system at a pressure of 60 mmHg on a modified Langendorff rig with an ‘umbilical’ system, allowing the heart to be lowered into the magnet whilst being supplied with physiological buffer at 37.5°C (Fig. 2.6). Hearts were positioned at the centre of the microimaging coil, and the bore of the magnet was kept at 37°C by circulating warm water through the imaging gradients. Hearts were enclosed within a modified thin-walled NMR tube containing a

'reference' sodium sample and bathed in coronary effluent, with an outflow siphoning line to prevent overflow. Physiological data (LVP) was recorded using a PowerLab 8/30 with BridgeAmp and LabChart 7 software. Note that the physiological buffer used in these experiments had a slightly modified composition (Table 2.1), as phosphorous spectra were collected during experiments and so the buffer could not contain phosphate.

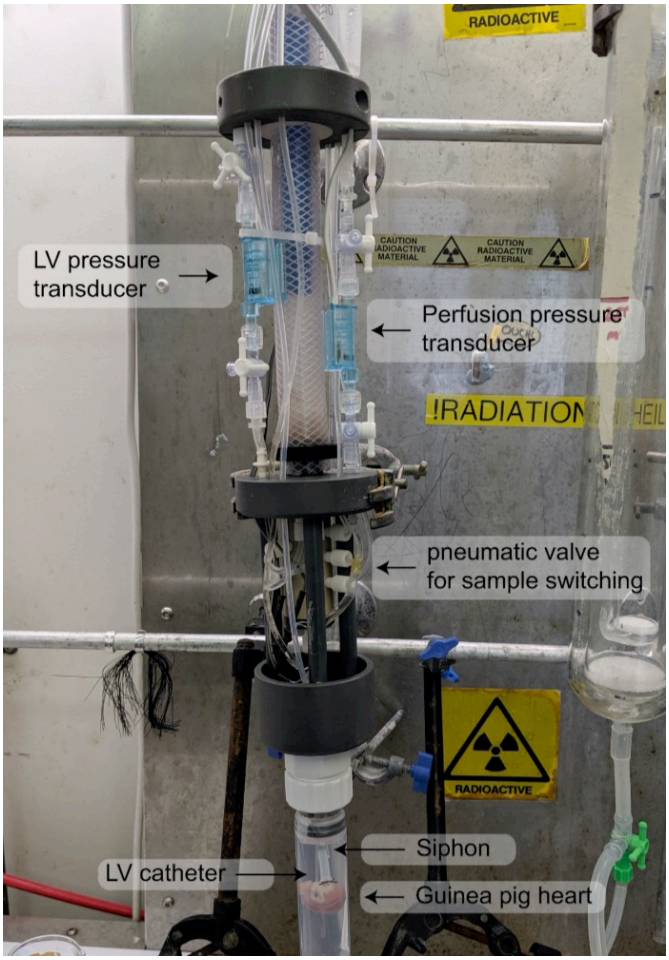

Figure 2.5 Instrumentation for NMR perfusion

Modified instrumentation of an isolated Langendorff-perfused guinea pig heart on the NMR perfusion rig. Hearts are enclosed within a double-walled glass NMR tube, which is filled by the coronary effluent and prevented from overflowing by a siphoning tube. Function is monitored via a fluid-filled catheter positioned within the left ventricle, coupled to a pressure transducer. A second pressure transducer is used to control perfusion pressure for the constant-pressure pump system. A pneumatic valve allows for switching between different buffers without a significant time lag.

Figure 2.6 NMR perfusion setup

Water-jacketed, constant-pressure pump perfusion system allows the heart to be supplied with physiological buffer at 37.5℃ and lowered into the magnet via an ‘umbilical’ system. The inclusion of multiple reservoirs allows for switching between buffers containing different concentrations of relevant pharmacological agents.

Table 2.1 Composition of physiological buffers used to perfuse isolated guinea pig hearts

Reagents were added to purified water (18.2MΩ.cm) with gentle stirring in the order listed, ensuring that the calcium chloride dihydrate was fully dissolved before adding remaining reagents in order to prevent precipitation. Buffer was filtered before use in experiments and kept at 4°C for a maximum of 5 days. Buffer was warmed and gassed with 95% O_2 + 5% CO_2 to maintain perfusate at a pH of 7.4 and temperature of 37.5°C. *N.B. This reagent was omitted from buffer used in NMR studies.

Reagent	*Concentration (mM)*
NaCl	114.0
$CaCl_2 2H_2O$	1.5
Sodium Pyruvate	2.0
Glucose	11.0
KCl	4.0
$NaH_2PO_4 2H_2O$*	1.1
$MgSO_4 7H_2O$	1.0
$NaHCO_3$	24.0

2.1.3 *In Vivo* Techniques

2.1.3.1 Unilateral Nephrectomy and DOCA Pellet Implantation

Guinea pigs (325-525g) underwent a unilateral nephrectomy and subcutaneous deoxycorticosterone acetate (DOCA) pellet (Innovative Research of America, 200mg, 60-day release) implantation in order to produce an animal model of diastolic dysfunction. Details of medications given to animals pre- and post-surgery are listed in Table 2.2. Anaesthesia was induced using 4% isoflurane inside an induction chamber and maintained using 2-2.5% isoflurane on a nose cone. A loss of pedal reflex and reaction to skin pinch at the incision site was used to indicate adequate depth of anaesthesia prior to commencing surgery. Animals were monitored throughout using a Rodent Surgical Monitor$^+$ system (Indus Instruments, USA) coupled with ECG and rectal temperature

probe, enabling core body temperature to be maintained throughout. Additional heating was provided with an infrared lamp as necessary. Aseptic technique was practiced throughout the procedure, with the use of sterile instruments, drapes, gown and gloves. Incision sites were prepared by shaving and thorough application of iodine-based surgical scrub. Removal of the left kidney was carried out via a 3cm abdominal incision slightly left of midline, which allowed sufficient space to remove a portion of the intestines and obtain a clear surgical field. Intestines were displaced onto the animal's abdomen onto sterile gauze swabs using cotton-tipped applicators and covered with gauze. They were kept moist using sterile 0.9% saline for the duration of the procedure. The blood vessels and ureter of the left kidney were occluded by using a curved metal 'introducer' to pass two 3-0 Mersilk sutures behind the renal hilum and tying off using surgical square knots (Fig. 2.7). Any additional arteries entering the kidney above or below the hilum were then identified and tied off (the presence of at least one additional artery was found to be common in guinea pigs). Once ischemia throughout the entire kidney was visually confirmed, the vessels were cut at the level of the surface of the kidney and the kidney was removed. The intestines were then replaced with the addition of several millilitres of saline to ensure adequate rehydration, and the abdominal muscle layers closed using 5-0 Vicryl and a simple continuous suture pattern. The skin layer was also closed using 5-0 Vicryl, but in this instance intradermal suturing with buried knots was used to prevent the animal reopening the wound upon recovery (Fig. 2.7). The incision site was then cleaned using reapplication of iodine surgical scrub followed by an ethanol rinse to reduce grooming around the incision site upon recovery.

Following completion of unilateral nephrectomy, the animal was positioned on its front and a 1-2cm incision made at the scruff of the neck. Round-ended scissors were used to create a subcutaneous pocket allowing for the insertion of two DOCA pellets. The wound was then closed using a simple interrupted suture pattern and cleaned with iodine surgical scrub, before recovering the animal (Fig. 2.7). Once conscious, animals were transferred to a recovery chamber at 27°C with food and water for several hours and monitored closely before being returned to their home cage. Sham animals underwent an identical abdominal incision and wound closure without the removal of the left kidney or implantation of DOCA pellets.

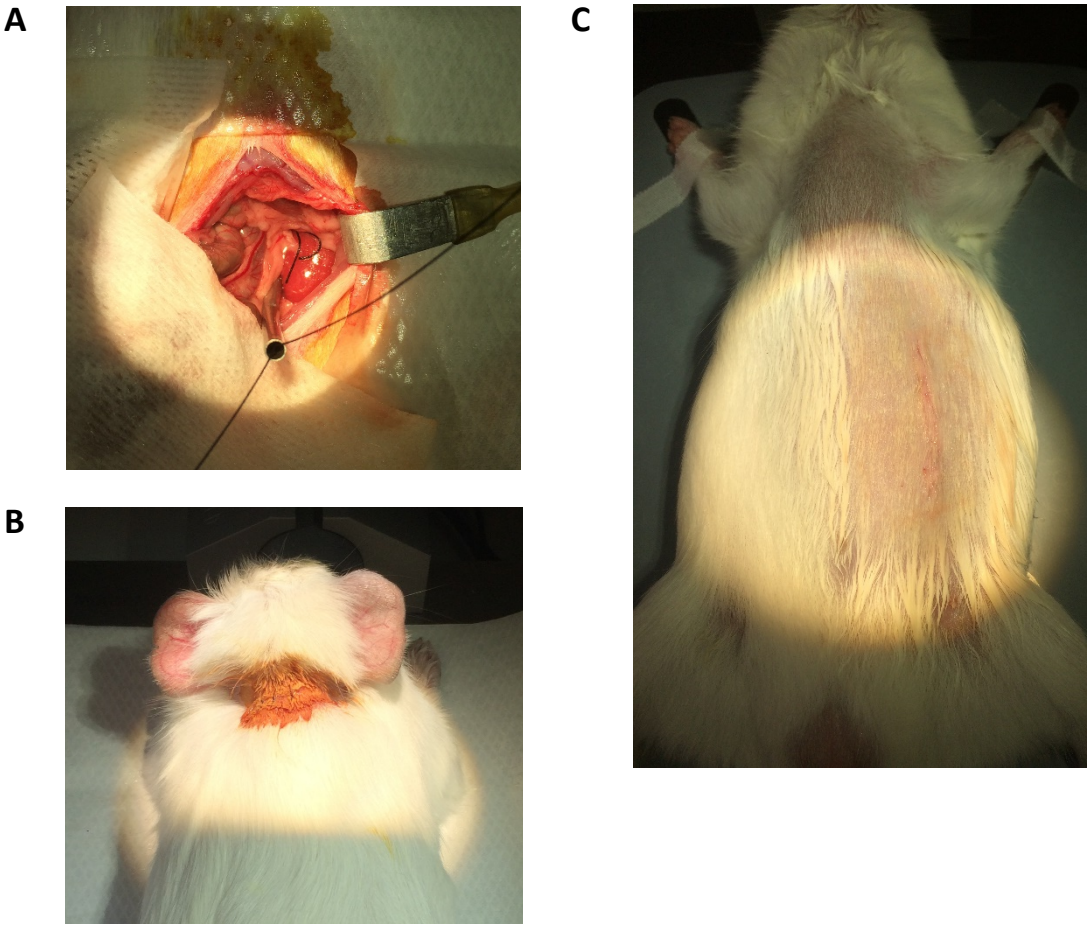

Figure 2.7 DOCA-salt model surgery

Animals included in the DOCA-salt diastolic dysfunction study underwent surgery for unilateral nephrectomy and DOCA pellet implantation. A) Image showing the method by with sutures were passed underneath the blood vessels and ureter of the renal hilum, using an L-shaped 'introducer'. B) Image showing the positioning of the incision used to implant the DOCA pellets. C) Image showing positioning of the abdominal incision through which the nephrectomy was performed, and the intradermal suturing pattern used for wound closure.

2.1.3.2 Telemetry Device Implantation

A proportion of animals used for the DOCA-salt HF model additionally underwent surgery to allow the implantation of combined ECG and blood pressure telemetry devices (HD-X11, DSI™, US). Not all animals could be telemetered owing to constraints on the number of telemetry devices and available hardware for recordings. Guinea pigs (325-525g) were anaesthetised and prepared for surgery as described above (Section 2.1.3.1).

The cap on the pressure catheter of the HD-X11 implant was removed and the device submerged in sterile saline prior to commencing surgery. A 2-3 cm horizontal incision was then made on the inside right hind leg, allowing visualisation of the femoral vein and artery. The skin and muscle on the proximal side of the wound was retracted to ensure a clear view of the vessels, and vessel dilators were used to carefully separate the femoral artery from the femoral vein and femoral nerve. Once this was achieved, 4 sutures were positioned underneath the vessel: 2 long sutures to permanently occlude the distal end of the artery and temporarily occlude the proximal end, and 2 short sutures ready to tie around the pressure catheter. A few drops of lignocaine (2% w/v) were then applied to the vessel in order to dilate the artery (it was found that the artery and vein were very tightly bonded, and the vessels did not remain patent during the procedure to separate them). The wound was covered with sterile gauze moistened with 0.9% sterile saline while the lignocaine took effect, and during this time the tip of the catheter was examined to check whether additional gel needed to be applied – this was done if any air bubbles were present, and the implant returned to the sterile saline. Once the femoral artery was visibly patent, the distal end was tied off using a surgical square knot and the long end of the suture used to tension the vessel slightly. The short sutures were loosely tied using a single square not, so that they were ready to be tightened over the catheter. The proximal end of the vessel was then occluded by tensioning a long suture passed underneath the vessel, using a pair of small forceps. Note, the femoral artery in the guinea pig was found to be too delicate for the use of a vessel clip in place of tension occlusion, and often remained collapsed after removal of the clip making it impossible to pass the catheter through the vessel. Once the vessel was occluded on both sides, a small incision was made in the vessel wall using curved vannas sprung scissors (DBIO, DE), and the pressure catheter introduced using a pair of cannulation forceps to grip the catheter and a pair of vessel dilators to grip the vessel wall. Once the catheter was passed far enough into the vessel, the short sutures were loosely tied, and tension was removed from the proximal end of the vessel. This allowed the catheter to be passed along the femoral artery until the tip reached the abdominal aorta, at which point the sutures could be securely fastened around the catheter to prevent any blood leakage. A subcutaneous pocket was then made in the flank of the animal in front of the hind limb, by blunt dissection with rounded scissors. This was flushed with sterile saline before positioning the implant within this

pocket, ensuring that the pressure catheter could lie flat with no kinks, and that the animal's movement would not be restricted.

Once the pressure catheter and implant were in place, the ECG leads could be positioned. This was done in a modified lead II formation, with the positive lead placed on the lower left side of the ribcage and the negative lead placed on the upper right chest wall. The leads were passed subcutaneously to these sites via a hollow metal rod with a rounded tip, which was first used to form a channel under the skin by blunt dissection. A small incision (1 cm) was made in the skin at both sites on the chest wall to expose the muscle layer to which the lead tips would be attached. The respective leads were cut to the appropriate length once passed under the skin to the site of attachment, leaving enough slack for growth and movement of the animal. The last 5 mm of the plastic coating was then removed from the lead by cutting through the coating with a scalpel blade and sliding the plastic sheath over the wire inside. This plastic coating was left covering the tip of the metal wire to prevent any irritation occurring. The wire was then sutured to the muscle of the chest wall using 4-0 Mersilk sutures and a square surgical knot at the level just below where the plastic coating had been cut. The remaining exposed section of wire was then buried by suturing the muscle on either side together, over the top of the lead. This ensured a good contact with the chest wall to obtain the best possible ECG quality.

The procedure was completed by suturing the incision in the hind limb using intradermal suturing and 5-0 Vicryl sutures and closing the chest wounds using simple interrupted sutures. Wounds were cleaned with iodine surgical scrub before recovering the animal and transferring to a recovery chamber at 27°C with food and water for several hours, prior to return to the home cage.

Table 2.2 Treatment regimen for guinea pigs undergoing surgical procedures

List of analgesics, antibiotics and supplements along with doses and routes of administration given to animals undergoing surgery in order to control pain and ensure rapid recovery from procedures.

Drug	*Route of Administration*	*Dose*	*Duration of Treatment*
Meloxicam (Metacam, 2mg/ml injectable solution for cats and 1.5mg/ml oral suspension for dogs)	Oral, s.c	0.2mg/kg	Orally for 2 days prior to surgery and 4 days after, s.c. on day of surgery
Enrofloxacin (Baytrill, 2.5% oral suspension)	Oral	5mg/kg	Orally (given as 1:3 dilution by syringe on day of surgery, and diluted in drinking water for 4 days following surgery)
Bupivacaine (Morcaine Polyamp, 0.25%)	s.c.	Max. 0.3ml/animal	Injected at incision sites prior to starting surgical procedure
Vitamin C (1000mg dispersible tablets)	Oral	Approx. 1420mg/L	Added to drinking water daily for 7 days either side of surgery

2.1.3.3 Cardiac Ultrasound

Animals were anaesthetised using 4% isoflurane in an induction chamber and maintained at 1.5-2% isoflurane on a nose cone. Body temperature was maintained during the procedure with the use of a homeothermic platform and rectal temperature probe, with additional warmth provided from an infrared lamp as required.

Prior to commencing cardiac ultrasound, an ECG was recorded for 1-2 minutes using a PowerLab 8/30 and BioAmp coupled to electrode pads on the homeothermic platform, onto which the animal's paws were secured. The recording of an ECG prior to starting the ultrasound allowed for any changes to heart rate and QT interval to be monitored thought the DOCA-salt study.

Cardiac ultrasound data was collected using a Vevo 3100 system with an MX201 10-22 MHz transducer (FUJIFILM VisualSonics Inc, Canada). Data was collected in the parasternal long axis (B-mode and M-mode), short axis (B-mode and M-mode) and apical two-chamber view (B-mode, pulsed-wave (PW) and tissue Doppler). These three views are illustrated in B-mode in Fig. 2.8. Data was collected free-hand, with the aid of a tilting platform to achieve a clear field of view for each parameter. After the ultrasound procedure animals were allowed to recover on the homeothermic platform and monitored for a short time, before return to their home cage.

Data was analysed using Vevo LAB 2.1.0 software (FUJIFILM VisualSonics Inc.). The timeline for the collection of cardiac ultrasound data from animals in the DOCA-salt study is shown in Fig. 2.9.

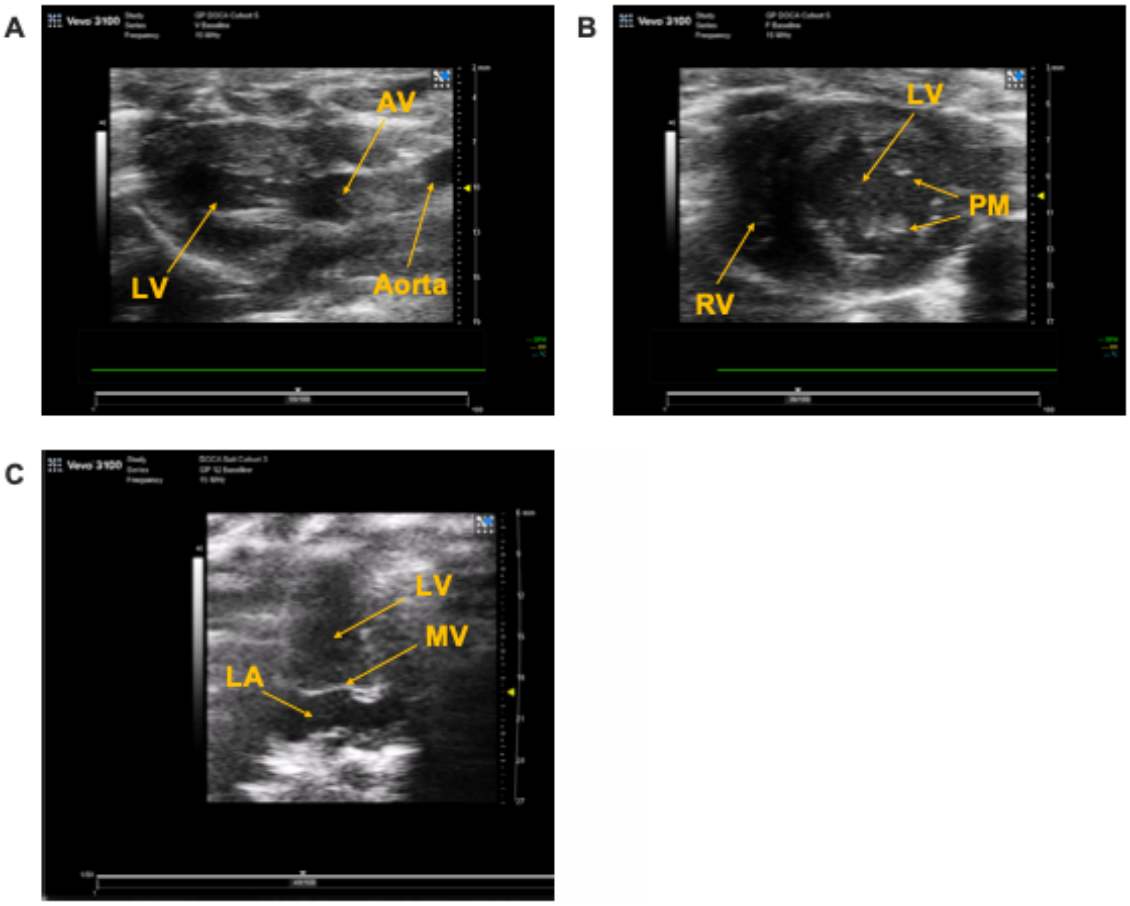

Figure 2.8 Views used in collection of cardiac ultrasound data

Representative B-mode images obtained in anaesthetised DOCA-salt and sham control guinea pigs. A) parasternal long axis (PLAX) view, B) short axis (SAX) view and C) apical two-chamber view. Additional analysis of cardiac structure and function was obtained in M-mode for PLAX and SAX views, while functional data from the apical two-chamber view was obtained using pulsed-wave and tissue Doppler. Abbreviations: left ventricle (LV), right ventricle (RV), left atrium (LA), aortic valve (AV), mitral valve (MV), papillary muscles (PM).

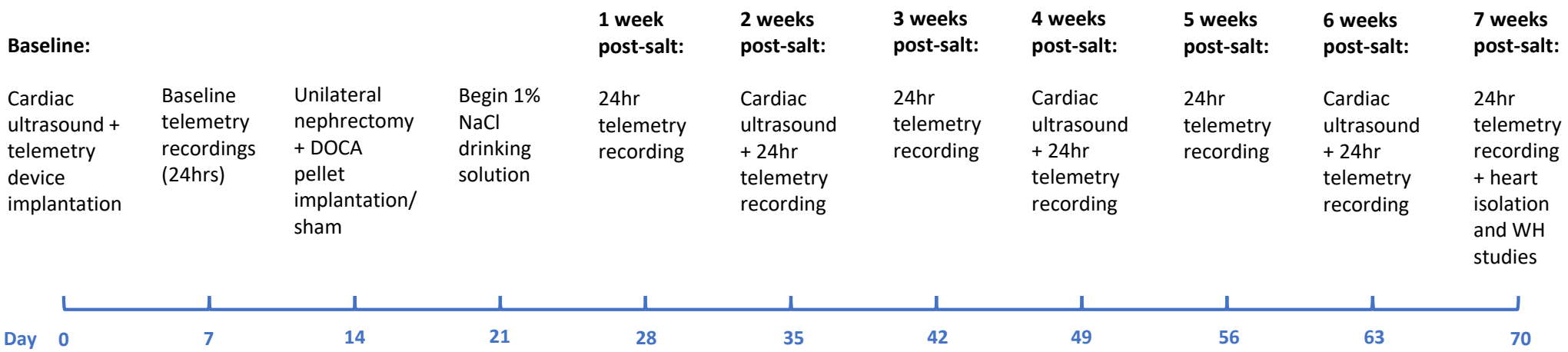

Figure 2.9 Timeline of DOCA-salt heart failure study

Details of the experimental timeline used for the DOCA-salt heart failure studies, including surgical procedures, serial monitoring using telemetry recording and cardiac ultrasound, and end-point function studies in isolated working hearts (WH).

2.1.4 Blood Pressure and ECG Telemetry Data Acquisition and Analysis

Telemetry studies were carried out using HD-X11 probes and PhysioTel™ RPC-1 receivers, coupled with Data Exchange Matrices and DataQuest A.R.T v4.33 software (DSI™, US). Blood pressure and ECG data was collected throughout a 24hr period on a weekly basis (Fig. 2.9), with sampling set to record 10s of data every minute during this period. Data was collected at weekends to minimise noise disturbance to the animals, and a 24hr period was recorded to control for any diurnal/nocturnal variation in blood pressure or ECG parameters. Animals undergoing telemetry recordings were single-housed in smaller home cages. Initial plans were to return these animals to group-housing with non-telemetered counterparts between recordings, however this proved impossible due to fighting occurring between animals following the period of separation.

Data was exported as a text file and opened in LabChart 8 for analysis. For blood pressure, data was averaged to provide hourly mean values which could then be further averaged to provide daytime and night-time values for the parameters of interest. An hour on either side of the switch between light and dark was excluded from this value to avoid error. For ECG, the ECG analysis module on LabChart was used to average 1500 beats allowing for manual measurement of the parameters of interest. An exception was made to this for one probe which had interrupted recordings, where 500 beats were averaged to allow mean values to be obtained using the ECG analysis software, despite the missing values. Similarly, these values were then averaged to give averages for the day and night with a central 6-hour window for day- and night-time used to provide these average values. Heart rate averages were obtained from the ECG data to provide a mean value for the same 6-hour day and night windows, thereby allowing QTc interval to be calculated. This was achieved using MATLAB R2019b software, which allowed the gaps in data (due to method used of acquiring 10s of data in every minute) and noise to be removed from the dataset and the remaining values averaged to provide an accurate heart rate for each animal.

2.1.5 NMR Spectra Acquisition and Analysis

Hearts for NMR studies were isolated and instrumented as described in section 2.1.2 and Fig. 2.5. The NMR tube holding the heart and perfusate inside the magnet consisted of two nested thin-walled NMR tubes. The outer tube (25mm diameter), contained a reference sample used to calibrate the ^{23}Na signal from one heart to another. This sample contained 500mM NaCl and 2.5mM Tm-DOTP shift reagent, set in 2% agarose. Agarose was used as a matrix medium to generate a triple quantum filtered (TQF) ^{23}Na signal, and the shift reagent was used to distinguish between the sodium signal originating from the heart/buffer and that which originates from the reference sample. The inner tube (24mm diameter), held the heart and perfusate.

^{31}P and ^{23}Na NMR spectra was acquired on the Bruker Advance III 400 MHz Spectrometer 9.4T vertical-bore magnet (Bruker, US) using a 30mm ^{31}P/^{23}Na microimaging coil. Spectra were visualised using the TopSpin 3.7pl software (Bruker, US). The coil was tuned and matched using the adjustment controls on the coil's probe. For every heart, shimming was carried out on the ^{23}Na channel.

Specific protocols and conditions used in studies examining the effects of ouabain and HF on intracellular sodium ($[Na_i]$) will be discussed in relevant results chapters. Briefly, time-resolved ^{23}Na spectra were acquired using TQF experiments with pulse sequences described by Eykyn and colleagues.[100] Interleaved TQF and double quantum filtering (DQF) NMR acquisitions, consisting of 192 scans and each lasting 1 min, were recorded throughout experiments. Cardiac energetics were determined before and after ouabain treatment through acquisition of ^{31}P spectra flanking the ^{23}Na experiments. Phosphorous spectra were acquired with a 60 flip angle, 64 scans and a total experiment duration of 5 min.

Two components were extracted from ^{31}P spectra for cardiac energetics assessment (Fig. 2.10). ATP-to-PCr ratio was obtained by the ratio of the integrated area under the ATP_β peak and PCr peak. The distance between the P_i and PCr peak (δ_{Pi}) was used to determine intracellular pH (pH_i) using the following equation:[101]

$$pH_i = 6.72 + \log\frac{(\delta_{Pi} - 3.17)}{(5.72 - \delta_{Pi})}$$

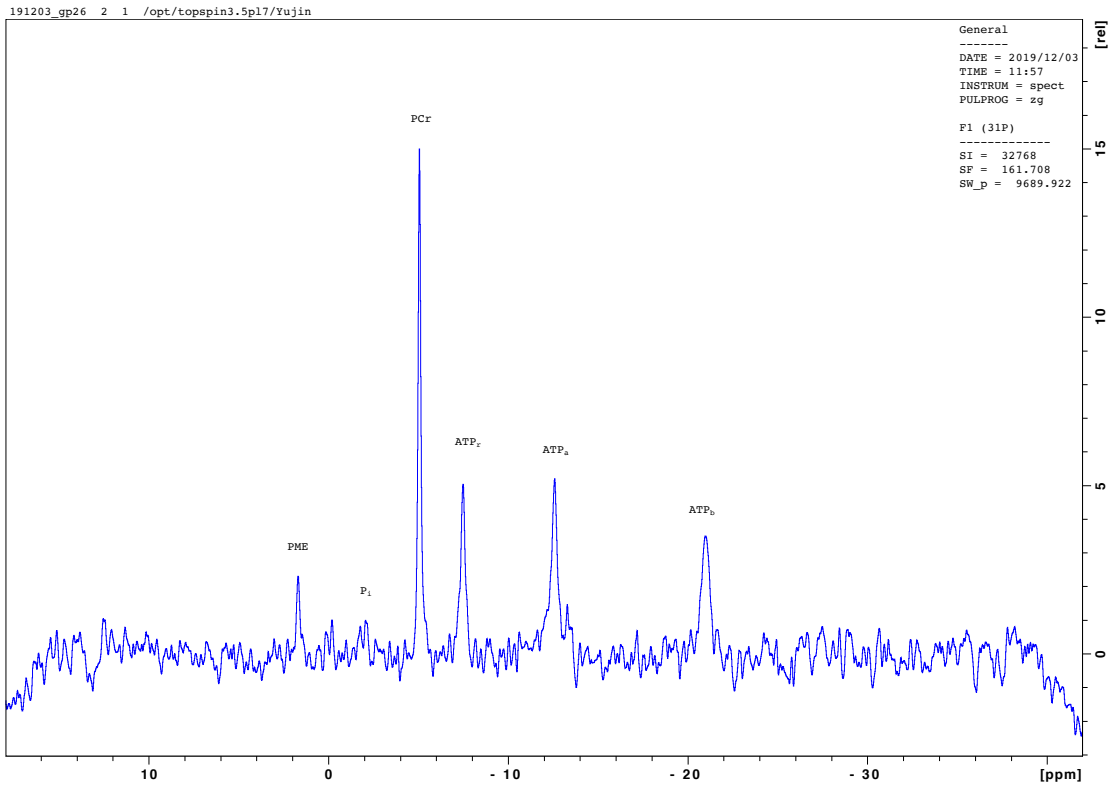

Figure 2.10 Representative ^{31}P NMR spectrum

Representative ^{31}P NMR spectrum obtained from a healthy Langendorff-perfused guinea pig heart under baseline conditions according to the methods described. Relevant peaks allowing for the calculation of intracellular pH using the above equation are labelled. Abbreviations: phosphomonoester (PME), inorganic phosphate (P_i), phosphocreatine (PCr), adenosine triphosphate (ATP).

For the analysis of ^{23}Na spectra, area under the reference sample peak and heart peak were integrated for each TQF and DQF spectrum (Fig. 2.11). The mean value of the signal coming from the reference samples was used to normalise the heart's signal to account for any differences in signal arising due to shim; the data was then further normalised to either heart weight (sham vs DOCA hearts) or to baseline (control vs ouabain/E4+HMR).

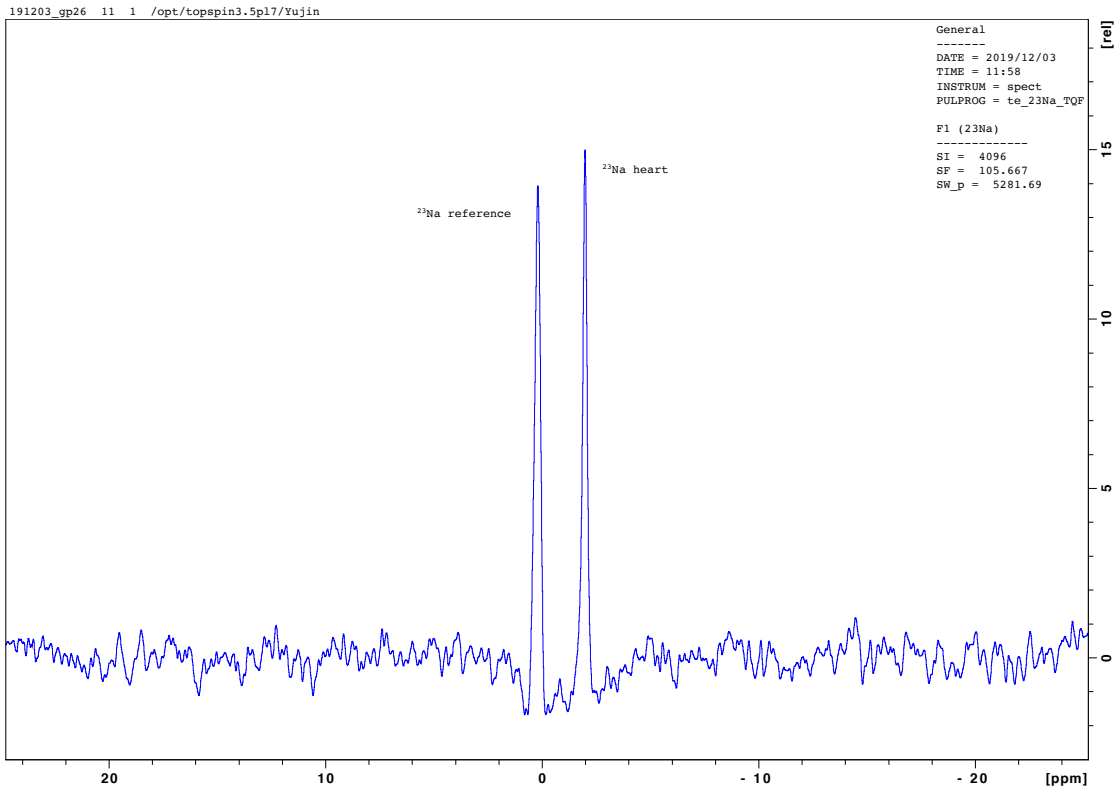

Figure 2.11 Representative ^{23}Na NMR spectrum

Representative triple quantum filtered (TQF) ^{23}Na NMR spectrum obtained from a healthy Langendorff-perfused guinea pig heart under baseline conditions according to the methods described. Relevant peaks originating from the sodium reference sample and the heart are labelled.

2.1.6 Western Blotting of Ventricular Tissue

2.1.6.1 Isolation and Homogenisation of Ventricular Tissue

Following completion of working heart study protocols in DOCA-salt animals, sections of tissue from the LV apex were isolated and placed into cryotubes before immediately submerging in liquid nitrogen. Tissue samples were stored at -80°C until homogenisation and biochemical analysis were carried out. Tissue samples were removed from -80°C and kept on dry ice.

Prior to homogenisation, tissue was weighed before adding a volume of homogenisation buffer equal to 10x tissue weight. The composition of the homogenisation buffer was as follows: 1:10 w/v MOPS buffer (20mM MOPS, 140mM NaCl, 5mM KCl, 1mM EDTA), 1:100 phosphatase inhibitor and 1:1000 protease inhibitor. Tissue and buffer were added to a homogenisation tube and kept on ice during homogenisation. This was carried out by using scissors to cut the sample into small pieces, before using an electric homogeniser for 30s to fully homogenise sample. Homogenate was transferred to eppendorff tubes and kept on ice until all samples were homogenised and a protein quantification assay could be performed. This was performed using a DC Protein Assay kit (Bio-Rad, US), with bovine serum albumin (BSA) as a protein standard and phosphate-buffered saline (PBS) as a diluent. A standard curve was produced using serial 1:2 dilutions of BSA, while tissue homogenates were serially diluted 1:10. A mixing plate was prepared in a 96-well plate according to manufacturer's instructions, before reading absorbance at 750nm. The protein concentration in each sample was then calculated from the standard curve and dilution factors. Samples were prepared at 10 mg/ml using PBS and 2x dilution with Laemelli buffer (Bio-Rad, US), before being heated at 65°C for 15 min at 1400rpm.

2.1.6.2 Western Blotting

Samples were loaded (200μg per well) into 4-20% TGX gels (Bio-Rad) alongside a protein colour standard (Bio-Rad, US) and run at 250V for 26 min, before a turbo system was used to transfer proteins to membranes (7 min). Membranes were blocked at room temperature for 1 hr with 1% casein in PBS (Bio-Rad, US), before incubating with primary antibodies overnight at 4°C on a plate rocker. Specific primary antibodies and concentrations used are listed in Table 2.3. Membranes were washed 4 times in PBST for 15 min at room temperature on a plate rocker, before being incubated with secondary antibody for 90 min at room temperature. Specific secondary antibodies and concentrations used are listed in Table 2.4. The washing step was then repeated to remove the secondary antibody before adding enhanced chemiluminescence (ECL) to membranes for 1 min at room temperature and developing films in a dark room. Films were scanned using a Bio-Rad GS800 scanner and ImageLab software (Bio-Rad, US) was used for analysis.

Table 2.3 Primary antibodies used in western blotting protocols

List of primary antibodies used, including concentration, manufacturer and product number. All primary antibodies were incubated with membranes overnight at 4°C on a plate rocker.

Antibody Target	*Product #*	*Manufacturer*	*Concentration*
GAPDH	2118S	CST	1:1000
NCX	MA3-926	ABR	1:1000
NKATPase α1	MA1-16731	Invitrogen	1:10,000
NKATPase α2	AB139094	Millipore	1:1000
NKATPase β1	05-38	Millipore	1:1000
NKATPase β2	06-171	Upstate Biotech	1:1000
PLB Phospho Thr 17	A010-913	Badrilla	1:1000
PLB Phospo Ser 16	A010-12	Badrilla	1:1000
PLB_{Total}	05-205	Millipore	1:10,000
PLM Phospho 63	S474C	Custom-made [102]	0.1µg/ml
PLM Phospho 68	S475C	Custom-made [102]	0.1µg/ml
PLM_{Total}	Ab76597	Abcam	1:10,000
SERCA2a	MA3-910	Invitrogen	1:1000

Table 2.4 Secondary antibodies used in western blotting protocols

List of secondary antibodies used, including concentration and manufacturer. All antibodies were incubated with membranes for 2 hours at room temperature on a plate rocker.

Secondary Antibody	*Species*	*Concentration*
GAPDH	Rabbit	1:5000
NCX	Mouse	1:2000
NKATPase α1	Mouse	1:2000
NKATPase α2	Rabbit	1:1000
NKATPase β1	Mouse	1:2000
NKATPase β2	Rabbit	1:1000
PLB Phospho Thr 17	Rabbit	1:2000
PLB Phospo Ser 16	Rabbit	1:1000
PLB_{Total}	Mouse	1:2000
PLM Phospho 63	Sheep	1:5000
PLM Phospho 68	Sheep	1:5000
PLM_{Total}	Rabbit	1:5000
SERCA2a	Mouse	1:5000

2.2 List of Reagents

Table 2.5 Reagents used in experimental protocols

List of reagents used in all experiments, including supplier. All salts listed were of reagent grade.

Reagent	*Supplier*
4-20% mini-PROTEAN TGX Gels	Bio-Rad Laboratories Ltd., UK
Bovine Serum Albumin (BSA)	Merck, UK
$CaCl_2 2H_2O$	VWR International, UK
DC Protein Assay Kit	Bio-Rad Laboratories Ltd., UK
ECL™ Blotting Reagents	GE Healthcare, UK
EDTA	Merck, UK
Glucose D (+)	VWR International, UK
KCl	VWR International, UK
Laemelli Buffer	Bio-Rad Laboratories Ltd., UK
$MgSO_4 7H_2O$	VWR International, UK
NaCl	VWR International, UK
$NaH_2PO_4 2H_2O$	VWR International, UK
$NaHCO_3$	VWR International, UK
PBS with 1% Casein	Bio-Rad Laboratories Ltd., UK

Phosphatase Inhibitors	Merck, UK
Phosphate Buffered Saline (PBS) (10x powder)	Fisher Scientific, UK
Precision Plus Protein Dual Colour Standards	Bio-Rad Laboratories Ltd., UK
Protease Inhibitor	Merck, UK
RH237	ThermoFisher, UK
Rhod-2, AM Ester	ThermoFisher, UK
Sodium Pyruvate	VWR International, UK
10x Tris/Glycine Buffer for Western Blots and Native Gels	Bio-Rad Laboratories Ltd., UK
Trans-Blot Turbo RTA Mini 0.2µm PVDF Transfer Kit	Bio-Rad Laboratories Ltd., UK
Tween 20	Merck, UK

2.3 List of Pharmacological Agents

Table 2.6 Pharmacological agents used in experimental protocols

List of pharmacological agents used in all studies, including supplier.

Pharmacological Agent	*Supplier*
Blebbistatin	Merck, UK

Bupivacaine Hydrochloride (Marcain Polyamp 0.25%)	AstraZeneca, UK
Cyclopiazonic Acid (CPA)	Merck, UK
Deoxycorticosterone Acetate (DOCA)	Innovative Research of America, US
E-4031 (hydrochloride)	Cambridge Bioscience, UK
Enrofloxacin (Baytril 2.5% Oral Solution)	Bayer, UK
HMR 1556	Bio-Techne Ltd, UK
Isoflurane (Isocare Inhalation Vapour)	Animalcare
Ivabradine Hydrochloride	Merck, UK
Meloxicam (Metacam)	Boehringer Ingelheim, UK
Ouabain Octahydrate	Merck, UK
Pentobarbitone Sodium (Pentoject 20% w/v Solution for Injection)	Animalcare
Veratridine	Merck, UK
Vitamin C, 1000mg Effervescent Tablets	Principle Healthcare, UK

3 LANGENDORFF HEART STUDIES

3.1 Introduction

The isolated, Langendorff-perfused heart remains a highly relevant technique in the field of cardiovascular research, with a broad range of applications.[103, 104] Using this model, it is straightforward to examine the effects of pharmacologically altered electrophysiology on cardiac function using a standard Langendorff perfusion with intraventricular balloon (IVB) and ECG/monophasic AP recordings.[105, 106] A modified Langendorff heart setup can also be employed to allow optical mapping of the ventricular myocardium and has useful applications for examining changes to ventricular electrophysiology.[107] This experimental model therefore provides an excellent means to answer initial questions surrounding the proposed hypothesis: namely, whether APD plays a role in determining calcium transient duration (CaTD), and whether APD affects cardiac diastolic function.

The guinea pig is an ideal animal model for investigating the potential link between repolarisation abnormalities and diastolic dysfunction, representing a small animal model with similar ventricular AP properties to those seen in humans. As discussed in section 1.2.1, there are numerous ion currents which contribute to the characteristic plateau and repolarisation phase of the ventricular AP, namely: I_{to}, $I_{Ca,L}$, $I_{Na,L}$, $I_{Na/Ca}$, I_{Kr}, I_{Ks} and I_{K1}. Expression of the relevant ion channels and the resultant contribution of these currents to the cardiac AP shows marked species variation, and it is important to consider this when designing experiments to examine the effects of altered repolarisation on ventricular relaxation. The guinea pig has several advantages over the more commonly used rat and mouse models in this regard, demonstrating both I_{Kr}, and I_{Ks}, as well as showing a significant contribution of $I_{Na,L}$ to the plateau phase and similar dependence on $I_{Na/Ca}$ for removal of cytosolic calcium.[22, 49, 108] In contrast, rats show predominantly I_{to}-driven repolarisation with a lack of AP plateau, which can be attributed to the very high heart rate which must be maintained in these species.[109] It should be noted that the ventricular AP of the guinea pig heart is not completely identical to that of humans and is commonly reported to lack I_{to} as well as demonstrating a more prominent I_{Ks}.[109] However, in terms of small animal species they provide the closest approximation, expressing most of the

major repolarising currents, and are therefore a very suitable model. In addition to similarities in ventricular ion channel expression, the guinea pig also represents a suitable model for the present studies owing to its similarity to humans in terms of EC coupling. It has been reported that guinea pigs and humans (along with rabbits) display similar contributions of NCX and SERCA to cytosolic calcium removal, with NCX accounting for around 28% and SERCA responsible for 70%. This is in contrast to rats (and mice) which demonstrate around 92% dependence on SERCA for calcium removal, with NCX accounting for only around 7%. [49-51] Given the importance of intracellular calcium handling to myocardial relaxation, and the potential role for changes to such calcium handling proteins in HF to disrupt this process (see Section 1.2.4), it is important that the chosen model is capable of mirroring the human situation as closely as possible. The guinea pig therefore represents the best choice of small animal model.

It has been shown that APD is prolonged in HF and that this is associated with changes to the intracellular calcium transient.[45-47] However, the relationship between APD and ventricular relaxation in the whole heart remains unclear. Before it was possible to try and address this, it was necessary to demonstrate that this relationship between APD and the intracellular calcium transient was present in the isolated guinea pig heart, using a whole-heart optical mapping approach. Subsequent studies could then determine whether prolongation of APD had any functional effects in the healthy heart.

Additional pathologies are also present in failing hearts and may affect any relationship between APD and ventricular diastolic function. One such pathology which is commonly reported in both human patients and animal models of HF is the reduction in expression and/or activity of SERCA.[58, 59, 110-112] As discussed in Section 1.2.2, SERCA is a key protein involved in the regulation of intracellular calcium and is the predominant mechanism by which calcium is removed from the cytosol, thereby allowing relaxation of the myofilaments to occur.[49] A diminished ability of SERCA to perform this function could therefore lead to elevated diastolic calcium levels, and so subsequent studies were designed to try and replicate this pathology of HF in order to determine whether the relationship between APD and diastolic function was altered in this setting.

3.1.1 Hypothesis and Objectives

Hypothesis: That repolarisation abnormalities commonly seen in HF act to prolong the underlying ventricular calcium transient and thereby contribute to impaired relaxation and diastolic dysfunction through altered intracellular calcium handling.

The objectives are therefore as follows:

1) To determine the relationship between APD and CaTD in the isolated, Langendorff-perfused guinea pig heart.
2) To assess whether APD prolongation had any functional implications in the healthy heart.
3) To assess the effect of APD prolongation on cardiac function in the Langendorff-perfused guinea pig heart when combined with SERCA inhibition.

3.2 Methods

The methods used to isolate, cannulate and instrument hearts for Langendorff perfusion are described in detail in Section 2.1.2. For the following Langendorff studies, male Dunkin Hartley guinea pigs weighing 500-700g were used. Where applicable, data were analysed using two-way ANOVA with Sidak's post-hoc test to determine whether significant differences were present between experimental groups at each time point and a p value of <0.05 was deemed statistically significant. Hearts were randomly assigned to experimental groups and data files were blinded prior to analysis.

3.2.1 Relationship between APD and CaTD in the Isolated Guinea Pig Heart

In order to properly test the experimental hypothesis, the first question to be addressed was whether there was a direct relationship between ventricular APD and the underlying CaTD. In order to do this, optical mapping techniques were used to measure simultaneous APs and calcium transients in the LV of isolated Langendorff-perfused guinea pig hearts (methods described Section 2.1.2).

Following cannulation and instrumentation, hearts were electromechanically uncoupled using blebbistatin (15μM) and loaded with voltage-sensitive RH237 (20μg in DMSO)

and calcium-sensitive Rhod-2 (200-400μg in DMSO) fluorescent dyes. Blebbistatin uncouples mechanical contraction from the electrical excitation of the tissue by binding to the myosin ADP-P_i complex, resulting in blockade of actin-myosin interaction.[113] Therefore, electrical activity of the heart is still present and may be recorded via an ECG, but contraction ceases to occur and motion artefact is removed. To allow pacing across a broad range of heart rates, hearts were perfused with ivabradine (10μM), which lowers intrinsic heart rate by selectively acting on the pacemaker current (I_f) in the sinoatrial node but does not affect cardiac repolarisation.[114] Following a stabilisation period for this to take effect, hearts were paced at a baseline rate of 2Hz (120bpm). Action potential duration was then varied by two methods: pacing across a range of pacing rates, and perfusion with a range of concentrations of E-4031 and HMR 1556 which block repolarising potassium currents I_{Kr} and I_{Ks}, respectively. The following pacing protocol was then carried out under control conditions and at each concentration of drug used in the study, with images captured at the end of each 2 min pacing period: 2Hz (2 min), 2.5Hz (2 min), 3Hz (2 min), 3.5Hz (2 min), 4Hz (2 min), 4.5Hz (2 min), 5Hz (2 min). The range of concentrations of E-4031 and HMR 1556 is detailed in Table 3.1.

Table 3.1 Concentrations of E-4031 and HMR 1556 used in optical mapping study

List of concentrations of E-4031 and HMR 1556 used to prolong APD during each phase of the experiment. Pacing protocol was performed once at each phase, with images captured at the end of a 2 min stabilisation period at each pacing rate.

	E-4031 + HMR 1556 (nM)
Baseline	0 + 0
Phase 1	100 + 0
Phase 2	100 + 300
Phase 3	100 + 1000

Images were captured using a MVX10 stereomicroscope (Olympus, JP) coupled to Evolve Delta 512 x 512 pixel EMCDD cameras (Teledyne Photometrics, US), and MetaMorph software (Molecular Devices LLC, CA). Data were sampled at 500Hz with a spatial resolution of 355μm^2 per pixel (64x64 pixels). Excitation wavelength was 530

± 25nm, with Rhod-2 emission light collected at 585 ± 20nm and RH237 emission light collected at >710nm. The optical setup for this experiment is depicted in Fig. 3.1.

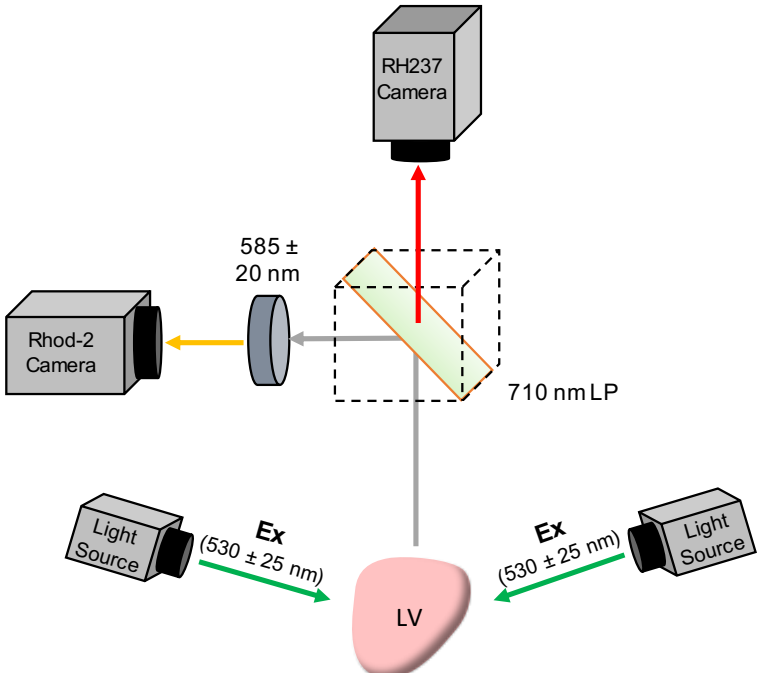

Figure 3.1 Optical setup of mapping experiments

Isolated guinea pig hearts were Langendorff-perfused in a horizontal orientation using a constant-pressure pump system. Hearts were loaded with RH237 and Rhod-2 dyes to enable the detection of changes in membrane voltage and intracellular calcium, respectively. LED light sources were used to illuminate the LV with an excitation wavelength (Ex) of 530 ± 25nm, and two separate detection cameras were used to collect emission light from RH237 (>710nm) and Rhod-2 (585 ± 20nm).

For analysis, Optiq software was used to extract the AP and calcium transient data (developed by Francis Burton at the University of Glasgow). Action potentials and calcium transients were taken as an average signal from 6 predetermined square regions across the left ventricle, as depicted in Fig. 3.2. APD/CaTDs were taken from three cardiac cycles at each pacing rate at each concentration of E-4031 and HMR 1556, with data displayed in several ways. Averaged APD90/50 vs cycle length: this is the APD averaged from 3 cardiac cycles across the 6 predetermined regions plotted against each cycle length (from the range of pacing rates). Averaged APDs at each cycle length at each concentration of E-4031 and HMR 1556 are plotted individually (Fig. 3.3 A and 3.4 A). The same approach is also used to display CaTD90/50 (Fig. 3.3 B and 3.4 B). In order to aid visualisation of APD90 vs CaTD90, representative examples were plotted and

overlaid for a heart paced at 2Hz under baseline conditions and in the presence of the maximum E-4031 and HMR 1556 concentration (Fig. 3.4 D).

Figures 3.3 C and 3.4 C show the relationship between the duration of the AP and the duration of the calcium transient plotted as a scatter plot from all pacing frequencies. In these plots, individual values for each of the three APs were taken from each of the six regions across the left ventricle and CaTD plotted as a function of the corresponding APD. This gives 18 individual points from each heart under each condition/pacing rate and was done for both APD/CaTD50 (Fig. 3.3 C) and APD/CaTD90 (Fig. 3.4 C).

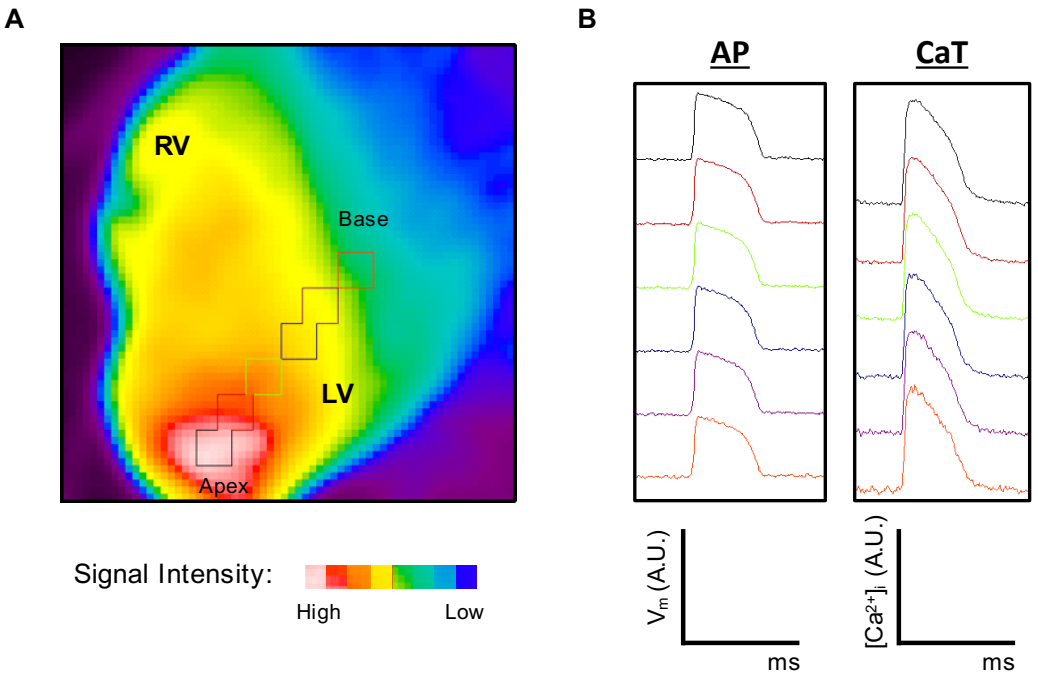

Figure 3.2 Left ventricular regions used for action potential and calcium transient analysis during optical mapping experiments

Representative image demonstrating regions across the left ventricle from which action potentials and calcium transients were obtained using Optiq software. A) Orientation of heart during endocardial pacing via a catheter positioned in the apex of the right ventricle (N.B. colours simply indicate signal intensity and did not form part of the analysis). Squares shown depict the six regions across the left ventricle from which averaged signals were taken to obtain action potentials and calcium transients used for analysis. B) Representative action potentials (AP) and calcium transients (CaT) from each of the squares indicated in (A).

3.2.2 Effect of Prolonging QT Interval in the Healthy Heart

After determining the relationship between APD and CaTD in the left ventricle, the next question to address was whether APD prolongation had any functional effect in the healthy heart. To this end, a study was conducted where Langendorff-perfused guinea pig hearts were perfused with incremental doses of APD-prolonging drugs, with QT interval used as a surrogate measure of APD. Two pharmacological mechanisms were used to prolong QT interval in this study: blockade of repolarising currents I_{Kr} and I_{Ks} using a combination of E-4031 and HMR 1556, as previously discussed, and augmentation of $I_{Na,L}$ using veratridine (for concentrations used see Table 3.2). The use of a range of doses in the healthy heart allowed for the selection of a dose which gives clinically relevant QT prolongation going forward, while the use of two separate mechanisms enables any differential effects of targeting different currents to be identified.

Table 3.2 Concentrations of E-4031 + HMR 1556 and veratridine used in QT prolongation study

List of concentrations of E-4031 + HMR 1556 or veratridine used to prolong QT interval in healthy Langendorff-perfused hearts (depending on experimental group).

	E-4031 + HMR 1556 (nM)	*Veratridine (nM)*
Baseline	0 + 0	0
Conc. 1	30 + 0	10
Conc. 2	100 + 0	30
Conc. 3	100 + 10	100
Conc. 4	100 + 30	300

In this study, hearts were isolated and instrumented as previously described (Section 2.1.2) and perfusion pressure was maintained at 65-70mmHg using a constant-pressure pump system. Hearts were paced at a rate of approximately 10bpm above their intrinsic rate, LVEDP set to 5-7mmHg by adjusting the IVB volume, and allowed to stabilise for 10min. An LVEDP of 5-7mmHg was chosen based on data from pilot hearts which

demonstrated that an LVEDP of this magnitude was required to give a sufficient left ventricular developed pressure (LVDP) (>80mmHg), whilst not being so high as to risk ischemic damage to the endocardium. Hearts were paced at a rate just above their intrinsic rate rather than at a predetermined, fixed rate to avoid having to pace some hearts significantly higher than their intrinsic rate, as pilot data had indicated that high pacing rates rapidly caused hearts to develop a high LVEDP owing to the short diastolic interval in guinea pig hearts. Since LVEDP was to be a key parameter used to measure diastolic function it was important to avoid distorting this at baseline.

Following stabilisation, hearts were subjected to a pacing protocol as follows: baseline pacing rate (2 min), +35bpm (2 min), baseline pacing rate (3 min), +70bpm (2 min), return to baseline pacing rate. Stable pacing was maintained for a minimum of 2 min at each pacing rate to allow LVDP to stabilise in response to increased pacing frequency. Hearts were then perfused with incremental concentrations of E-4031 + HMR 1556, veratridine, or vehicle control (DMSO) (Table 3.2) and stabilised for 10 min to allow the drug to take effect, before repeating the pacing protocol at each drug dose.

For analysis, LabChart 8 Pro with ECG and Peak Analysis modules was used. ECG parameters were measured using the ECG analysis tool to average 10 beats, with manual correction of the detection of ECG features (Fig. 3.5 A-C, Fig. 3.9 B). To analyse LVP, 30s of data was analysed using the cyclic measurements on the data pad tool to give an average value for LVDP and LVEDP at each drug dose (Fig. 3.6 A, C, E and Fig. 3.7 A, C, E). Time from pacing spike to peak ventricular pressure was analysed manually using scope view to average multiple pressure cycles (Fig. 3.6 B, D, F). The peak analysis tool was used to analyse the average time from peak ventricular pressure to 75% relaxation for the same 30s section of data (Fig. 3.7 B, D, F). To aid visualisation of the effect of QT prolongation on LV pressure generation, data from a complete cardiac cycle was exported from LabChart and plotted against time on GraphPad Prism 8. Representative examples were selected by identifying hearts which displayed diastolic function most similar to the group average, with the data shown taken from baseline pacing rates at the highest drug dose or corresponding timepoint for vehicle control (Fig. 3.8). Coronary flows were calculated continuously using a calibrated LabChart channel coupled to the pressure transducer and STH Pump Controller (ADInstruments, Australia) which

monitored perfusion pressure and flow rate. Reported coronary flows represent the average flow rate from the 30s of data selected at the end of each pacing protocol (Fig. 3.9 A).

3.2.3 Effect of Prolonging QT Interval in the Presence of Ivabradine

This study aimed to build on the findings of the previous study by examining the effects of prolonging QT interval in the healthy heart. Although guinea pigs display a similar, plateaued ventricular AP to humans, they have a much shorter diastolic interval owing to the higher heart rate in guinea pigs. This limits the extent to which APD can be pharmacologically prolonged without the heart becoming refractory, especially in an isolated heart where there is no sympathetic tone. This is because guinea pigs express a prominent I_{Ks}, and this current is augmented by sympathetic stimulation which has been reported as a possible mechanism for APD adaptation at higher heart rates.[28, 29, 109] To this end, it was decided to treat hearts with ivabradine and pace at a much slower heart rates, thereby allowing for a much longer diastolic interval and greater QT prolongation. The veratridine group was also dropped in subsequent studies owing to unexpected results from the previous study where it was found that veratridine lowered LVEDP.

In this study, hearts were isolated and instrumented as previously described (Section 2.1.2) and perfusion pressure was maintained at 70mmHg (±5mmHg) using a simplified, gravity-fed perfusion system. Using this system, coronary flows were measured by collecting and weighing the coronary effluent at the end of each relevant time point. Hearts were initially allowed to stabilise for 10 min following instrumentation, before beginning perfusion with 10μM ivabradine. After a further 20 min stabilisation, hearts were paced at 120bpm and LVEDP was set to 6-7mmHg by adjusting the volume within the IVB. Hearts were then subjected to the following pacing protocol: 120bpm (1 min), 170bpm (1 min), 220bpm (1 min), return to baseline. This protocol was then repeated following perfusion with each incremental concentration of E-4031 + HMR 1556/DMSO, allowing 15 min for stabilisation after switching to each dose (Table 3.3).

For analysis, LabChart 8 Pro with ECG and Peak Analysis modules was used. ECG parameters were measured using the ECG analysis tool to average 10 beats, with manual

correction of the detection of ECG features (Fig. 3.10 A-C, Fig. 3.14 B). To analyse LVP, 30s of data was analysed using the cyclic measurements on the data pad tool to give an average value for LVDP and LVEDP at each drug dose (Fig. 3.11 A, C, E and Fig. 3.12 A, C, E). Time from pacing spike to peak ventricular pressure was analysed manually using scope view to average multiple pressure cycles (Fig. 3.11 B, D, F). The peak analysis tool was used to analyse the average time from peak ventricular pressure to 75% relaxation for the same 30s section of data (Fig. 3.12 B, D, F). To aid visualisation of the effect of QT prolongation on LV pressure generation, data from a complete cardiac cycle was exported from LabChart and plotted against time on GraphPad Prism 8. Representative examples were selected by identifying hearts which displayed diastolic function most similar to the group average, with the data shown taken from baseline pacing rates at the highest drug dose or corresponding timepoint for vehicle control (Fig. 3.13). Coronary flow was calculated by collecting and weighing the coronary effluent for 15s at the end of each pacing protocol or stabilisation period (Fig. 3.14 A).

Table 3.3 Concentrations of E-4031 + HMR 1556 used in QT prolongation with ivabradine study

List of concentrations of E-4031 + HMR 1556 used to prolong QT interval in healthy Langendorff-perfused hearts treated with 10μM ivabradine.

	E-4031 + HMR 1556 (nM)
Baseline	0 + 0
Conc. 1	100 + 0
Conc. 2	100 + 100
Conc. 3	100 + 300

3.2.4 Effect of Prolonging QT Interval in the Presence of SERCA Inhibition

The next study aimed to build on previous studies examining the relationship between APD prolongation and cardiac function in the healthy heart, and determine whether

clinically relevant levels of QT prolongation would begin to impair diastolic function in the presence of a common co-pathology of HF. Therefore, this study used E-4031 and HMR 1556 to prolong QT interval in isolated guinea pig hearts perfused with cyclopiazonic acid (CPA) in order to inhibit SERCA activity. Under such conditions the heart may be less able to cope with increased influx of calcium as a result of prolonged APD since there is a reduced ability to return calcium to the SR, potentially causing elevated diastolic calcium levels and impaired relaxation.

In this study, hearts were isolated and instrumented as previously described (Section 2.1.2) and perfusion pressure was maintained at 70mmHg (±5mmHg) using a gravity-fed perfusion system. Hearts were initially allowed to stabilise for 15 min before being paced at 300bpm. During a 5 min stabilisation period at this pacing rate LVEDP was set to 6-7mmHg by adjusting the volume of the IVB, before switching hearts to physiological buffer containing 1μM CPA and stabilising for 10 min. LVEDP was not adjusted after switching to 1μM CPA, and coronary flow was measured at the end of this period. Hearts were then subjected to the following pacing protocol: 300bpm (1 min), 335bpm (1 min), 370bpm (1 min), return to baseline. Pacing protocol and coronary flow measurements were then repeated following the switch to perfusion with 100nM E-4031 + 30nM HMR 1556 (in addition to 1μM CPA), allowing 15 min for stabilisation.

For analysis, LabChart 8 Pro with ECG and Peak Analysis modules was used. ECG parameters were measured using the ECG analysis tool to average 10 beats and manually correcting the detection of ECG features (Fig. 3.15 A-C, Fig. 3.19 B). To analyse LVP, 30s of data was analysed using the cyclic measurements on the data pad tool to give an average value for LVDP and LVEDP at each drug dose (Fig. 3.16 A, C, E and Fig. 3.17 A, C, E). The peak analysis tool was used to analyse the average time from pacing spike to peak ventricular pressure and time from peak ventricular pressure to 75% relaxation for the same 30s section of data (Fig. 3.16 & 3.17 B, D, F). To aid visualisation of the effect of QT prolongation on LV pressure generation, data from a complete cardiac cycle was exported from LabChart and plotted against time on GraphPad Prism 8. Representative examples were selected by identifying hearts which displayed diastolic function most similar to the group average, with the data shown taken from baseline

pacing rates at the highest drug dose or corresponding timepoint for vehicle control (Fig. 3.18). Coronary flow was calculated by collecting and weighing the coronary effluent for 15s at the end of each pacing protocol or stabilisation period (Fig. 3.19 A).

3.3 Results

3.3.1 Relationship between APD and CaTD in the Isolated Guinea Pig Heart

As cycle length increases and repolarising currents I_{Kr} and I_{Ks} are blocked, there is a corresponding increase in APD within the left ventricle (Fig. 3.3 A and 3.4 A). The same is true of CaTD (Fig.3.3 B and 3.4 B). When APD is plotted against CaTD the data reveal a clear relationship between these two parameters, with interventions which cause an increase in APD resulting in a corresponding increase in CaTD (Fig. 3.3 C and 3.4 C). This is illustrated in Fig 3.4 D, which depicts overlaid APs and calcium transients from a heart paced at 2Hz under baseline conditions and following exposure to 100nM E-4031 and 1000nM HMR 1556.

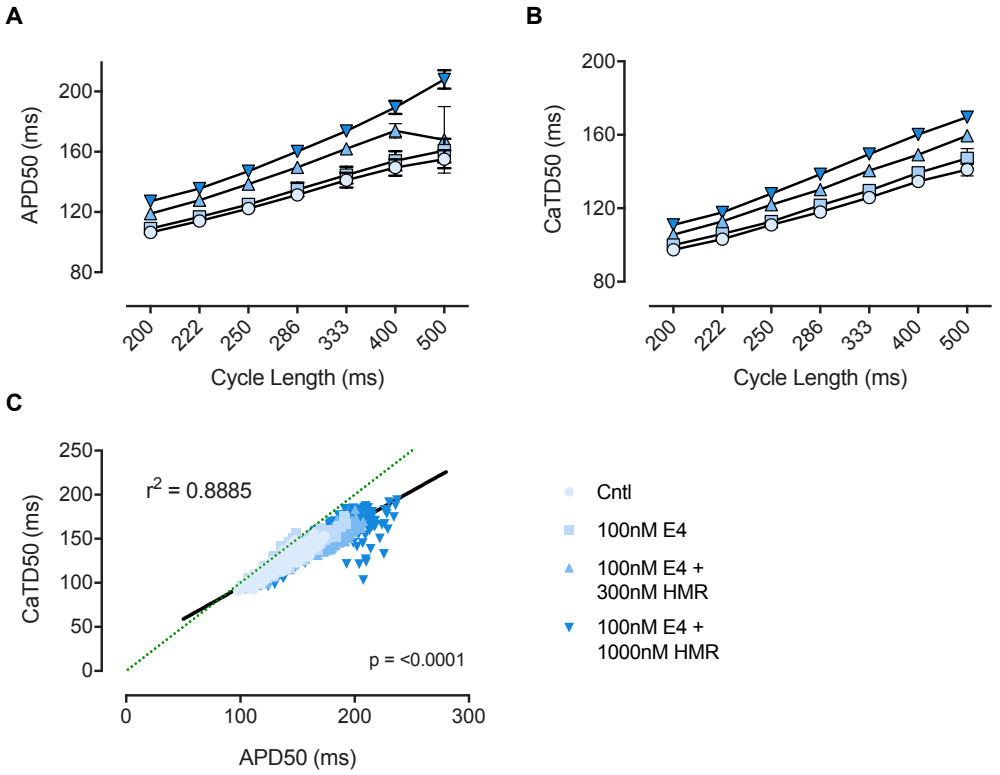

Figure 3.3 Relationship between APD50 and CaTD50 in the left ventricle

A) Average APD50 vs. cycle length at each concentration of E-4031 and HMR 1556. B) Average CaTD50 vs. cycle length at each concentration of E-4031 and HMR1556. C) Individual APD50 values vs. corresponding CaTD50 values across the range of cycle lengths and concentrations of E-4031 and HMR 1556 for each heart. Linear regression slope shown in black with corresponding r^2 and p value, dotted green line shows the line of identity. n=4 hearts, average data plotted as mean ±SEM.

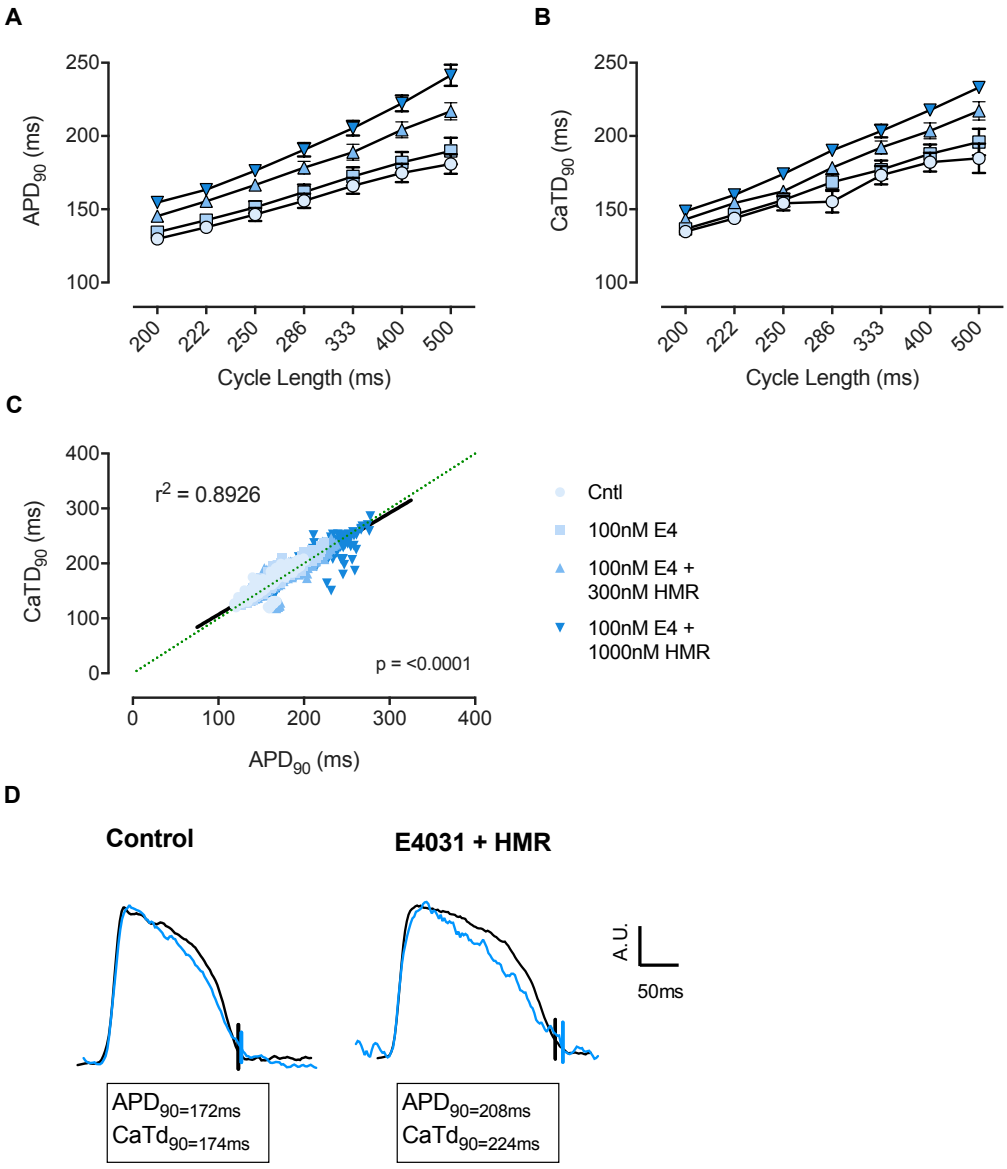

Figure 3.4 Relationship between APD90 and CaTD90 in the left ventricle

A) Average APD90 vs. cycle length at each concentration of E-4031 and HMR 1556. B) Average CaTD90 vs. cycle length at each concentration of E-4031 and HMR1556. C) Individual APD90 values vs. corresponding CaTD90 values across the range of cycle lengths and concentrations of E-4031 and HMR 1556 for each heart. Linear regression slope shown in black with corresponding r^2 and p value, dotted green line shows the line of identity. n=4 hearts, average data plotted as mean ±SEM. D) Representative AP and corresponding calcium transient from a heart paced at 2Hz under control conditions and after perfusion with 100nM E-4031 + 1000nM HMR 1556. AP shown in black, calcium transient shown in blue, with vertical line indicating 90% repolarisation/return to baseline. N.B. Traces are overlaid for ease of comparison, analysis did not allow for resolution of the timing of calcium transient upstroke vs AP upstroke.

3.3.2 Effect of Prolonging QT Interval in the Healthy Heart

A significant and comparable QT prolongation was achieved in both the veratridine and E-4031 + HMR 1556-treated groups at all pacing rates (Fig. 3.5 A-C). This equated to a 14.5% QT prolongation in the E-4031 + HMR 1556-treated group and a 13.3% QT prolongation in the veratridine-treated group at conc. 4, relative to control at baseline pacing rates. A slight but significant increase in the baseline heart rate of the veratridine-treated group relative to control was observed, but this did not result in any differences in QT interval between groups at baseline (Fig. 3.5 D).

Treatment with incremental doses of E-4031 + HMR 1556 had no effect on LVDP relative to control at any pacing rate (Fig. 3.6 A, C, E). Veratridine, however, appeared to have a positive inotropic effect, with this group demonstrating a higher developed pressure at the maximum concentration used. This effect was apparent at baseline and +35bpm pacing rates but appeared to be diminished at +70bpm. These results are reflected in the time taken from the pacing spike to maximum LVP, with E-4031 + HMR 1556 having no effect at any dose or pacing rate (Fig. 3.6 B, D, F). Treatment with veratridine, on the other hand, resulted in a reduction in this parameter at conc. 3 & 4 at all three pacing rates, indicative of an increased rate of contraction in the LV.

The systolic effects of E-4031 + HMR 1556 and veratridine are mirrored when looking at the diastolic function. Treatment with E-4031 + HMR 1556 had no effect on LVEDP at any dose or pacing rate, relative to control (Fig. 3.7 A, C, E). Treatment with veratridine, however, results in a clear reduction in LVEDP relative to control at all but the lowest dose. This effect is apparent at all three pacing rates. Neither treatment with E- 4031 + HMR 1556 nor veratridine has any effect on the time from LVP peak to 75% relaxation (Fig. 3.7 B, D, F).

These effects can be visualised by comparing LV pressure traces from hearts in each of the three treatment groups, with veratridine treatment resulting in a faster rate of pressure generation in the LV and earlier peak contraction, increasing the available time for subsequent relaxation to occur and enabling a lower LVEDP to be reached (Fig. 3.8).

Coronary flow rate and QRS duration were also measured to check for any off-target effects of veratridine and E-4031 + HMR 1556 on vascular tone or cardiac conduction. Neither drug had any effect on either of these parameters across the range of concentrations tested (Fig. 3.9 A & B).

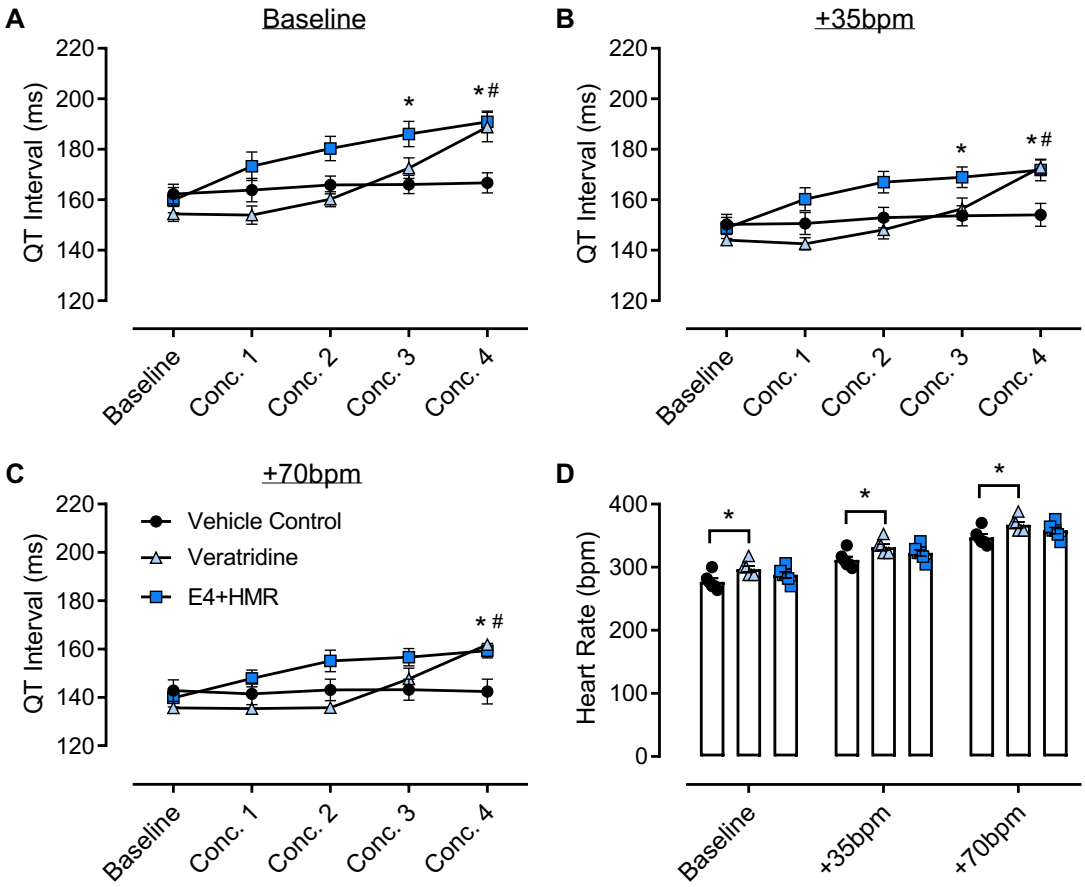

Figure 3.5 QT prolongation in the healthy heart

Effect of treatment with incremental doses of veratridine or E-4031 + HMR 1556 vs vehicle control on QT interval in the healthy Langendorff-perfused guinea pig heart at three different pacing rates. Change to QT interval with increasing drug dose at A) baseline pacing rate, B) +35bpm, C) +70bpm. D) Heart rates of different treatment groups at baseline and increased pacing rates. Doses of veratridine/E-4031 + HMR 1556 (nM) as follows: Conc. 1=10/30+0, Conc. 2=30/100+0, Conc. 3=100/100+10, Conc. 4=300/100+30, respectively. Data presented as mean ±SEM, n=6 hearts, # = $p<0.05$ in veratridine vs. vehicle control group, * = $p<0.05$ in E-4031 + HMR 1556 vs. vehicle control group.

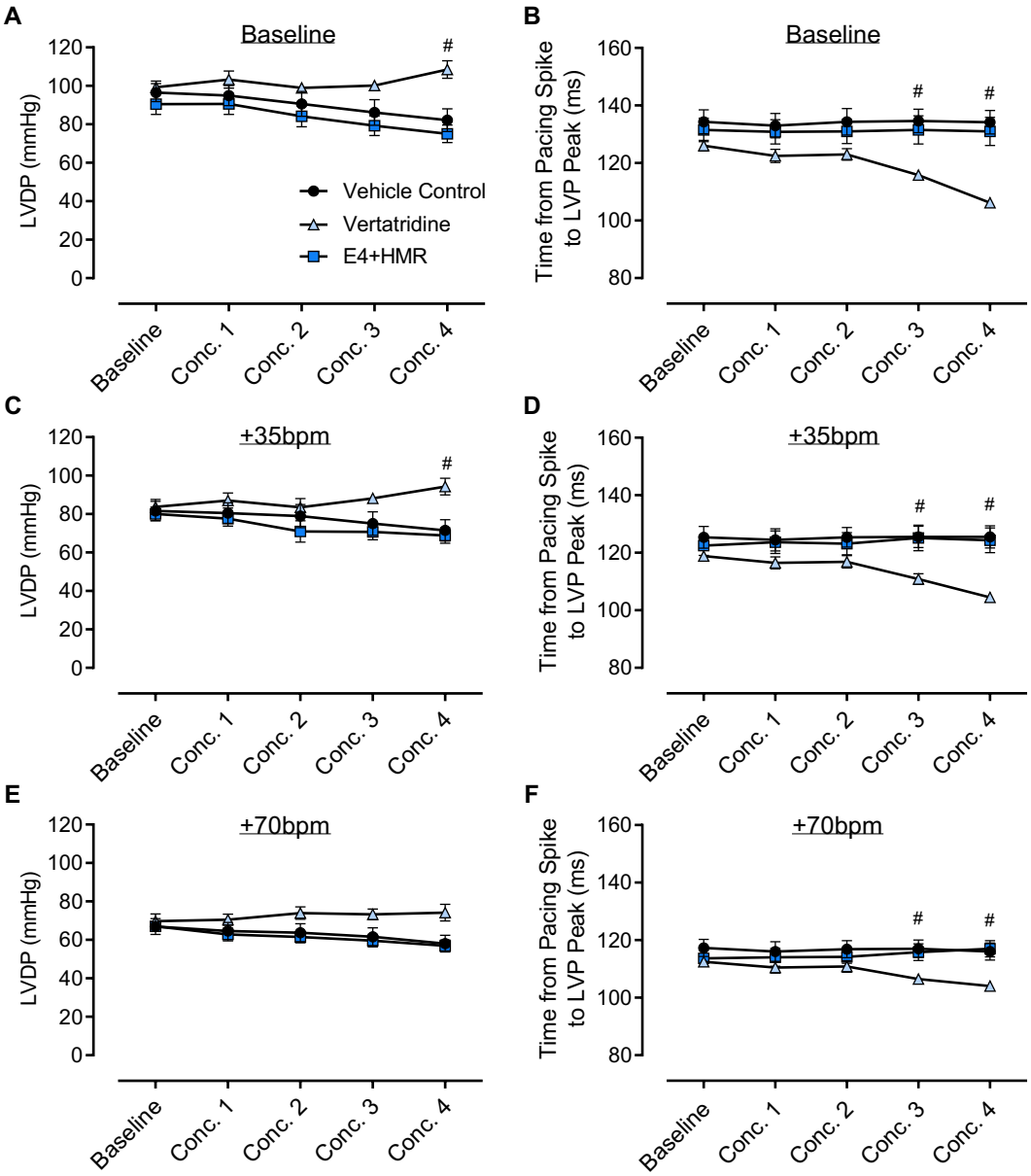

Figure 3.6 Effect of QT prolongation on systolic function in the healthy heart

Effect of QT prolongation using incremental doses of veratridine or E-4031 + HMR 1556 vs vehicle control on systolic function in the healthy Langendorff-perfused guinea pig heart at three different pacing rates. Change in LVDP with increasing drug dose at A) baseline pacing rate, C) +35bpm, E) +70bpm. Change in time from pacing spike to peak LVP with increasing drug dose at B) baseline pacing rate, D) +35bpm, F) +70bpm. Doses of veratridine/E-4031 + HMR 1556 (nM) as follows: Conc. 1=10/30+0, Conc. 2=30/100+0, Conc. 3=100/100+10, Conc. 4=300/100+30, respectively. Data presented as mean ±SEM, n=6 hearts, # = $p<0.05$ in veratridine vs. vehicle control group.

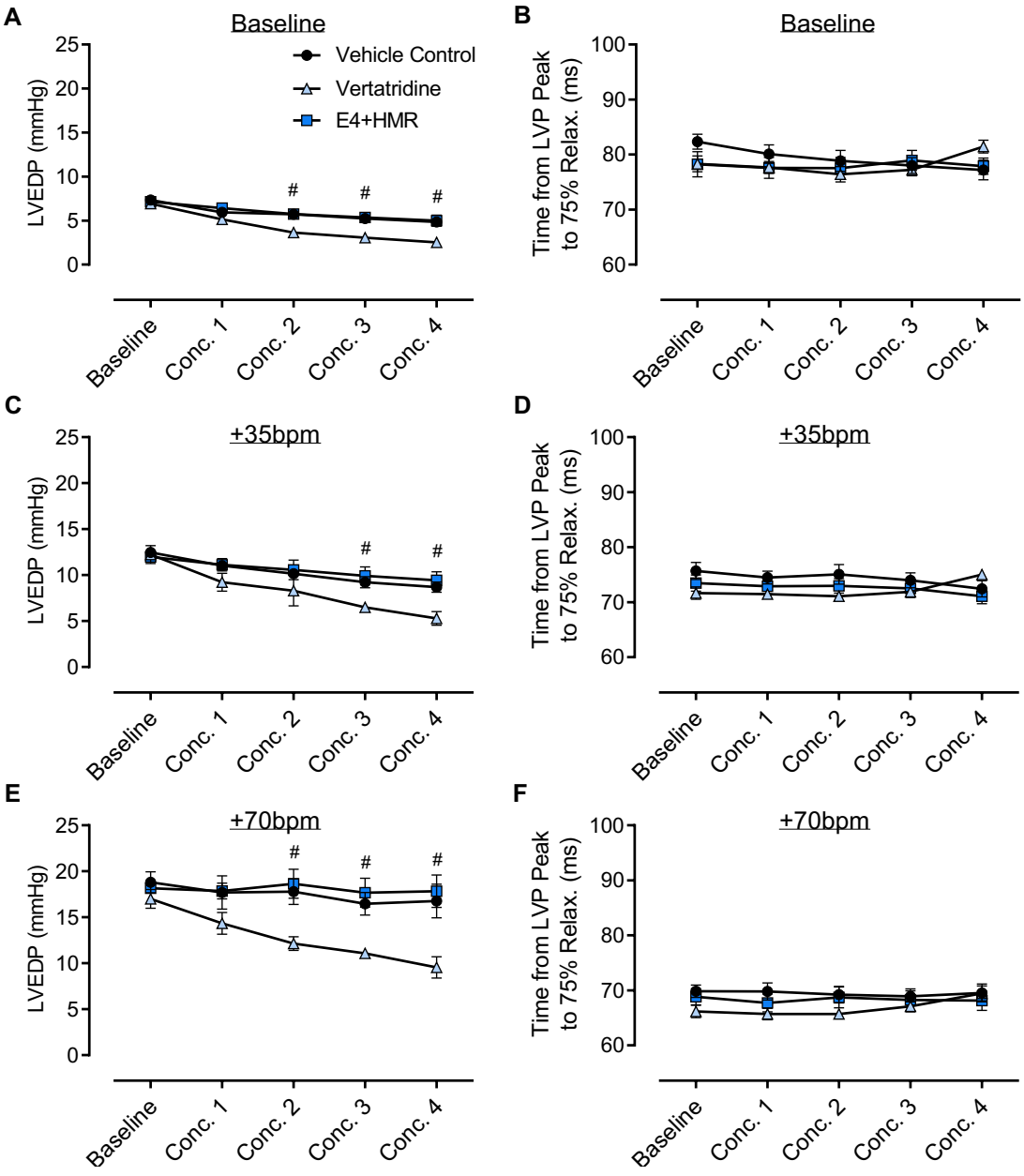

Figure 3.7 Effect of QT prolongation on diastolic function in the healthy heart

Effect of QT prolongation using incremental doses of veratridine or E-4031 + HMR 1556 vs vehicle control on diastolic function in the healthy Langendorff-perfused guinea pig heart at three different pacing rates. Change in LVEDP with increasing drug dose at A) baseline pacing rate, C) +35bpm, E) +70bpm. Change in time from LVP peak to 75% relaxation with increasing drug dose at B) baseline pacing rate, D) +35bpm, F) +70bpm. Doses of veratridine/E-4031 + HMR 1556 (nM) as follows: Conc. 1=10/30+0, Conc. 2=30/100+0, Conc. 3=100/100+10, Conc. 4=300/100+30, respectively. Data presented as mean ±SEM, n=6 hearts, # = $p<0.05$ in veratridine vs. vehicle control group.

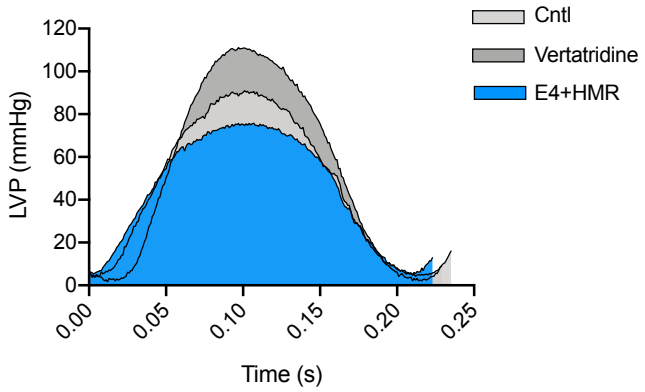

Figure 3.8 Effect of QT prolongation on pressure generation in the left ventricle

Representative left ventricular pressure throughout a complete cardiac cycle from hearts treated with 100nM E-4031 + 300nM HMR 1556, 300nM veratridine or vehicle control at baseline pacing rate. Traces aligned to peak LVP to aid visualisation.

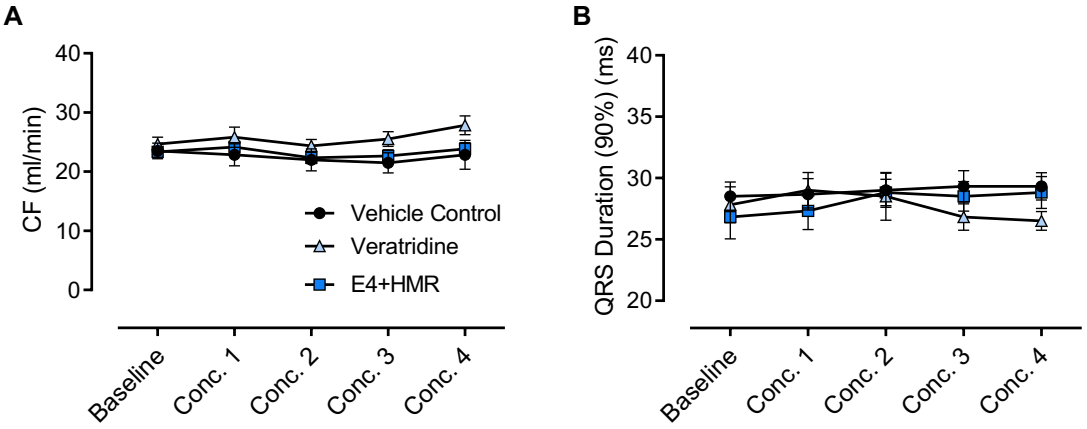

Figure 3.9 Effect of QT prolongation on coronary flow and QRS duration in the healthy heart

Effect of QT prolongation using incremental doses of veratridine or E-4031 + HMR 1556 vs vehicle control on coronary flow (CF) and QRS duration (to 90% repolarisation) in the healthy Langendorff-perfused guinea pig heart. A) Change in CF with increasing drug dose at baseline pacing rate. B) Change in QRS duration with increasing drug dose at baseline pacing rate. Doses of veratridine/E-4031 + HMR 1556 (nM) as follows: Conc. 1=10/30+0, Conc. 2=30/100+0, Conc. 3=100/100+10, Conc. 4=300/100+30, respectively. Data presented as mean ±SEM, n=6 hearts.

3.3.3 Effect of Prolonging QT Interval in the Presence of Ivabradine

A significant QT prolongation was achieved using incremental concentrations of E-4031 + HMR 1556 in ivabradine-treated hearts at all three pacing rates (Fig. 3.10 A-C). At the highest concentration (100nM E-4031 + 300nM HMR 1556), this equated to a 34% QT prolongation at 120bpm relative to the vehicle control group.

Treatment with E-4031 and HMR1556 had no effect on systolic function in hearts treated with 10μM ivabradine. This was true of at all drug concentrations and at each pacing rate, when using LVDP (Fig. 3.11 A, C, E) and time from pacing spike to peak LVP (Fig. 3.11 B, D, F) as markers of systolic function.

Interestingly, however, prolongation of QT interval using E-4031 and HMR 1556 did appear to affect diastolic function in ivabradine-treated hearts. When looking at LVEDP (Fig. 3.12 A, C, E), there was no apparent difference between E-4031 + HMR 1556 and vehicle control groups at any pacing rate or drug dose. However, when looking at time from LVP peak to 75% relaxation as a marker of diastolic function (Fig. 3.12 B, D, F), there was a significant increase in the relaxation time in the E-4031 + HMR 1556 group at the highest dose at all three pacing rates. This is suggestive of a decreased rate of relaxation in these hearts in response to this greater degree of QT prolongation.

This effect on relaxation time can be visualised by comparing LV pressure traces from control and E-4031 + HMR 1556-treated hearts, with QT prolongation demonstrating no effect on the time taken to reach peak LV pressure but resulting in slower decline of pressure within the LV (Fig. 3.13).

No difference in coronary flow was observed between the E-4031 + HMR 1556-treated and vehicle control groups at any point throughout the protocol (Fig. 3.14 A). There is an apparent reduction in flow once hearts have been treated with ivabradine, however, this is likely to reflect the reduced heart rate and therefore diminished cardiac metabolic demand.[115] The same is true of QRS duration (Fig. 3.14 B), with no differences being observed between the experimental groups during the protocol. This suggests that E-4031 and HMR 1556 did not have any off-target effects on cardiac conduction or vascular tone in the presence of ivabradine.

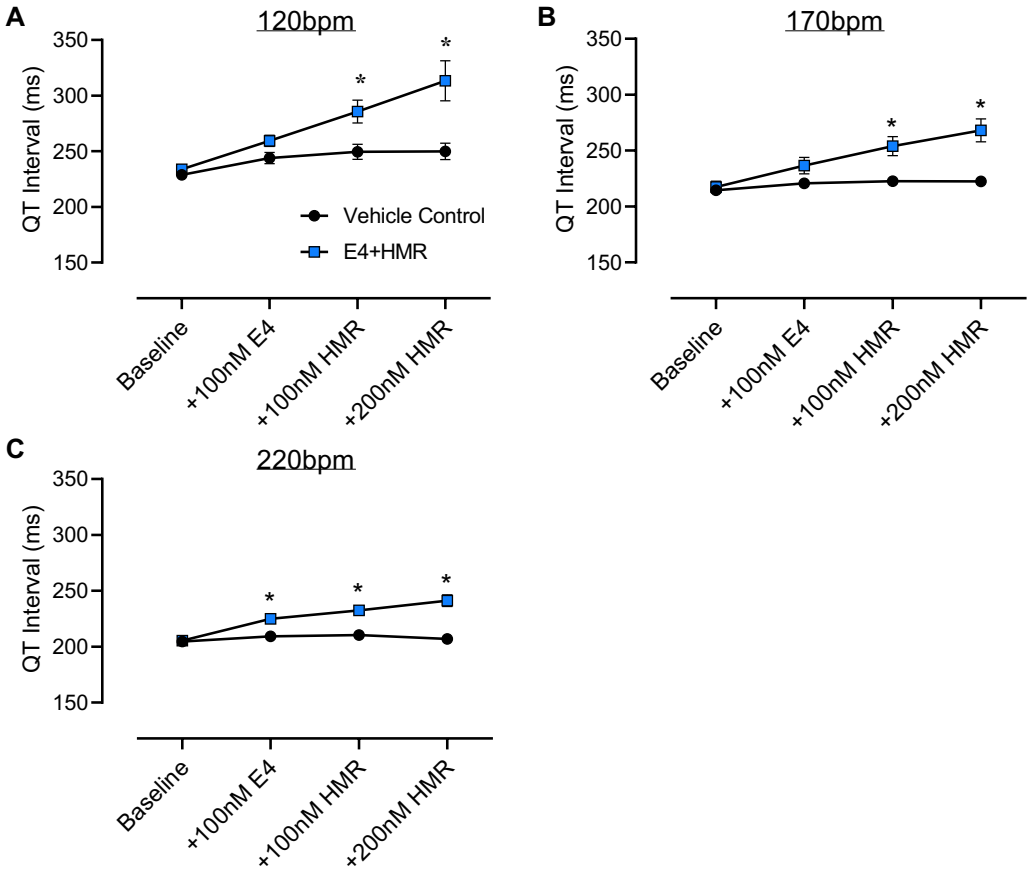

Figure 3.10 QT prolongation in the presence of ivabradine

Effect of treatment with incremental doses of E-4031 + HMR 1556 vs vehicle control on QT interval in the healthy Langendorff-perfused guinea pig heart treated with 10μM ivabradine at three different pacing rates. Change to QT interval with increasing drug dose at A) 120bpm, B) 170bpm, C) 220bpm. Data presented as mean ±SEM, n=8 hearts, * = $p<0.05$ in E-4031 + HMR 1556 vs. vehicle control group.

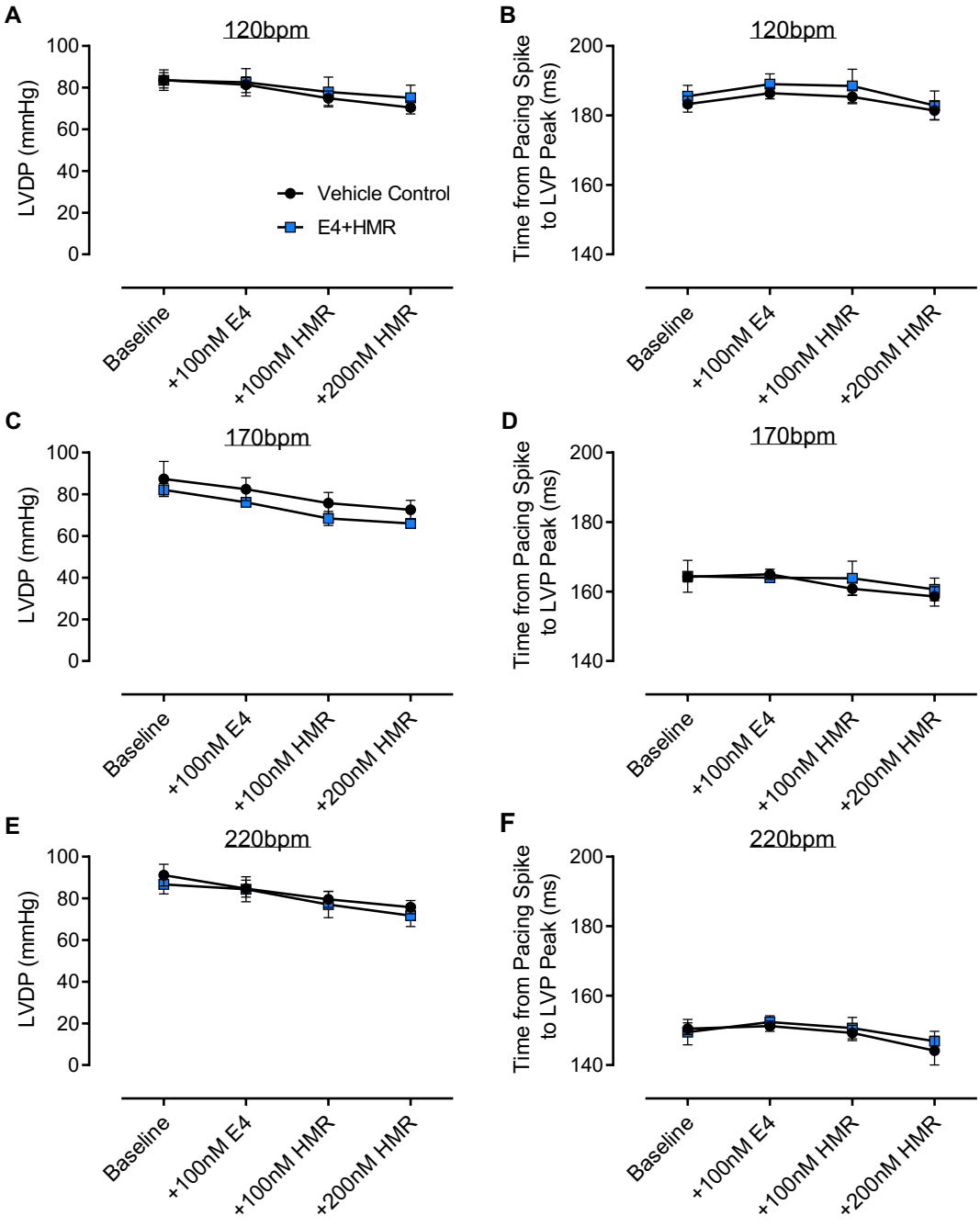

Figure 3.11 Effect of QT prolongation on systolic parameters in the presence of ivabradine

Effect of QT prolongation using incremental doses of E-4031 + HMR 1556 vs vehicle control on systolic function in the healthy Langendorff-perfused guinea pig heart treated with 10μM ivabradine at three different pacing rates. Change in LVDP with increasing drug dose at A) 120bpm, C) 170bpm, E) 220bpm. Change in time from pacing spike to peak LVP with increasing drug dose at B) 120bpm, D) 170bpm, F) 220bpm. Data presented as mean ±SEM, n=8 hearts.

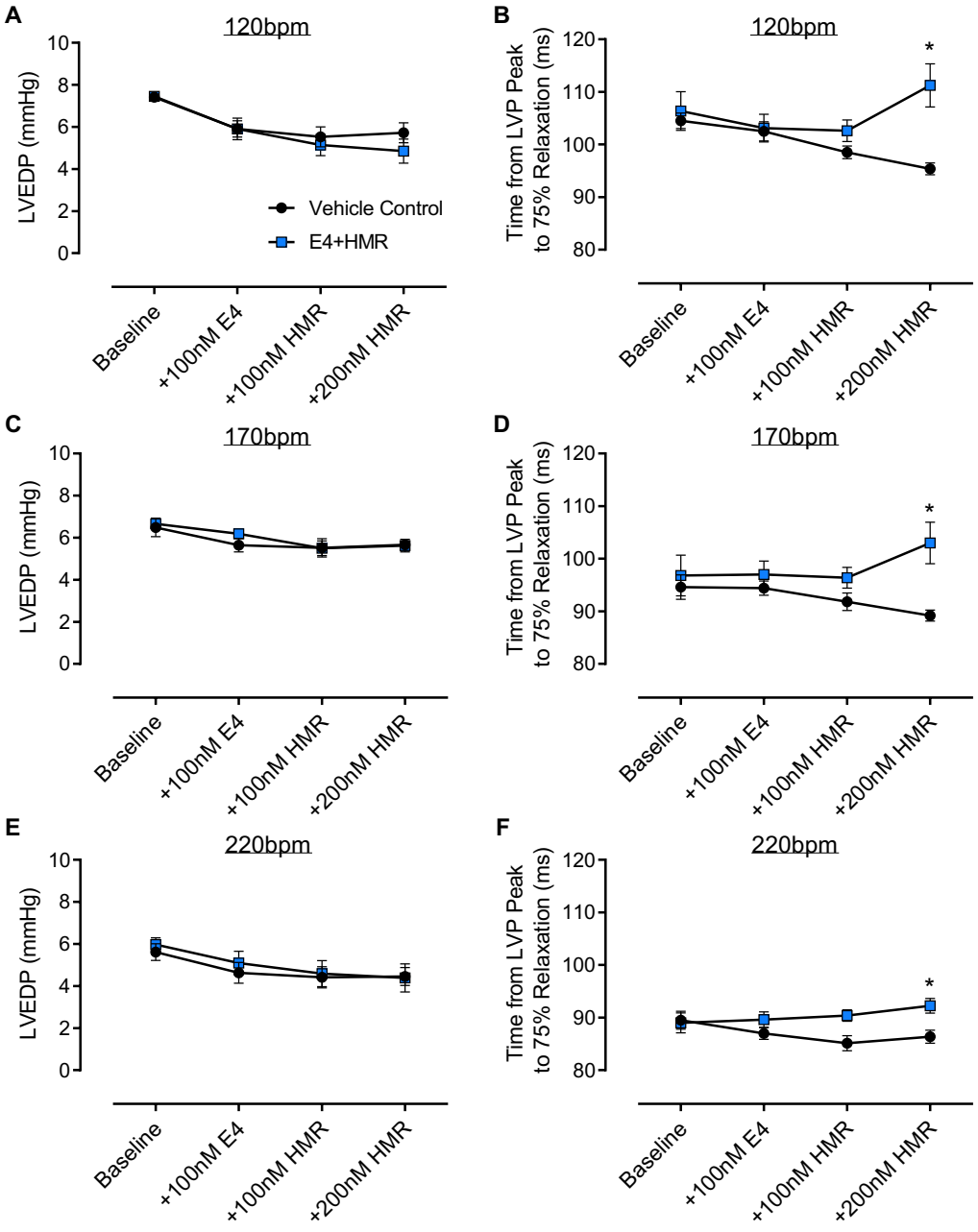

Figure 3.12 Effect of QT prolongation on diastolic parameters in the presence of ivabradine

Effect of QT prolongation using incremental doses of E-4031 + HMR 1556 vs vehicle control on diastolic function in the healthy Langendorff-perfused guinea pig heart treated with 10μM ivabradine at three different pacing rates. Change in LVEDP with increasing drug dose at A) 120bpm, C) 170bpm, E) 220bpm. Change in time from LVP peak to 75% relaxation with increasing drug dose at B) 120bpm, D) 170bpm, F) 220bpm. Data presented as mean ±SEM, n=8 hearts, * = $p<0.05$ in E-4031 + HMR 1556 vs. vehicle control group.

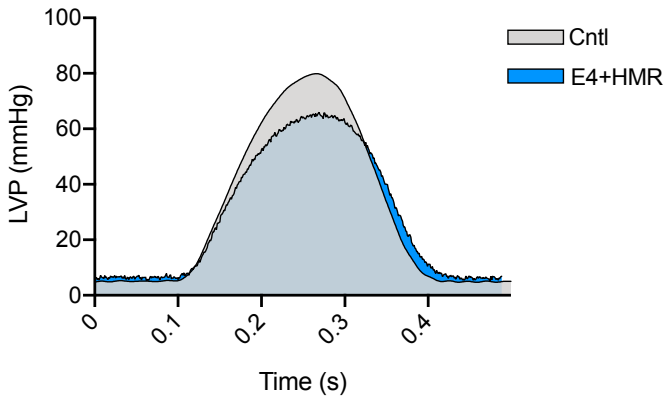

Figure 3.13 Effect of QT prolongation on pressure generation in the left ventricle in the presence of ivabradine

Representative left ventricular pressure throughout a complete cardiac cycle from hearts treated with 10μM ivabradine and 100nM E-4031 + 300nM HMR 1556 or vehicle control at baseline pacing rate (120bpm). Traces aligned to peak LVP to aid visualisation.

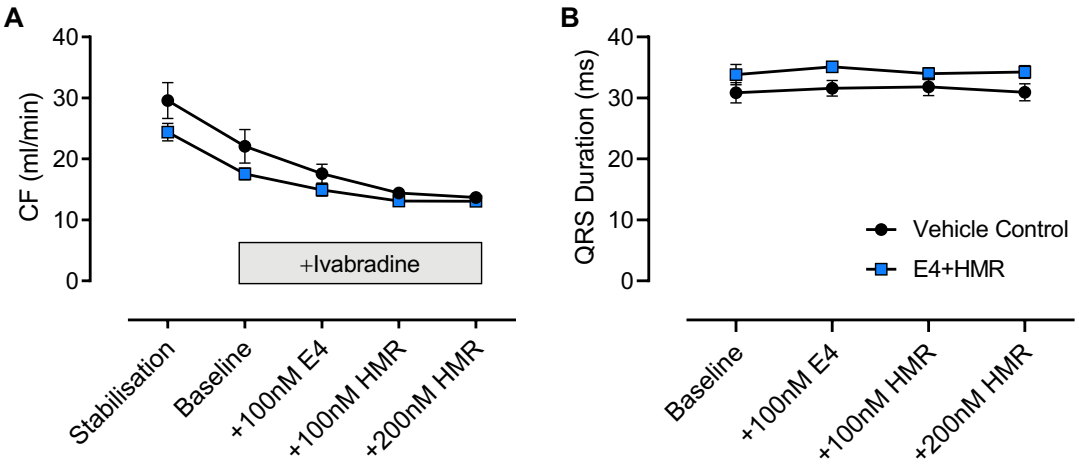

Figure 3.14 Effect of QT prolongation on coronary flow and QRS duration in the presence of ivabradine

Effect of QT prolongation using incremental doses of E-4031 + HMR 1556 vs vehicle control on coronary flow (CF) and QRS duration in the healthy Langendorff-perfused guinea pig heart treated with 10μM ivabradine. A) Change in CF with increasing drug dose at baseline pacing rate (120bpm). B) Change in QRS duration with increasing drug dose at baseline pacing rate (120bpm). Data presented as mean ±SEM, n=8 hearts.

3.3.4 Effect of QT Prolongation in the Presence of SERCA Inhibition

A modest but significant prolongation of QT interval was achieved using 100nM E-4031 + 30nM HMR 1556 in hearts treated with 1μM CPA at all tree pacing rates (Fig. 3.15 A-C). This amounted to a 7.2% QT prolongation in the E4+HMR group, relative to the vehicle control group at baseline pacing rate (300bpm).

Treatment with E-4031 and HMR1556 had no effect on systolic variables in hearts treated with 1μM CPA. This was true when looking at LVDP (Fig. 3.16 A, C, E) and time from pacing spike to peak LVP (Fig. 3.16 B, D, F) as markers of systolic function, and remained the case at all tree pacing rates. Importantly, both experimental groups demonstrate a similar impairment of systolic function in response the CPA treatment, as shown by a reduced LVDP and an increased time to LVP peak at all three pacing rates.

Interestingly, modest prolongation of QT interval in the presence of SERCA inhibition did appear to impair diastolic function, with LVEDP showing a significant increase in the E-4031 + HMR 1556-treated group, relative to vehicle control (Fig. 3.17 A, C, E). This increase in LVEDP is apparent at all three pacing rates but does not reach significance at the highest pacing rate (370bpm). However, when we look at time from LVP peak to 75% relaxation, there is no significant effect of prolonging QT (Fig. 3.17 B, D, F), although there does appear to be a modest trend for the relaxation time to be longer in the E-4031 + HMR 1556-treated hearts at all pacing rates. Of note, again, there is a clear effect of treating hearts with 1μM CPA, with an impairment of diastolic function evidenced in both groups by an increased LVEDP and time to 75% relaxation.

This effect on LVEDP can be visualised by comparing LV pressure traces from control and E-4031 + HMR 1556-treated hearts treated with CPA. QT prolongation demonstrated no appreciable effect on peak LVP but did cause subtle slowing of the rate of both pressure generation and decline in the LV, resulting in an elevated LVEDP in the E4 + HMR group at baseline pacing rate (300bpm) (Fig. 3.18).

No difference in coronary flow was observed between the E-4031 + HMR 1556-treated and vehicle control groups at any point throughout the protocol (Fig. 3.19 A), the same being true of QRS duration (Fig. 3.19 B). This suggests that E-4031 and HMR 1556 did

not have any off-target effects on cardiac conduction or vascular tone in the presence of CPA.

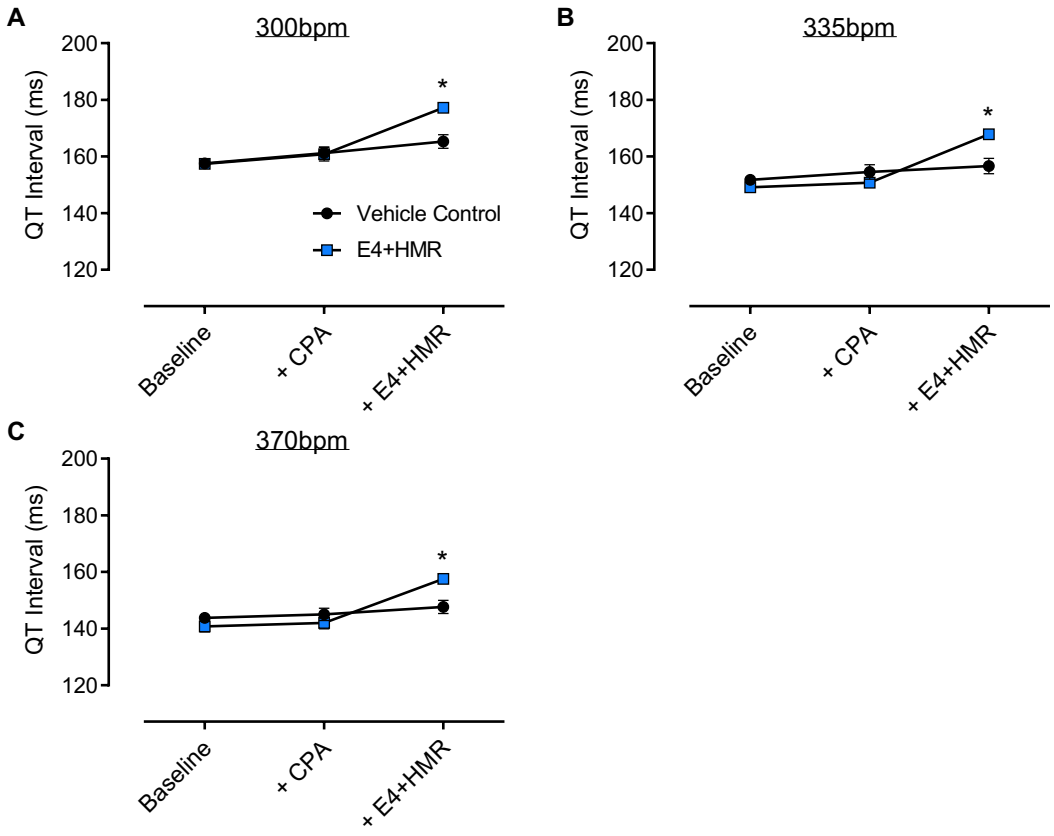

Figure 3.15 Effect of QT prolongation in the presence of SERCA inhibition

Effect of treatment with 100nM E-4031 + 30nM HMR 1556 vs vehicle control on QT interval in the Langendorff-perfused guinea pig heart treated with 1μM cyclopiazonic acid (CPA) at three different pacing rates. Change to QT interval with drug treatment at A) 300bpm, B) 335bpm, C) 370bpm. Data presented as mean ±SEM, n=9 hearts, * = $p<0.05$ in E-4031 + HMR 1556 vs. vehicle control group.

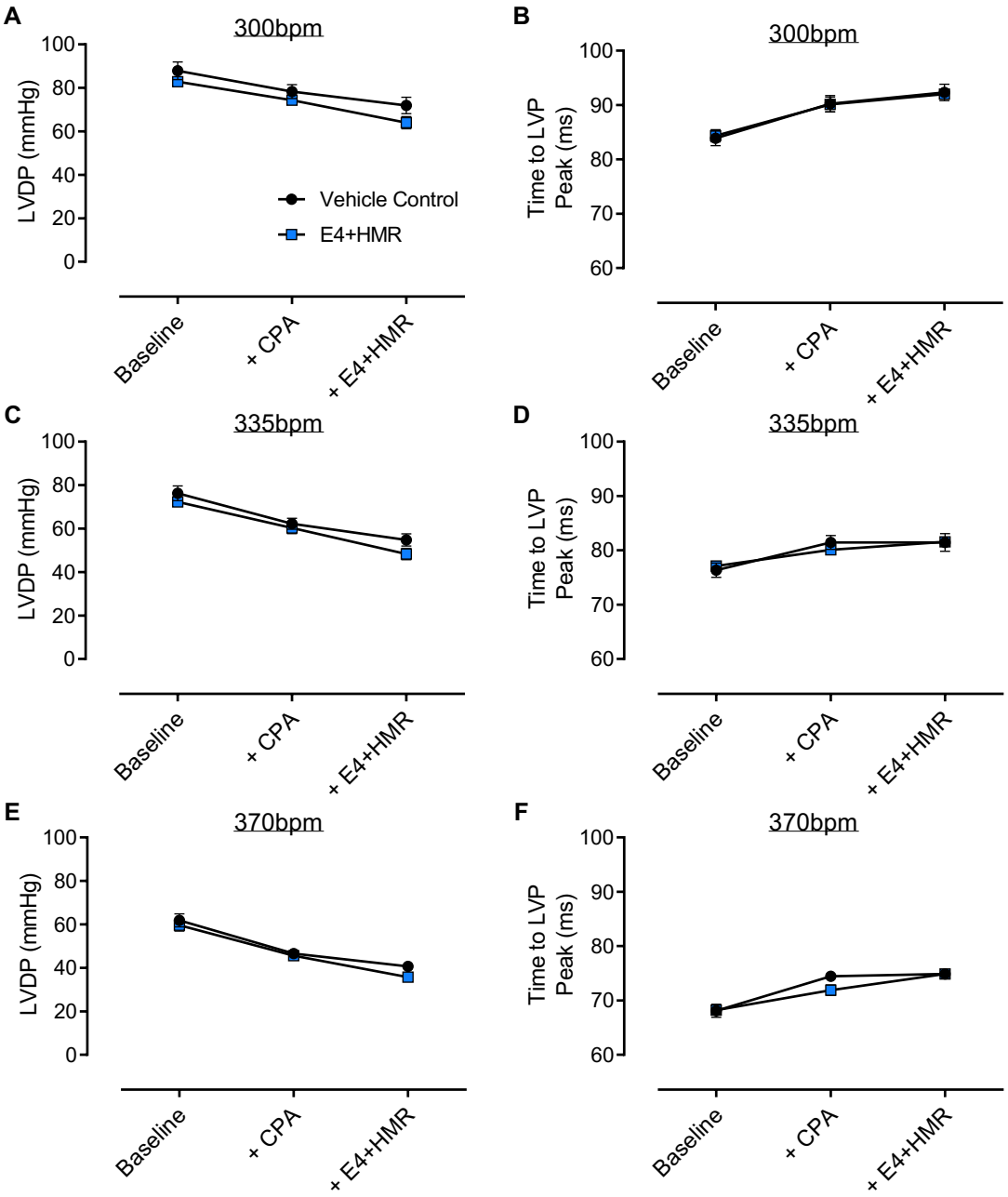

Figure 3.16 Effect of QT prolongation on systolic function in the presence of SERCA inhibition

Effect of QT prolongation using 100nM E-4031 + 30nM HMR 1556 vs vehicle control on systolic function in the Langendorff-perfused guinea pig heart treated with 1μM cyclopiazonic acid (CPA) at three different pacing rates. Change in LVDP with drug treatment at A) 300bpm, C) 335bpm, E) 370bpm. Change in time from pacing spike to peak LVP with increasing drug treatment at B) 300bpm, D) 335bpm, F) 370bpm. Data presented as mean ±SEM, n=9 hearts.

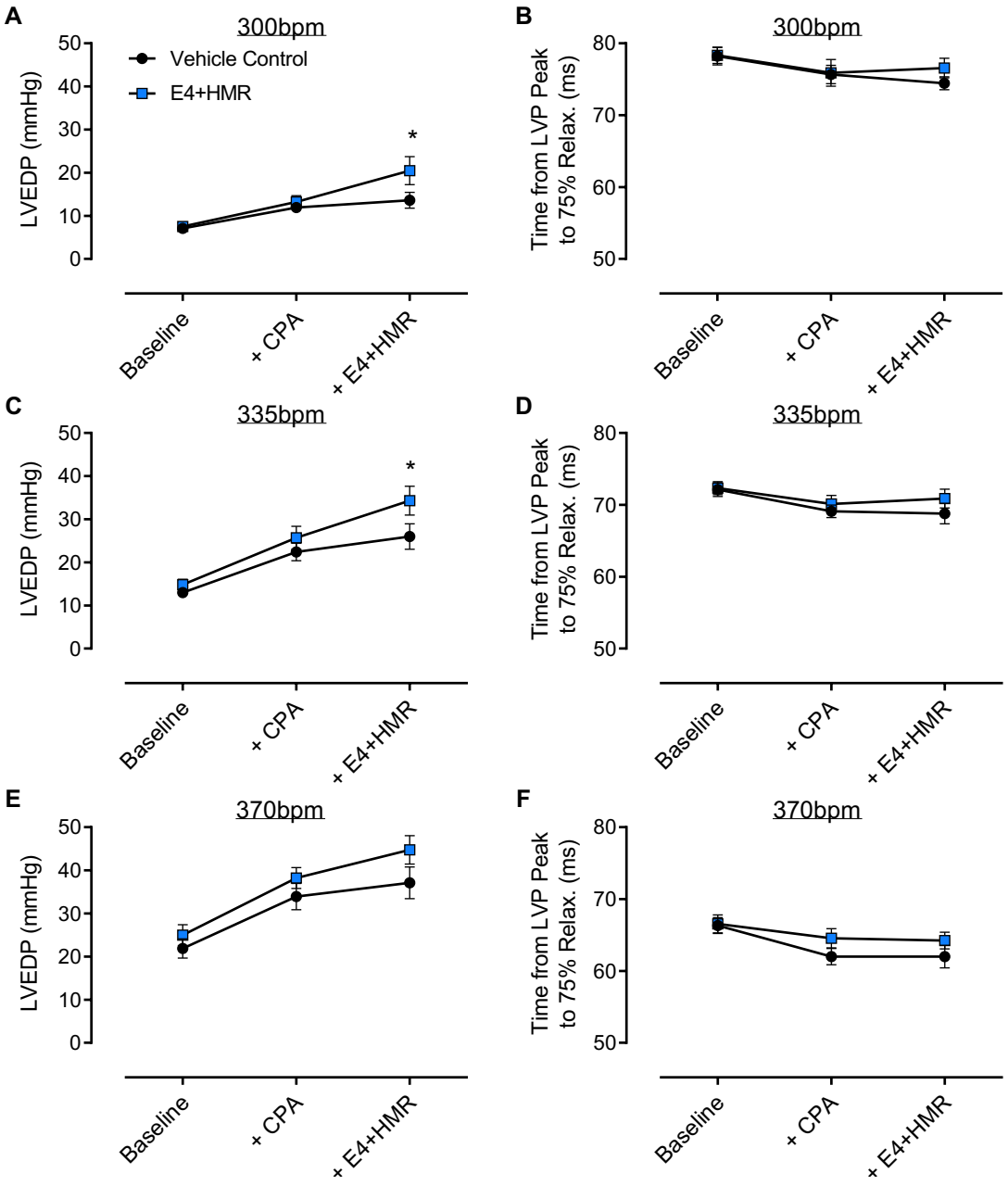

Figure 3.17 Effect of QT prolongation on diastolic function in the presence of SERCA inhibition

Effect of QT prolongation using 100nM E-4031 + 30nM HMR 1556 vs vehicle control on diastolic function in the Langendorff-perfused guinea pig heart treated with 1μM cyclopiazonic acid (CPA) at three different pacing rates. Change in LVEDP with drug treatment at A) 300bpm, C) 335bpm, E) 370bpm. Change in time from LVP peak to 75% relaxation with drug treatment at B) 300bpm, D) 335bpm, F) 370bpm. Data presented as mean ±SEM, n=9 hearts, * = $p<0.05$ in E-4031 + HMR 1556 vs. vehicle control group.

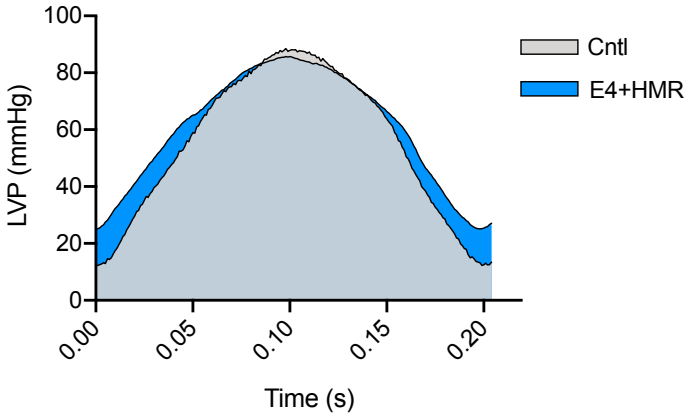

Figure 3.18 Effect of QT prolongation on pressure generation in the left ventricle in the presence of SERCA inhibition

Representative left ventricular pressure throughout a complete cardiac cycle from hearts treated with 1μM cyclopiazonic acid (CPA) and 100nM E-4031 + 30nM HMR 1556 or vehicle control at baseline pacing rate (300bpm). Traces aligned to peak LVP to aid visualisation.

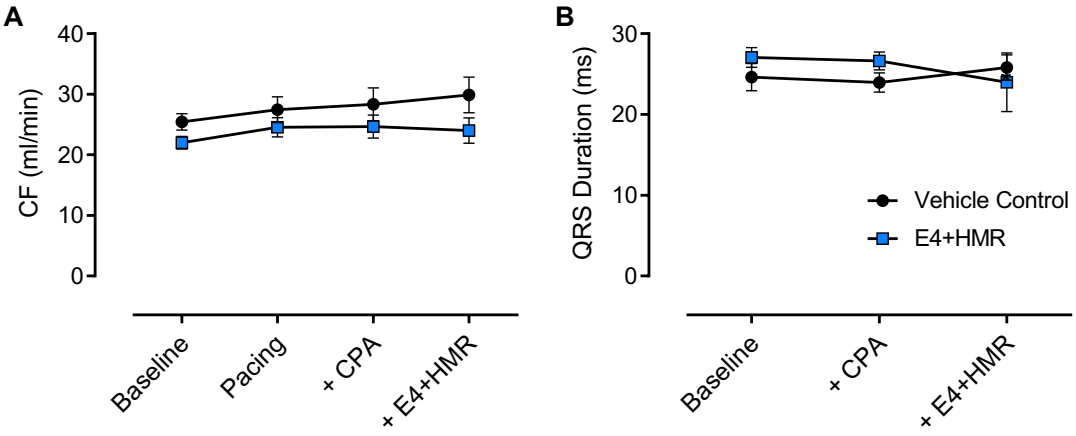

Figure 3.19 Effect of QT prolongation on coronary flow and QRS duration in the presence of SERCA inhibition

Effect of QT prolongation using 100nM E-4031 + 30nM HMR 1556 vs vehicle control on coronary flow (CF) and QRS duration in the Langendorff-perfused guinea pig heart treated with 1μM cyclopiazonic acid (CPA). A) Change in CF with drug treatment at baseline pacing rate (300bpm). B) Change in QRS duration with drug treatment at baseline pacing rate (300bpm). Data presented as mean ±SEM, n=9 hearts.

3.4 Discussion

There is good evidence from clinical studies that amongst HF patients, repolarisation abnormalities identified using electrocardiograms are predictive of presentation with diastolic dysfunction, as determined by echocardiography.[12, 86, 87] What these studies cannot determine, however, is whether such repolarisation abnormalities represent a causal mechanism by which impaired myocardial relaxation occurs in HF. Studies using isolated cells or tissue preparations from patients with HF have illustrated an association between APD prolongation and altered intracellular calcium handling,[46] as well as between APD prolongation, abnormal intracellular calcium handling and impaired relaxation.[45] Manipulation of APD in healthy cells results in a larger influx of calcium into the cell, with a slower decay of the calcium transient and a reduced rate of relaxation.[43] In the whole heart, if calcium clearance could not be matched to this larger influx of calcium due to prolonged APD, this could result in elevated diastolic calcium levels and cause impaired relaxation. This scenario may be particularly likely in the setting of HF, where studies report a reduction in SERCA activity and/or expression which would hinder cytosolic calcium clearance within cells.[58, 59, 110-112] However, the extent to which isolated cell/tissue work extends into a whole-heart setting remains unclear. Therefore, the present studies aimed firstly to demonstrate the relationship between APD and CaTD in the guinea pig Langendorff heart model, and secondly to explore the effects of prolonging APD on cardiac function.

3.4.1 Relationship Between APD and CaTD in the Left Ventricle

The optical mapping data clearly demonstrate a positive linear relationship between APD and CaTD in the left ventricle of the isolated Langendorff-perfused guinea pig heart. This means that when the AP is prolonged, there is a concomitant increase in the duration of the calcium transient. This study provides proof-of-principle for the proposed mechanism by which repolarisation abnormalities may act to impair diastolic function by perturbing normal intracellular calcium handling, resulting in delayed relaxation and possible elevation of diastolic calcium concentration.

Data from this study reveals that calcium transients and APs demonstrate an almost one-to-one ratio in terms of duration in the isolated guinea pig heart preparation (Fig. 3.3 and 3.4). It has previously been reported that the intracellular calcium transient triggered by cardiac APs is significantly longer that the AP itself.[39] However, many studies have been conducted in isolated cell preparations rather than whole hearts and may not have recorded simultaneous APs and calcium transients at physiological temperatures and heart rates, both of which could affect the results. Indeed, data from the present study is in close agreement with similar studies using human ventricular wedge preparations, with one such study using a near-identical experimental setup, recording APD and CaTD simultaneously using optical mapping with RH237 and Rhod-2 fluorescent dyes.[74] Data from this study used the parameter CaTD80-APD80 to report transmural differences in the duration of the calcium transients and APs, and demonstrated that CaTD80 was modestly greater than APD80, with the most closely-related APD and CaTD found in the sub-epicardial layer (where the difference between the durations of the calcium and electrical transients (CaTD80-APD80) was approximately 50 ms, with a baseline APD of approximately 400 ms). That is, the calcium transient was about 10% longer than the prevailing AP at all cycle lengths. Bearing in mind that optical mapping of the whole heart provides data from the epicardial surface of the heart, the data from these human heart preparations is essentially similar to the measurements in the present guinea pig optical mapping study. A second study also made use of optical mapping to simultaneously record APD and CaTD in isolated Langendorff-perfused rabbit hearts and reported very similar durations of APs and calcium transients at a given cycle length, with CaTD being slightly shorter than APD in this instance.[116] Data from isolated guinea pig ventricular myocytes has previously demonstrated that the calcium transient is completed within approximately the same time frame as the AP.[117] Studies in isolated rabbit cardiomyocytes which simultaneously measured calcium transients and APs reported a modestly greater CaTD80 relative to APD90 at physiological stimulation frequencies (around 12% at 2 Hz), however, this increased to give much greater relative duration of calcium transients at non-physiological stimulation frequencies commonly used in isolated cell studies (approx. 37% at 0.2 Hz).[55] Another study demonstrated significantly longer CaTD relative to APD in isolated guinea pig myocytes, however, experiments in

this instance were conducted at room temperature and at a non-physiological stimulation frequency (0.25Hz).[118]

It is worth noting that Rhod-2 can, under some circumstances, become sequestered into mitochondria rather than remaining in the cytosol. This can lead to a portion of the positive signal arising due to mitochondrial calcium transients, rather than cytosolic calcium transients following CICR, which could confuse findings. Indeed, one study using isolated rat trabeculae reported 55% of Rhod-2 fluorescence arose from mitochondria following selective permeabilization of mitochondrial and sarcolemmal membranes.[119] However, sequestering of Rhod-2 into mitochondria is influenced by the loading conditions used, with many studies using isolated cardiomyocytes and a cold-warm loading protocol to induce mitochondrial Rhod-2 loading and loss of Rhod-2 from the cytosol.[120] In addition, a study using isolated guinea pig cardiomyocytes demonstrated Rhod-2 fluorescence to originate predominantly from the cytoplasm using confocal microscopy. Rhod-2 fluorescence localisation was compared to that of a probe which is sequestered into the mitochondria (TMRE). Membrane permeabilization was then employed to confirm the cytosolic localisation of the calcium signal.[121] Therefore, given that the present study was conducted under conditions of warm loading with subsequent imaging conducted in a timely manner, in a species previously demonstrated to show cytosolic Rhod-2 loading, it is likely that the confounding effects of mitochondrial Rhod-2 loading are minimal.

Furthermore, simultaneous recording of APs and calcium transients in isolated guinea pig hearts using optical mapping with RH237 and Rhod-2 has been well characterised in a study by Choi & Salama.[122] This study demonstrated that these fluorescent dyes can successfully be used together for the simultaneous detection of calcium transients and APs, with no evidence of 'cross-talk' between the dyes. Data from this study also indicated that the calcium transient was not substantially longer than the AP at cycle lengths of 300ms, and so does not contradict the findings from the present study. These findings were also true of a second study using a similar approach but with different dyes in isolated guinea pig hearts.[123] Of note, the authors of the first study determined that an acquisition speed of 4kHz was required in order to accurately resolve the delay between AP and calcium transient upstrokes, and also averaged voltage and calcium signals from

very small regions of ventricular epicardium (0.8mm^2). Given that the present optical mapping study was conducted with a sampling speed of 500Hz and spatial averaging across much larger regions of the ventricular surface, this may go some way to explaining the lack of resolution between the rate of the upstrokes of the AP and calcium transients, potentially resulting in a loss of resolution of transient morphologies. Despite this, the present study provides good evidence of a potential mechanism by which repolarisation abnormalities could perturb normal intracellular calcium handling, thereby contributing to diastolic dysfunction in HF.

3.4.2 Effect of QT Prolongation on Cardiac Function

The first study examining the effect of QT prolongation on cardiac function in this chapter highlights the relevance of the method of QT prolongation that is employed. It was initially decided to have two QT prolongation groups, one using veratridine to prolong QT interval by augmentation of the late sodium current, and one using E-4031 and HMR 1556 to prolong QT through blockade of the delayed rectifier potassium currents. This was in order to reproduce methods used to prolong APD in previous studies by other groups[66, 124] and to replicate mechanisms known to prolong QT in both acquired and inherited LQTS (i.e. sodium channel gain of function and potassium channel loss of function). Data from the present study revealed that a clinically relevant level of QT prolongation (13-15% relative to control) had no impact on cardiac function when blockade of I_{Kr} and I_{Ks} was the pharmacological method used. However, when $I_{Na,L}$ was augmented a significant increase in LVDP and rate of contraction was observed, alongside a significant decrease in LVEDP. These positive inotropic and lusitropic effects likely reflect increased intracellular calcium stores as a result of reduced NCX activity (forward mode) or increased reverse-mode NCX activity, which occurs in response to the resultant elevated intracellular sodium.[54] Indeed, elevated intracellular sodium concentration is a reported effect from studies using similar drugs to augment the late sodium current.[125] This would cause positive inotropy due to greater calcium influx/reduced calcium efflux via NCX and therefore increased SR loading, with a resultant increased rate of contraction. The shortening of time-to-peak contraction and fall in LVEDP as a result of veratridine treatment was unexpected and the mechanism uncertain. Greater inotropy and reduced forward mode NCX might be expected to raise

rather than lower LVEDP, however, it is possible that these two unexpected effects are related. That is, the decreased time-to-peak contraction appears to allow for earlier relaxation, hence allowing a lower end diastolic pressure to be achieved. Of note, this effect on LVEDP may be unique to the guinea pig Langendorff model, since the short diastolic interval in these animals (as a result of the long AP to high heart rate ratio) means that there is no significant 'diastolic pause' in LVP between contractions (i.e. LVP is effectively sinusoidal). Regardless of mechanism, the observed functional effects following veratridine treatment are likely independent of any direct effects of APD prolongation on ventricular relaxation itself, given the similar degree of QT prolongation achieved in the E4+HMR group which showed no functional differences. This difficulty in attributing functional effects to AP duration alone when targeting $I_{Na,L}$ lead to the decision to only continue with I_{Kr} and I_{Ks} blockade going forward.

As discussed above, the nature of the relationship between APD and heart rate in the guinea pig is such that there is a limited scope for prolonging QT interval in isolated heart preparations. This is likely compounded by the fact that guinea pigs demonstrate a very prominent I_{Ks},[109] which would normally act to shorten APD in the presence of β-adrenergic stimulation (and thus high heart rates) *in vivo*, an element which is lacking in a denervated isolated preparation. To this end, it was decided to conduct an experiment under conditions where the heart rate could be slowed in the isolated guinea pig heart to create a longer diastolic pause, mimicking that seen in humans. This provided the scope to prolong QT interval to a greater extent and understand whether QT prolongation alone could begin to have measurable effects on cardiac relaxation. Therefore, hearts were perfused with ivabradine prior to blockade of I_{Kr} and I_{Ks}, allowing them to be paced at a much slower rate (120bpm) and a maximum QT prolongation of 34% to be achieved. Clinically speaking, this is equivalent to the QT prolongation which might be seen in patients with symptomatic LQTS[91] and is therefore a substantial but clinically relevant effect size (although it does exceed that observed in HF). In this study, an increase in the time to 75% relaxation was observed with maximal QT prolongation, suggesting that ventricular relaxation was indeed impaired under these conditions. This provides evidence that calcium handling may be altered in the presence of marked APD

prolongation in the healthy heart, although the functional effect appears to be small in this case given that LVEDP remained unaffected.

The degree of QT prolongation achieved in the isolated guinea pig heart in these studies compares favourably to the reported QT prolongation seen in diastolic dysfunction and LQTS patients in the literature. The percentage QT prolongation achieved using veratridine in the first study varied from 4-22% with increasing drug dose, whereas the QT prolongation with E4+HMR treatment ranged from 8-23%. This increased to 34% when a higher dose of E4+HMR was used in conjunction with ivabradine in the second study. From the literature, percentage prolongation of heart rate-corrected QT interval (QTc) in patients with diastolic dysfunction has been reported at 7.4% in Grade I diastolic dysfunction, 9% in grade II diastolic dysfunction, and 11% in grade III diastolic dysfunction.[86] If this is expanded to include QTc prolongation in LQTS patients, studies report a prolongation of 18% and 23% in asymptomatic and symptomatic single mutation carriers, respectively. This increases to 43% in double mutation carriers.[91] Therefore, the percentage of pharmacologically induced QT prolongation achieved in the present study falls within the range observed in humans with disorders associated with cardiac repolarisation abnormalities.

Thus far, data suggest that in the healthy heart where calcium handling is not impaired and maladaptation (e.g. fibrosis) is not present, APD prolongation alone is not sufficient to result in a significant impairment of ventricular relaxation. Healthy hearts may be able to cope with any minor increases in calcium entry to the cell or delays in the onset of relaxation without displaying diastolic dysfunction. Going forward, it was therefore important to replicate some the common co-pathologies of HF in the isolated heart model and determine whether this affected the relationship between APD and diastolic function.

Data from the present study indicate that modest QT prolongation in the presence of SERCA inhibition results in diastolic dysfunction, as evidenced by an elevated LVEDP. This was in the absence of any significant change in the rate of ventricular relaxation and may be indicative of elevated diastolic calcium levels under these conditions, resulting in impaired ventricular relaxation. The return of calcium to SR stores by SERCA is the major mechanism for calcium removal from the cytoplasm following a ventricular AP. It

has been shown that the level of SERCA expression is reduced in failing hearts. One study reported a 47% reduction in mRNA levels for this protein relative to ventricular samples from control hearts.[58] A similar study examined the protein levels of SERCA and reported a decrease of 36% in failing vs non-failing human heart tissue.[59] In addition to contributing to reduced SR loading and contractile dysfunction, this could also serve to impede cytosolic calcium clearance and impair ventricular relaxation. Therefore, it seems possible that such changes to SERCA activity may leave hearts vulnerable to impaired diastolic function as a result of altered calcium transient dynamics caused by APD prolongation.

3.4.3 Limitations of the Langendorff Model

Whilst studies in the isolated, Langendorff-perfused guinea pig heart have provided some insight into the possible relationship between APD and diastolic function in the whole heart, there are some issues with this approach. Although some changes to parameters associated with relaxation (i.e. time to 75% relaxation, or LVEDP) were observed with substantial QT prolongation or QT prolongation in the presence of SERCA inhibition, they were not evident simultaneously. This suggests the phenotype was either very mild or that this model was not sensitive enough to detect subtle changes in diastolic function. This possibility was also indicated by some inconsistencies observed with the general setup of the guinea pig Langendorff heart. It was found that the IVB volume required to give a starting LVEDP of 5-7mmHg was very variable, suggesting that positioning/morphology of the balloon was having an effect on the reported end diastolic pressure. The presence of the balloon also appeared to make hearts prone to arrhythmia, such that the pacing rate had to be set substantially higher than the intrinsic heart rate to achieve stable pacing, contributing to the issue of a lack of diastolic interval previously discussed. From the data, increasing pacing rate had a clear effect on LVEDP at higher heart rates but not at lower the heart rates used in the ivabradine study, indicating that hearts were functioning at the upper limits of normal physiological reserve at baseline. Given that LVEDP represented the main readout for diastolic function in these studies, this brought into question the sensitivity/reliability of measuring this variable in this manner. In addition, isovolumic relaxation is only a component of normal auxotonic relaxation in the heart *in vivo*. Measuring isovolumic function may therefore give a

distorted or insensitive index of diastolic function. As such, going forward it was decided to develop an isolated working guinea pig heart as a model, which may provide more sensitive and reliable physiological information about the influence of QT prolongation on diastolic function in an auxotonically contracting working heart preparation.

3.4.4 Summary and Conclusions

In the isolated guinea pig heart ventricular CaTD is closely linked to APD, and will show a corresponding increase in duration in response to interventions which prolong AP. This has potential implications for diastolic function in the presence of prolonged APD due to the essential role of calcium removal from the cytoplasm in ventricular relaxation. Clinically relevant levels of APD prolongation alone are not sufficient to impair diastolic function in the healthy heart, however, there is evidence that larger APD prolongation possible at lower heart rates does act to slow the rate of ventricular relaxation, and that diastolic function is impaired by APD prolongation in the presence of impaired intracellular calcium handling.

4 WORKING HEART STUDIES

4.1 Introduction

The isolated working heart is another well-established experimental model used in cardiovascular physiology and pharmacology.[126-131] It is a versatile model with many applications; however, the working heart may have a particular advantage over the Langendorff heart when it comes to studying cardiac contractility due to its closer approximation of normal physiology in this regard. In the working heart, the left side of the heart is filled with physiological buffer that is then ejected via the aorta against a defined hydrostatic pressure forming the 'afterload', which in turn determines perfusion of the coronary vasculature (Section 2.1.2, Fig. 2.4). This is far more similar to the situation *in vivo* than that seen in the Langendorff heart, where the left ventricle is undergoing isometric contraction against a fixed volume (in the form of a fluid filled IVB).

In the working heart, as *in vivo*, contraction is initially isovolumic (although, as a result of torsion, not necessarily isometric) which is then followed by a period of shortening against an afterload after the aortic valve opens and ventricular ejection proceeds. In this way, the isolated heart performs external work. After peak ejection, the fall in aortic pressure is initially influenced by aortic compliance and Windkessel effects. However, after the closure of the aortic valve, relaxation proceeds initially isovolumically before the mitral valve reopens and the ventricle refills. Both contraction and relaxation can therefore be considered to be auxotonic and very similar to that *in vivo*.

The Langendorff heart, instrumented with an IVB, is also potentially prone to error as a means of recording intraventricular pressure, with factors such as air bubbles and gauge/rigidity of the plastic line chosen to connect the balloon to the pressure transducer having the potential to dampen the signal, resonate or introduce noise.[132] In addition to this, there is some discussion as to whether the measurement of the rate of pressure decline in the isolated heart provides an accurate assessment of calcium-dependent changes to the rate of relaxation under conditions of isometric contraction. It has been

proposed that under these conditions factors other than removal of cytosolic calcium may determine the rate of relaxation, unlike unloaded myocytes where calcium clearance from the cytosol is the major mechanism behind initiation of relaxation.[133-135]

In addition to a more physiologically relevant contraction and relaxation cycle, another advantage of the working heart is that a pressure-volume catheter can be introduced into the left ventricle to record high-fidelity physiological data. We have therefore used a working heart with an admittance catheter introduced into the left ventricle via the aortic valve to record beat-to-beat ventricular pressures and volumes. Due to the small size of the catheter, there is no interference with normal cardiac contraction, and no irritation to the endocardium resulting in the proarrhythmic state observed in the guinea pig Langendorff heart in the previous studies. Given that no markedly different effects were observed at the higher pacing rates in the Langendorff studies (Chapter 3), this meant that isolated working hearts could be allowed to run at their intrinsic rate for the most part during these studies, thereby removing the potential for causing impaired diastolic function at baseline due to high pacing rates.

The use of an admittance catheter provides a large number of clinically familiar variables useful for the assessment of subtle changes in cardiac function. These include maximal rates of pressure increase and decline (dP/dt max and dP/dt min), time constants of relaxation (tau) and the potential for measuring end-systolic and end-diastolic pressure-volume relationships (as indices of ventricular contractility and compliance, respectively) by performing partial 'preload occlusions' (Fig. 2.4 and 4.2). The acquisition of pressure-volume data in this manner represents the gold standard measure of systolic and diastolic function both experimentally (*in vivo*) and in clinical settings.[136-138]

Given the absence of significant changes to diastolic function with QT prolongation in the Langendorff heart, it was considered necessary to move to the working heart where the hypothesis could be tested in a more physiologically relevant model. The studies described in this chapter therefore aim to build on those in Chapter 3 and further explore the relationship between APD and diastolic function. In addition, the role of concomitant co-pathologies of HF will be explored.

As has already been discussed in Chapter 1 (Section 1.2.4), changes in the expression and/or activity of SERCA are known to occur in HF and these will profoundly influence the shape and recovery of the cytosolic calcium transient. This decline in intracellular calcium uptake is counterbalanced in the failing heart by an increase in sarcolemmal calcium extrusion via increased expression and activity of NCX. The shift from intracellular calcium uptake to sarcolemmal extrusion is likely to render calcium removal from the cytoplasm more dependent on: i) membrane potential, and ii) intracellular sodium concentration. The former would increase the likelihood of APD influencing relaxation of the calcium transient, and the latter is a co-morbidity widely associated with HF.[53-56]

4.1.1 Hypothesis and Objectives

Hypothesis: Prolonged APD in the presence of elevated intracellular sodium and impaired SERCA function will act to impair ventricular relaxation via alterations to intracellular calcium handling. This hypothesis is best tested in an auxotonically contracting working heart model using clinically recognised indices of systolic and diastolic function.

Objectives are, therefore:

1) To develop and fully characterise a working guinea pig heart model, with respect to normal function and identification of useful systolic and diastolic functional variables.
2) To investigate the relationship between APD/ventricular repolarisation and diastolic function the healthy working heart.
3) To determine whether the presence of pharmacologically induced impairment of intracellular calcium handling (replicating that seen in HF) affects the relationship between APD and repolarisation in the working heart.

4.2 Methods

The methods used to isolate, cannulate and instrument hearts for working heart perfusions are described in detail in Section 2.1.2. Where applicable, data were analysed using two-

way ANOVA with Sidak's post-hoc test to determine whether significant differences were present between experimental groups at each time point and a p value of <0.05 was deemed statistically significant. Hearts were randomised to study groups and experiments and analysis were conducted in a blinded fashion.

4.2.1 Characterisation of the Working Guinea Pig Heart

Before it was possible to tackle any more of the questions surrounding the hypothesis, it was first necessary to characterise the working guinea pig heart model. Although the working heart experimental setup enabled preload and afterload to be altered (Fig. 2.4), the pressures used in these protocols were informed by a study which looked at the metabolic performance of a working guinea pig heart over a range of preloads and afterloads.[139] The working hearts in the present study were therefore set to work under a preload of 15mmHg and an afterload of 55mmHg, to enable performance at maximal efficiency.

Figure 4.1 shows a representative trace from an IVB used in a Langendorff-perfused guinea pig heart (in red), compared to a trace obtained using a PV catheter in a working guinea pig heart (in black). From these traces it can be seen that there are substantial differences in the morphology of the LV pressure trace obtained with these two experimental models, with the Langendorff heart showing a very symmetrical shape and no appreciable diastolic interval. In comparison, the working heart shows different rates of contraction and relaxation, with an asymmetric LV pressure trace more typical of that observed *in vivo*. In addition, there is a greater diastolic pause with a true end diastolic pressure morphology. This difference in the morphology of the pressure trace and the closer approximation to what is observed *in vivo* gives confidence that the PV catheter provides more physiological data which may be more sensitive to changes in cardiac function. In addition, studies conducted to examine the frequency-response characteristics of similar IVB setups have demonstrated a flat frequency response at frequencies ranging well beyond those seen in the contracting guinea pig heart.[132] Thus, the differing morphology obtained between pressure catheter and IVB is unlikely to be due to any artificial dampening of the pressure signal. The presence of a 'true' end diastolic pressure also means that this parameter, which formed the major readout of

diastolic function in the Langendorff studies, may provide more reliable data on the diastolic function of the heart.

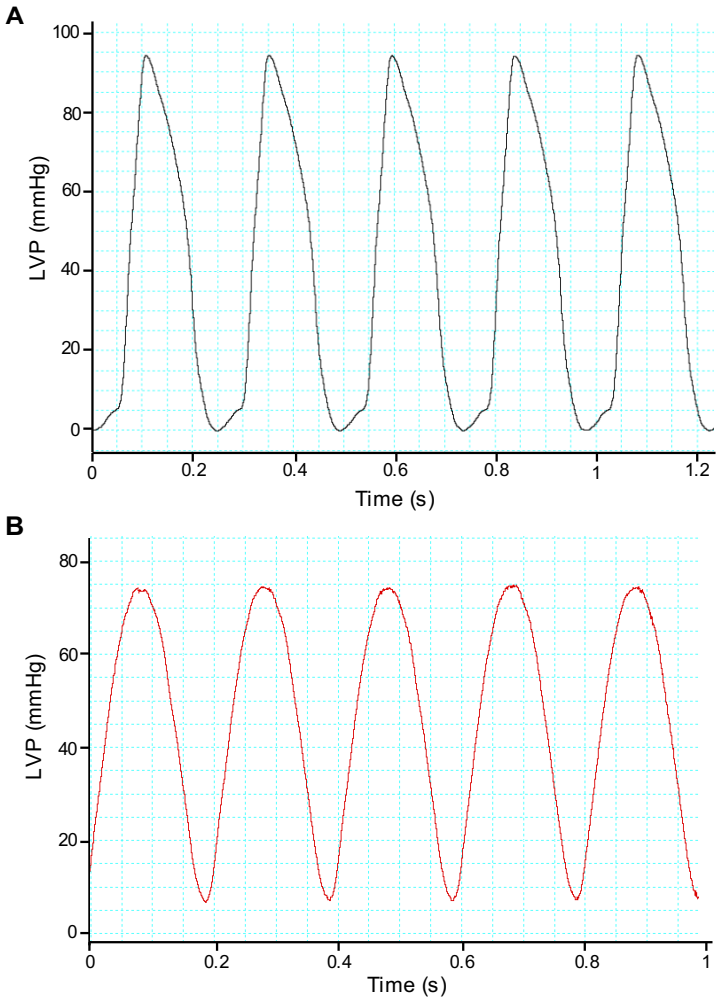

Figure 4.1 Comparison of LVP trace from PV catheter and IVB

Comparison of left ventricular pressure trace from A) a pressure-volume (PV) catheter positioned within the left ventricle of a working heart, introduced via the aortic valve, and B) an intraventricular fluid-filled balloon (IVB) coupled to a pressure transducer, introduced into the left ventricle of a Langendorff-perfused heart via the left atrium. Note the symmetrical appearance and lack of true diastolic pause in the Langendorff pressure trace (red), whereas the working heart trace (black) shows a true EDP morphology and different rates of contraction and relaxation during the cardiac cycle, as would be seen *in vivo*.

Examples of the pressure-conductance loops and preload occlusions obtained in the guinea pig working heart model are shown in Fig. 4.2. Good quality loops were obtained in most hearts, although it can be seen that the morphology of the ejection phase differs

slightly from the domed appearance of loops obtained *in vivo*, which is likely a reflection of the abnormal afterload experienced by isolated working hearts. Other phases of the cardiac cycle appeared similar to that observed *in vivo*, and the end diastolic point was generally well detected by LabChart PV loop analysis software when analysing occlusions, however, it was found that the rounded ejection phase often made the accurate detection of the end systolic point challenging.

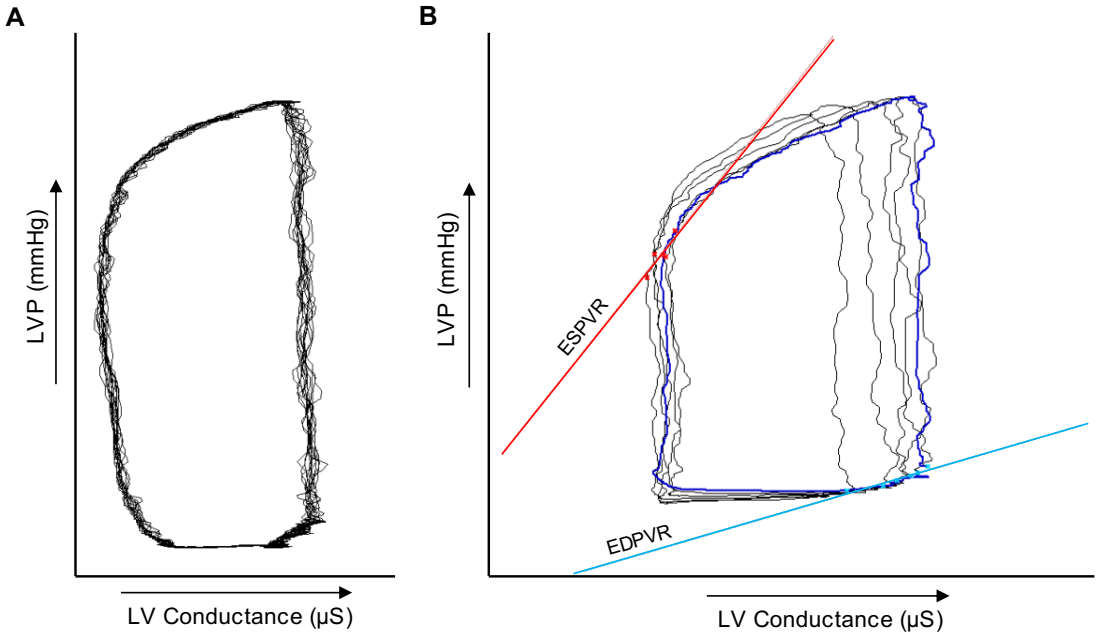

Figure 4.2 Example PV loop and 'IVC' occlusion from working heart setup

Representative examples of A) pressure-volume (PV) loops obtained using a PV catheter within the left ventricle of an isolated working guinea pig heart and B) modified 'IVC' occlusions performed by abruptly partially occluding inflow to the left side of the working heart to enable end diastolic- and end systolic pressure-volume relationships to be determined – referred to as preload occlusions (blue and red lines, respectively). N.B. Raw LV conductance data displayed on x-axis owing to inability to correctly calibrate volume calculation on ADV500 PV System used (see discussion Section 4.4.1).

Once it had been established that the combination of the working guinea pig heart and PV catheter provided a good means of collecting accurate data about cardiac function, it was necessary to characterise the relationship between various functional parameters and heart rate. This was to avoid the need to pace hearts in future studies, thus avoiding the issue of potentially stressing hearts at high pacing rates under baseline conditions. In addition, the fact that the working heart preparation was found to be very stable (i.e. did not

demonstrate the same propensity for arrythmias observed in the Langendorff preparation when using an IVB) and that little effect of high heart rate was observed in the previous Langendorff studies rendered pacing unnecessary. However, given that pharmacological interventions used in subsequent studies would affect heart rate it was important to understand how functional variables would change in response to heart rate under baseline conditions.

To this end a study was conducted where healthy hearts were treated with low, incremental doses of ivabradine to gradually lower heart rate, before atrial pacing was used to gradually increase heart rate again in a series of small steps. Hearts were initially cannulated and allowed to stabilise in Langendorff-mode for 15 min, before switching to working mode and allowing a further 15 min for stabilisation. Incremental concentrations of ivabradine were then added to the physiological buffer in 0.2μM steps (up to a maximum concentration of 0.6μM) to gradually lower heart rate to approximately 120bpm. Heart rate was then gradually increased again using atrial pacing (at 1.5x capture threshold) in 20bpm steps (allowing 2 min at each pacing rate) up to a maximum heart rate of 310bpm. This allowed data to be recorded across the range of physiological heart rates which would be observed in subsequent studies, and the relationship between various cardiac parameters and cardiac cycle length (i.e. RR interval) could then be plotted (Fig. 4.3-4.5).

For analysis, data from 8 individual hearts were plotted with 10s of data analysed for each heart rate (both paced and unpaced during ivabradine application, with data analysed after each 10bpm reduction in heart rate). For analysis, LabChart 8 Pro with blood pressure and ECG analysis modules was used (Fig. 4.3-4.5). To analyse LVP variables, the blood pressure analysis module was used to analyse LVP and new channels created for dP/dt max, dP/dt min, systolic duration, diastolic duration, tau and end diastolic pressure. ECG variables were measured using the ECG analysis tool to average 10 beats, with manual correction of the detection of ECG features. Each point was plotted against the corresponding RR interval to give the relationship between heart rate and each variable of interest, and a linear regression analysis carried out on the combined group data to give the slope and r^2 value for each parameter.

The average heart rate in the working guinea pig heart was determined by taking the average from these 8 hearts following the 30 min stabilisation period at the start of the protocol and was determined to be 242bpm. This, combined with the slope of the relationship between RR interval and each functional parameter, allowed a formula to be calculated which would allow parameters to be corrected for heart rate in subsequent studies. The formula used was:

$$a(c) = a + \frac{b(HR - 242)}{1000}$$

For the above equation, *a* was equal to the recorded value of the parameter of interest at any given heart rate, *b* was equal to the slope of the relationship between that parameter and RR interval, and HR was equal to the heart rate at which the parameter was recorded. The corrected value was referred to as *a*(c) (e.g. LVEDP became LVEDP(c)).

4.2.2 Measuring Dysfunction in the Working Heart

Having set up a satisfactory working heart model and established the relationship between various functional parameters and cardiac cycle length, it was next important to understand which of these parameters could provide useful and reliable information about the presence of cardiac dysfunction. Table 4.1 outlines the different functional parameters measured in working heart preparations, and how these values are obtained from the raw data.

Table 4.1 Functional parameters measured in isolated working guinea pig hearts

List of functional parameters measured, alongside physiological significance and method of deriving values from the raw pressure-conductance/coronary and aortic flow data in working heart studies. Abbreviations: stroke volume (SV), coronary flow (CF), aortic flow (AF), heart rate (HR), cardiac output (CO), stroke work (SW), end-systolic pressure-volume relationship (ESPVR), end-diastolic pressure-volume relationship (EDPVR), left ventricular developed pressure (LVDP), systolic duration (SD), left ventricular end diastolic pressure (LVEDP), diastolic duration (DD). * See Fig. 4.2 for example.

Functional Parameter	*Definition/Method of Calculation*	*Physiological Significance*
SV	Volume ejected per cardiac cycle: (CF+AF)/HR.	Systolic and diastolic function: largely influenced by contractility and ventricular compliance in the working heart (where filling and afterload pressure are fixed).
CO	CF+AF per unit time. Expressed per gram of ventricular mass to account for differences in heart size.	Systolic and diastolic function: product of SV and HR.
SW	Area of the pressure-conductance loop: product of LVP and conductance/volume.	Systolic function: measure of the work performed by the LV to eject blood during each contraction.

ESPVR	The beat-to-beat relationship between end-systolic pressure-volume points under variable preload. Measured by temporary, partial occlusion of preload line.*	Systolic function: the slope of the ESPVR provides a load-independent measure of ventricular contractility.
EDPVR	The beat-to-beat relationship between end-diastolic pressure-volume points under variable preload. Measured by temporary, partial occlusion of preload line.*	Diastolic function: the slope of the EDPVR provides a measure of passive ventricular stiffness.
LVDP	Maximum pressure reached within the LV during the cardiac cycle, minus LVEDP.	Systolic function: reduced LVDP may indicate reduced contractility.
dP/dt(max)	Maximum rate of pressure increase within the LV.	Systolic function: increased dP/dt(max) reflects increased contractility during isovolumic contraction.
SD	Time from the start of the cardiac cycle (at LVEDP) to dP/dt(min).	Systolic function: duration may be influenced by rate of contraction.

LVEDP	Pressure within the LV at end diastole (following atrial contraction, prior to ventricular contraction).	Diastolic function: elevated LVEDP at a fixed filling pressure indicates reduced ventricular compliance.
dP/dt(min)	Maximum rate of pressure decline within the left ventricle.	Diastolic function: increased dP/dt(min) reflects improved relaxation during isovolumic relaxation.
DD	Time from dP/dt(min) to end of cardiac cycle.	Diastolic function: duration may be influenced by the rate of relaxation.
Tau	Exponential time constant of ventricular pressure decay during isovolumic relaxation.	Diastolic function: pre-load independent measure of relaxation during the isovolumic phase.

In order to determine which of these parameters provided the best indication of changes to cardiac function, a study was conducted where working guinea pig hearts were treated with incremental concentrations of CPA. Given that inhibition of SERCA activity with CPA should affect both systolic and diastolic function, this allowed various functional parameters to be assessed at each concentration of CPA to determine which parameters were best able to detect the resultant perturbation of normal cardiac function. The specific protocol for this study is as follows. Hearts were initially cannulated and allowed to stabilise in Langendorff-mode for 15 min, before switching to working mode and allowing a further 15 min for stabilisation. Baseline measurements were recorded at this point, and preload occlusions performed. CPA was then added to the physiological buffer at a concentration of 1μM and given 20 min to take full effect, before repeating measurements and occlusions. This was repeated for 5 and 10μM concentrations of CPA.

For analysis, LabChart 8 Pro with blood pressure and PV loop modules was used (Fig. 4.6-4.9). To analyse LVP variables, the blood pressure analysis module was used to analyse LVP and new channels created for dP/dt max, dP/dt min, systolic duration, diastolic duration, tau and end diastolic pressure, with 10s of data analysed for each time point. Parameters associated with LVP were presented as corrected values to account for differences in heart rate using the formula determined in the previous study (Section 4.2.1). Cardiac output was calculated by collecting and weighing the coronary effluent for 15s at the end of each time point and combining this with the aortic flow obtained from a flow meter in the afterload line. The ventricles were weighed at the end of each experiment, allowing cardiac output to be expressed as ml/min/g of ventricular mass. Stroke volume was calculated by dividing the total cardiac output by the heart rate. The ESPVR and EDPVR was calculated by analysing the preload occlusions performed at each time point using the PV loop module.

4.2.3 Effect of QT Prolongation in the Healthy Working Heart

Having determined that cardiac dysfunction could be successfully detected in the working heart model, the first stage of addressing the experimental hypothesis was to examine the effects of prolonging the AP in the healthy heart. Therefore, a simple study was designed where QT interval was prolonged using a combination of E-4031 and HMR 1556 in healthy working guinea pig hearts.

Hearts were initially cannulated and allowed to stabilise in Langendorff-mode for 15 min, before switching to working mode and allowing a further 15 min for stabilisation. Baseline measurements were recorded at this point before adding 100nM E-4031 and 30nM HMR 1556 or DMSO vehicle control to the physiological buffer, allowing 20 min for the drugs to take full effect, and repeating measurements.

For analysis, LabChart 8 Pro with blood pressure and ECG analysis modules was used (Fig. 4.10-4.12). To analyse LVP variables, the blood pressure analysis module was used to analyse LVP and new channels created for dP/dt max, dP/dt min, systolic duration, diastolic duration, tau and end diastolic pressure, with 10s of data analysed for each time point. Variables associated with LVP were presented as corrected values to account for

differences in heart rate using the formula determined in the previous study (Section 4.2.1). ECG parameters were measured using the ECG analysis tool to average 10 beats, with manual correction of the detection of ECG features and QT interval presented as QTc, according to the appropriate formula. To aid visualisation of the effect of QT prolongation on LV pressure generation, data from a complete cardiac cycle was exported from LabChart and plotted against time on GraphPad Prism 8. Representative examples were selected by identifying hearts which displayed diastolic function most similar to the group average. Cardiac output was calculated by collecting and weighing the coronary effluent for 15s at the end of each time point and combining this with the aortic flow obtained from a flow meter in the afterload line. The ventricles were weighed at the end of each experiment, allowing cardiac output to be expressed as ml/min/g of ventricular mass. Stroke volume was calculated by dividing the total cardiac output by the heart rate.

4.2.4 Effect of QT Prolongation in the Presence of SERCA Inhibition

Once the relationship between APD and cardiac function had been examined in the healthy heart, it was next important to determine how this might be affected by common co-pathologies associated with HF. Therefore, a study was conducted where hearts were treated with E-4031 and HMR 1556 to prolong QT interval in the presence of SERCA inhibition.

Initially, hearts were cannulated and allowed to stabilise in Langendorff-mode for 15 min, before switching to working mode and allowing a further 15 min for stabilisation. Baseline measurements were recorded at this point before adding 5μM CPA to the physiological buffer and allowing 15 mins for the drug to take effect before measurements were recorded. Hearts were then treated sequentially with 100nM E-4031 followed by 30nM HMR 1556 (or DMSO vehicle control), allowing 15 min for stabilisation at each dose before repeating measurements.

For analysis, LabChart 8 Pro with blood pressure and ECG analysis modules was used (Fig. 4.13-4.15). To analyse LVP variables, the blood pressure analysis module was used to analyse LVP and new channels created for dP/dt max, dP/dt min, systolic duration, diastolic duration, tau and end diastolic pressure, with 10s of data analysed for each time

point. Variables associated with LVP were presented as corrected values to account for differences in heart rate using the formula determined in the previous study (Section 4.2.1). ECG parameters were measured using the ECG analysis tool to average 10 beats, with manual correction of the detection of ECG features and QT interval was presented as QTc, according to the appropriate formula. To aid visualisation of the effect of QT prolongation on LV pressure generation, data from a complete cardiac cycle was exported from LabChart and plotted against time on GraphPad Prism 8. Representative examples were selected by identifying hearts which displayed diastolic function most similar to the group average. Cardiac output was calculated by collecting and weighing the coronary effluent for 15s at the end of each time point and combining this with the aortic flow obtained from a flow meter in the afterload line. The ventricles were weighed at the end of each experiment, allowing cardiac output to be expressed as ml/min/g of ventricular mass. Stroke volume was calculated by dividing the total cardiac output by the heart rate.

4.2.5 Effect of QT Prolongation in the Presence of SERCA Inhibition and Elevated Intracellular Sodium

In order to build on the premise of investigating the relationship between APD and cardiac function in the failing heart, the next study aimed to prolong QT interval in the presence of both SERCA inhibition and elevated intracellular sodium. To achieve this, working guinea pig hearts were treated with a combination of CPA and ouabain before using E-4031 and HMR 1556 to prolong QT.

Before this study could be carried out it was necessary to identify a suitable dose of ouabain which would act to elevate intracellular sodium, as would be apparent by the presence of positive inotropy in the healthy heart. To this end, a preliminary study was conducted where working hearts were exposed to incremental concentrations of ouabain, and the effects on systolic parameters recorded. Hearts were cannulated and allowed 15 min to stabilise in Langendorff-mode, before switching to working mode and allowing a further 15 min for stabilisation. Baseline measurements were recorded at this point before the following concentrations of ouabain were added: 100nM, 200nM and 300nM. Each dose was given 20 min to take effect and functional parameters were recorded at 5 min intervals.

Following the identification of 200nM ouabain as an appropriate dose to elevate intracellular sodium, the study examining the effects of APD prolongation on cardiac function in the presence of HF co-pathologies was conducted. Hearts were initially cannulated and allowed to stabilise in Langendorff-mode for 15 min, before switching to working mode and allowing a further 15 min for stabilisation. Baseline measurements were recorded at this point before adding 5μM CPA and 200nM ouabain to the physiological buffer and allowing 15 mins for the drugs to take effect before measurements were recorded. Hearts were then treated with 100nM E-4031 and 30nM HMR 1556 (or DMSO vehicle control), allowing 15 min for stabilisation before repeating measurements.

For analysis, LabChart 8 Pro with blood pressure and ECG analysis modules was used (Fig. 4.16-4.19). To analyse LVP variables, the blood pressure analysis module was used to analyse LVP and new channels created for dP/dt max, dP/dt min, systolic duration, diastolic duration, tau and end diastolic pressure, with 10s of data analysed for each time point. Variables associated with LVP were presented as corrected values to account for differences in heart rate using the formula determined in the previous study (Section 4.2.1). For the ouabain dose-finding study, only systolic parameters were calculated, and were expressed as raw values to avoid errors in the detection of positive inotropy. ECG parameters were measured using the ECG analysis tool to average 10 beats, with manual correction of the detection of ECG features and QT interval was presented as QTc, according to the appropriate formula. To aid visualisation of the effect of QT prolongation on LV pressure generation, data from a complete cardiac cycle was exported from LabChart and plotted against time on GraphPad Prism 8. Representative examples were selected by identifying hearts which displayed diastolic function most similar to the group average. Cardiac output was calculated by collecting and weighing the coronary effluent for 15s at the end of each time point and combining this with the aortic flow obtained from a flow meter in the afterload line. The ventricles were weighed at the end of each experiment, allowing cardiac output to be expressed as ml/min/g of ventricular mass. Stroke volume was calculated by dividing the total cardiac output by the heart rate.

4.3 Results

4.3.1 Characterisation of the Working Guinea Pig Heart

Of the ECG parameters measured, QT interval demonstrated the closest relationship with RR interval, demonstrating a clear positive correlation with a relatively high goodness of fit ($r^2 = 0.73$) (Fig. 4.3 A). This means that as heart rate slows QT interval becomes longer and is the expected effect as APD adapts to slower heart rate. The other ECG parameters examined, namely Tp-Te interval, PR interval and QRS duration, show little to no relationship with RR interval, and as such do not vary much in response to altered heart rate (Fig.4.3 B-D).

When looking at the relationship between systolic parameters and heart rate, LVDP demonstrates a negative correlation with RR interval (Fig. 4.4 A). This means that LVDP will increase at higher heart rates, which is as expected given the positive force-frequency relationship in the guinea pig heart. This is backed up by a negative dP/dt max- and positive systolic duration-RR correlation, which means that at higher heart rates the ventricular myocardium contracts at a faster rate and so spends a shorter period of time in systole (Fig. 4.4 B and C). These parameters all show clear relationships with heart rate, and so will benefit from correction using the calculated formula (Section 4.2.1).

The diastolic functional parameters examined also show a relationship with heart rate (Fig. 4.5 A-D). LVEDP and dP/dt min both appear to show a modest positive correlation with RR interval, with hearts demonstrating a higher EDP and slower rate of relaxation at slower heart rates. A more substantial positive tau- and diastolic duration-RR correlation is demonstrated, indicating that hearts relax more slowly and thus spend a longer time in diastole at slower heart rates. Again, these parameters will benefit from being presented in a corrected format using the appropriate formula, thus enabling results in future studies to be analysed independently from heart rate effects.

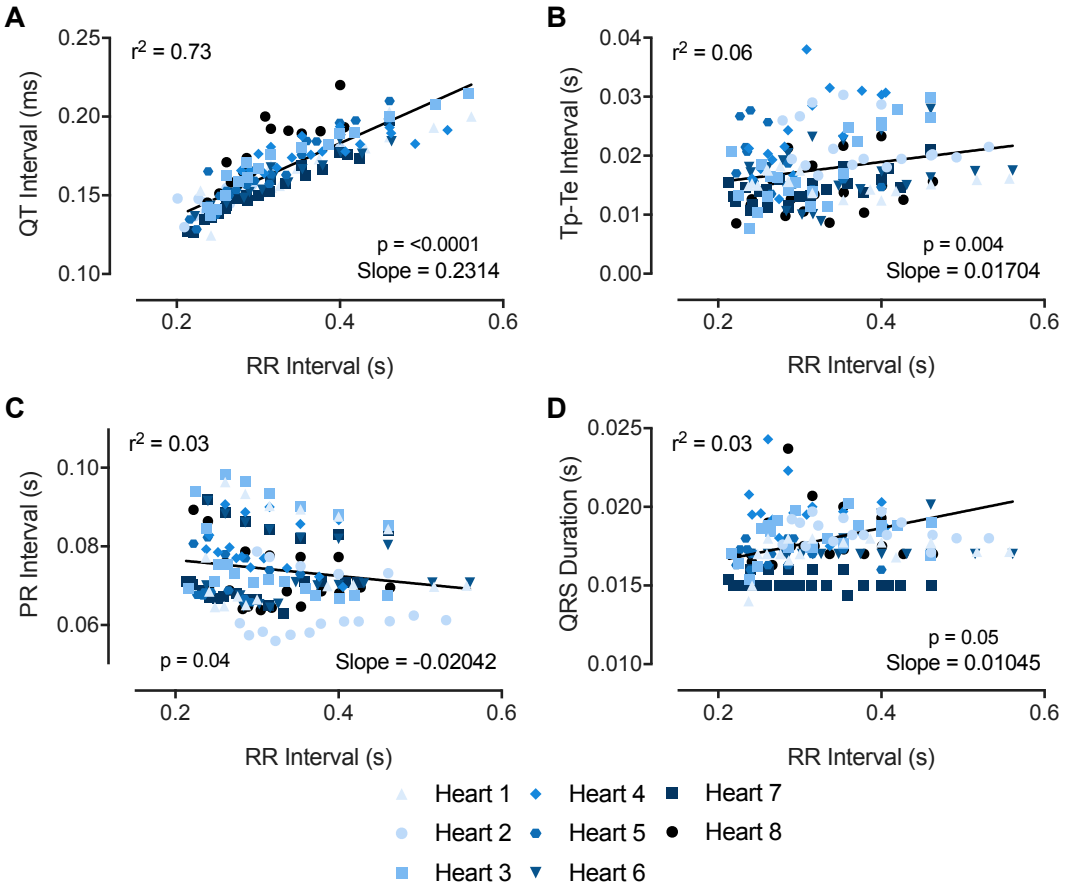

Figure 4.3 Relationship between RR interval and ECG parameters

Relationship between RR interval (i.e. cardiac cycle length) and ECG parameters in working guinea pig hearts paced across a range of heart rates in the presence of ivabradine (max. 0.6μM). Relationships between A) QT interval, B) Tp-Te interval, C) PR interval and D) QRS duration and RR interval are shown. Slope of relationship with r^2 and p value for each parameter are also given and relate to a linear regression analysis of group data from all 8 hearts.

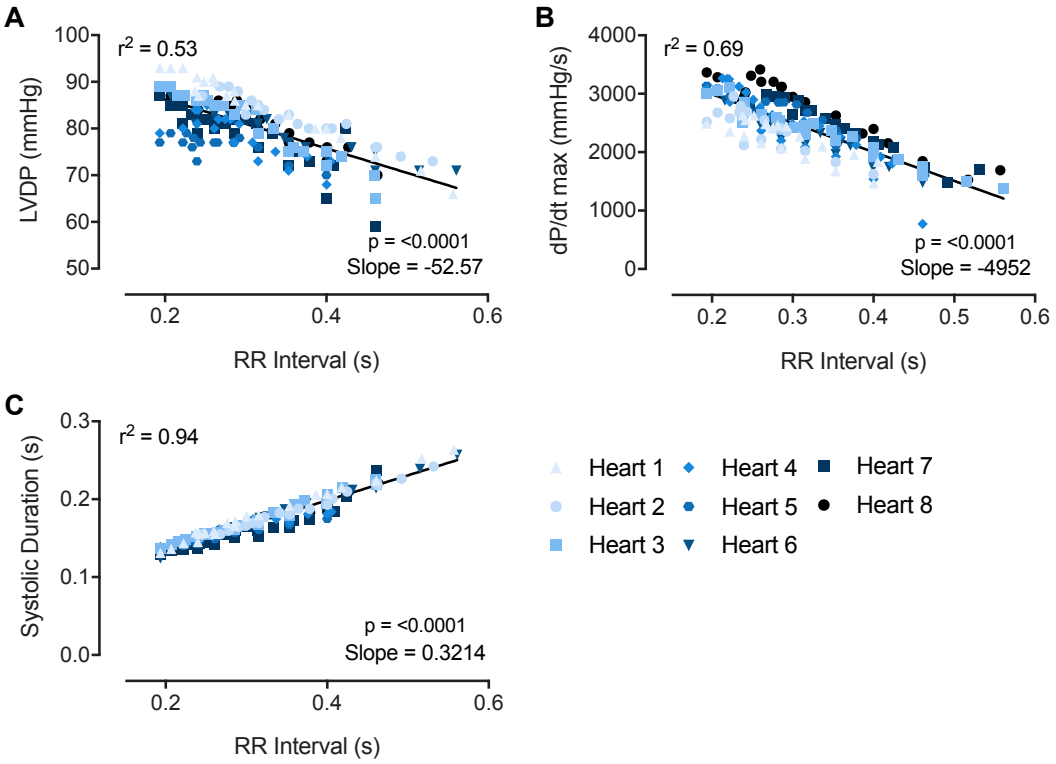

Figure 4.4 Relationship between RR interval and systolic parameters

Relationship between RR interval (i.e. cardiac cycle length) and ECG parameters in working guinea pig hearts paced across a range of heart rates in the presence of ivabradine (max. 0.6μM). Relationships between A) LVDP, B) dP/dt max, and C) systolic duration and RR interval are shown. Slope of relationship with r^2 and p value for each parameter are also given and relate to a linear regression analysis of group data from all 8 hearts.

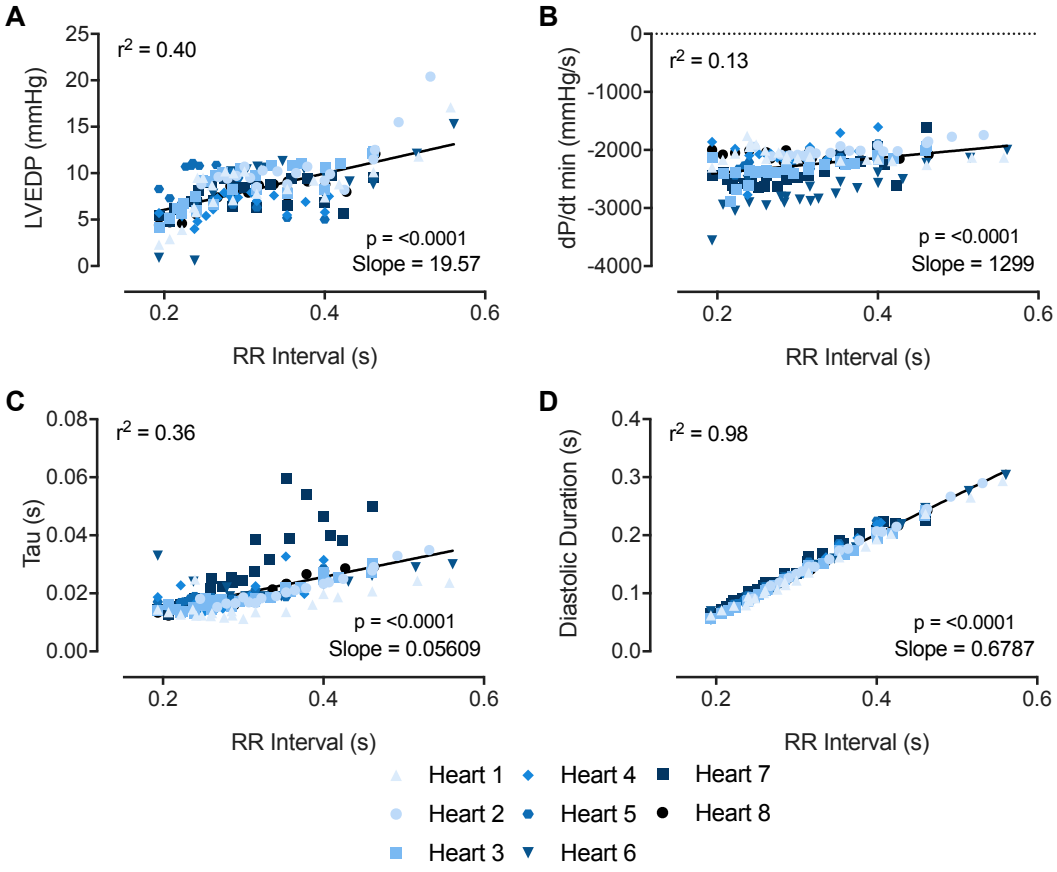

Figure 4.5 Relationship between RR interval and diastolic parameters

Relationship between RR interval (i.e. cardiac cycle length) and ECG parameters in working guinea pig hearts paced across a range of heart rates in the presence of ivabradine (max. 0.6µM). Relationships between A) LVEDP, B) dP/dt min, C) tau, and D) diastolic duration and RR interval are shown. Slope of relationship with r^2 and p value for each parameter are also given and relate to a linear regression analysis of group data from all 8 hearts.

4.3.2 Measuring Dysfunction in the Working Heart

Treatment with CPA causes a reduction in heart rate, with this effect becoming significant at 5µM (Fig. 4.6 A). This is accompanied by a reduction in cardiac output and stroke volume, both of which also display significance at 5µM (Fig. 4.6 B & C). The fact that the reduction in cardiac output occurs alongside a reduction in stroke volume indicates that this effect is likely independent of the reduced heart rate.

Data obtained from PV loops and preload occlusions were also analysed to determine whether useful information about cardiac function could be obtained in this manner from the working guinea pig heart preparation. Fig 4.7 A demonstrates that stroke work (i.e. the area of the PV loop) closely mirrors the effects seen on cardiac output and stroke volume, demonstrating a significant reduction with increasing doses of CPA, reaching significance at a concentration of 5μM. The ESPVR and EDPVR were also examined but showed no change at any dose of CPA (Fig. 4.7 B & C). The EDPVR in particular demonstrates large variation between hearts and thus is unlikely to detect changes in cardiac function with the group sizes used in these studies.

Treatment with CPA enabled a clear impairment of systolic function to be detected in working guinea pig hearts (Fig. 4.8 A-C). Corrected LVDP was reduced in the presence of increasing concentrations of CPA, with this reduction reaching significance at 5μM. The rate of pressure development within the ventricle appeared to be more sensitive to the effects of CPA, with dP/dt max(c) demonstrating a significant reduction from the lowest concentration of 1μM. Similarly, corrected systolic duration showed a large increase in response to CPA treatment, although this only became apparent at 5 and 10μM concentrations.

Impairment of diastolic function was also detected in working guinea pig hearts treated with CPA (Fig. 4.9 A-C). Interestingly, LVEDP(c) did not appear to be sensitive to impaired ventricular relaxation as a result of SERCA inhibition, demonstrating little or no change at any concentration of CPA. The rate of pressure decline in the ventricle did respond to CPA treatment however, with dP/dt min(c) showing a dose-dependent reduction in response to CPA, although this did not reach significance until 10μM. This was mirrored by an increase in tau(c) in response to CPA, indicating a slowing of relaxation, although this reached significance from 5μM concentrations. Corrected diastolic duration, perhaps unexpectedly, showed a significant decrease in response to CPA treatment, although this effect appeared to be lost at 10μM.

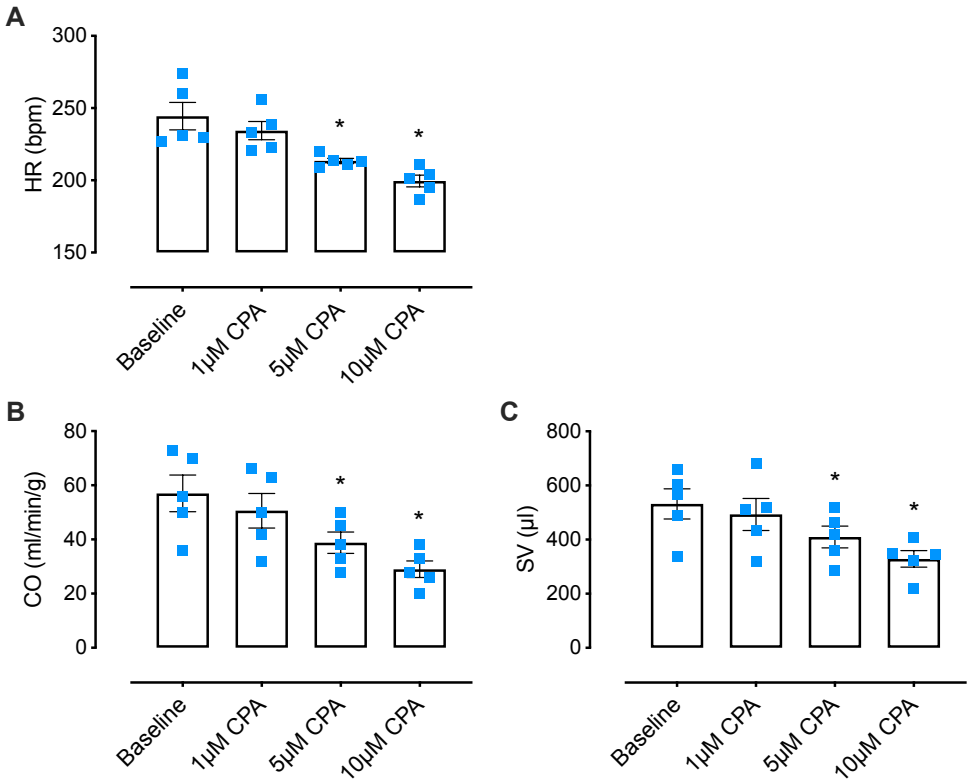

Figure 4.6 Effect of CPA on function in the working heart

Effect of incremental doses (max. 10µM) of cyclopiazonic acid (CPA) on function in the isolated working guinea pig heart. The effects of each dose of CPA on A) heart rate, B) cardiac output and C) stroke volume are shown. Data presented as mean ±SEM, n=5 hearts, * = $p<0.05$ vs. baseline.

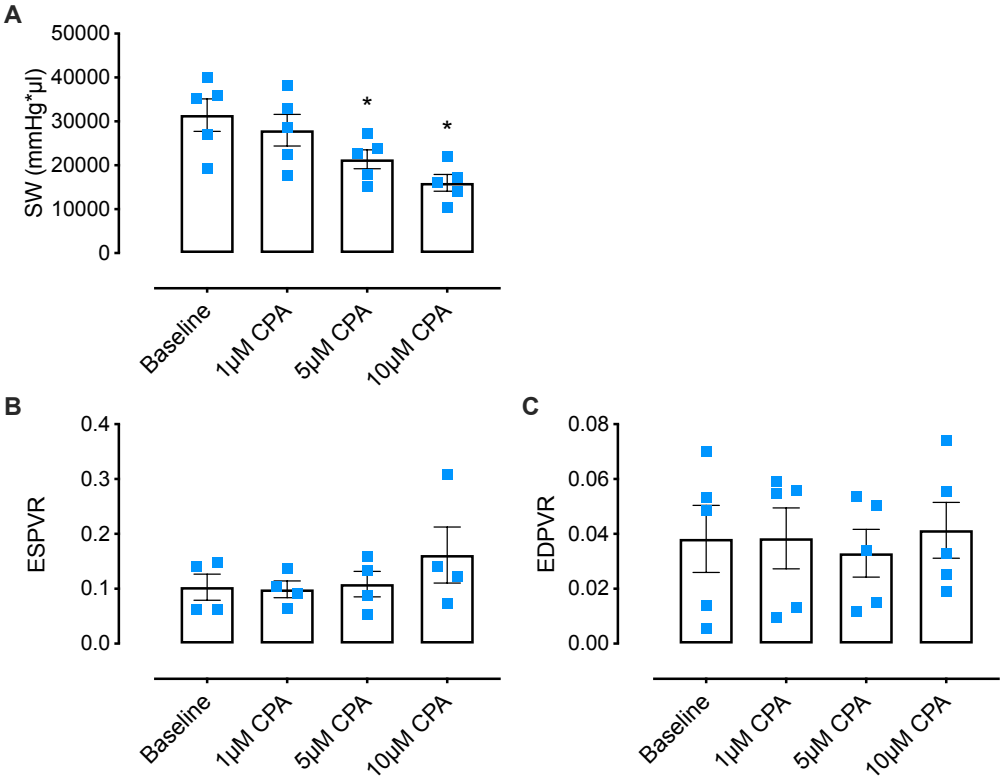

Figure 4.7 Effect of CPA on function in the working heart

Effect of incremental doses (max. 10µM) of cyclopiazonic acid (CPA) on function in the isolated working guinea pig heart, as measured by pressure-volume loop parameters. The effects of each dose of CPA on A) stroke work, B) end systolic pressure-volume relationship and C) end diastolic pressure-volume relationship are shown. Data presented as mean ±SEM, n=4-5 hearts (parameters only recorded if high-quality pressure-volume loops were obtained), * = $p<0.05$ vs. baseline.

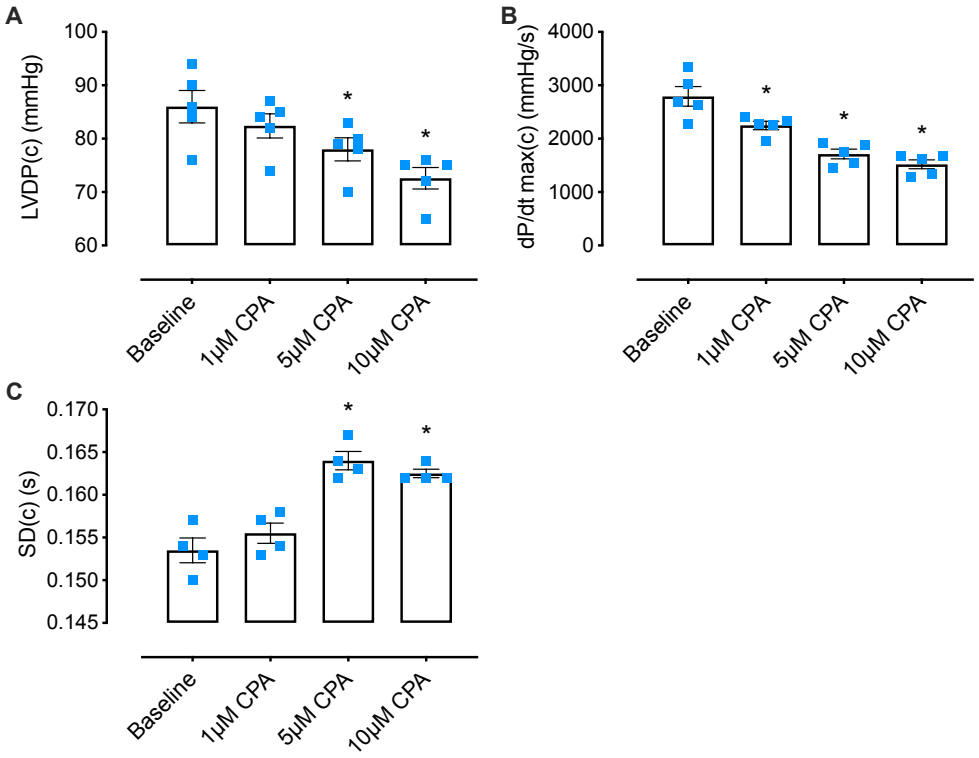

Figure 4.8 Effect of CPA on systolic function in the working heart

Effect of incremental doses (max. 10μM) of cyclopiazonic acid (CPA) on systolic function in the isolated working guinea pig heart. The effects of each dose of CPA on A) LVDP, B) dP/dt max and C) systolic duration. Data presented as mean ±SEM, n=4-5 hearts, * = $p<0.05$ vs. baseline.

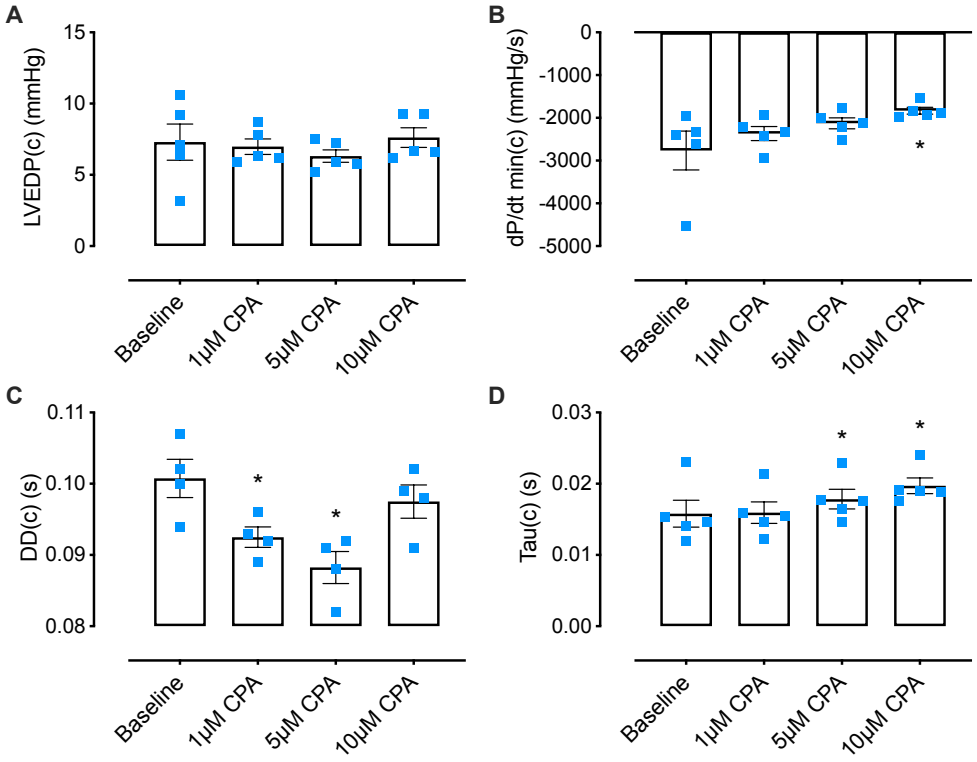

Figure 4.9 Effect of CPA on diastolic function in the working heart

Effect of incremental doses (max. 10μM) of cyclopiazonic acid (CPA) on diastolic function in the isolated working guinea pig heart. The effects of each dose of CPA on A) LVEDP, B) dP/dt min C) diastolic duration and D) tau. Data presented as mean ±SEM, n=4-5 hearts, * = p<0.05 vs. baseline.

4.3.3 Effect of QT Prolongation in the Healthy Working Heart

Treatment with E-4031 and HMR 1556 caused a significant prolongation of QTc interval alongside a significant reduction in heart rate in working guinea pig hearts (Fig. 4.10 A & B). No effects on coronary flow were observed and although a slight but non-significant reduction was seen in cardiac output, stroke volume remained unchanged suggesting that this was a heart rate-dependent effect (Fig. 4.10 C-E).

Prolongation of the AP with E-4031 and HMR 1556 had no effect on systolic function in the working guinea pig heart (Fig. 4.11 A-C). This was apparent from the lack of change in LVDP(c), dP/dt max(c) and SD(c) in response to treatment with E-4031 and HMR 1556.

Diastolic function did demonstrate some change in response to QT prolongation in the working guinea pig heart, independent of effects on heart rate (Fig. 4.12 A-C). Whilst LVEDP(c) showed no change in response to E-4031 + HMR 1556 treatment, DD(c) and tau(c) both showed a significant increase in response to treatment, relative to vehicle control. This was accompanied by a slight but non-significant reduction in dP/dt min(c) and suggests that ventricular relaxation was slowed in response to APD prolongation.

Visualisation of LVP traces from control and E-4031 + HMR 1556-treated hearts reveals that QT prolongation may have resulted in a slight slowing of pressure generation and decline in the LV during all but early pressure development (Fig. 4.13). It should be noted that these LVP traces represent raw data which is not corrected for the effects of variation in heart rate following QT prolongation.

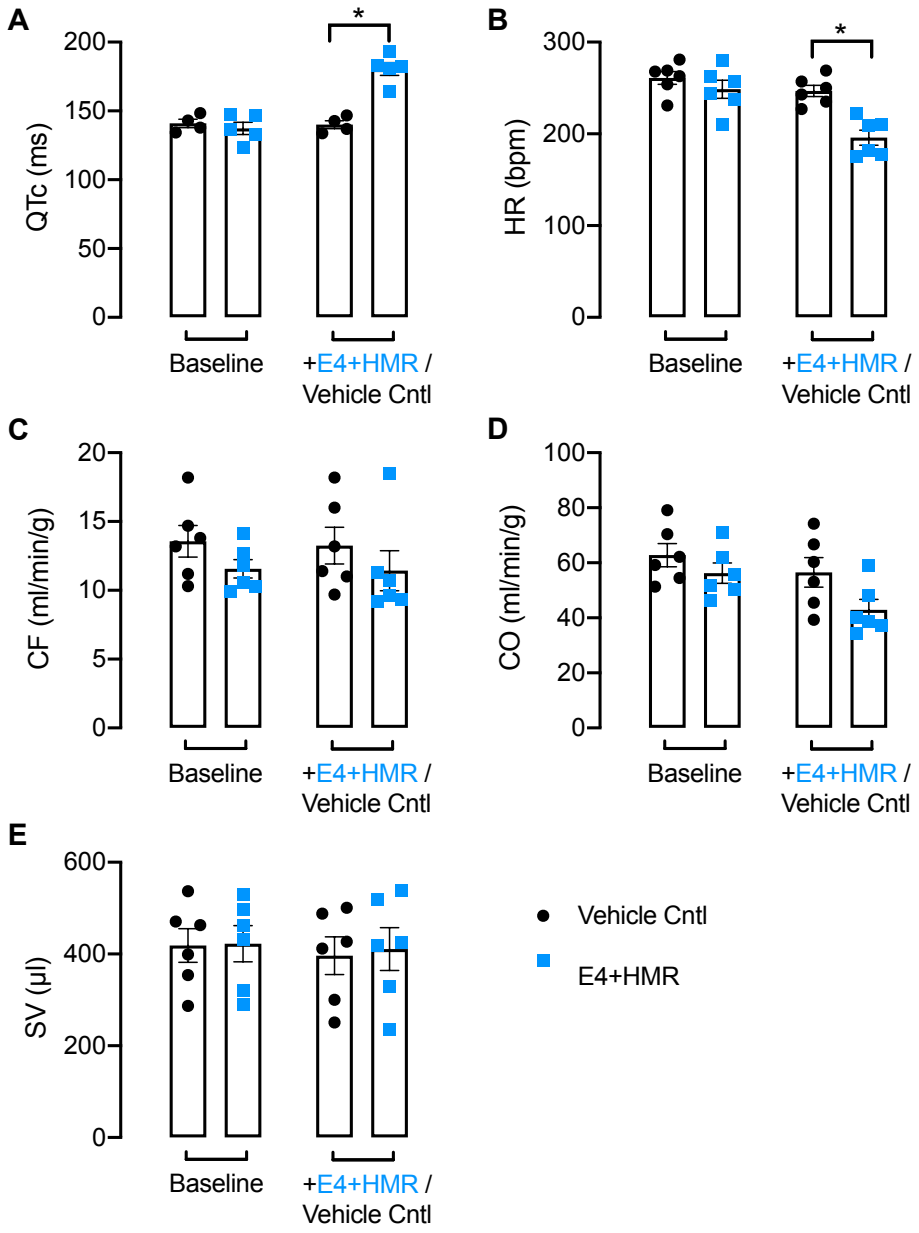

Figure 4.10 Effect of QT prolongation in the healthy working heart

Effect of treatment with 100nM E-4031 + 30nM HMR 1556 vs vehicle control in the healthy working guinea pig heart. Effect of treatment with E-4031+HMR 1556 on A) QTc interval, B) heart rate, C) coronary flow, D) cardiac output and E) stroke volume. Data presented as mean ±SEM, n=6 hearts, * = $p<0.05$ in E-4031 + HMR 1556 vs. vehicle control group.

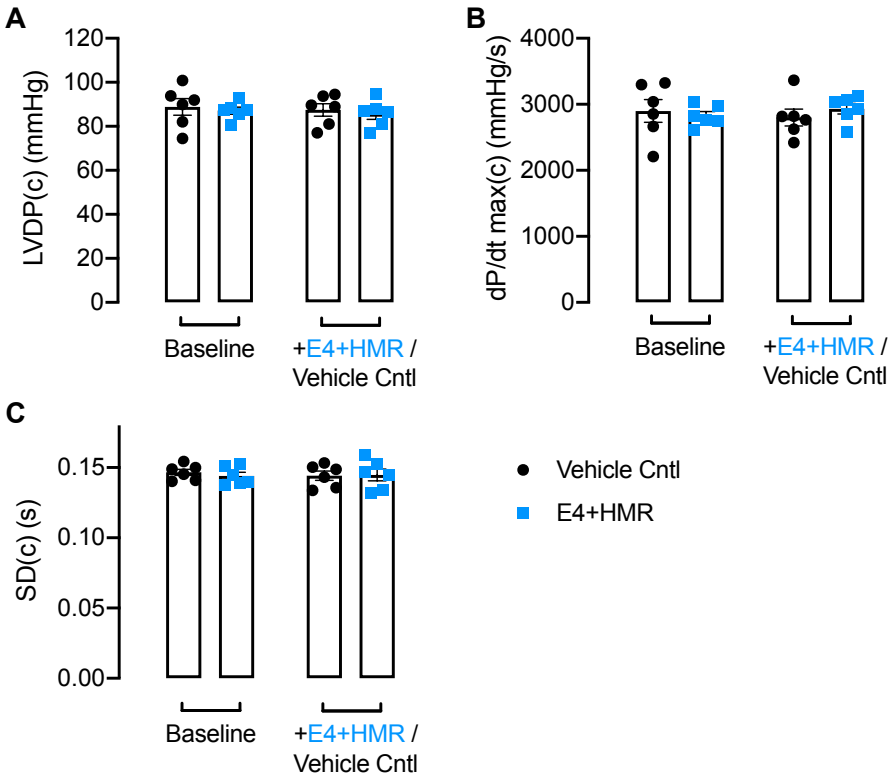

Figure 4.11 Effect of QT prolongation on systolic function in the healthy working heart

Effect of treatment with 100nM E-4031 + 30nM HMR 1556 vs vehicle control on systolic functional parameters corrected for heart rate in the healthy working guinea pig heart. Effect of treatment with E-4031+HMR 1556 on A) LVDP(c), B) dP/dt max(c) and C) systolic duration(c). Data presented as mean ±SEM, n=6 hearts.

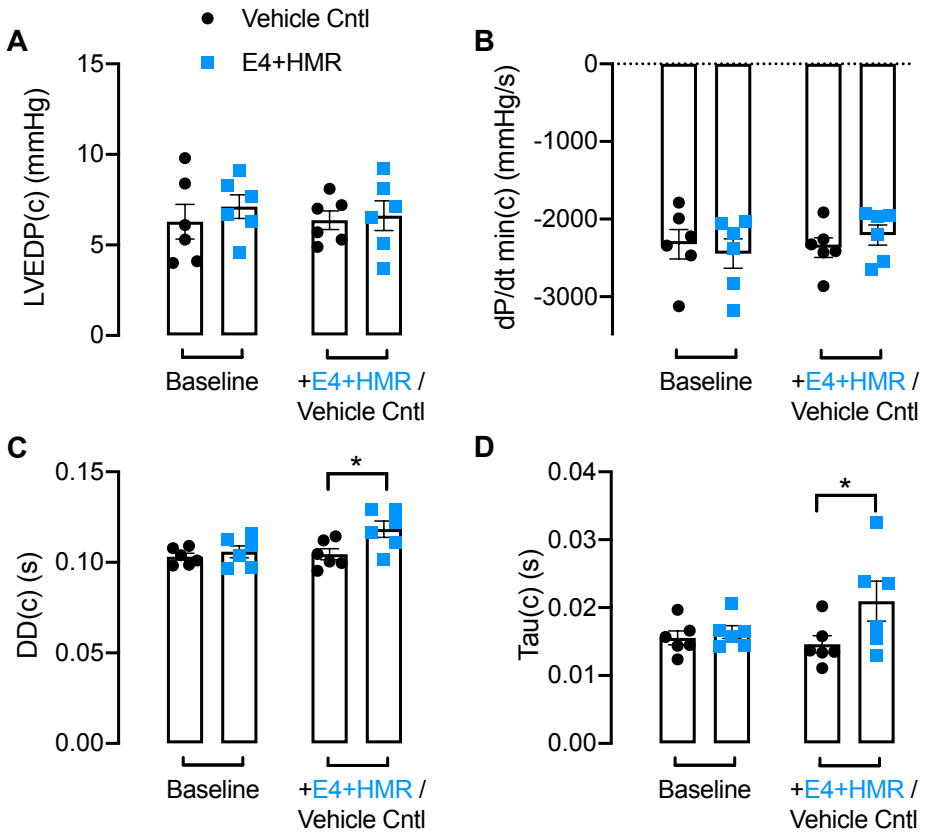

Figure 4.12 Effect of QT prolongation on diastolic function in the healthy working heart

Effect of treatment with 100nM E-4031 + 30nM HMR 1556 vs vehicle control on diastolic functional parameters corrected for heart rate in the healthy working guinea pig heart. Effect of treatment with E-4031+HMR 1556 on A) LVEDP(c), B) dP/dt min(c), C) diastolic duration(c) and D) tau(c). Data presented as mean ±SEM, n=6 hearts, * = $p<0.05$ in E-4031 + HMR 1556 vs. vehicle control group.

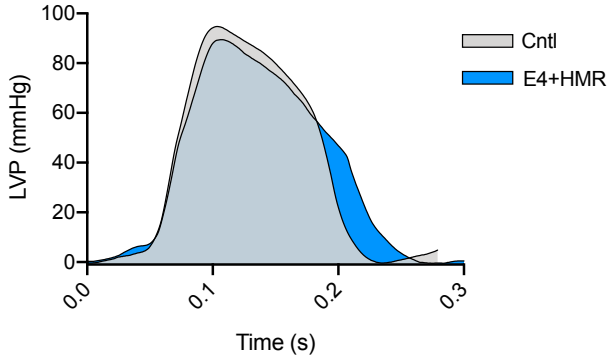

Figure 4.13 Effect of QT prolongation on pressure generation in the left ventricle in the healthy working heart

Representative left ventricular pressure throughout a complete cardiac cycle from working guinea pig hearts treated with 100nM E-4031 + 30nM HMR 1556 or vehicle control (unpaced). Traces aligned to peak LVP to aid visualisation.

4.3.4 Effect of QT Prolongation in the Presence of SERCA Inhibition

Treatment with E-4031 + HMR 1556 in the presence of CPA resulted in a significant increase in QTc and a significant decrease in heart rate relative to vehicle control (Fig. 4.14 A & B). Although treatment with 5µM CPA caused an apparent reduction in coronary flow, cardiac output and stroke volume this did not differ between the experimental groups and there was no further effect of treatment with E-4031 and HMR 1556 on these parameters (Fig. 4.14 C-E).

There was no evident impairment of systolic function in response to QT prolongation in the presence of SERCA inhibition (Fig. 4.15 A-C). Although treatment with CPA resulted in a substantial reduction in dP/dt max(c), there was no further effect of E-4031 and HMR 1556, and no effect of QT prolongation on LVDP(c) or SD(c).

Diastolic function was similarly unaffected by QT prolongation in the presence of SERCA inhibition (Fig. 4.16 A-C). Again, there was an apparent effect of CPA on dP/dt min(c), but no further effect of treatment with E-4031 and HMR 1556. LVEDP(c), DD(c) and tau(c) were similarly unaffected by QT prolongation with E-4031 and HMR 1556, relative to vehicle control.

Visualisation of the LVP traces from E-4031 + HMR 1556-treated hearts reveals a slight slowing of the rate of pressure generation in the left ventricle, alongside a slowing of the early phase of pressure decline compared to control hearts (Fig. 4.17). QT prolongation appeared to have little effect on the maximum rate of pressure decline or LVEDP, although LVDP was slightly reduced. Again, these LVP traces represent raw data which is not corrected for the effects of variation in heart rate following QT prolongation.

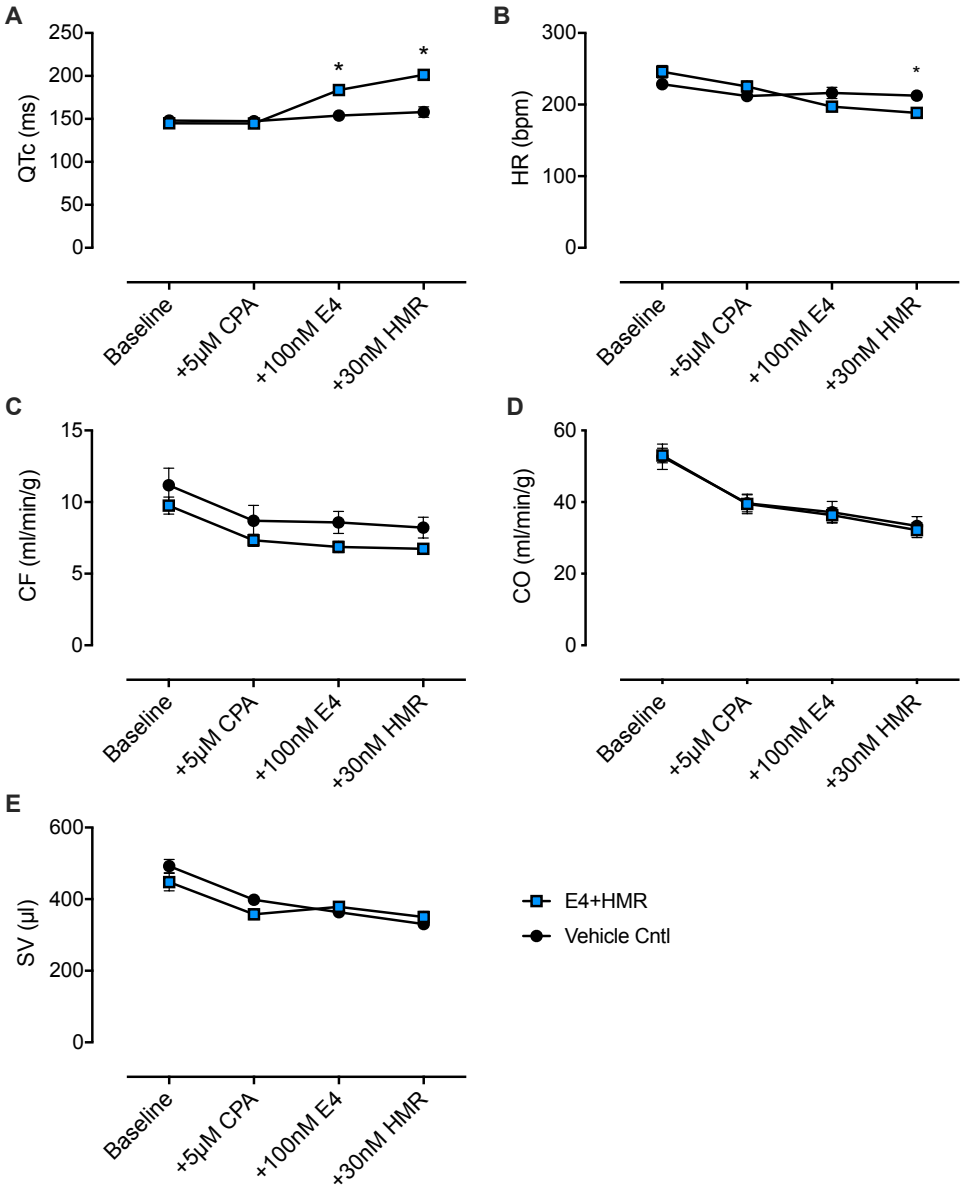

Figure 4.14 Effect of QT prolongation in the presence of SERCA inhibition

Effect of treatment with 100nM E-4031 + 30nM HMR 1556 vs vehicle control in the presence of 5µM cyclopiazonic acid (CPA) in the working guinea pig heart. Effect of treatment with E-4031+HMR 1556 on A) QTc interval, B) heart rate, C) coronary flow, D) cardiac output and E) stroke volume in the presence of SERCA inhibition. Data presented as mean ±SEM, n=6 hearts, * = $p<0.05$ in E-4031 + HMR 1556 vs. vehicle control group.

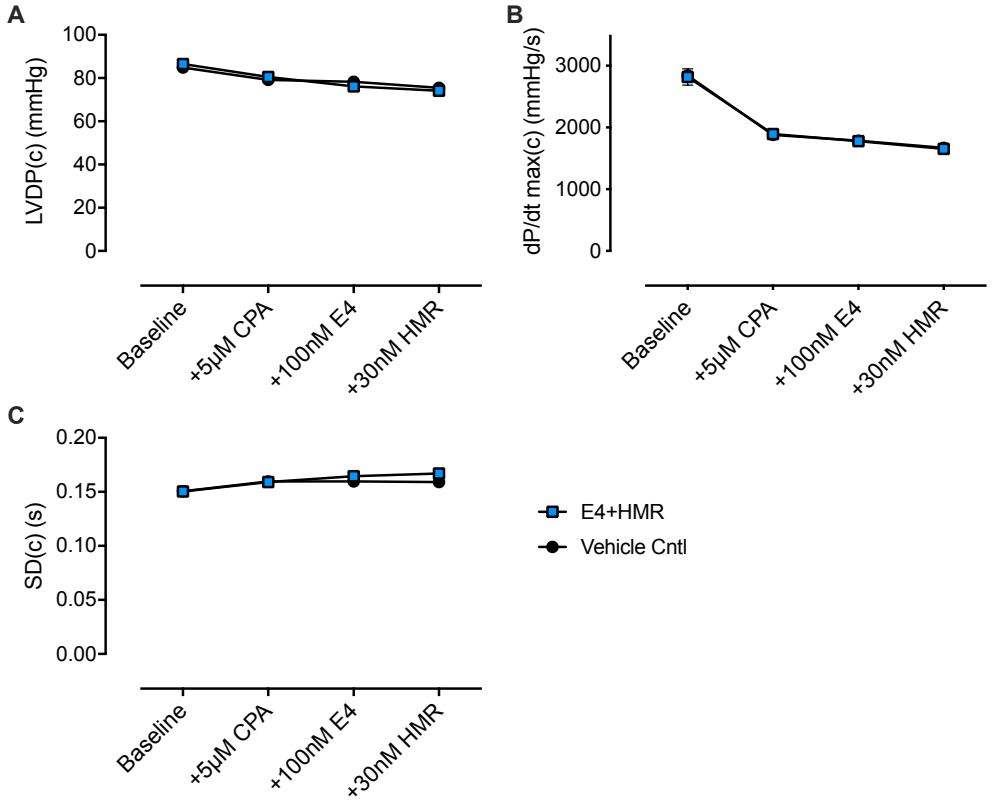

Figure 4.15 Effect of QT prolongation on systolic function in the presence of SERCA inhibition

Effect of treatment with 100nM E-4031 + 30nM HMR 1556 vs vehicle control on systolic functional parameters corrected for heart rate in the presence of 5μM cyclopiazonic acid (CPA) in the working guinea pig heart. Effect of treatment with E-4031+HMR 1556 on A) LVDP(c), B) dP/dt max(c) and C) systolic duration(c). Data presented as mean ±SEM, n=6 hearts.

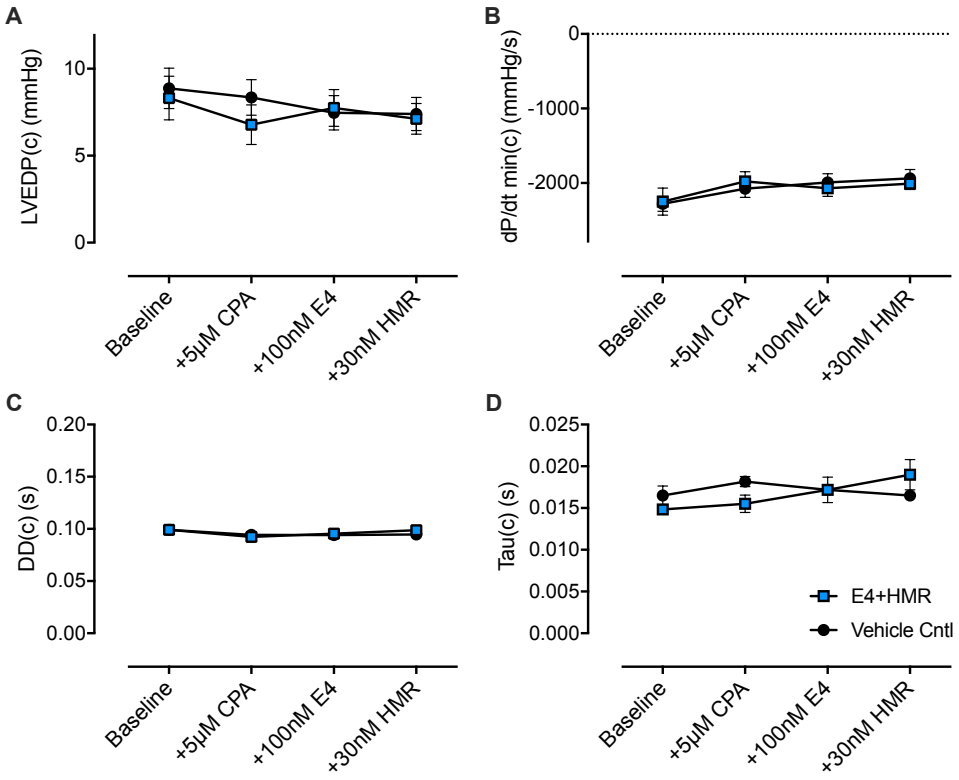

Figure 4.16 Effect of QT prolongation on diastolic function in the presence of SERCA inhibition

Effect of treatment with 100nM E-4031 + 30nM HMR 1556 vs vehicle control on diastolic functional parameters corrected for heart rate in the presence of 5μM cyclopiazonic acid (CPA) in the working guinea pig heart. Effect of treatment with E-4031+HMR 1556 on A) LVEDP(c), B) dP/dt min(c), C) diastolic duration(c) and D) tau(c). Data presented as mean ±SEM, n=6 hearts.

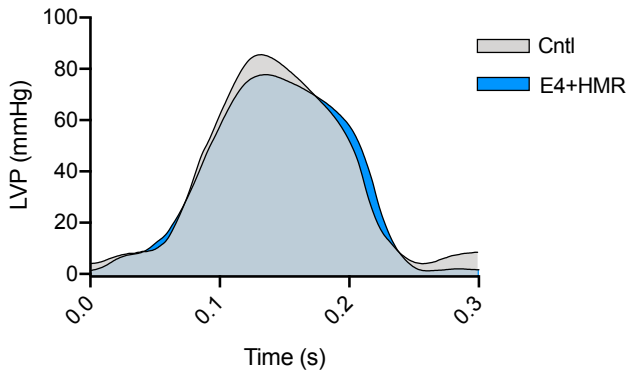

Figure 4.17 Effect of QT prolongation on pressure generation in the left ventricle in the presence of SERCA inhibition

Representative left ventricular pressure throughout a complete cardiac cycle from hearts treated with 5μM cyclopiazonic acid (CPA) and 100nM E-4031 + 30nM HMR 1556 or vehicle control on working guinea pig hearts (unpaced). Traces aligned to peak LVP to aid visualisation.

4.3.5 Effect of QT Prolongation in the Presence of SERCA Inhibition and Elevated Intracellular Sodium

Treatment of working guinea pig hearts with ouabain resulted in a modest positive inotropic effect (Fig. 4.18 A-F). Heart rate demonstrated an increase at 200nM concentrations, and this was accompanied by a modest increase in cardiac output in the absence of any significant effect on stroke volume. The rate of pressure development was also affected by ouabain treatment, with dP/dt max showing an increase at both concentrations. Although not significant, an increase in LVDP was also observed at both concentrations of ouabain alongside a significant decrease in systolic duration. Altogether, these changes are indicative of a positive inotropic effect of ouabain treatment, which was greater at a 200nM concentration.

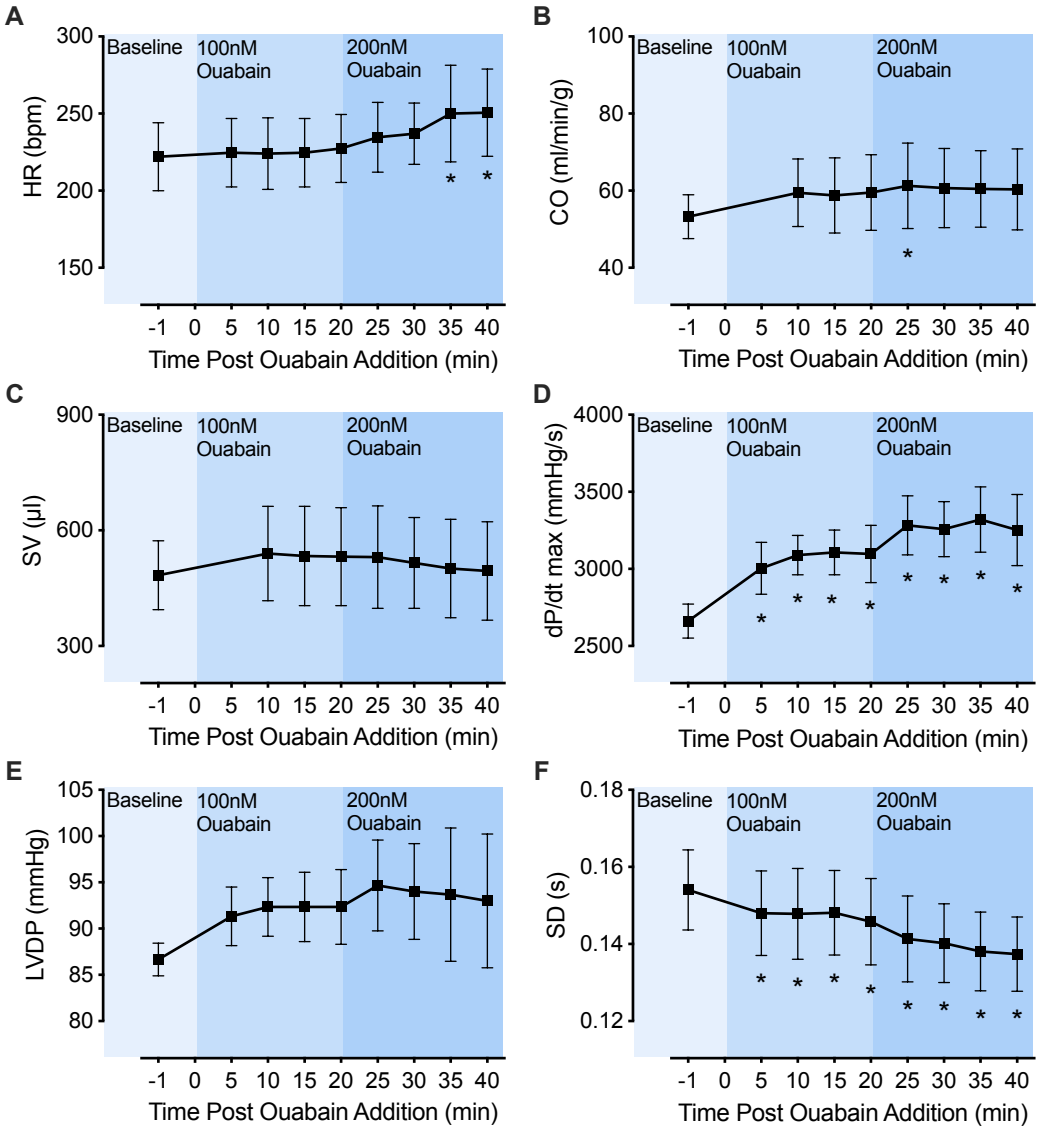

Figure 4.18 Effect of ouabain treatment on systolic function of the working heart

Effect of treatment with incremental doses of ouabain (max. 200nM) on systolic function in the working guinea pig heart. Effect of treatment with ouabain on A) heart rate, B) cardiac output, C) stroke volume, D) dP/dt max, E) LVDP and F) systolic duration. Data presented as mean ±SEM, n=3 hearts, * = $p<0.05$ vs. baseline.

Treatment with E-4031 and HMR 1556 in the presence of SERCA inhibition and elevated intracellular sodium resulted in an increase in QTc in the absence of any effects on heart rate (Fig. 4.19 A & B). Initial treatment with CPA and ouabain resulted in an apparent decrease in heart rate, coronary flow, cardiac output and stroke volume (Fig. 4.19 B-E). There was no apparent further effect of prolonging QT interval on these parameters, and

although coronary flow was significantly different between E4+HMR and vehicle control groups at the last time point, this may have arisen due to a difference between the groups at baseline (Fig. 4.19 C).

A slight effect on systolic function was observed in response to prolongation of QTc by E-4031 and HMR 1556 in the presence of SERCA inhibition and elevated intracellular sodium (Fig. 4.20 A-C). Whilst no effect of CPA + ouabain treatment was observed on LVDP(c) or SD(c), a modest decrease in dP/dt max(c) was observed. Treatment with E- 4031 and HMR 1556 resulted in a modest but significant increase in SD(c) relative to vehicle control, suggestive of an increased contraction time in the LV and possible mild systolic impairment.

Diastolic function was unaffected by QT prolongation in the presence of SERCA inhibition and elevated intracellular sodium (Fig. 4.21 A-C). Treatment with CPA and ouabain appeared to result in a decrease in dP/dt min(c), alongside a modest increase in DD(c) and tau(c). Upon subsequent prolongation of QTc by treatment with E-4031 and HMR 1556, there was no effect on any of the measured diastolic parameters relative to vehicle control.

Visualisation of the LVP traces from control and E-4031 + HMR 1556-treated hearts reveals little effect of QT prolongation on LVDP/LVEDP or on the maximal rates of pressure increase or decline in the LV, in agreement with the reported average results (Fig. 4.22). Again, there does appear to be a slowing of the early phase of pressure decline in the LV following QT prolongation in the E4 + HMR group relative to vehicle control.

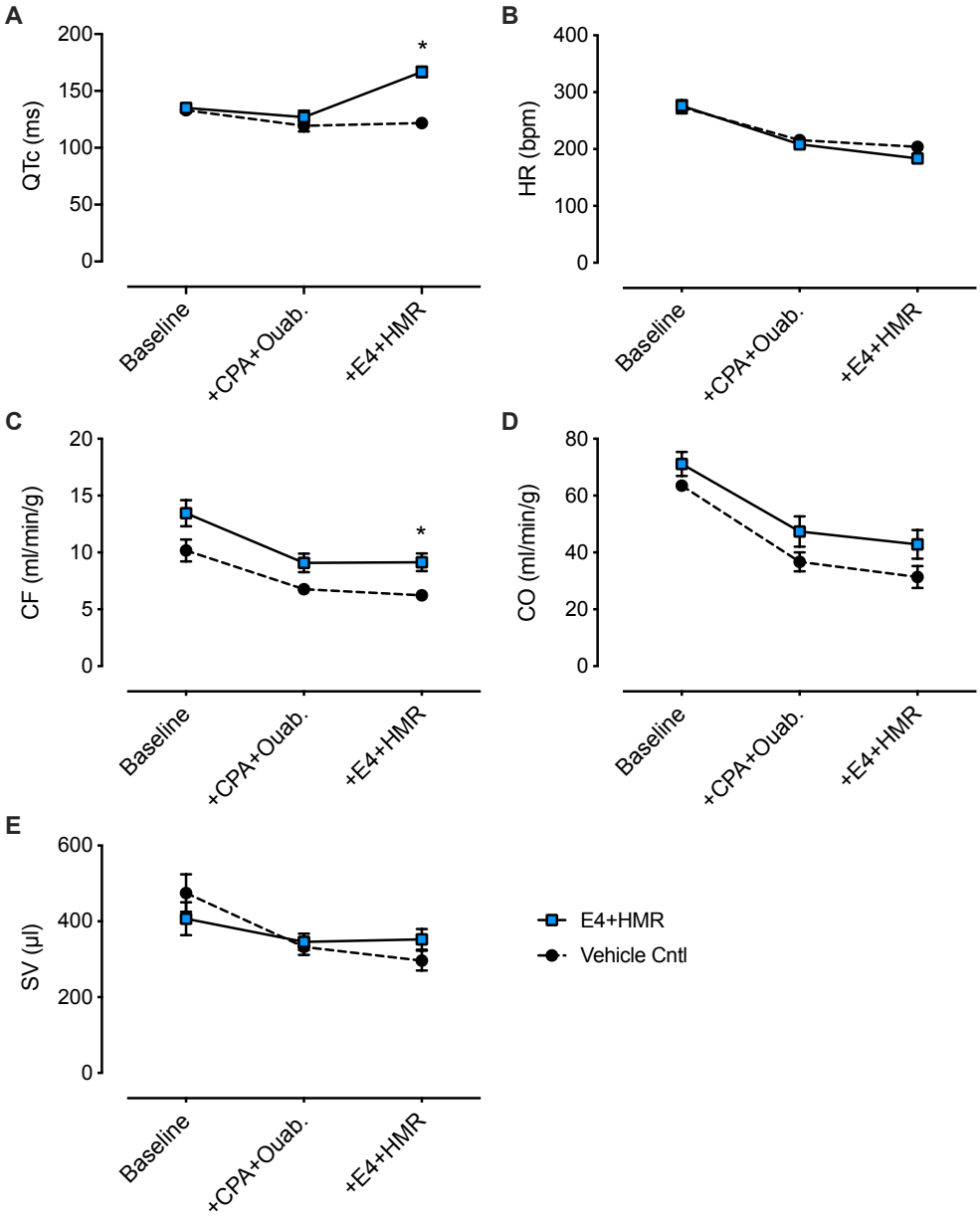

Figure 4.19 Effect of QT prolongation in the presence of SERCA inhibition and elevated intracellular sodium

Effect of treatment with 100nM E-4031 + 30nM HMR 1556 vs vehicle control in the presence of 5µM cyclopiazonic acid (CPA) and 200nM ouabain in the working guinea pig heart. Effect of treatment with E-4031+HMR 1556 on A) QTc interval, B) heart rate, C) coronary flow, D) cardiac output and E) stroke volume in the presence of SERCA inhibition and elevated intracellular sodium. Data presented as mean ±SEM, n=6 hearts, * = $p<0.05$ in E-4031 + HMR 1556 vs. vehicle control group.

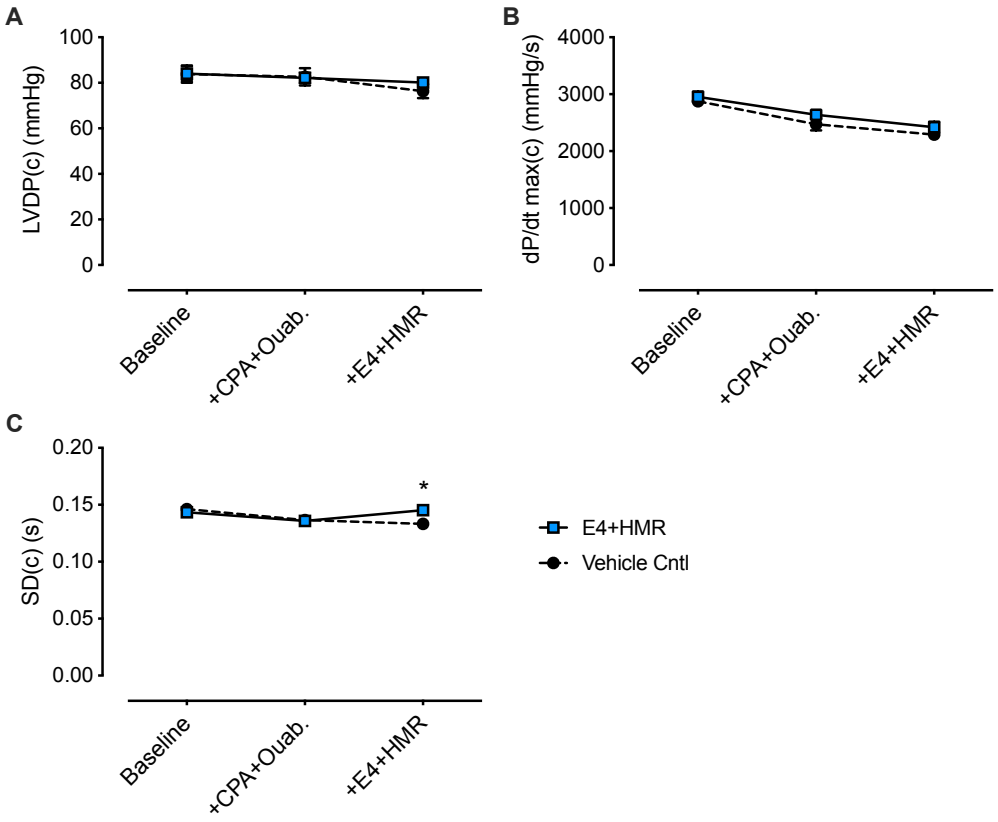

Figure 4.20 Effect of QT prolongation on systolic function in the presence of SERCA inhibition and elevated intracellular sodium

Effect of treatment with 100nM E-4031 + 30nM HMR 1556 vs vehicle control on systolic functional parameters corrected for heart rate in the presence of 5μM cyclopiazonic acid (CPA) and 200nM ouabain in the working guinea pig heart. Effect of treatment with E-4031+HMR 1556 on A) LVDP(c), B) dP/dt max(c) and C) systolic duration(c). Data presented as mean ±SEM, n=6 hearts, * = $p<0.05$ in E-4031 + HMR 1556 vs. vehicle control group.

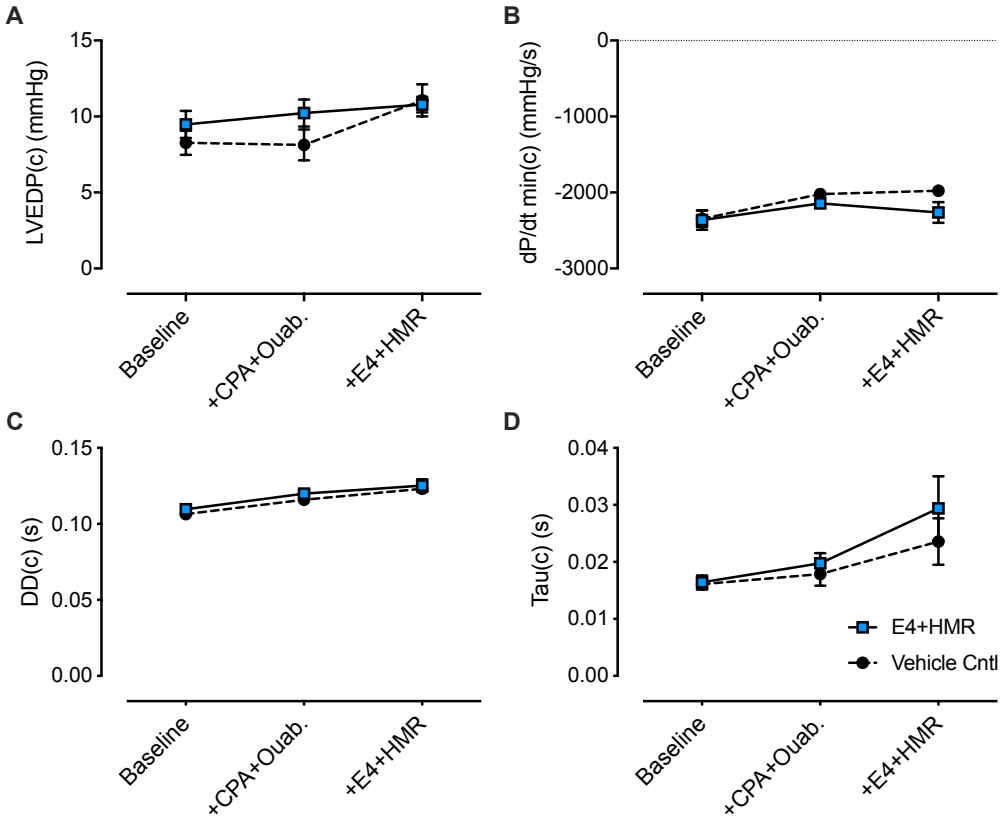

Figure 4.21 Effect of QT prolongation on diastolic function in the presence of SERCA inhibition and elevated intracellular sodium

Effect of treatment with 100nM E-4031 + 30nM HMR 1556 vs vehicle control on diastolic functional parameters corrected for heart rate in the presence of 5μM cyclopiazonic acid (CPA) and 200nM ouabain in the working guinea pig heart. Effect of treatment with E-4031+HMR 1556 on A) LVEDP(c), B) dP/dt min(c), C) diastolic duration(c) and D) tau(c). Data presented as mean ±SEM, n=6 hearts.

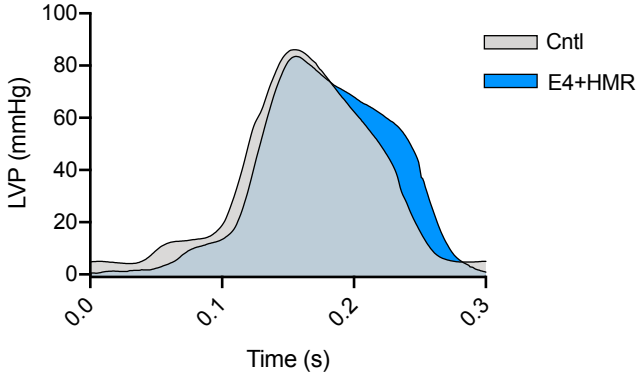

Figure 4.22 Effect of QT prolongation on pressure generation in the left ventricle in the presence of SERCA inhibition and elevated intracellular sodium

Representative left ventricular pressure throughout a complete cardiac cycle from working guinea pig hearts treated with 5μM cyclopiazonic acid (CPA) and 200nM ouabain in the presence of 100nM E-4031 + 30nM HMR 1556 or vehicle control. Traces aligned to peak LVP to aid visualisation.

4.4 Discussion

4.4.1 Characterisation of the Working Guinea Pig Heart

The working guinea pig heart was found to provide a physiological and stable model which circumvented the need to pace hearts during protocols, avoiding the issues associated with this approach. The admittance catheter provided high-fidelity data, allowing for detailed assessment of LV function.

One issue which was encountered with this experimental setup related to the use of the admittance catheter and the calculation of volume within the left ventricle. Calculation of volume using admittance catheters relies in part upon knowing the resistivity of the blood within the left ventricle.[136] Although this can be measured and inputted into the hardware for use in this calculation, it was discovered that the resistivity of the physiological crystalloid buffer used in these experiments differed from blood to the extent that it lay outside the range allowed for by the software on the ADV500 PV System used, rendering the system unable to calculate volumes accurately. As this problem could not be resolved without making the system permanently unsuitable for use *in vivo*, it was decided to

continue experiments with raw pressure-conductance (uncalibrated volume) loops, rather than pressure-volume loops. Stroke volume could still be calculated based on cardiac output, and so this did not affect the scope of data available from studies to a large extent, with the exception of not being able to calculate EF.

The ivabradine study provided a good insight into the relationship between heart rate and various parameters in the working heart preparation, and informed future studies. Using this approach, it was possible to develop a formula which allowed functional/electrophysiological variables to be corrected for variation in heart rate in subsequent studies. This was particularly important given that the interventions used were known to affect heart rate and so differences between groups could be related to changes in heart rate rather than the intervention per se. This study also highlighted that Tp-Te, which is often used as a measure of ventricular dispersion of repolarisation,[66, 87] was not reliable as a means of measuring changes in repolarisation in this preparation. This was due to morphological variability in the T wave recorded in the ECG's which occurred between hearts and between experimental protocols, often making it difficult to determine the peak of the T wave. However, QT interval was unaffected by this and QTc was therefore used to measure changes to repolarisation. This had the added benefit of providing a surrogate for APD which was useful when comparing data to existing studies which may use APD or QT interval as a readout for ventricular repolarisation.

The next question which was addressed when characterising the working guinea pig heart was how dysfunction could be measured, i.e. which functional variables would provide sensitive and reliable detection of changes to systolic and diastolic function? This was addressed by treating healthy hearts with incremental doses of CPA to impair SERCA activity, which would act to impair both systolic and diastolic function.[140-142] This enabled various parameters to be measured and their sensitivity to dysfunction determined by looking at the effects of CPA at increasing doses, as well as allowing an appropriate dose of CPA to be identified for use in later studies. The results demonstrate that the effects of CPA are easily apparent from basic cardiac parameters such as heart rate, cardiac output and stroke volume. However, when looking at data from 'pressure-volume' loops, changes to stroke work precisely mirrored those seen in cardiac output and stroke volume and therefore did not provide further useful information. When looking at the ESPVR and

EDPVR obtained from preload occlusions, no change in systolic and diastolic function was apparent using this approach. Indeed, the ESPVR did not successfully detect systolic impairment at any concentration of CPA and it was found that the LabChart PV loop analysis module was not able to reliably identify the true end systolic point, given the more sloping appearance of the ejection phase from loops obtained in the working heart. Similarly, the reported EDPVR using this approach was found to be so variable as to be unable to detect any change in diastolic function. Therefore, these loop parameters were not considered to be the best method of assessing changes to ventricular function in studies going forward. Parameters collected from the LV pressure trace, on the other hand, were found to provide much better sensitivity in detecting functional changes as a result of CPA treatment. To measure systolic function, LVDP, dP/dt max and systolic duration (all corrected for heart rate) were all able to detect the impairment of systolic function with CPA treatment, with dP/dt max appearing to be the most sensitive, showing a significant reduction from the lowest concentration of CPA. The results for diastolic function appeared to be a little more complicated, with LVEDP(c) found to be somewhat variable and unable to detect changes to diastolic function. Corrected dP/dt min and tau both demonstrated a concentration-dependent effects of CPA treatment indicating a slowing of relaxation, with tau appearing to be the most sensitive. However, corrected diastolic duration demonstrated a perhaps unexpected reduction with CPA treatment which was lost at the highest concentration. This may be indicative of a slowed rate/initiation of contraction due to reduced SR calcium release, thereby causing a delay in the onset of relaxation. This would tie in with the increase in systolic duration observed but does not explain why the effect on diastolic duration was lost at the highest concentration of CPA, perhaps demonstrating that this parameter is not a reliable indicator of diastolic impairment.

One point of note is the morphological change observed in the LVP traces in working hearts following treatment with E-4031 and HMR 1556. It appears as though QT prolongation results in a slowing of the first portion of pressure decline in the LV following peak systolic pressure. It is likely that this portion of the cardiac cycle relates to the ejection phase during systole, prior to closure of the aortic valve. This is supported by the fact that the working heart rig operates at a fixed afterload of 55mmHg, which

coincides with the approximate pressure at which this slowed phase of LVP decline increases again. Therefore, this observation relates to reduced contractility rather than impaired active relaxation and is not detected by variables such as dP/dtmin and LVEDP, which measure effects during later portions of the cardiac cycle. As such, these variables likely provide a good measure of changes to active relaxation and so are ideal for the purposes of the present study. It is likely that these changes to contractility following treatment with E-4031 and HMR 1556 can be explained by the reduction in heart rate following QT prolongation in these hearts resulting in reduced cardiac contractility, owing to the positive force-frequency response in the guinea pig heart. This ties in with the general lack of changes in measured systolic variables, which were corrected for differences in heart rate.

Therefore, the present study was able to establish that the working guinea pig heart demonstrated improved physiological function over the Langendorff-perfused heart. A comprehensive characterisation study making use of ivabradine and atrial pacing in healthy hearts was able to reveal the relationship between variables of interest and heart rate, allowing the creation of a formula to calculate corrected values obtained in subsequent unpaced studies and account for differences in heart rate. A further characterisation study using CPA to impair cardiac function was able to identify which parameters obtained using the admittance catheter were best able to detect impairment of systolic and diastolic function, and so represented suitable parameters to examine in future studies. Therefore, the working guinea pig heart setup used in these studies has been thoroughly characterised and determined to be a more suitable model to conduct studies going forward in order to address the remaining research questions.

4.4.2 Relationship between QT Interval and Cardiac Function

Given the change of experimental model it was necessary to repeat the baseline study to examine the relationship between QT interval and diastolic function in the healthy isolated heart. The findings in the working heart differed from those in the Langendorff-perfused heart, highlighting the difference in these preparations. In the working heart prolongation of the QT interval had no impact on systolic function but did result in an increase in corrected diastolic duration and tau, indicating a slowing of ventricular

relaxation. This is in agreement with studies in healthy isolated ventricular myocytes that have shown a slowing in the onset and rate of decline of the calcium transient with subsequent slowing of relaxation in response to prolonged APD.[43] This has been proposed to occur due to various factors, including a delay in the closing of L-type calcium channels, and an increased calcium influx/reduced calcium efflux via NCX in response to the prolonged membrane depolarisation.[24, 43] Therefore, the results from this study support the hypothesis that repolarisation abnormalities such as prolonged APD/delayed repolarisation can impair ventricular relaxation by delaying or reducing cytosolic calcium removal.

Since the data from the baseline study in the working heart differs to that observed in the Langendorff-perfused heart, it was important to repeat the study which aimed to examine the relationship between QT prolongation and diastolic function in the presence of reduced SERCA activity, as is often observed in HF.[58, 59, 110-112] The dose of CPA used to achieve this was informed from the CPA characterisation study carried out in working hearts and was higher than that used previously in Langendorff-perfused hearts (5μM vs. 1μM), since it was apparently better-tolerated in the working heart. The chosen dose caused detectable systolic and diastolic dysfunction without being so severe as to risk impaired coronary flow due to excessive reduction of cardiac output. Under these conditions, prolongation of QT interval using the same concentration of E-4031 and HMR 1556 as in the baseline study caused no detectable impairment to systolic or diastolic function, relative to control. This is perhaps surprising, since it might be assumed that inhibition of SERCA activity would exacerbate the slowing of relaxation observed in the baseline study which presumably occurred as a result of altered intracellular calcium handling. Based on the experimental hypothesis, impaired relaxation as a result of prolonged APD would occur because of a delayed or slowed removal of calcium from the cytosol, thereby impeding myofilament dissociation and relaxation. A reduction in the activity of SERCA should act to compound this by further reducing the removal of cytosolic calcium. However, it is also possible that this effect is balanced out by reduced SR loading as a result of SERCA inhibition in this setting. Perhaps this slowed relaxation is no longer seen in this study because the impaired SERCA activity results in smaller SR stores and a subsequent smaller release of calcium. This resultant smaller calcium

transient (which is evident from the reduced LVDP(c) in response to CPA treatment) may be able to be removed at a sufficient rate so as not to impede relaxation in the ventricle.

Given that it is known that APD prolongation and reduced SERCA activity/expression are commonly reported alongside diastolic impairment in HF, it is perhaps the case that the model used in the above study did not sufficiently replicate the failing heart for the true relationship between repolarisation and diastolic function to be determined. Another commonly reported abnormality in failing hearts is elevated intracellular sodium.[53-55] This may act to further impair intracellular calcium handling by altering the activity of NCX, thereby working to decrease calcium extrusion or even increase calcium influx via this mechanism as a result of the altered sodium gradient across the sarcolemmal membrane.[57] Given that the combination of reduced SERCA activity and elevated intracellular sodium could interact to further perturb intracellular calcium handling, it was important to conduct a study which would combine these factors in the presence of abnormal repolarisation. In order to achieve this, a combination of ouabain and CPA was used to elevate intracellular sodium and impair cytosolic calcium removal by reducing N^+,K^+-ATPase and SERCA activity.

An initial study using ouabain alone was used to identify an appropriate dose of ouabain to use in the isolated working guinea pig heart that would elevate intracellular sodium (as confirmed by the presence of positive inotropy). A concentration of 200nM was selected for use in further studies since this demonstrated a mild positive inotropy and higher doses (300nM) were found to cause most hearts to go into ventricular fibrillation. When hearts were treated with E-4031 and HMR 1556 to prolong QT interval in the presence of both elevated intracellular sodium and impaired SERCA activity in a subsequent study, there was little evidence of any impairment of cardiac function. This was with the exception of a modest increase in corrected systolic duration, indicating a possible mild systolic impairment, although this was not accompanied by any change in LVDP(c) or dP/dtmax(c) that would give confidence in this observation. Therefore, although baseline studies did appear to show an effect of prolonging APD on diastolic function in the working heart, this effect was absent when common co-pathologies of HF were pharmacologically induced alongside QT prolongation. This may reflect the interplay between the systolic and diastolic functional effects of impairing SERCA activity, i.e.

both will be affected since both cytosolic calcium removal and SR calcium stores will be reduced. The reduction in the size of the calcium transient may enable cardiomyocytes to cope with a larger influx of calcium due to prolonged APD without relaxation becoming impaired. Elevation of intracellular sodium and the resultant effects on NCX activity may not be enough to counteract these effects on SR calcium stores, and as such will not change the fact that APD prolongation is insufficient to impair intracellular calcium handling and induce diastolic dysfunction in this setting.

4.4.3 Limitations of this Experimental Approach

Although the present study has established that the working guinea pig heart represents a stable experimental model which displays good physiological function, it is unclear whether these experiments have disproven the hypothesis or merely not succeeded in pharmacologically replicating key elements of HF. Whilst it can be assumed with some confidence that CPA and ouabain treatment resulted in impaired SERCA activity and elevated intracellular sodium, what cannot be known is the relative effect size compared to that observed in HF. This could be critical in how these factors interact with alterations to repolarisation and affect the calcium transient. Additionally, not all factors commonly reported in HF could be replicated. One other change that is commonly reported is an increase in NCX expression, which can contribute to altered calcium handling in HF by increasing calcium entry into the cell via reverse-mode function.[143, 144] Indeed, this could be central to the hypothesis and explain some of the results thus far, since an increase in calcium entry via this mechanism could override the reduced calcium release from depleted SR stores. This could potentially exacerbate delayed calcium removal from the cell as a result of prolonged APD and reduced SERCA activity and may have altered the outcome of the present studies if this could have been replicated. Additionally, many other factors which contribute to intracellular calcium handling in the ventricular myocardium could be affected in HF and may affect the relationship between repolarisation and relaxation. These include factors which would be affected by altered phosphorylation status in a diseased heart (e.g. as a result of the increased β-adrenergic signalling often seen[145, 146]) and include altered phosphorylation of calcium handling proteins such as L-type calcium channels, ryanodine receptors and phospholamban, as well as factors like myofilament calcium sensitivity and titin phosphorylation. Additionally, structural

remodelling of the heart (including hypertrophy and fibrosis) is likely to play a key role in impaired relaxation.

4.4.4 Summary and Conclusions

The working guinea pig heart has been shown to provide a good experimental model in which changes to systolic and diastolic function can be detected. There is some evidence that prolongation of APD in this model causes impairment of diastolic function in the absence of other impairments to intracellular calcium handling. However, attempts to replicate common co-pathologies of HF using pharmacological means in this model have not yielded clear answers to the research questions posed. There is a clear need to elaborate on these findings and investigate the relationship between repolarisation abnormalities and diastolic function in failing hearts which will more accurately represent the broad range of pathological changes which affect intracellular calcium handling and are commonly observed in HF. Therefore, an animal model of HF with diastolic dysfunction will be developed in order to achieve this.

5 *IN VIVO* STUDIES

5.1 Introduction

One of the major challenges associated with understanding the mechanisms behind HFpEF is the identification and characterisation of a suitable animal model. The literature reveals HFpEF to be a very heterogeneous condition, with a broad patient demographic presenting with a range of comorbidities (Section 1.1.1). This is also apparent in the lack of effect of novel therapies investigated in clinical trials and may be partially attributable to the failure to identify suitable patient groups for a therapy, with patient cohorts either being too broad or too narrow in their definitions (Section 1.1.2). Developing an animal model which encompasses the myriad of conditions associated with HFpEF is clearly not practical, but it is important to choose a model which displays appropriate cardiac features when planning experiments to explore the underlying mechanisms of diastolic dysfunction.

One model which has been proposed to provide a good model of HFpEF is the DOCA-salt rodent model. This model has typically been used to study hypertension in rats and mice but has also been shown to progress into cardiac hypertrophy and failure with suitable dose and duration of exposure to DOCA, combined with a high salt intake exacerbated by the removal of one kidney. It has been demonstrated that, in mice, this model displays many of the features associated with HFpEF including preserved EF, reduced E/e', elevated LVEDP and increased slope of the EDPVR.[147] Interestingly, this model has also been shown to produce cardiac hypertrophy and clinical signs of HF in the guinea pig, although no functional cardiac studies were performed.[148, 149] Given the advantages of using a guinea pig model when studying cardiac repolarisation abnormalities (Section 3.1) and the stated suitability of the DOCA-salt model in mice from the literature,[147] it was decided to establish and characterise a guinea pig DOCA-salt model of diastolic dysfunction and HF in which to further explore the relationship between ventricular repolarisation and diastolic function in the failing heart.

Since the guinea pig DOCA-salt model is not well established and no functional data is available to characterise disease progression, it was important to generate data to address this during the development of this model as a novel model of HFpEF. Functional changes to diastolic function can be monitored *in vivo* using cardiac ultrasound, with such data forming a critical part of the diagnostic criteria for HFpEF clinically.[6] Certain cardiac ultrasound parameters have been reported to be particularly indicative of diastolic dysfunction in murine models of HF. These include left atrial area (LAA) and isovolumic relaxation time (IVRT), both of which will increase in response to impaired active relaxation in the left ventricle.[150] These parameters, along with other systolic and diastolic functional markers, were monitored during disease progression in the guinea pig DOCA-salt model so that comparisons to the literature concerning patients and animal models with diastolic dysfunction could be made. See Table 5.1 for details. It is not known whether the guinea pig DOCA-salt model demonstrates abnormalities of cardiac repolarisation with disease progression, as is often observed in HFpEF patients.[12, 86, 87] To address this, QTc interval was monitored in both conscious animals using radiotelemetry, and in anaesthetised animals during the collection of cardiac ultrasound data. Since hypertension is another well-established comorbidity of HFpEF[6] and feature of the rodent DOCA-salt model,[147, 149, 151] blood pressure was also monitored throughout the study in conscious telemetered animals.

Having characterised the progression to cardiac dysfunction and hypertension in the guinea pig DOCA-salt model *in vivo*, further studies were conducted using isolated hearts and ventricular tissue to determine whether other common features of HF were present and test how *ex vivo* cardiac function compared to healthy hearts. One of the key features which a suitable model of HF with diastolic function should demonstrate is changes to the activity and/or expression of proteins involved in intracellular calcium handling. In the literature, this has been reported to involve a reduction in SERCA expression, which may also be associated with reduced SERCA activity as result of reduced phospholamban phosphorylation.[58, 59, 110-112] The expression levels of NCX have also been reported to be increased in some models of HF, with resultant implications for calcium handling (Section 1.2.4). Changes to the expression of proteins involved in calcium handling have not previously been reported in the guinea pig DOCA-salt model, therefore the present

study assessed this using western blotting. Physical changes to the myocardium were also determined at the macroscopic level by weighing myocardial tissue to determine the presence of hypertrophy in DOCA-salt hearts.

Another frequently reported change observed in failing hearts is elevated intracellular sodium.[53-55, 58, 59, 110-112] This has important implications for intracellular sodium handling due to resultant changes to NCX activity and may exacerbate the effect of repolarisation abnormalities on intracellular calcium handling (Section 1.2.4.2). One way in which this can be measured in the isolated Langendorff-perfused heart is with the application of multiple quantum filtered ^{23}Na nuclear magnetic resonance (NMR) spectroscopy.[100] A full technical description of the mechanism behind this technique is outwith the scope of this report, for a detailed review see Hutchison *et. al.* 1991.[152] Briefly, previous studies have demonstrated that intracellular sodium in the heart can be distinguished from extracellular sodium by comparing triple quantum filtered (TQF) and double quantum filtered (DQF) sodium spectra obtained using a ^{23}Na microimaging NMR coil and a reference sample of known sodium concentration.[100] It has been shown in rats that the DQF signal originates solely from the extracellular portion of sodium, whereas the TQF signal is composed of intracellular sodium signal with a 64% contribution from extracellular sodium.[153] In mice, there has been shown to be a smaller extracellular sodium contribution to the TQF signal at 47%.[100] An increase in TQF signal in the absence of an increase in the DQF signal would therefore correspond to an increase in intracellular sodium levels in the heart, when appropriately normalised to a reference sodium sample.

Finally, the questions raised by the experimental hypothesis could be addressed by examining the relationship between abnormal ventricular repolarisation and diastolic dysfunction in failing hearts expressing key characteristics of HFpEF. This was achieved by building on the foundations outlined in the previous results chapter, using the guinea pig working heart preparation and inducing prolonged ventricular repolarisation by treatment with E-4031 and HMR 1556 to achieve pharmacological blockade of I_{Kr} and I_{Ks}.

5.1.1 Hypothesis and Objectives

Hypothesis: Repolarisation abnormalities contribute to impairment of diastolic function in the failing heart.

The objectives were therefore as follows:

1) To develop and characterise a guinea pig DOCA-salt model of HF with impaired diastolic function.
2) To determine whether repolarisation abnormalities contribute to diastolic dysfunction in the failing heart in this model.

5.2 Methods

The general methods used in this chapter are discussed in Chapter 2. The following section will provide details of the specific protocols used in individual studies.

5.2.1 Model Characterisation

The first portion of this chapter deals with the development and characterisation of the guinea pig DOCA-salt model as a novel model of diastolic dysfunction in HF. The methods used to provide a detailed understanding of the pathophysiological characteristics of this model will be described, before going on to discuss the use of the characterised model to address the questions raised by the experimental hypothesis.

5.2.1.1 Unilateral Nephrectomy and DOCA Pellet Implantation

Guinea pigs (325-525g) underwent unilateral nephrectomy and DOCA pellet implantation according to the surgical method described in Section 2.1.3. A DOCA dose of 6.67mg/day was delivered via two subcutaneously implanted pellets with a 60-day release time. DOCA-salt animals were given a 1% NaCl drinking solution from 7 days post-surgery, while sham controls remained on tap water throughout the study.

5.2.1.2 Conscious Blood Pressure and ECG Monitoring

A subset of guinea pigs from two DOCA-salt cohorts underwent additional surgical procedures to enable the implantation of combined blood pressure and ECG telemetry devices (HD-X11 probes, DSI™). Details of the surgical procedure for this process are given in Section 2.1.3.2, while details of the hardware, software and approach to data collection and analysis are given in Section 2.1.4. Data was collected at baseline (7 days after recovery from telemetry device implantation), and then weekly after animals had started on 1% NaCl drinking water (Fig. 2.8). In the second telemetered cohort, control animals had telemetry device implantation combined with sham nephrectomy surgery in order to limit the number of surgical procedures, and so recordings began 1 week following the switch to 1% NaCl drinking water in this group. Approximately half of the animals in each cohort were telemetered in order to provide information about changes to blood pressure and ECG parameters, with half remaining untelemetered owing to constraints on the available hardware. Longitudinal data on mean arterial pressure (MAP), HR and QTc were analysed, although statistical analysis was not performed owing to small group sizes.

5.2.1.3 Echocardiography and Anaesthetised ECG Recording

In order to monitor *in vivo* cardiac functional changes, all animals undergoing the DOCA-salt protocol underwent serial cardiac ultrasound scans at baseline and every two weeks following commencement of the switch to 1% NaCl drinking water. Details of the methods used to collect cardiac ultrasound data are given in Section 2.1.3.3. Animal I.D's were coded at the time of data to collection so that the files could be analysed in a blinded fashion at a later date, avoiding any biasing of results. Files were only unblinded after analysis on Vevo LAB 2.1.0 software (FUJIFILM VisualSonics). EF for each animal was taken as the average value obtained from three different measurements: parasternal long axis LV trace (B-mode), parasternal long axis LV trace (M-mode) and short axis LV trace (B-mode). Tissue doppler measurements were taken from the mitral annulus of the left ventricular free wall and pulsed wave doppler used to measure mitral flow, and an average of three measurements was used to obtain the values for IVRT, E, A, e' and S wave velocity. The apical two-chamber view was used to determine LAA at peak atrial diastole.

Statistical analysis was performed using two-way ANOVA with Sidak's post hoc test, with a p value of less than 0.05 deemed statistically significant.

Table 5.1 Echocardiographic parameters measured in anaesthetised DOCA-salt guinea pigs

List of parameters measured, alongside method of deriving values from cardiac ultrasound data in anaesthetised DOCA-salt animals and physiological significance/limitations. Abbreviations: ejection fraction (EF), parasternal long axis view (PLAX), short axis view (SAX), end diastolic volume (EDV), end systolic volume (ESV), cardiac output (CO), stroke volume (SV), left ventricular (LV), isovolumic relaxation time (IVRT), left atrial area (LAA), diastolic dysfunction (DD). *See Fig. 5.7 for example.

Functional Parameter	*Definition/Method of Calculation*	*Physiological Significance/Limitations*
EF	Taken as average from: M-mode LV trace in PLAX, M-mode LV trace in SAX and B-mode LV trace in PLAX	Systolic function: reduced EF is indicative of reduced contractility and therefore SV. EF can remain normal in diastolic HF as EDV falls proportionately with SV due to reduced ventricular compliance.
CO	Calculated from M-mode LV trace in PLAX	Systolic and diastolic function: product of SV and HR.
SV	Difference between EDV and ESV. Calculated from M-mode LV trace in PLAX	Systolic and diastolic function: influenced by preload, afterload and contractility. SV in failing hearts is more susceptible to changes in afterload.
LV Mass	Calculated from M-mode LV trace in PLAX	Increases in LV mass indicate LV hypertrophy.

S Wave Velocity	Peak S wave velocity, measured from the mitral annulus of the LV free wall using tissue doppler	Systolic function: represents longitudinal LV contraction. Correlates well with EF.[154]
IVRT	Measured using pulsed wave doppler as the time from aortic valve closure to mitral valve opening in the apical two-chamber view*	Diastolic function: reflects the time constant of relaxation, tau. Prolongations indicates slowed relaxation; however, this parameter can be affected by loading conditions and HR. Can undergo pseudonormalisation as mitral valve opens earlier under conditions of elevated LA pressures.[155-157]
LAA	Traced at peak atrial diastole in the apical two-chamber view	Diastolic function: increased LA size is an indicator of chronically elevated LV filling pressures.[158]
E Wave Velocity	Early mitral inflow velocity. Measured using pulsed wave doppler in the apical two-chamber view*	Diastolic function: proportional to the ratio between LA pressure and the time constant of relaxation, tau. Correlates with LA/filling pressure only in the presence of HF, Measurement can become difficult at high HR if waves fuse.[159]
A Wave Velocity	Late mitral inflow velocity, measured using pulsed wave doppler in the apical two-chamber view*	Diastolic function: increases to A wave velocity (relative to E wave velocity) are indicative of a greater reliance on the atrial contribution to LV filling. Measurement can become difficult at high HR if waves fuse.

e' Velocity	Early diastolic velocity of the mitral annulus. Measured from the mitral annulus of the LV free wall using tissue doppler	Diastolic function: inversely proportional to the time constant of relaxation, tau. Provides a relatively load-independent measure of early ventricular relaxation and elastic recoil. Value varies at different sites of measurement within the LV.[159, 160]
E/A	Ratio of peak early mitral inflow velocity (E) to peak late mitral inflow velocity (A).	Diastolic function: correlates with LA/filling pressure. Poor correlation in the presence of preserved systolic function (EF>50%). Reversal may indicate DD as LV filling becomes dependent on atrial contribution, however, pseudonormalisation may occur with disease progression. Value declines with age.[161-163]
E/e'	Ratio of peak early mitral inflow velocity (E) to peak early diastolic velocity of the mitral annulus (e')	Diastolic function: correlates with LA/filling pressure with both impaired (EF<50%) and preserved systolic function (EF>50%). Increased E/e' is associated with increased risk of mortality in HF patients. Correlation with LV filling pressures may be lost in the presence of mitral regurgitation or abnormal septal motion.[159, 161, 164]

While animals were anaesthetised, ECGs were recorded prior to the collection of cardiac ultrasound data, as described in Section 2.1.3.3. This data was used to provide information about changes to cardiac repolarisation and heart rate in response to DOCA-salt treatment. For analysis, LabChart 8 software with the ECG analysis module was used, with an average of 50 beats used to determine the QT interval and heart rate for each animal. The QT interval was corrected according to the formula described in Section 4.2.1 and

statistical analysis was performed using two-way ANOVA with Sidak's post hoc test, with a p value of less than 0.05 deemed statistically significant.

5.2.1.4 Dissection of DOCA-Salt Hearts

Following completion of isolated heart protocols, the myocardium was dissected and weighed to provide information relating to gross anatomical changes as a result of DOCA-salt treatment. The atria were first removed and weighed separately, before removing and weighing the right ventricular free wall. The apex of the remaining ventricular myocardium was then removed, weighed and snap frozen by immediate submersion in liquid nitrogen for biochemical analysis. The remaining myocardial mass was then weighed to provide the total heart mass for each animal. In addition to heart tissues, a section of lung was removed, blotted dry and weighed at the point of heart isolation, before being dried overnight in an oven at 60°C to provide a wet-to-dry lung mass ratio. This would enable any evidence of oedema as a result of HF to be detected. Finally, the right tibia of each animal was removed, and the length measured using a calliper to enable heart mass to tibia length ratio to be determined for each animal. This was deemed a more reliable measure of cardiac hypertrophy then heart mass to body mass ratio, given that it was found that DOCA-salt animals did not gain as much weight as their sham counterparts during the study.

5.2.1.5 Western Blotting

Western blotting was used to identify changes in the expression of key calcium-handling proteins in the left ventricle in response to DOCA-salt treatment. The details of the precise protocol used for western blotting, including antibody concentrations, are given in Section 2.1.6.

5.2.1.6 Function of Working DOCA-Salt Hearts

Following completion of the DOCA-salt protocol at 7 weeks post-salt, animals were terminally anaesthetised with an overdose of pentobarbitone (i.p.) and hearts excised and perfused under working conditions as described in Section 2.1.2. The initial aim of these

working heart studies was to determine the differences in cardiac function between DOCA and sham animals under baseline conditions. To this end, hearts were cannulated and allowed to stabilise for 15 min under Langendorff conditions, before switching to working mode and allowing an additional 15 min of stabilisation. Hearts were instrumented with an intraventricular pressure-volume catheter and silver wire ECG electrodes in a modified lead II arrangement during this stabilisation period, as described in Section 2.1.2.2. Once stabilisation was complete, baseline measurements, including coronary and aortic flow were collected to form the basis of the functional assessment of failing DOCA vs. healthy sham hearts.

For analysis, LabChart 8 with ECG and blood pressure analysis modules was used, with average values acquired from 10s of continuous data recording at the end of the stabilisation period. Where relevant (i.e. a relationship between the parameter and heart rate exists), these data were displayed as a corrected value to account for differences in heart rate between individual preparations. This process is described in Section 4.2.1. The presence of significant differences between DOCA and sham groups was determined using an unpaired Student's t-test, with a p value of less than 0.05 deemed to be statistically significant.

Following the collection of baseline data both groups were treated with 100nM E-4031 + 30nM HMR 1556 to induce delayed cardiac repolarisation, recorded as increased QT interval. Hearts were allowed to stabilise for 20 min following the addition of drug before functional data was collected, including coronary and aortic flow, enabling a comparison of the functional effects of abnormal cardiac repolarisation in healthy vs. failing hearts to be made (Section 5.2.2.1). Once this portion of the protocol was complete hearts were dissected and the relevant tissue portions weighed and/or snap-frozen for further analysis (Section 5.2.1.3).

5.2.2 Hypothesis Testing

The latter portion of this chapter largely involves the use of the characterised DOCA-salt model of HF with diastolic dysfunction to test whether any relationship exists between repolarisation abnormalities and diastolic function in HF.

5.2.2.1 Effect of Repolarisation Abnormalities on Diastolic Dysfunction in Failing Hearts

In order to determine whether diastolic dysfunction in the failing heart is augmented by repolarisation abnormalities, data from working DOCA-salt and sham control hearts were collected following exposure of hearts to 100nM E-4031 + 30nM HMR 1556, as described in Section 5.2.1.5 above. In this instance, data for each variable were displayed as change from baseline values obtained prior to the addition of E4+HMR. This allowed for a comparison of the effect of QT prolongation in failing vs. healthy hearts to be made, i.e. do failing hearts show a different functional response to abnormal repolarisation than healthy hearts due to the underlying pathophysiological changes discussed previously? LabChart 8 with ECG and blood pressure analysis modules was used to obtain average values acquired from 10s of continuous data recording following treatment with 100nM E-4031 and 30nM HMR 1556. Where relevant (i.e. a relationship between the variable and heart rate exists), data were corrected to account for differences in heart rate between individual preparations. This process is described in Section 4.2.1. The presence of significant differences between DOCA and sham groups was determined using an unpaired Student's t-test, with a p value of less than 0.05 deemed to be statistically significant.

5.2.2.2 Effect of Repolarisation Abnormalities on Intracellular Sodium Levels in Failing Hearts

An additional cohort of DOCA-salt animals was established in order to examine the potential role of intracellular sodium elevation in the pathologies seen in the DOCA-salt animals, and whether repolarisation abnormalities may affect this. This was explored using ^{23}Na NMR spectra acquisition and determining whether the TQF signal (a large portion of which relates to intracellular sodium levels) changes in response to different conditions. The specific details of the experimental setup and hardware/software used to achieve this are given in the General Methods Chapter, Section 2.1.5. Briefly, hearts were isolated and cannulated for this purpose as described in Section 2.1.2 & 2.1.2.4. Initial NMR studies were carried out in healthy guinea pig hearts and used ouabain to elevate intracellular sodium via blockade of the Na^+,K^+-ATPase in the presence or absence of

100nM E-4031 + 30nM HMR 1556. In this study, the hearts used were the same as those used in the working heart study used to examine the effect of QT prolongation on cardiac function under baseline conditions in the working heart. At the end of the working heart protocol, the cannula to which the aorta was fixed was removed from the working heart rig with the heart still attached and immediately submerged in ice-cold physiological buffer, before being immediately transferred to the NMR rig and reperfused with warmed physiological buffer. Hearts which had been assigned to the E4+HMR experimental group were perfused with the same concentration of these drugs from the outset (100nM E-4031 + 30nM HMR 1556), and those which had been assigned to the vehicle control group were perfused with control buffer from the outset. Following instrumentation and stabilisation, hearts were lowered into the magnet and allowed a further 10 min to stabilise before subjected to the following protocol: ^{31}P spectra acquisition, 15 min of ^{23}Na spectra acquisition under baseline conditions, switch to physiological buffer containing 200nM ouabain and a further 35 min of ^{23}Na spectra acquisition, before carrying out a final ^{31}P spectra acquisition. Triple- and double-quantum filtered ^{23}Na spectra were acquired in an interleaved fashion throughout the relevant period of the protocol, as described in Section 2.1.5. Acquisition of ^{31}P spectra at the start and end of the protocol allowed for the assessment of cardiac energetics and intracellular pH, thereby assessing the stability of the isolated heart preparations throughout the protocol (Section 2.1.5).

For analysis, TQF heart spectra were integrated and first normalised to the averaged reference spectrum under baseline conditions, before being normalised to baseline experimental values so that the effect of ouabain on sodium load within hearts could be established. The DQF heart spectra were first integrated and normalised to the average reference DQF spectrum under baseline conditions, before being normalised to experimental baseline values. The ^{31}P spectra were used to calculate the ATP to PCr ratio and intracellular pH, as described in Section 2.1.5. The presence of statistically significant differences between groups was determined using two-way ANOVA with Sidak's post hoc test or an unpaired Student's t-test, as appropriate to the number of comparisons being made, and a p value of less than 0.05 was deemed to be statistically significant.

Having determined a strategy for measuring intracellular sodium elevation in healthy isolated guinea pig hearts, a subsequent study aimed to measure intracellular sodium

levels in DOCA vs sham hearts, and address whether repolarisation abnormalities affect intracellular sodium levels in the failing heart. An additional DOCA-salt cohort was characterised using cardiac ultrasound, anaesthetised ECG/heart rate recordings and identification of gross cardiac anatomical changes to ensure the same cardiac phenotype was achieved (see General Methods and Section 5.2.1). Following completion of the DOCA-salt protocol at 7 weeks post-salt, animals were anaesthetised by an overdose of pentobarbitone (i.p.) and hearts excised and perfused for ^{23}Na NMR spectra acquisition as described in Section 2.1.5. The protocol for the NMR study was as follows: hearts were allowed to stabilise for 15 min before baseline ^{31}P spectra acquisition, then 10 min of ^{23}Na spectra acquisition under baseline conditions before switching to physiological buffer containing 100nM E-4031 + 30nM HMR 1556 and a further 20 min of ^{23}Na spectra acquisition, before carrying out a final ^{31}P spectra acquisition.

For analysis, TQF heart spectra were integrated and first normalised to the averaged reference spectrum under baseline conditions, before being normalised to heart weight to account for cardiac hypertrophy in DOCA animals. The DQF heart spectra were first integrated and normalised to the average reference DQF spectrum under baseline conditions, before being normalised to experimental baseline values. The ^{31}P spectra were used to calculate the ATP to PCr ratio and intracellular pH, as described in Section 2.1.5. The presence of statistically significant differences between groups was determined using two-way ANOVA with Sidak's post hoc test or an unpaired t test, as appropriate to the number of comparisons being made, and a p value of less than 0.05 was deemed to be statistically significant.

5.3 Results

5.3.1 Model Characterisation

Initial studies were conducted in order to characterise the guinea pig DOCA-salt model as a novel model of HF with diastolic dysfunction. This section will describe data which were collected in order to characterise model progression and determine the resultant effects on cardiac function.

5.3.1.1 Effect of DOCA-Salt Treatment on Blood Pressure, Heart Rate and QTc

Radiotelemetry was used in a subset of animals throughout the DOCA-salt protocol to monitor changes to blood pressure, heart rate and cardiac repolarisation in conscious animals. Heart rate and QTc interval were additionally measured at intervals throughout the protocol in anaesthetised animals prior to performing cardiac ultrasound scans.

There was a clear effect of DOCA-salt treatment on MAP and heart rate, with DOCA animals demonstrating apparent increases in these variables relative to their sham counterparts from 4 weeks post-salt (Fig. 5.1 A-D). There was no obvious effect of DOCA-salt treatment on QTc interval in the limited number of animals from which telemetry data was available (Fig. 5.1 E & F). Another interesting observation from the telemetry data was a lack of any strong circadian rhythm in the guinea pig. Although there may be a subtle elevation in nighttime heart rate (Fig. 5.2 A), this appears to be variable, and is not reflected in any obvious cyclic changes to mean arterial pressure (Fig. 5.2 B). Similarly, the average weekly values across all variables did not appear to differ between day and night-time (Fig. 5.1).

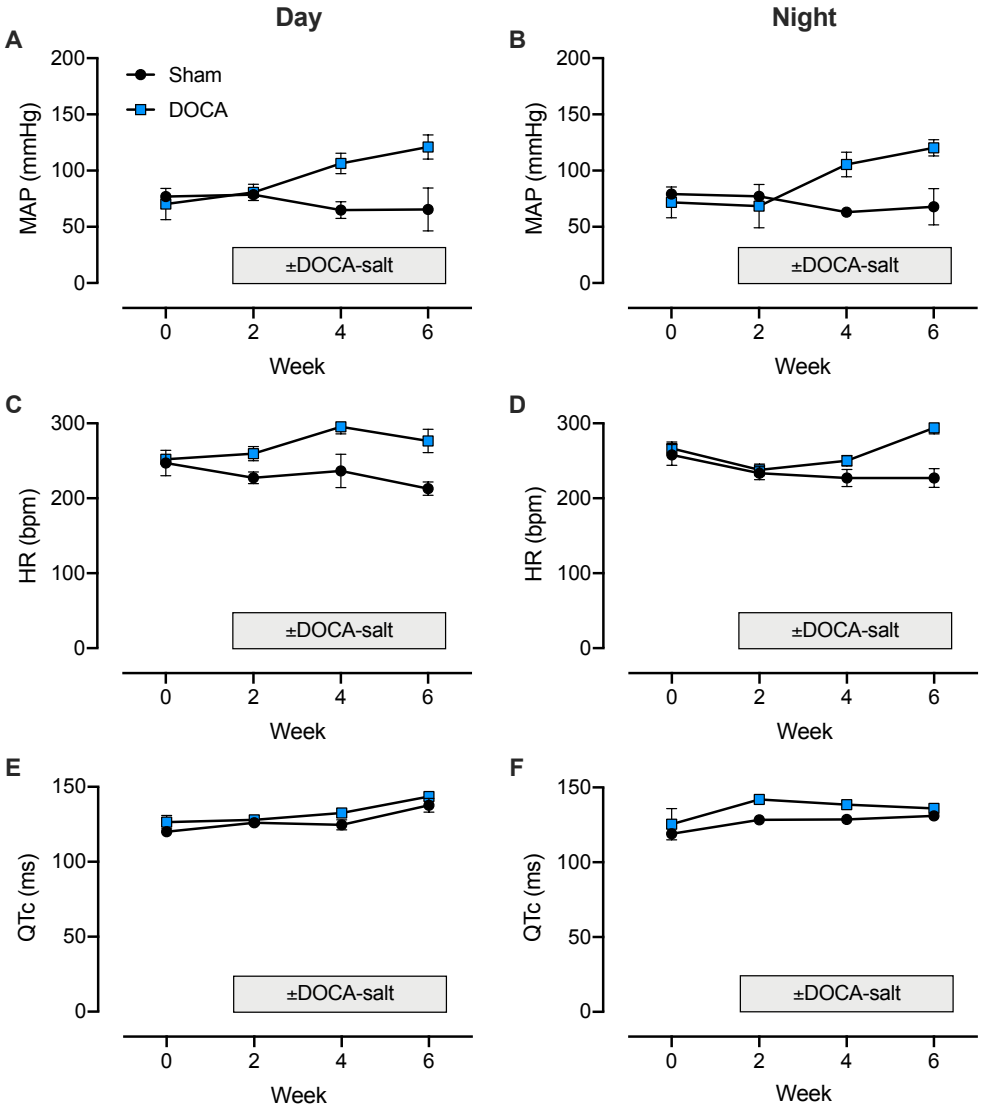

Figure 5.1 Impact of DOCA-salt treatment on blood pressure, heart rate and QTc interval in conscious animals

Data gathered from conscious DOCA and sham guinea pigs using combined blood pressure and ECG telemetry at baseline (week 0), 2, 4 and 6 weeks post-salt. Daytime averages for mean arterial pressure (A), heart rate (C) and QTc interval (E). Night-time averages for mean arterial pressure (B), heart rate (D) and QTc interval (F). Data presented as mean ± S.E.M., n=2-3, statistical analysis not performed due to low group sizes.

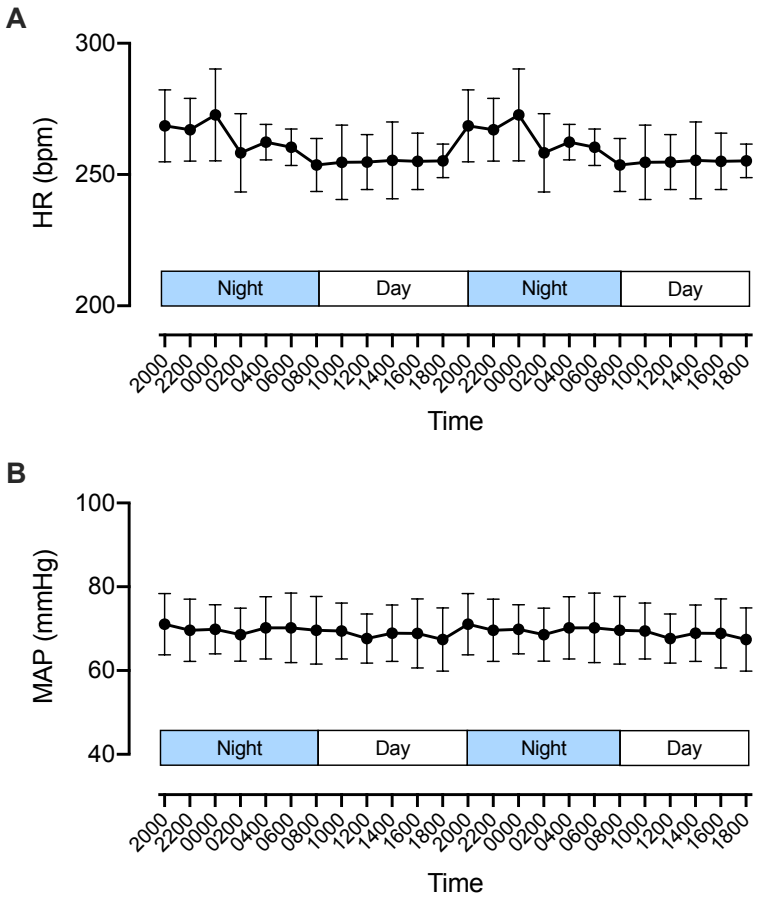

Figure 5.2 Baseline circadian rhythm in telemetered guinea pigs

Data gathered from conscious radiotelemetered guinea pigs under baseline conditions. Average heart rate obtained during continuous recording during day and night-time periods (A) and average mean arterial pressure during day and night-time periods (B). Data presented as mean ± S.E.M., n=4. N.B. Data recorded over a continuous 24hr period and duplicated on the x-axis to allow for visualisation of any circadian rhythm present.

In anaesthetised DOCA and sham animals no differences were observed in heart rate between groups, however, a significant increase in QTc interval was apparent in DOCA animals relative to their sham counterparts from 4 weeks post-salt (Fig. 5.3).

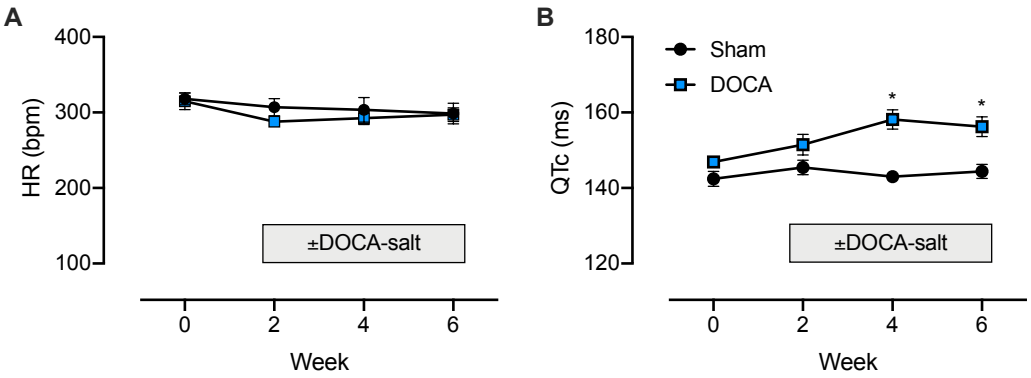

Figure 5.3 Impact of DOCA-salt treatment on heart rate and QTc interval in anaesthetised animals

Heart rate and QTc interval changes in anaesthetised DOCA and sham guinea pigs at baseline (week 0), 2, 4 and 6 weeks post-salt. A) Heart rate and B) QTc interval. Data presented as mean ± S.E.M., n=7-8, * = p<0.05 vs. sham.

5.3.1.2 Effect of DOCA-Salt Treatment on Cardiac Function In Vivo

Serial cardiac ultrasound measurements were performed throughout the DOCA-salt protocol in order to monitor cardiac function. Owing to the smaller body mass observed in DOCA animals relative to their sham counterparts as a result of the DOCA protocol (Fig. 5.8), certain cardiac ultrasound parameters which are likely to change with body mass under baseline conditions (e.g. LV mass) were expressed as a ratio of body mass to allow for better comparison between groups.

Systolic function was preserved in DOCA animals, with no differences between groups observed for any of the parameters measured (Fig. 5.4). This was true for EF, a key observation in HFpEF patients, as well as for cardiac output, stroke volume and S wave velocity, which reflects the rate of left ventricular contraction as determined by tissue Doppler imaging. Whilst no significant increase in calculated LV mass was observed in the DOCA group, there does appear to be a trend towards increased LV mass to body mass ratio in this group compared to sham animals. Indeed, LV hypertrophy was apparent when looking at B-mode images from sham vs DOCA animals at 6 weeks post-salt (Fig. 5.5).

In contrast, several markers of diastolic dysfunction were observed in DOCA-salt treated animals (Fig. 5.6). There was a rapid and sustained elevation in IVRT in the DOCA group that is indicative of impaired ventricular relaxation. This was accompanied by a significant increase in LAA, reportedly also a key marker of diastolic dysfunction as ventricular filling becomes more dependent on the atrial contribution. No change was observed in the ratio of early and late mitral inflow velocity (E/A) on average in the DOCA group relative to sham counterparts, nor in the ratio of the early mitral inflow velocity and early diastolic velocity of the mitral anulus (E/e'). The increase in IVRT was clearly visible in the DOCA group when looking at mitral flow velocities using pulsed-wave Doppler (Fig. 5.7).

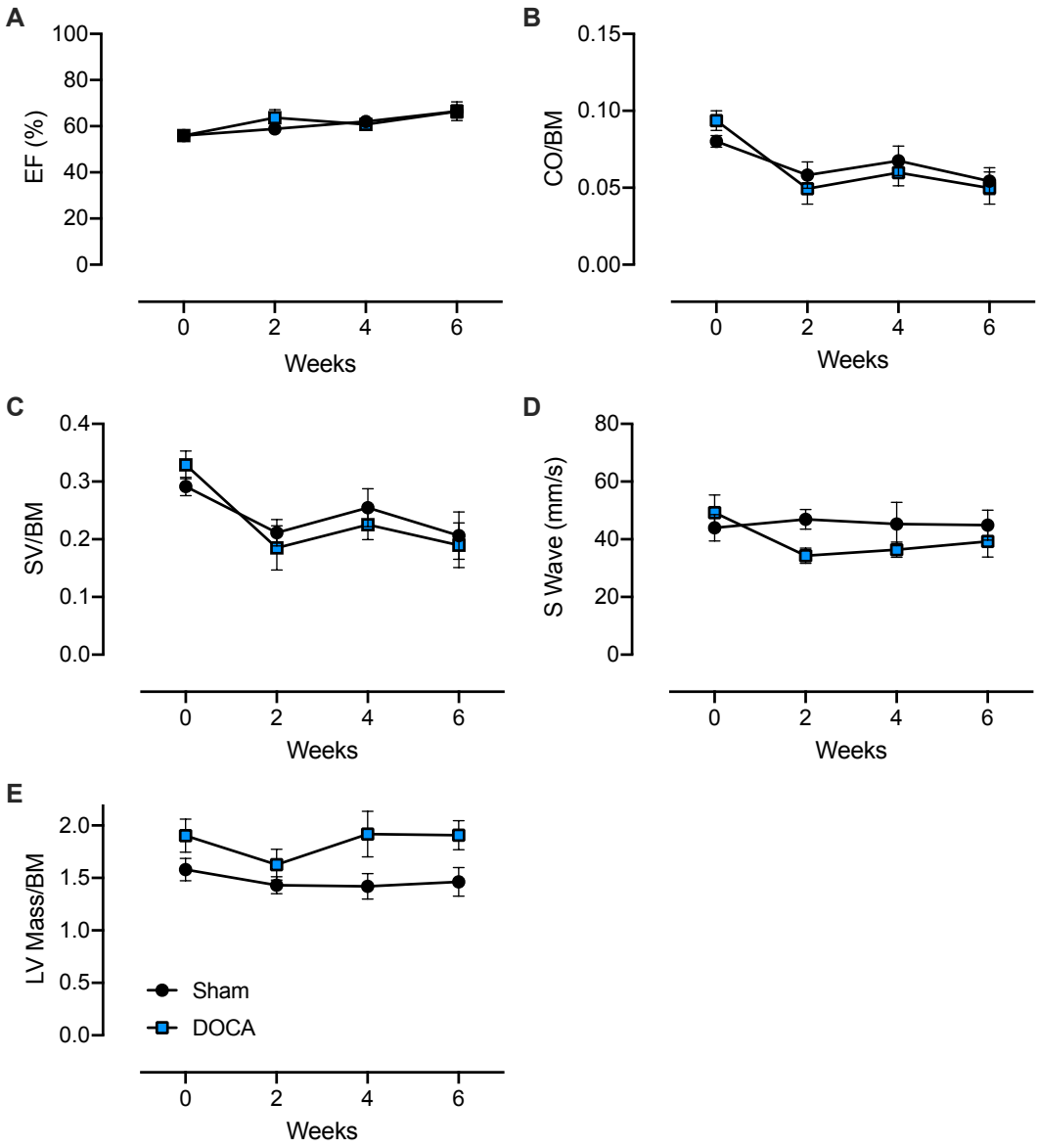

Figure 5.4 Impact of DOCA-salt treatment on systolic function *in vivo*

Cardiac systolic function in anaesthetised DOCA and sham guinea pigs at baseline (week 0), 2, 4 and 6 weeks post-salt, as determined using cardiac ultrasound. A) Ejection fraction, B) cardiac output/body mass, C) stroke volume/body mass, D) S wave velocity and E) left ventricular mass/body mass. Data presented as mean ± S.E.M., n=5-8.

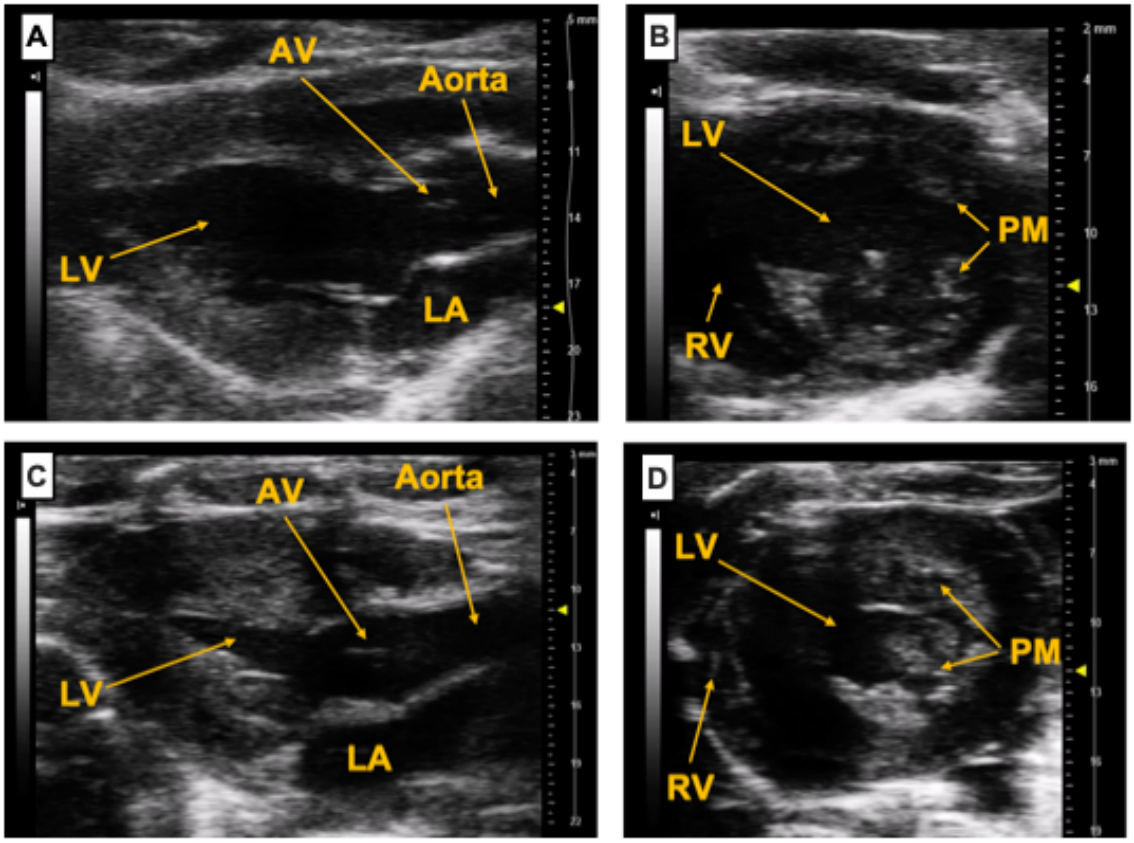

Figure 5.5 Cardiac ultrasound images demonstrating left ventricular hypertrophy following DOCA-salt treatment

Cardiac ultrasound images obtained from anaesthetised DOCA and sham guinea pigs at 6 weeks post-salt. Parasternal long axis view of sham (A) and DOCA (C) hearts, taken on closure of the aortic valve at end systole. Short axis view of sham (B) and DOCA (D) hearts, taken at peak diastole. Abbreviations: left ventricle (LV), right ventricle (RV), left atrium (LA), aortic valve (AV), papillary muscles (PM).

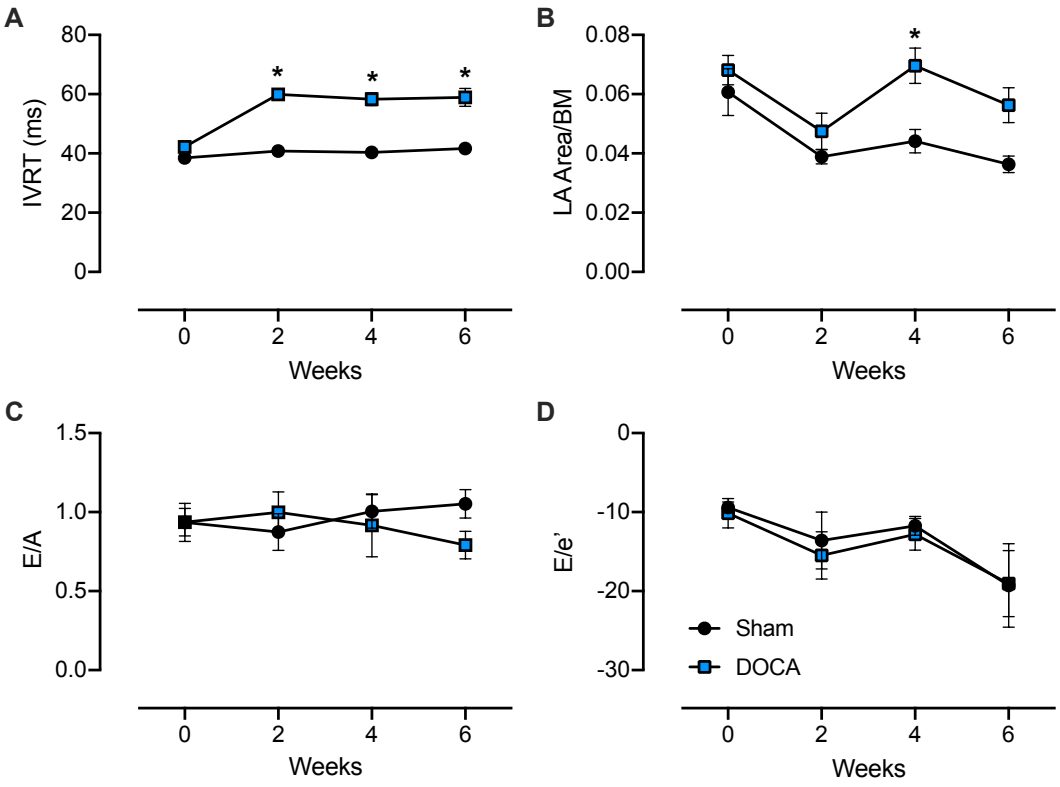

Figure 5.6 Impact of DOCA-salt treatment on diastolic function *in vivo*

Cardiac diastolic function in anaesthetised DOCA and sham guinea pigs at baseline (week 0), 2, 4 and 6 weeks post-salt, as determined using cardiac ultrasound. A) Isovolumic relaxation time, B) left atrial area/body mass, C) E/A ratio and D) E/e' ratio. Data presented as mean ± S.E.M., n=5-8, * = $p<0.05$ vs. sham.

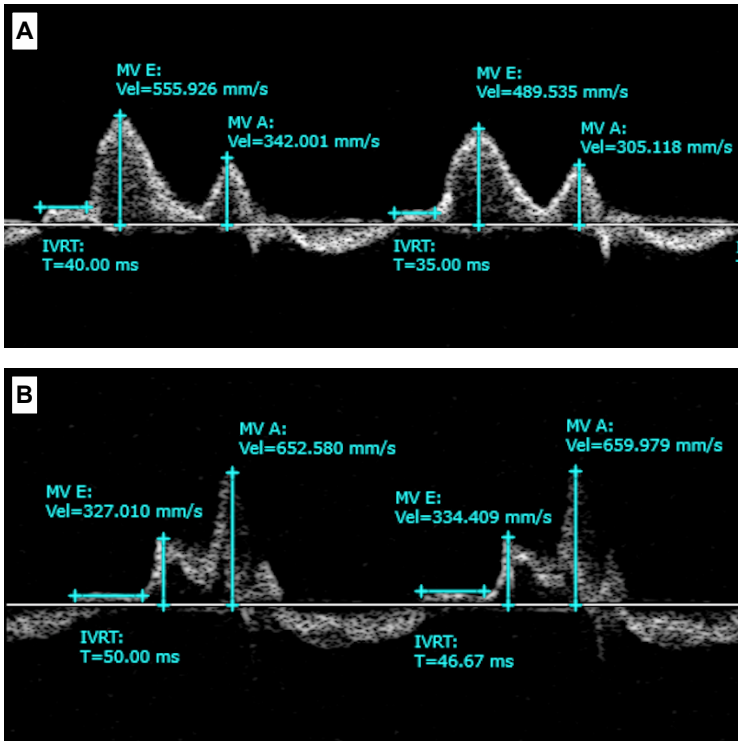

Figure 5.7 Mitral flow velocities from DOCA and sham guinea pigs

Mitral flow velocities obtained using pulsed-wave Doppler in the apical two-chamber view in anaesthetised sham (A) and DOCA (B) guinea pigs at 6 weeks post-salt. DOCA animals demonstrate clear prolongation of isovolumic relaxation time (IVRT) and, in this example, a reversal of the E/A ratio indicating impaired ventricular relaxation and increased reliance on left atrial contribution to ventricular filling.

5.3.1.3 Effect of DOCA-Salt Treatment on Cardiac Gross Anatomy

Treatment with DOCA-salt had a significant impact on the growth of DOCA animals compared to their sham counterparts (Fig. 5.8). There was no difference in body mass between groups at baseline and while both groups gained weight during the protocol, DOCA animals were significantly smaller at termination of the protocol.

Based on the observed effects on body mass, cardiac gross anatomy (i.e. mass of cardiac tissues) was expressed as a ratio relative to the tibia length of each animal (Fig. 5.9). While right atrial (RA) mass ratio showed no change in DOCA animals relative to sham, there was a significant increase in LA mass ratio in DOCA animals, indicative of LA hypertrophy. LV hypertrophy in DOCA animals was also apparent while, perhaps

unexpectedly, right ventricular (RV) mass ratio was lower in DOCA-salt animals. It should be noted that this represents the mass of the RV free wall relative to tibia length, with the intraventricular septum being included in the LV mass calculation.

No evidence of pulmonary oedema was evident in DOCA-salt animals relative to sham counterparts, as determined by wet to dry lung mass ratio (Fig. 5.10).

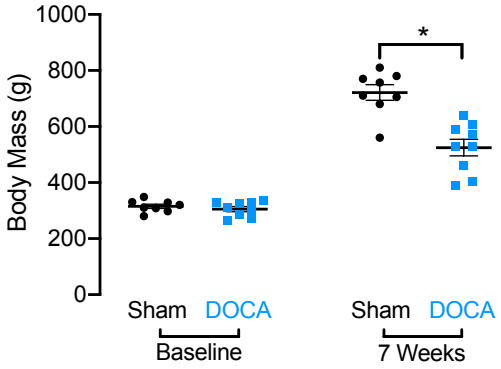

Figure 5.8 Impact of DOCA-salt treatment on body mass

The body mass of sham and DOCA-salt treated guinea pigs at A) baseline and B) termination of protocol (7 weeks post-salt). Data presented as mean ± S.E.M. with all individual values shown, n=8-9, * = $p<0.05$ vs sham.

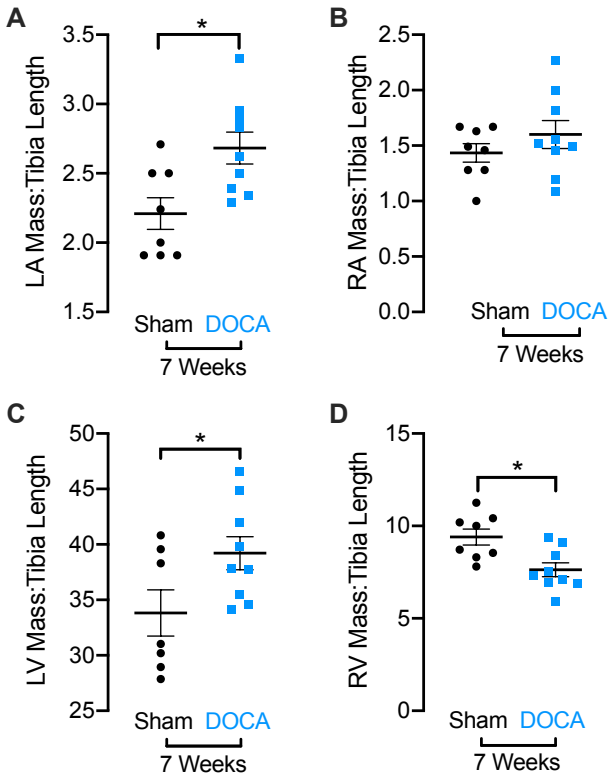

Figure 5.9 Impact of DOCA-salt treatment on cardiac gross anatomy

The myocardial mass of sham and DOCA-salt treated guinea pigs at termination of protocol (7 weeks post-salt), expressed vs. tibia length. A) Left atrial mass:tibia length ratio, B) right atrial mass:tibia length ratio, C) left ventricular mass:tibia length ratio and D) right ventricular mass:tibia length ratio. Data presented as mean ± S.E.M. with all individual values shown, n=7-9, *= p<0.05 vs sham.

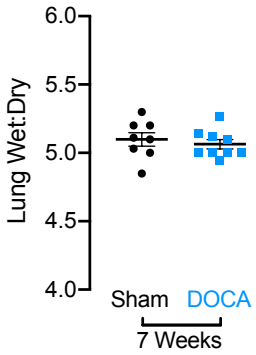

Figure 5.10 Impact of DOCA-salt treatment on lung wet:dry mass

Wet:dry ratio of lung tissue in sham and DOCA-salt treated guinea pigs at termination of protocol (7 weeks post-salt). Data presented as mean ± S.E.M. with all individual values shown, n=8-9.

5.3.1.4 Protein Expression in DOCA-Salt Hearts

Western blotting was used to determine any changes in the level of expression of several key proteins that play a role in intracellular calcium handling in the myocardium in response to DOCA-salt treatment. A significant increase in the expression of NCX was observed in DOCA animals, alongside a significant decrease in SERCA2a relative to GAPDH (Fig. 5.11 A & B). No significant changes were observed in the level of expression of total phospholamban or in the levels of phospholamban phosphorylated at serine-16 or threonine-17, although there appears to be a trend towards reduced threonine-17 phosphorylation in DOCA animals (Fig. 5.11 C & D). The α_2 and β_1 subunits of the Na^+,K^+-ATPase also demonstrated an increase in response to DOCA-salt treatment, with a possible trend towards an increase in the β_2 subunit as well (Fig. 5.12 A & B). No changes in the expression of Na^+,K^+-ATPase regulatory protein phospholemman (total or phosphorylated) were observed in DOCA animals relative to their sham counterparts (Fig. 5.12 C & D).

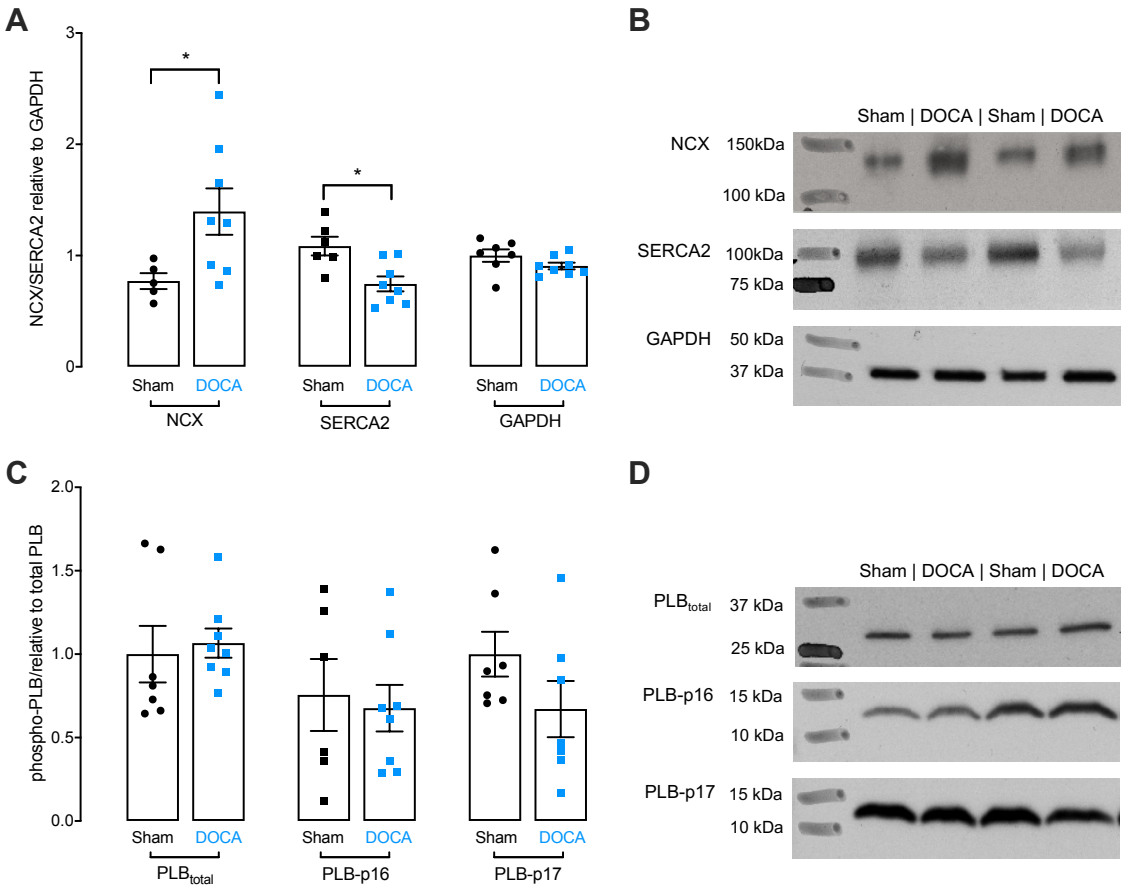

Figure 5.11 Impact of DOCA-salt treatment on expression of cardiac intracellular calcium handling proteins

Effect of DOCA-salt treatment on the level of expression of key proteins involved in intracellular calcium handling in left ventricular tissue at 7 weeks post-salt. A) Quantified level of expression of the sodium-calcium exchanger and SERCA2a relative to GAPDH, B) representative blots showing expression of NCX, SERCA2a and GAPDH in sham and DOCA animals, C) quantified level of serine-16 and threonine-17 phospholamban phosphorylation, relative to total phospholamban expression and D) representative blots showing phosphorylated and total phospholamban expression in sham and DOCA animals. Data presented as mean ±S.E,M., n=6-8, * = p<0.05 relative to sham. **Blots performed and analysed by Dr Lauren Albee.**

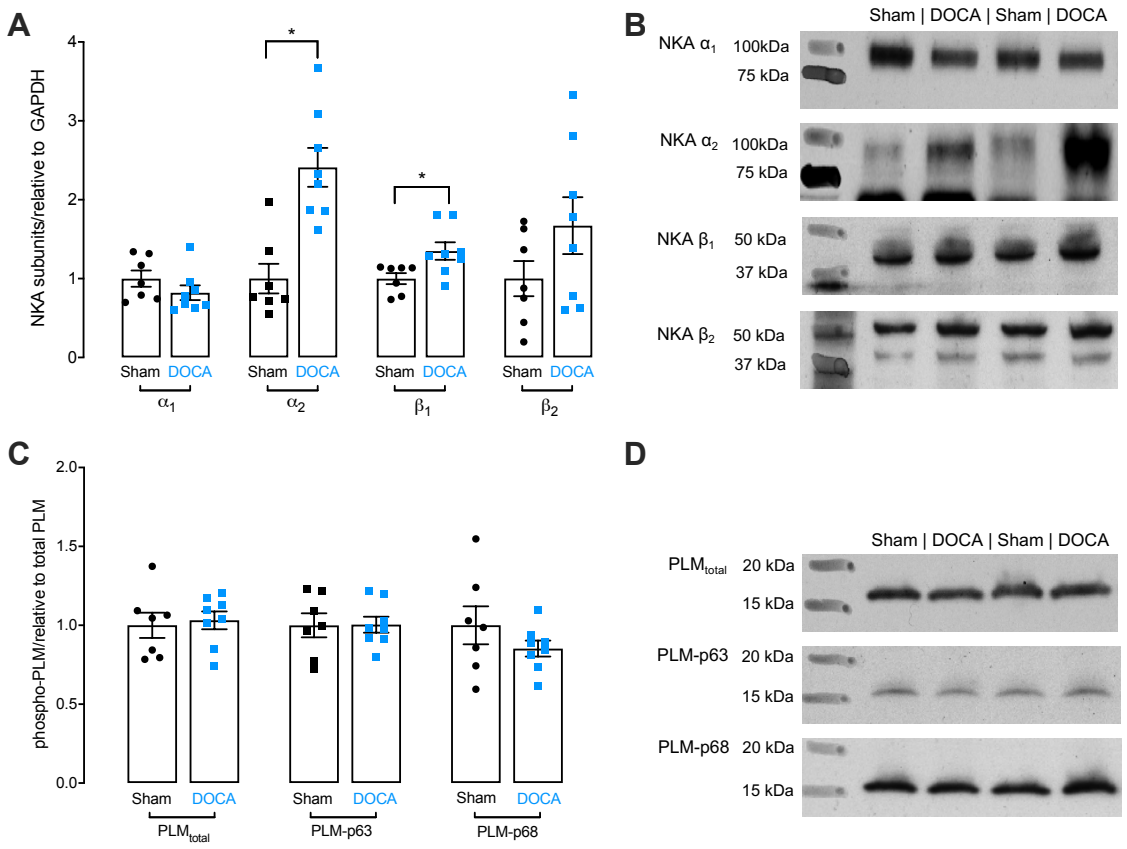

Figure 5.12 Impact of DOCA-salt treatment on expression of cardiac intracellular calcium handling proteins

Effect of DOCA-salt treatment on the level of expression of key proteins involved in intracellular calcium handling in left ventricular tissue at 7 weeks post-salt. A) Quantified level of expression of the sodium-potassium ATPase subunits relative to GAPDH, B) representative blots showing sodium-potassium ATPase subunit expression in sham and DOCA animals, C) quantified level of serine-63 and serine-68 phospholemman phosphorylation relative to total phospholemman expression and D) representative blots showing phosphorylated and total phospholemman expression in sham and DOCA animals. Data presented as mean ±S.E,M., n=6-8, * = p<0.05 relative to sham. **Blots performed and analysed by Dr Lauren Albee.**

5.3.1.5 Baseline Function of Working DOCA-Salt Hearts

Following the 7-week DOCA-salt protocol, hearts were isolated from DOCA and sham animals and perfused under working conditions. Under baseline conditions, no difference was observed in QTc interval or heart rate in DOCA-salt hearts compared to sham counterparts (Fig. 5.13 A & B). There appeared to be a trend towards a reduced stroke

volume in DOCA hearts, while coronary flow and cardiac output (adjusted for ventricular mass) were both significantly decreased in DOCA hearts (Fig. 5.13 C-E).

Clear systolic dysfunction was observed in failing DOCA hearts, which demonstrated reduced LVDP, reduced maximum rate of left ventricular pressure increase and increased systolic duration (Fig. 5.14).

Diastolic dysfunction was also evident in DOCA hearts under baseline conditions (Fig. 5.15). A significant increase in LVEDP was observed in DOCA hearts, alongside a reduction in the maximum rate of pressure decline within the left ventricle and decreased diastolic duration. No significant changes were observed in the time constant of relaxation (Tau).

These systolic and diastolic effects can be visualised by examining LVP traces from DOCA and sham hearts (Fig. 5.16). Failing hearts demonstrate a clear reduction in the rate of pressure development in the LV, also showing a reduced maximum rate of pressure decline and an elevated LVEDP.

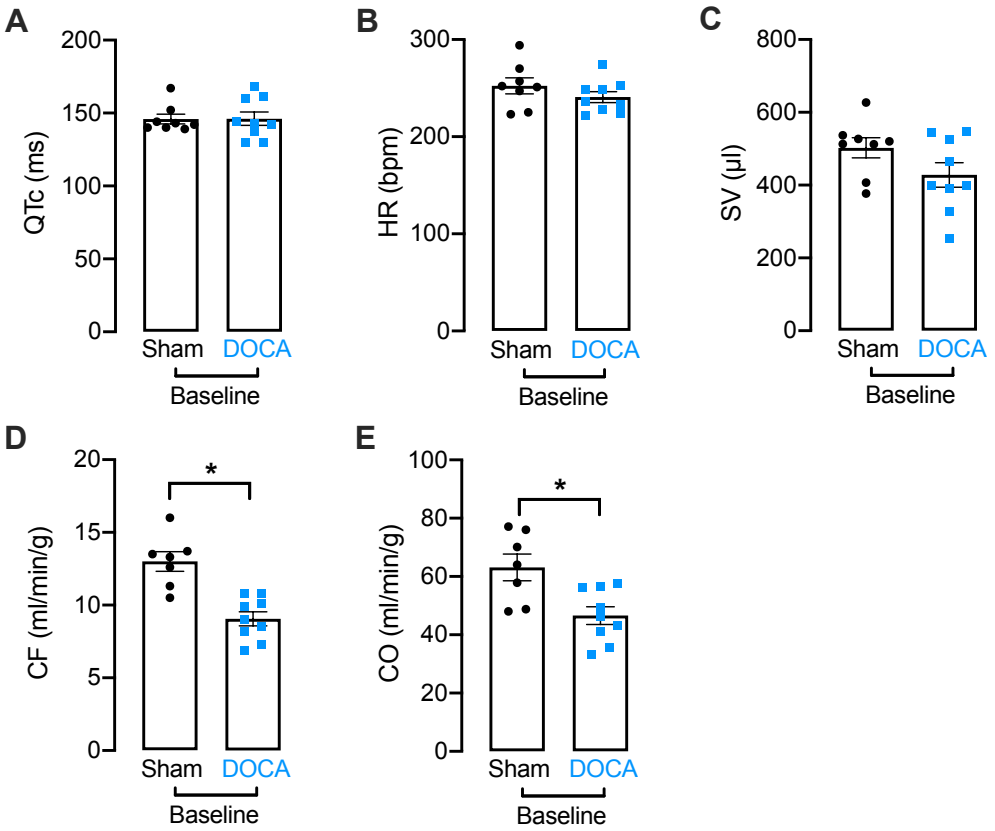

Figure 5.13 Baseline function in the working DOCA-salt heart

Baseline functional parameters in working DOCA-salt hearts at 7 weeks post salt, relative to sham hearts. A) QTc interval, B) heart rate, C) stroke volume, D) coronary flow and E) cardiac output in DOCA vs. sham hearts under baseline conditions following stabilisation period. Data presented as mean ±SEM, n=7-9, * = $p<0.05$ in DOCA vs. sham group.

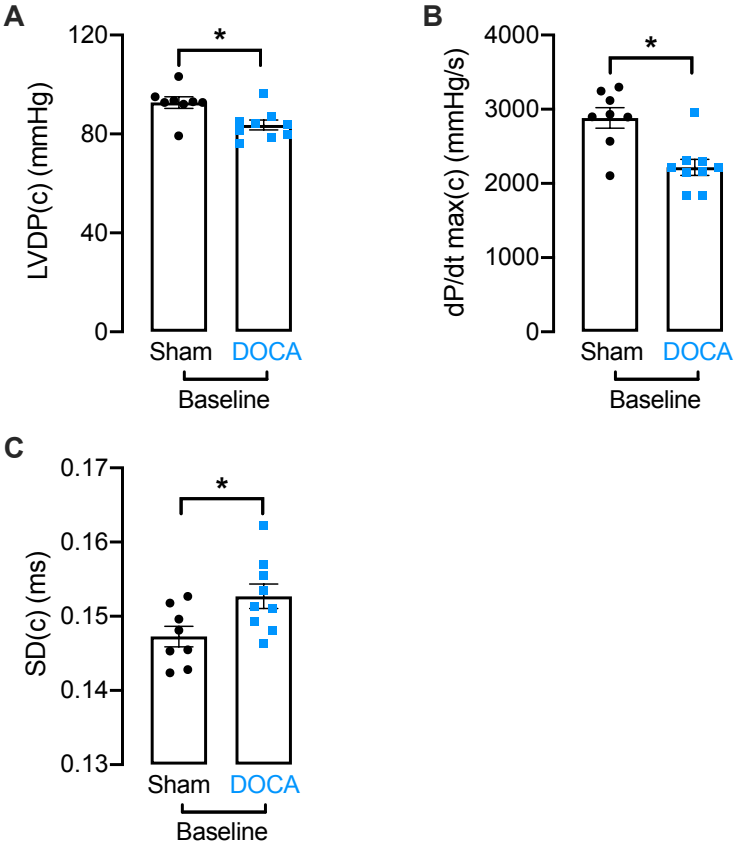

Figure 5.14 Baseline systolic function in the working DOCA-salt heart

Baseline systolic function in working DOCA-salt hearts at 7 weeks post salt, relative to sham hearts. Values shown are corrected for heart rate: A) left ventricular developed pressure, B) dP/dt max and C) systolic duration in DOCA vs. sham hearts under baseline conditions following stabilisation period. Data presented as mean ±SEM, n=7-9, * = $p<0.05$ in DOCA vs. sham group.

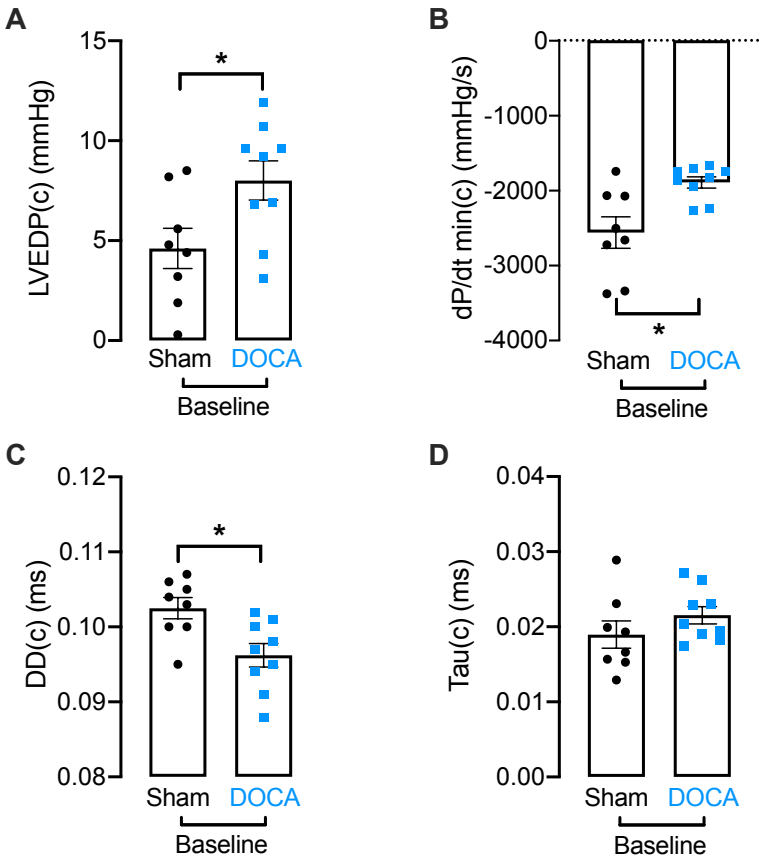

Figure 5.15 Baseline diastolic function in the working DOCA-salt heart

Baseline diastolic function in working DOCA-salt hearts at 7 weeks post salt, relative to sham hearts. Values shown are corrected for heart rate: A) left ventricular end diastolic pressure, B) dP/dt min and C) diastolic duration in DOCA vs. sham hearts under baseline conditions following stabilisation period. Data presented as mean ±SEM, n=7-9, * = $p<0.05$ in DOCA vs. sham group.

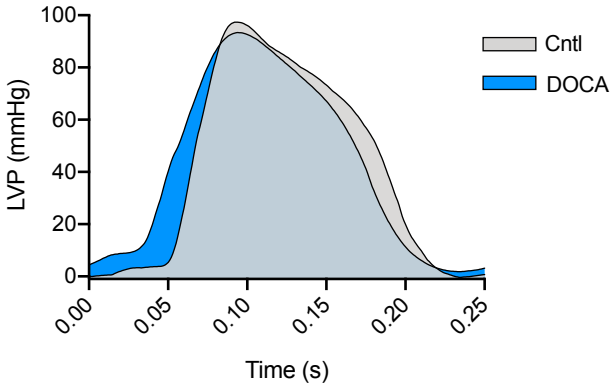

Figure 5.16 Pressure generation in the left ventricle in failing DOCA-salt hearts

Representative left ventricular pressure throughout a complete cardiac cycle from working DOCA-salt or sham control guinea pig hearts. Traces aligned at peak LVP for ease of comparison.

5.3.2 Hypothesis Testing

This section will describe studies which were conducted to examine the relationship between ventricular repolarisation and diastolic dysfunction in HF, using the guinea pig DOCA-salt model of HFpEF following the determination of this to be a suitable model based on characterisation data.

5.3.2.1 Effect of Repolarisation Abnormalities on Diastolic Dysfunction in Failing Hearts

Following the 7-week DOCA-salt protocol, hearts were isolated form DOCA and sham animals and perfused under working conditions. Results are displayed as change from baseline values following the addition of 100nM E-4031 + 30nM HMR1556 in order to determine any difference in the response of failing DOCA hearts to altered cardiac repolarisation, relative to control hearts.

A similar degree of QT prolongation was achieved in DOCA-salt and sham control hearts using treatment with 100nM E-4031 and HMR 1556, and there was no difference in the resultant change to heart rate between groups (Fig. 5.17 A & B). Changes to coronary flow and cardiac output following treatment with E4+HMR were also similar in DOCA-

salt hearts relative to nonfailing sham hearts, although stroke volume appeared to be slightly reduced in response to E4+HMR in DOCA animals, while in sham animals stroke volume was increased (Fig. 5.17 C-E).

Systolic function in DOCA hearts demonstrated a similar response to that of sham hearts following QT prolongation with E4+HMR (Fig. 5.18). Increases to dP/dt max and systolic duration were observed in both groups, while LVDP was largely unaffected.

Whilst not significant, some differences in response to E4+HMR treatment were observed in DOCA hearts relative to sham in terms of diastolic functional parameters (Fig. 5.19). Whilst diastolic duration and tau tended to increase in both groups, LVEDP decreased in the DOCA group in response to QT prolongation while in the sham group LVEDP increased. A similar trend was seen with dP/dt min, with the DOCA group demonstrating a greater mean dP/dt min following treatment with E4+HMR while the sham group demonstrated a reduced dP/dt min. However, it should be noted that these apparent differences in response were subtle.

This lack of significant functional effect of QT prolongation on cardiac function in DOCA-salt hearts is illustrated in Fig. 5.20, which shows that similar morphological differences are present between LVP traces of DOCA and sham hearts following E4 + HMR treatment when compared to baseline conditions (Fig. 5.16).

These effects are summarised in Table 5.2, which demonstrates the mean response of DOCA vs sham hearts to altered myocardial repolarisation as a result of treatment with 100nM E-4031 + 100nM HMR 1556 for the parameters discussed.

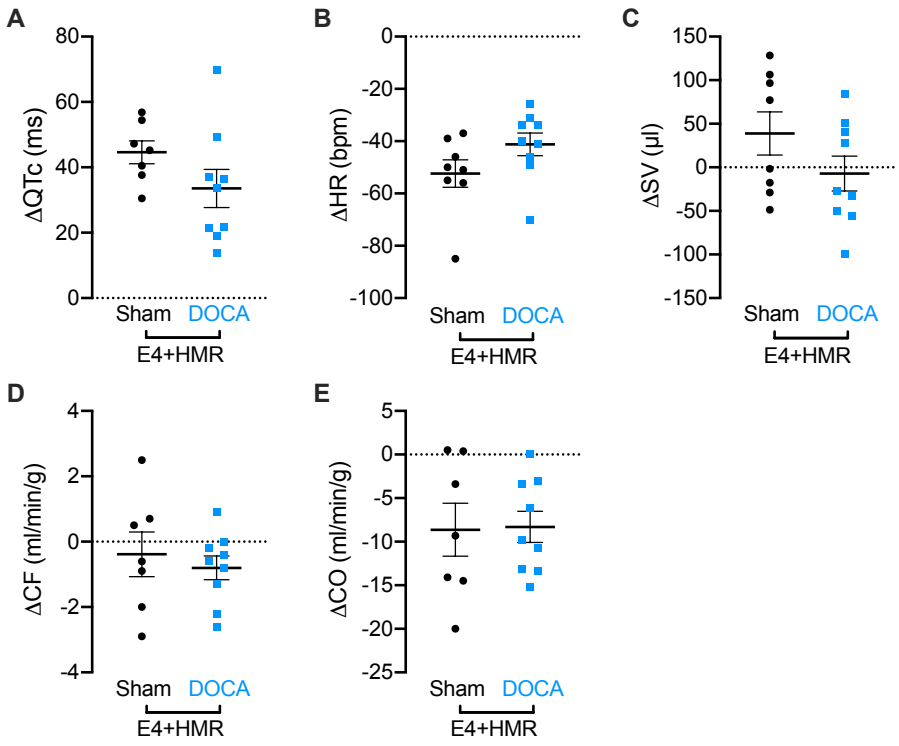

Figure 5.17 Effect of QT prolongation in the working DOCA-salt heart

Effect of treatment with 100nM E-4031 + 30nM HMR 1556 on functional parameters in working DOCA-salt hearts at 7 weeks post salt, relative to sham hearts. A) QTc interval, B) heart rate, C) stroke volume, D) coronary flow and E) cardiac output in DOCA vs. sham hearts following QT prolongation. Data presented as mean change relative to baseline values (i.e. before addition of E4+HMR) ±S.E.M., n=7-9.

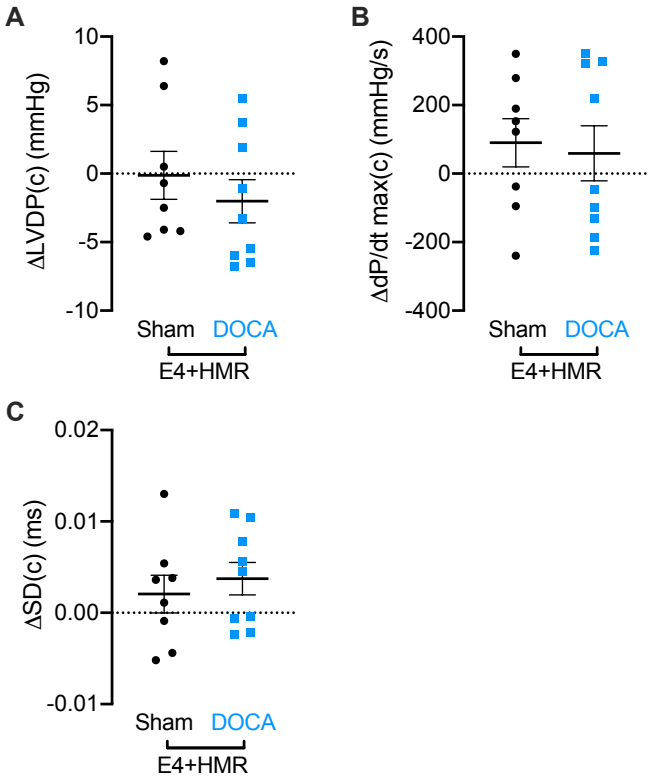

Figure 5.18 Effect of QT prolongation on systolic function in the working DOCA-salt heart

Effect of treatment with 100nM E-4031 + 30nM HMR 1556 on systolic function in working DOCA-salt hearts at 7 weeks post salt, relative to sham hearts. Values shown are corrected for heart rate: A) left ventricular developed pressure, B) dP/dt max and C) systolic duration in DOCA vs. sham hearts following QT prolongation. Data presented as mean ±SEM, n=7-9, * = $p<0.05$ in DOCA vs. sham group.

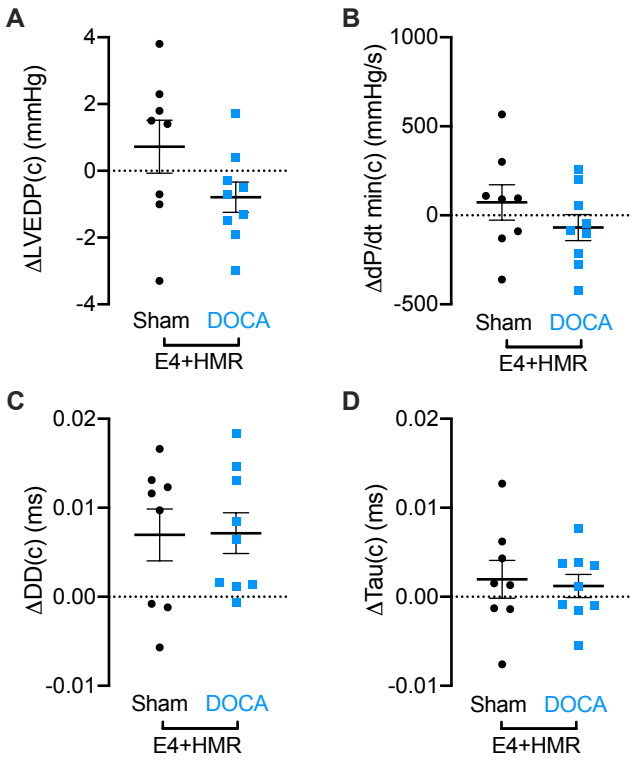

Figure 5.19 Effect of QT prolongation on diastolic function in the working DOCA-salt heart

Effect of treatment with 100nM E-4031 + 30nM HMR 1556 on diastolic function in working DOCA-salt hearts at 7 weeks post salt, relative to sham hearts. Values shown are corrected for heart rate: A) left ventricular end diastolic pressure, B) dP/dt min and C) diastolic duration in DOCA vs. sham hearts following QT prolongation. Data presented as mean ±SEM, n=7-9, * = $p<0.05$ in DOCA vs. sham group.

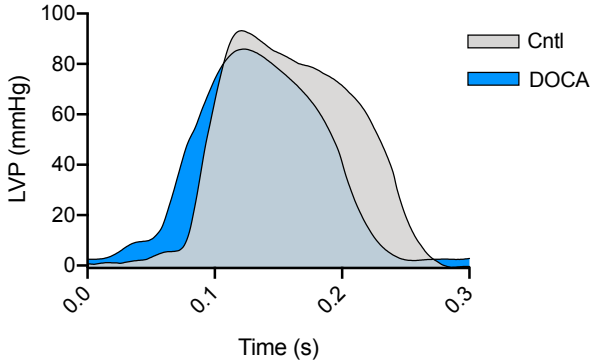

Figure 5.20 Effect of QT prolongation on pressure generation in the left ventricle in failing DOCA-salt hearts

Representative left ventricular pressure throughout a complete cardiac cycle from working DOCA-salt or sham control guinea pig hearts treated with 100nM E-4031 + 30nM HMR 1556. Traces are aligned to peak LVP for ease of comparison.

Table 5.2 Summary of effects of altered myocardial repolarisation in working DOCA-salt hearts

Summary data showing the functional effects of altered myocardial repolarisation as a result of treatment with E4+HMR in working DOCA-salt hearts, relative to sham counterparts. Values shown represent the mean group values for each functional parameter under baseline conditions and following the addition of 100nM E-4031 + 30nM HMR 1556 to prolong QT interval. Yellow highlighting denotes parameters which have increased in response to E4+HMR treatment, relative to baseline, while blue highlighting denotes parameters which have decreased. Green boxes indicate parameters which demonstrate an opposite response to E4+HMR treatment in failing DOCA-salt hearts relative to sham controls.

		QTc (ms)	HR (bpm)	SV (µl)	CO (ml/min/g)	LVDP(c) (mmHg)	dP/dt max(c) (mmHg/s)	SD(c) (s)	LVEDP(c) (mmHg)	dP/dt min(c) (mmHg/s)	DD(c) (s)	Tau(c) (s)
SHAM	Baseline	146	252	503	63	93	2882	0.147	4.6	-2566	0.103	0.019
	+E4+HMR	187	200	541	55	93	2972	0.149	5.3	-2493	0.110	0.021
DOCA	Baseline	146	241	428	47	84	2218	0.153	8.0	-1896	0.096	0.022
	+E4+HMR	180	199	420	38	82	2277	0.156	7.2	-1965	0.103	0.023

5.3.2.2 Effect of Repolarisation Abnormalities on Intracellular Sodium Levels in Failing Hearts

An additional cohort of DOCA-salt animals was established in order to determine the potential role for elevated intracellular sodium in diastolic dysfunction, and any relationship between this and delayed ventricular repolarisation. Initial data concerns the characterisation of this cohort to ensure that the same cardiac phenotype was achieved.

In anaesthetised animals, differences in baseline heart rate (and therefore QTc) were observed in this cohort and therefore additional comparisons were made between baseline and 6 weeks (shown in red), as well as between DOCA and sham animals at each time point (shown in black) to enable interpretation of the data (Fig. 5.21). As a result of these baseline differences, changes to QT interval are less clear in this cohort: DOCA animals demonstrate a higher QTc interval at 6 weeks relative to their sham counterparts, but this occurs alongside a reduction in QTc from baseline values in the sham group. DOCA animals also had a lower HR at the 6 weeks post-salt ECG recording, relative to baseline values. Such differences in HR between baseline and 6 weeks make any effects on QTc difficult to determine, particularly given the correction formula for QT interval was developed in working hearts and cannot be validated *in vivo*. Sham animals demonstrated a reduced QTc interval at 6 weeks vs baseline. This may simply be a reflection of inconsistent anaesthetic levels at the 6 week ECG recording in this group, with both heart rate and QTc in sham animals demonstrating larger variance at this timepoint. Overall, baseline differences in ECG and HR recordings between DOCA and sham animals make it difficult to draw conclusions about the effect of DOCA-salt treatment on QTc interval in this cohort of animals.

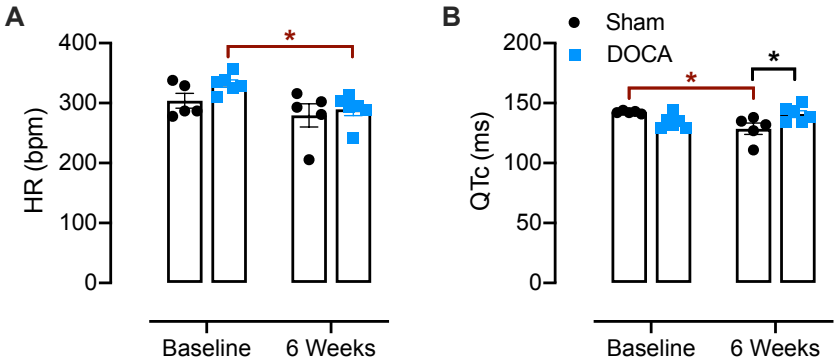

Figure 5.21 Impact of DOCA-salt treatment on heart rate and QTc interval in anaesthetised animals

Heart rate and QTc interval changes in anaesthetised DOCA and sham guinea pigs at baseline (week 0) and 6 weeks post-salt. A) Heart rate and B) QTc interval. Data presented as mean ± S.E.M., n=5-6, * = $p<0.05$ vs. sham. N.B. Statistical comparisons shown for baseline vs 6 weeks (in red) and for DOCA vs. sham at each timepoint (in black) owing to differences in HR and QTc at baseline.

Cardiac ultrasound data reveals the same preservation of systolic function (Fig. 5.22) alongside impairment of diastolic function (Fig. 5.23) previously observed. DOCA animals demonstrate preserved EF, and show similar cardiac output, stroke volume and S wave velocity to their sham counterparts. Calculated LV mass does not show an increase.

Diastolic function does, however, show some impairment in DOCA-salt animals (Fig. 5.23). Although DOCA animals did demonstrate a slightly lower IVRT at baseline, this was markedly elevated at 6 weeks post-salt, while the IVRT of sham animals remained unchanged. LAA was also significantly elevated in DOCA animals compared to sham counterparts at 6 weeks post-salt. It should be noted that a reduction in LAArea/BM at 6 weeks is an expected effect in healthy animals due to growth (statistical analysis shown in red). This was demonstrated by serial cardiac ultrasound scans in previous cohorts (see Fig. 5.6). A loss of this reduction in LAArea/BM is reflective of higher LAA in DOCA animals relative to sham counterparts (raw data not shown). Displaying data as LAArea/BM helps to account for the reduced body mass of DOCA animals. No significant changes to E/A or E/e' ratios were observed in response to DOCA-salt treatment.

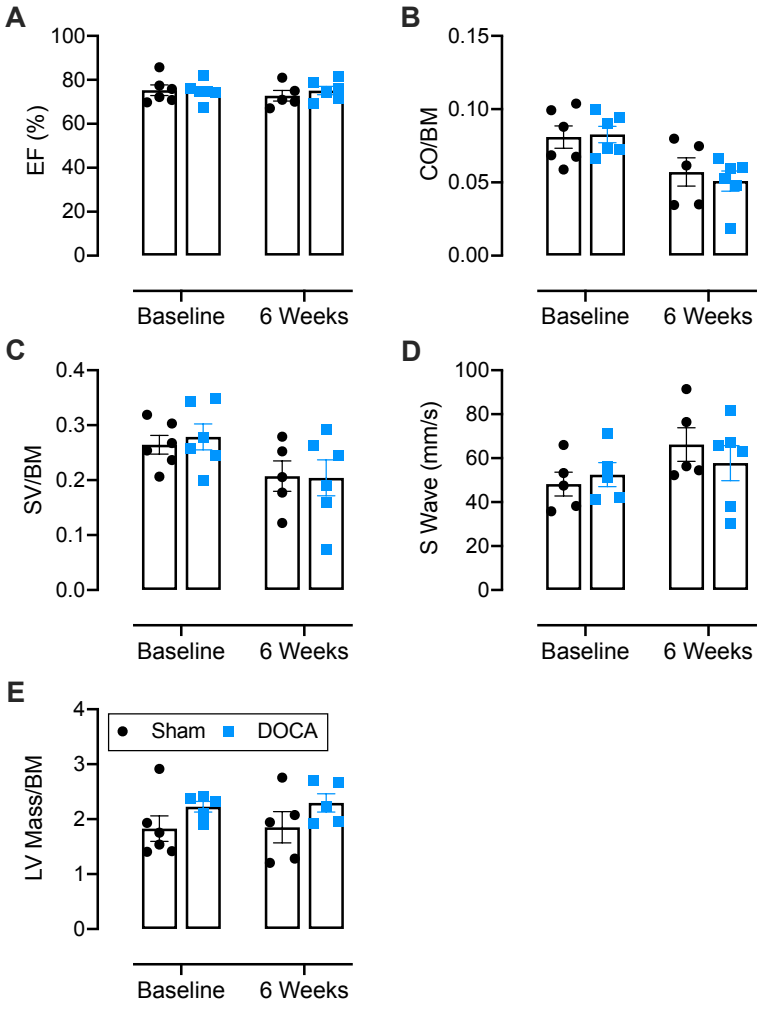

Figure 5.22 Impact of DOCA-salt treatment on systolic function *in vivo*

Cardiac systolic function in anaesthetised DOCA and sham guinea pigs at baseline (week 0) and 6 weeks post-salt, determined by cardiac ultrasound. A) Ejection fraction, B) cardiac output/body mass, C) stroke volume/body mass, D) S wave velocity and E) left ventricular mass/body mass. Data presented as mean ± S.E.M., n=5-6.

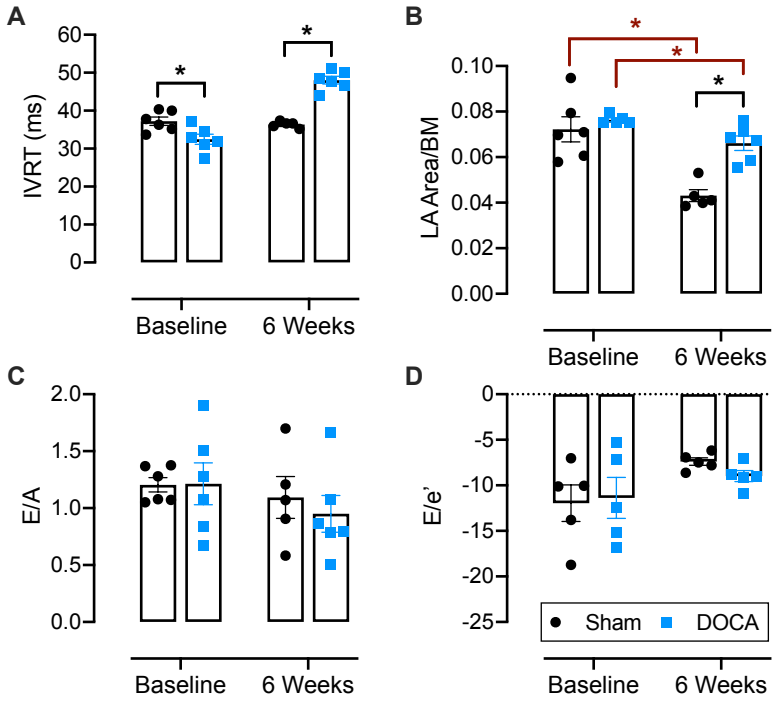

Figure 5.23 Impact of DOCA-salt treatment on diastolic function *in vivo*

Cardiac diastolic function in anaesthetised DOCA and sham guinea pigs at baseline (week 0) and 6 weeks post-salt, determined by cardiac ultrasound. A) Isovolumic relaxation time, B) left atrial area/body mass, C) E/A ratio and D) E/e' ratio. Data presented as mean ± S.E.M., n=5-6, * = $p<0.05$. N.B. Additional statistical comparisons comparing baseline to 6 weeks within DOCA and sham groups are shown for LAA/BM (graph B, in red).

No significant increase in LA mass was found in DOCA animals at 7 weeks post salt when hearts were isolated, with the same being true of RA mass (Fig. 5.24 A & B). LV mass, relative to tibia length, appeared to trend towards being higher in DOCA animals relative to sham, while RV mass was significantly lower in DOCA animals, as previously observed (Fig. 5.24 C & D).

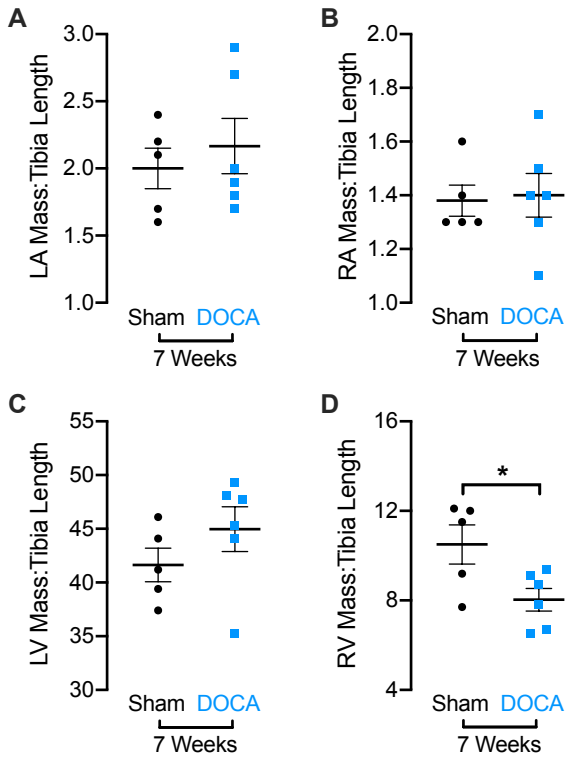

Figure 5.24 Impact of DOCA-salt treatment on cardiac gross anatomy

The myocardial mass of sham and DOCA-salt treated guinea pigs at termination of protocol (7 weeks post-salt), expressed vs. tibia length. A) Left atrial mass:tibia length ratio, B) right atrial mass:tibia length ratio, C) left ventricular mass:tibia length ratio and D) right ventricular mass:tibia length ratio. Data presented as mean ±S.E,M,, n=5-6, *= p<0.05 vs sham.

Prior to measuring intracellular sodium in DOCA-salt hearts, a study was conducted to measure sodium in healthy guinea pig hearts with 200nM ouabain used to elevate intracellular sodium in the presence or absence of 100nM E-4031 and 30nM HMR 1556. This allowed the ability to detect sodium elevation using NMR in isolated guinea pig hearts to be determined.

A modest but consistent increase in ^{23}Na TQF signal is observed in response to 200nM ouabain in both E4+HMR and vehicle control groups (Fig. 5.25 A). The ^{23}Na DQF signal appears less stable but shows no significant changes in response to ouabain in either group (Fig. 5.25 B). Although not achieving significance, the average ^{23}Na TQF signal is lower at baseline when compared to the average signal following treatment with ouabain (amounting to an 11% increase), indicative of elevated intracellular sodium (Fig. 5.25 C).

Prolongation of QT interval by treatment with E-4031 + HMR 1556 had no impact on intracellular sodium elevation by ouabain (Fig. 5.25 D). No significant changes to cardiac energetics (ATP to phosphocreatine ratio) or intracellular pH occurred throughout the experimental protocol, indicating that the isolated heart preparations remained in good condition throughout (Fig.5.25 E & F).

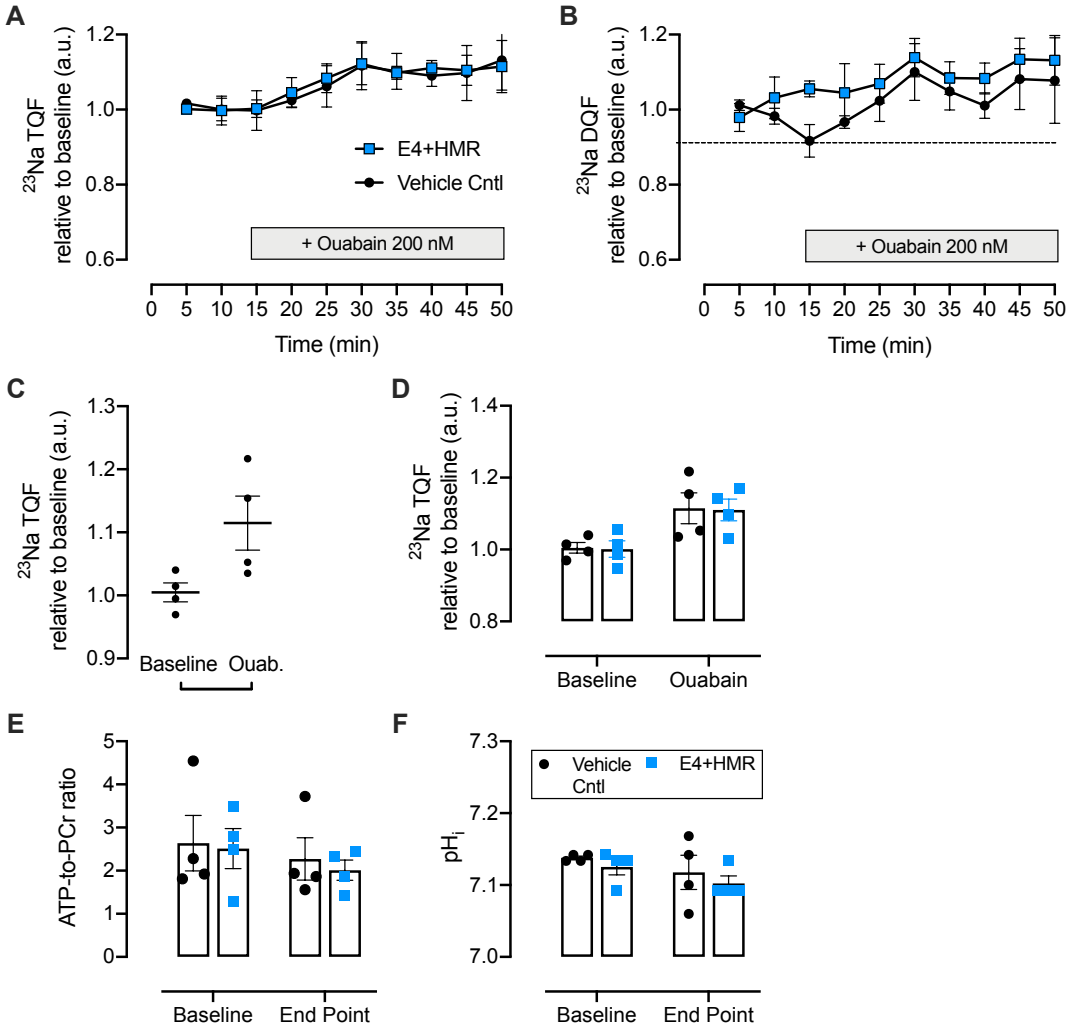

Figure 5.25 Impact of ouabain on intracellular sodium levels in isolated guinea pig hearts

Effect of treatment with 200nM ouabain on intracellular sodium levels in the presence/absence of 100nM E-4031 + HMR 1556 in isolated guinea pig hearts, as determined using ^{23}Na NMR. A) Triple quantum filtered (TQF) ^{23}Na signal representative of intracellular sodium concentration, B) double quantum filtered ^{23}Na signal representative of extracellular sodium concentration, C) average 23Na TQF signal at baseline and following addition of 200nM ouabain in vehicle control hearts, D) average 23Na TQF signal at baseline and following addition of 200nM ouabain in vehicle control vs. E4+HMR group, E) ATP to phosphocreatine ratio at the start and end of the protocol and F) intracellular pH at the start and end of the protocol. Data presented as mean ±S.E.M., n=4. **NMR studies conducted and analysed by Dr Yujin Chung.**

Hearts from DOCA-salt animals demonstrate a modest but consistent increase in ^{23}Na TQF signal relative to heart mass compared to sham counterparts (Fig. 5.26 A). The ^{23}Na DQF signal remains relatively stable throughout the course of the protocol and does not

vary between groups (Fig. 5.26 B). The average baseline ^{23}Na TQF signal relative to heart mass is significantly higher in DOCA hearts (~24% vs. sham), however, treatment with 100nM E-4031 + 30nM HMR 1556 has no effect on intracellular sodium in either group (Fig. 5.26 C & D). DOCA hearts demonstrate a significant increase in ATP to phosphocreatine ratio from baseline to the end of protocol, indicative of improved cardiac energetics (Fig. 5.26 E). No significant changes to intracellular pH occurred throughout the experimental protocol, indicating that the isolated heart preparations remained in good condition throughout (Fig.5.26 F).

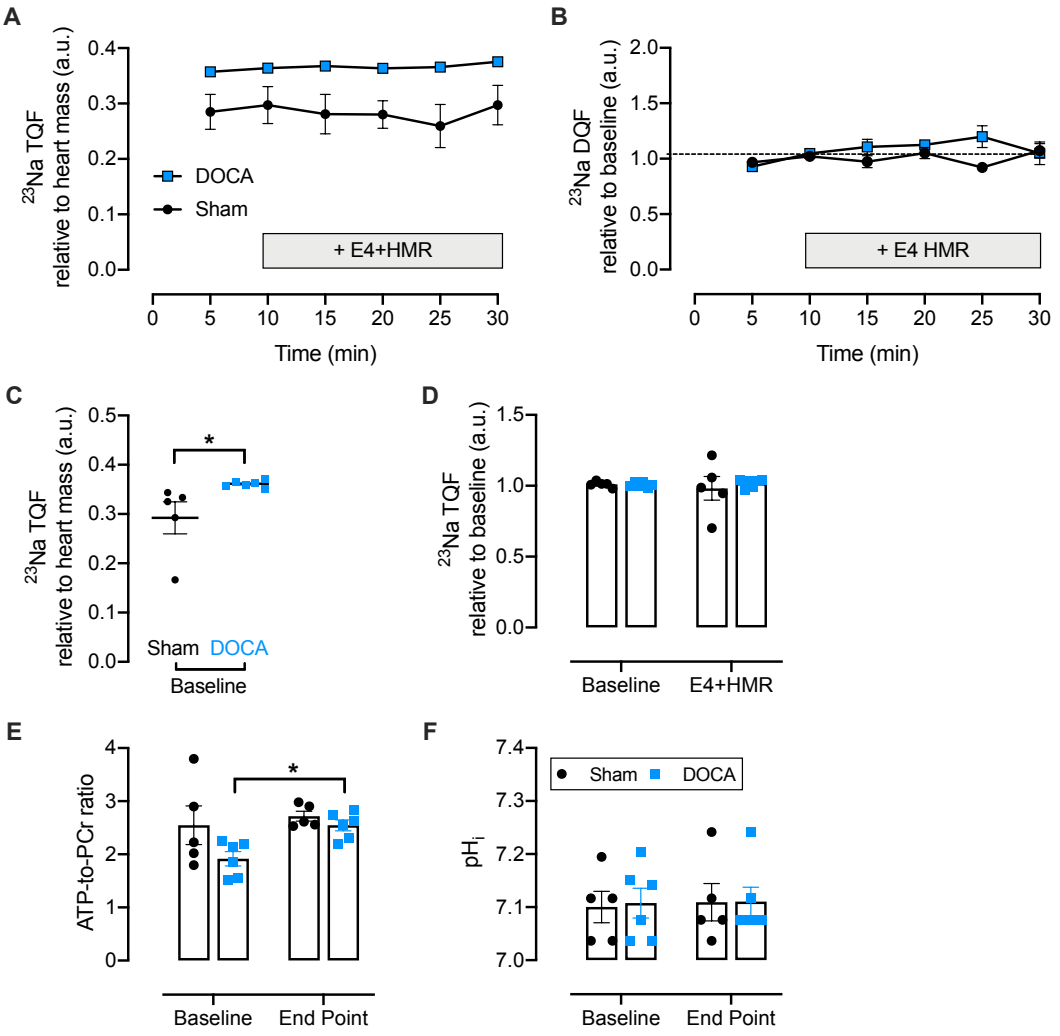

Figure 5.26 Impact of QT prolongation on intracellular sodium levels in isolated failing guinea pig hearts

Effect of QT prolongation with 100nM E-4031 + HMR 1556 on intracellular sodium levels in hearts isolated from DOCA-salt or sham-treated guinea pigs at 7 weeks post-salt, as determined using ^{23}Na NMR. A) Triple quantum filtered (TQF) ^{23}Na signal representative of intracellular sodium concentration, B) double quantum filtered ^{23}Na signal representative of extracellular sodium concentration, C) average 23Na TQF signal at baseline in sham and DOCA hearts, D) average 23Na TQF signal at baseline and following addition of 100nM E-4031 + 30nM HMR 155 in sham vs. DOCA group, E) ATP to phosphocreatine ratio at the start and end of the protocol and F) intracellular pH at the start and end of the protocol. Data presented as mean ±S.E.M., n=5-6. **NMR studies conducted and analysed by Dr Yujin Chung.**

5.4 Discussion

5.4.1 Model Characterisation

This study has been able to demonstrate that the guinea pig DOCA-salt model represents a very effective model of HF with diastolic dysfunction, displaying many of the associated characteristics observed both clinically and in other animal models of HF.

The initial challenge associated with setting up the guinea pig DOCA-salt model was establishing the correct dose and route of administration of DOCA. The DOCA-salt model is widely used in rats and mice for both hypertension and HF studies, and as a result has very variable reported doses, routes of administration and durations of exposure.[148, 149, 165-169] The only reported use of the DOCA-salt model in guinea pigs was from two studies published by the Tritilli group,[148, 149] which contained two different methods of drug administration (subcuticular pellet and 5x weekly intramuscular injections) that varied greatly in dosage. After consideration of the literature it was decided that subcutaneous pellet-delivery of a continuous daily dose of DOCA was the most appropriate method, and a dose was selected which could be modified as appropriate (each animal was to be implanted with 3x 200mg pellets, therefore the number of pellets could be adjusted to alter the dose). The Tiritilli studies also used a 0.9% NaCl + 0.2% KCl drinking solution, instead of the more usual 0.9-1% NaCl. Given that no justification was provided for this change, a solution of 1% NaCl was chosen for the present study. An initial pilot study with the chosen dose (data not shown) revealed that DOCA animals lost weight following the switch to 1% NaCl drinking solution, indicating that the DOCA dose was too high. Anorexia and trembling were reported as side-effects of high DOCA dose in guinea pigs by the Tiritilli group, therefore this initial pilot study was terminated and a second pilot cohort performed with a reduced dose (2x 200mg pellets/animal, 6.67mg/day). This lower dose was selected as a suitable dose since animals gained weight throughout the study (albeit at a slower rate than their sham counterparts) and exhibited normal behaviour.

Having established a suitable surgical method and dosing protocol, a subsection of the next two cohorts of animals were telemetered with combined ECG and blood pressure

radiotelemetry devices to provide information about ventricular repolarisation (QTc interval) and blood pressure in conscious animals. This did not yield very large group sizes owing to failure to successfully record physiological data from a number of telemetered animals, which displayed signal noise rather than ECG/blood pressure traces in the weeks after implantation, despite apparently successful surgery. The reason for this did not become clear until the end of the protocol, at which point the probes were removed from the animals under terminal anaesthesia at the time of heart excision for working heart studies. It was discovered that in most of these telemetered animals, the ECG leads had become detached from their anchor points in the chest wall (originally in a modified lead II positioning) and had become wound lengthwise around the body of the probe itself (Fig. 5.23). In many cases this had resulted in twisting of the pressure catheter as well due to rotation of the probe, thus resulting in a loss of ECG and blood pressure data. Strangely, the longitudinal wrapping of the ECG lead around the probe was remarkably neat. The reason for this is unclear but seemed to be a consistent effect with femoral artery cannulation and positioning of the probe in the right flank. The neatness and reproducibility of the longitudinal lead-wrapping suggests that there is a fundamental problem with this placement in this guinea pig model. However, time and cost constraints prevented the repetition of this cohort and exploration other placement options.

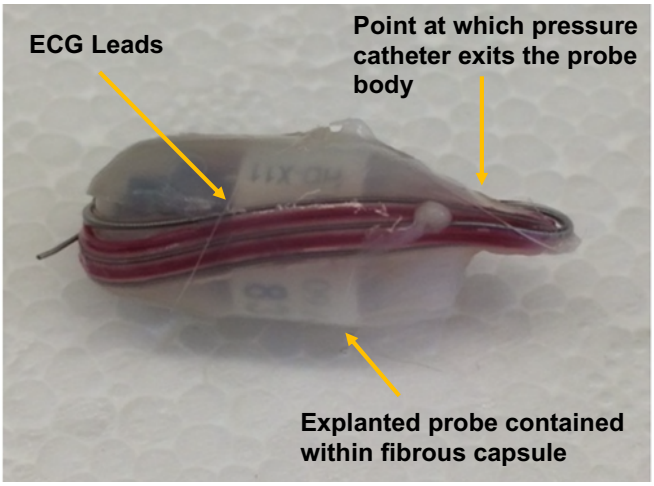

Figure 5.27 HD-X11 radiotelemetry probe upon explantation

Representative image showing HD-X11 combined blood pressure and ECG radiotelemetry probe upon explantation at 7 weeks post-salt. Probes were contained within a fibrous capsule upon explantation, fixing ECG leads in the position in which they had been held inside the animal. It was found in many of the animals that the ECG leads (positive lead in red silicone casing, negative lead in clear silicone casing) became detached from their anchor points in the chest wall and wrapped around the probe, resulting in a loss of ECG signal and, often, twisting of the pressure catheter with resultant additional loss of pressure signal.

Despite this, remaining data from probes which did successfully record physiological data throughout the protocol indicate that guinea pigs have a MAP of around 60-70 mmHg, which shows a substantial increase to around 110 mmHg by 6 weeks post-salt. This may be a slightly lower baseline blood pressure when compared to mice or rats, but this observation is in good agreement with the limited literature available on conscious guinea pigs.[170, 171] Telemetry data also suggests that conscious DOCA-salt guinea pigs may develop a higher heart rate than sham counterparts. This may reflect an increased sympathetic tone due to the presence of HF, as is reported to be the case both clinically and in animal models.[172-175] Telemetry data revealed no difference in QTc interval between conscious DOCA and sham animals.

In comparison, data from anaesthetised animals reveals that no difference in heart rate between groups was observed, whilst a clear prolongation of QTc interval was present in DOCA-salt animals relative to their sham counterparts. It should be noted that the group sizes in the anaesthetised recordings are much larger than for the conscious telemetry data

(due to the issues with the telemetry probes described above), and so any increase in QTc interval may simply have been lost due to low group sizes in conscious animals. Certainly, any effect of anaesthetic would have been equal between groups and light anaesthesia was maintained throughout recording, as evidenced by the physiological heart rate. Indeed, the heart rate in anaesthetised animals was in fact higher than that of conscious animals, which is perhaps contradictory to what one might expect. This is likely an effect of the stress of handling and removal from home cage prior to the recording of ECG's, since this was done immediately upon induction of anaesthesia. It should also be noted that direct comparison of *in vivo* and *ex vivo* QTc intervals may not be advisable, since the formula used to correct for heart rate variation was developed using data from isolated hearts which are free from the influence of circulating catecholamines which will affect the relationship between QT interval and heart rate. However, there was no difference in heart rate between anaesthetised DOCA and sham animals and so there will have been no skewing of the data by application of the correction factor i.e. the difference between groups is genuine.

The echo data reveals a strong phenotype of diastolic dysfunction with preserved systolic function in DOCA-salt animals. This is typical of HFpEF and is in good agreement with other reports from animal models of diastolic dysfunction. Of note is the rapid and sustained increase in IVRT in DOCA-salt animals as well as the increased LAA, which have both been reported to be of particular significance when assessing the presence of diastolic dysfunction in mouse models of HF.[150] In the present study, LAA was used as a surrogate of LA volume and measurements normalised to the body mass of individual animals to account for differences in LA size, which is known to vary with body size.[176] LAA and/or LA volume are accepted as important and sensitive markers of diastolic dysfunction clinically, indeed, LA maximum volume index (LA peak systolic volume corrected for body surface area) is recommended as one of four diagnostic variables to be assessed in order to establish the presence of diastolic dysfunction by the American Society of Echocardiography and the European Association of Cardiovascular Imaging.[177] LA volume has been found to increase in line with disease severity and has been proposed to act as a marker of chronic diastolic dysfunction, as opposed to the 'snapshot' of ventricular filling pressures provided by other measures such as E/e'.[178-180] Although not

routinely used as an independent diagnostic marker in the clinic, changes to IVRT as a result of diastolic dysfunction are well-established. The lack of utilisation of IVRT for diagnostic purposes is due to the complexity of the relationship between IVRT and ventricular relaxation, since both increases and decreases to this parameter can be indicative of diastolic dysfunction.[177, 181] An increase in IVRT as observed in the present study has been suggested to represent underlying impairment of ventricular relaxation, whilst a shortening of IVRT is characteristic of restrictive filling patterns. Indeed, in mouse models of HF LAA has been recommended to provide the best indication of chronic diastolic dysfunction, with IVRT providing a means to further distinguish between impaired ventricular relaxation vs restrictive filling phenotype.[150] The key diagnostic marker of diastolic dysfunction cited for use in the clinic is the E/e' ratio, with E/A ratio considered to be useful for the assessment of diastolic function when other parameters are also suggestive of diastolic dysfunction but not definitive.[177, 182] Data from the present study reveals no strong association between these parameters and diastolic dysfunction in the DOCA-salt guinea pig model, however, there may be several contributing factors to this observation. One such factor relates to the technical challenge of acquiring a good apical 4-chamber view in the guinea pig. There is very limited data available concerning the use of echocardiography in guinea pigs, and so establishing whether mitral flow/tissue doppler measurements reflected normal physiological values was not possible from the literature. Additionally, it is well-reported that achieving consistent readings of early and late mitral flow velocities is very challenging in species with a high heart rate, with the peaks often fusing together. The presence of increases to E/e' is also reported to be model-dependent, with a mouse model of HFpEF showing no change to this parameter despite the presence of other markers of diastolic dysfunction.[150] Together, these observations may account for the lack of change in these parameters in this model. Overall, cardiac ultrasound data revealed DOCA-salt guinea pigs to display overt markers of diastolic dysfunction with preserved ejection fraction, indicating that it may provide a suitable model of HFpEF.

Baseline data from isolated working heart preparations was in good agreement with the diastolic findings from the echo data, demonstrating a clear diastolic dysfunction in DOCA-salt hearts under baseline conditions. This was evident from a significant increase

in LVEDP alongside a significant reduction in dP/dt min, which have been reported to be indicative of impaired ventricular filling and active relaxation, respectively.[183] The value of LVEDP is known to be load-dependant, and as such will vary with factors external to the heart. This may be accounted for by collecting the value of LVEDP over a range of loading conditions and expressing the result as an EDPVR.[183, 184] However, in the present study sham and failing hearts were assessed under isolated working conditions and experienced identical preload and afterload. As such, this could be argued to represent a load-independent 'version' of LVEDP values which are normally obtained *in vivo*, providing a readout of diastolic function comparable to that of the EDPVR. The same load-dependence is reported for dP/dt min which, again, may be somewhat controlled for by assessing this parameter under isolated working conditions.[183, 185-187]

Interestingly, unlike the echo data, systolic function was also found to be impaired in working DOCA-salt hearts. This, taken alongside the fact that seemingly apparent differences in heart rate and QTc interval in DOCA animals detected using telemetry and anaesthetised ECG recordings were also lost, may indicate increased sympathetic tone in DOCA-salt animals *in vivo*. It may be the case that the development of increased sympathetic tone in DOCA-salt animals arose in order to maintain cardiac output, resulting in a 'masking' of systolic failure and an elevated resting heart rate. Upon isolation of the hearts and removal of sympathetic tone, this compensatory increase in systolic function would be lost, resulting in the functional phenotype seen in the isolated hearts. Indeed, increased sympathetic tone is commonly reported in HF.[172-175]

This isolation-induced loss of adrenergic tone may also account for the loss of QTc prolongation in isolated DOCA-salt hearts. Adrenergic signalling is clearly important in modulating I_{Ks}, which is known to play a predominant role in determining APD in the guinea pig ventricle.[109] This may seem counterintuitive since adrenergic stimulation is known to increase I_{Ks} and therefore shorten the ventricular AP, however, it is possible that I_{Ks} may have become downregulated in the face of excessive stimulation therefore prolonging QT interval. Upon subsequent isolation of the hearts, rather than the DOCA-salt hearts 'losing' the QTc prolongation observed *in vivo*, the sham control hearts underwent a prolongation of QTc interval in response to the loss of baseline sympathetic tone, as one would expect. There are numerous reports of I_{Ks} downregulation in models

of HF which often also display APD/QTc prolongation that could support this theory.[75, 109, 188, 189] However, one reported mechanism by which this occurs (phosphorylation of KCNE1 by activated PKC)[190] is not present in guinea pigs and has in fact been reported to increase I_{Ks} current amplitude.[191] However, downregulation of I_{Ks} alongside QTc prolongation in guinea pig models of LV hypertrophy has still been reported previously.[192] Additionally, the degree of QT prolongation achieved using the combination of E-4031 and HMR 1556 to achieve blockade of I_{Kr} and I_{Ks} was almost identical (22.5% vs. 22.8% in sham) which may seem surprising if I_{Ks} is downregulated. However, this is not necessarily contradictory if I_{Ks} is minimally active under baseline conditions in the absence of sympathetic activation, as has been reported to be the case.[28, 30, 193] Under such circumstances the majority of the QT prolongation seen in response to E4+HMR treatment would stem from the effects of E-4031 on I_{Kr}. Therefore, the mechanism of QT prolongation in the guinea pig DOCA-salt model may involve downregulation of I_{Ks} in response to a prolonged increase in sympathetic tone, but further investigations would be required to confirm this.

Data concerning alterations to expression of key proteins involved in intracellular calcium handling reveal clear differences between DOCA-salt and sham animals. Ventricular tissue from failing hearts demonstrated increased NCX protein levels and decreased SERCA2a protein levels, both of which are widely reported in both human and animal failing hearts.[59, 143, 194-197] Indeed, elevated NCX expression in a setting of reduced SERCA activity/expression is proposed to be one mechanism by which systolic function could be preserved in failing hearts. This would occur as a result of increased calcium entry into the cell via reverse-mode NCX during early repolarisation, thus supplementing the depleted SR calcium stores in the face of reduced SERCA function. However, this altered NCX activity is proposed to be protective only at lower heart rates, with higher heart rates resulting in elevated diastolic intracellular calcium levels and further impairment of ventricular relaxation.[57]

DOCA-salt animals also demonstrated an increase in the protein expression of the α_2 and β_1 subunits of the Na^+,K^+-ATPase, with what appears to be a trend towards an increase in the β_2 subunit expression. The increase in the α_2 subunit is particularly marked (~141% vs sham) and is in contrast with the prevailing observations from the literature, which

often report a decrease in this subunit in other animal models of hypertension or hypertrophy/HF,[60-63] whilst there are reports of this subunit expression remaining unchanged in failing human hearts.[198, 199] Interestingly, another study using a guinea pig aortic banding model found a significant increase in the expression of the α_2 subunit alongside increased NCX expression and decreased SERCA2a, in line with the findings of the present study.[200] However, this is not true of all guinea pig models, with the study by Ke et al. demonstrating decreases in the expression of both α_1 and α_2 Na^+,K^+-ATPase subunits in a guinea pig aortic banding model. This study is particularly interesting as two separate time points were examined which, based on functional cardiac ultrasound data, represented a compensated hypertrophy phase (60 days post-banding) and subsequent progression into HF (150 days post-banding).[63] Western blotting and immunofluorescence staining revealed a significant decrease in α_1 subunit expression at both timepoints alongside a decrease in the α_2 subunit at 150 days, although this decrease appeared to be less marked compared to α_1 (the expression of the α_2 subunit was not examined at the 60-day timepoint). The authors proposed that a decrease in the Na^+,K^+-ATPase current, alongside an increase in $I_{Na,late}$, alters calcium exchange by NCX to limit systolic impairment in the compensated hypertrophy phase. A subsequent decrease in SERCA function was reported during the HF phase, which coincided with contractile impairment and an increased relative contribution of NCX to calcium extrusion. This is clearly in contrast to the findings of the present study, which reported increased Na^+,K^+-ATPase subunit expression alongside decreased SERCA and increased NCX expression. However, these interactions are complex, and the relative expression of the individual subunits is likely to be important. Na^+,K^+-ATPase is composed of an α subunit core which provides the catalytic binding sites for sodium, potassium, cardiotonic steroids (e.g. ouabain) and ATP, while the outer β subunit is required for trafficking to the sarcolemmal membrane.[201] The α_2 isoform demonstrates a preferential localisation to transverse tubule membranes over the α_1 isoform[202, 203] and has been suggested to play an important role in indirectly regulating intracellular calcium stores as a result of co-localisation with NCX in this restricted cytosolic region.[204-206] Indeed, it has been demonstrated that the α_2 subunit and NCX share the same subcellular localisation[205, 207] and there is some evidence that changes to Na^+,K^+-ATPase subunit expression can drive compensatory changes to NCX expression.[60] It is known that inhibition of Na^+,K^+-ATPase (e.g. with ouabain) has a

positively inotropic effect due to the resultant decrease in calcium efflux via NCX exchange in response to the reduced sodium gradient, thereby increasing intracellular stores.[60] In a setting where NCX expression is increased in response to reduced α-NKA subunit expression (as is often reported in HF), it is proposed that this would work to prevent any changes to intracellular calcium stores by compensating for the reduced sodium gradient with increased calcium extrusion.[60] In our model the increase in α_2 isoform expression is accompanied by an increase in NCX which, according to this theory, would actually increase the overall calcium extrusion from the cell. However, we also see elevated intracellular sodium and AP prolongation in our model, alongside a preservation of systolic function *in vivo*, which could imply that NCX is also being driven to lower calcium extrusion/increased calcium influx due to these other factors known to affect its activity. These interactions are complex and should not be oversimplified.

Gross anatomy also revealed DOCA-salt guinea pigs to demonstrate LV hypertrophy in accordance with other models of HFpEF (Fig. 5.9), although there was an absence of any pulmonary oedema (Fig. 5.10). This may reflect an incomplete transition from the compensated hypertrophy phase to overt HF in this model, phases which were identified in the guinea pig aortic banding model by Ke *et. al*.[63] However, DOCA animals did demonstrate a clear loss of SERCA expression, and a loss of SERCA function was shown to correspond with the transition to HF in the aortic banding model, and so defining when this transition occurs is likely not straightforward. It may be of interest in future experiments to extend the length of exposure to DOCA-salt treatment and determine whether more overt clinical signs of HF manifest as a result.

5.4.2 Hypothesis Testing

Having established a suitable model of diastolic dysfunction in HF, it remained to test the experimental hypothesis that altered ventricular repolarisation may act to further impair diastolic function in the failing heart. In order to do this, isolated working DOCA-salt and sham control hearts were exposed to pharmacological prolongation of QT interval, as was previously performed under the same experimental setup (Results Chapter 2). Using this experimental approach was appropriate since baseline characterisation revealed that QTc prolongation was not present in isolated working DOCA-salt hearts, and this intervention

had been previously well-characterised in terms of the effect on function in healthy hearts in the isolated setting. Data was displayed as a change in each parameter relative to baseline values, so that it could be determined whether failing hearts responded differently to abnormal repolarisation compared to healthy counterparts. Although no significant differences were observed between DOCA and sham heart response to QT prolongation, there were three parameters in which DOCA hearts demonstrated an opposite response to treatment when compared to sham counterparts: stroke volume, LVEDP and dP/dt min (Table 5.2). It is not clear whether these responses represent a true difference in the function of DOCA vs sham hearts, owing to the modest size of the changes and the lack of statistical significance. However, such differences are interesting because, in contrast to sham hearts, DOCA hearts demonstrate a reduction in LVEDP in response to QT prolongation alongside an increased maximum rate of pressure decline, both of which are indicative of an improvement of diastolic function and would be in contrast to the experimental hypothesis. In hindsight, it would perhaps have been of benefit to perform an incremental prolongation of QT interval with E4+HMR in isolated DOCA-salt and sham hearts, to determine whether this effect demonstrated a dose-dependent relationship.

Given the importance of intracellular sodium concentration in the interplay between ventricular repolarisation and intracellular calcium handling, it was decided that it was important to understand how our interventions might affect sodium levels in the failing heart. Initial studies were conducted in order to demonstrate that changes to intracellular sodium could be measured in the isolated Langendorff-perfused guinea pig heart using ^{23}Na NMR spectroscopy, and to determine the effect of altered ventricular repolarisation on intracellular sodium levels in the healthy heart. Whilst ouabain resulted in an apparently modest but measurable increase in intracellular sodium (~11% from baseline) there was no effect of pharmacological prolongation of QT interval in this setting, in agreement with earlier working heart studies which demonstrated no functional changes under such conditions. An additional cohort of DOCA-salt animals revealed that failing hearts demonstrate a greater degree of elevated intracellular sodium, approx. 24% relative to sham hearts. This elevated intracellular sodium in DOCA-salt hearts is in line with the reported findings from both clinical studies and animal models of HF, including other

guinea pig models of HF.[53-56] Such an elevation of intracellular sodium would likely contribute to altered NCX activity, potentially leading to altered intracellular calcium handling[57] (Section 1.2.4.2). However, this is likely to have complex effects given that we also see an upregulation of NCX protein expression and a prolongation of APD in DOCA-salt animals, and we have no measure of intracellular calcium concentration in our model. All of these factors will also feed into NCX activity and direction of function. The working DOCA-salt heart studies reveal a modest improvement to LVEDP and dP/dt min in DOCA-salt hearts with QT prolongation whilst control hearts show a modest trend in the opposite direction. Could it be possible that the increased APD in this setting simply allows a larger window for NCX (which is upregulated in this setting) and SERCA to remove more calcium from the cytoplasm and aid ventricular relaxation? Further information about changes to the intracellular calcium transient kinetics would be required in our model to interpret these findings. Whole-heart optical mapping or isolated myocyte calcium recordings would be invaluable in understanding the potential mechanisms involved. However, we do know that treatment with E4+HMR did not affect intracellular sodium levels in either healthy or failing hearts, and so any effects observed are independent of alterations to the sodium gradient.

One other limitation of the current study is the lack of data concerning potential structural changes to the myocardium which could impair relaxation via passive mechanisms (e.g. fibrosis, titin phosphorylation etc.). It may be that a major source of diastolic dysfunction in this model relates to changes in the physical properties of the ventricular myocardium as a result of remodelling, rather than changes to calcium transient dynamics. It would be useful to be able to address the balance of causal factors in future studies.

5.4.3 Summary and Conclusions

Extensive characterisation data gathered as part of this study indicates that guinea pigs treated according to the outlined DOCA-salt protocol provide a very suitable model of diastolic dysfunction in HF. *In vivo* data reveals prolongation of QTc interval alongside increased IVRT and LAA with preserved EF, typical of models of HFpEF. Myocardial dysfunction (both systolic and diastolic) was also confirmed in isolated working heart preparations using a pressure-volume catheter. In addition to this, DOCA-salt hearts also

demonstrated elevated NCX protein expression with reduced SERCA expression and elevated intracellular sodium levels. Overall, these data indicate that this is a novel model of diastolic dysfunction in HF which will be of great value to future studies investigating the mechanisms of this disease – particularly where the different electrophysiological characteristics of the rat and mouse heart make these species less suitable as models of human disease.

In terms of the experimental hypothesis, data from failing DOCA-salt guinea pig hearts indicated that ventricular repolarisation abnormalities do not contribute to diastolic dysfunction in this model. This is in agreement with previous preliminary studies conducted in healthy working guinea pig hearts, in which key features of HF were replicated pharmacologically (Results Chapter 2). Further studies would be needed to understand the underlying mechanisms of diastolic dysfunction in the present model of HF, however, data from the present study provides valuable insight into the role of ventricular repolarisation in diastolic dysfunction.

6 GENERAL DISCUSSION

6.1 Summary of Major Findings

Recent studies have revealed a correlation between ventricular repolarisation abnormalities and diastolic dysfunction in failing hearts, however, it is unclear whether or not this represents a causal relationship. The present study has aimed to address this question using a direct approach to determine the relationship between diastolic function and ventricular repolarisation in the whole heart, beginning in healthy Langendorff-perfused hearts and progressing to isolated working hearts from a novel guinea pig model of HF with diastolic dysfunction. In non-HF models, APD was prolonged via pharmacological blockade of repolarising currents I_{Kr} and I_{Ks} to replicate the changes to QT interval seen in the clinic. This was then built upon by pharmacologically replicating other factors which are commonly reported to be present in HF, namely elevated intracellular sodium and impaired SERCA function. Such factors affect intracellular calcium handling and are therefore likely to be relevant to the proposed mechanism by which altered ventricular repolarisation could affect diastolic function (i.e. perturbed intracellular calcium handling leading to a delay or reduction in the removal of cytosolic calcium during diastole). These experiments culminated in the development of a novel guinea pig model of HF with diastolic dysfunction, allowing the relationship between ventricular repolarisation and diastolic function to be assessed in a setting of HF.

Initial studies utilising optical mapping in healthy, Langendorff-perfused guinea pig hearts demonstrated that the intracellular calcium transient is prolonged in response to prolongation of the AP. This effect occurs with both APD prolongation due to altered pacing frequency and pharmacological blockade of repolarising currents. Subsequent studies in healthy Langendorff-perfused hearts demonstrated no functional effect of prolonging APD at normal heart rates. However, when heart rate was slowed to allow more extensive APD prolongation, or when SERCA activity was pharmacologically impaired, subtle changes to diastolic function were detected, namely an increased relaxation time and elevated LVEDP, respectively. These conditions are relevant to the experimental hypothesis because QT prolongation is able to occur to a greater extent in

the human heart, owing to the increased 'diastolic pause' seen at lower heart rates, and a reduction in SERCA expression and/or activity is commonly reported in failing hearts. Ultimately, it was apparent that the Langendorff-perfused heart, coupled with an IVB to measure LVP, could not provide a sensitive enough measure of subtle changes to diastolic function, prompting a switch to the working guinea pig heart with an intraventricular pressure-volume catheter as the experimental model in subsequent experiments.

Extensive characterisation of the working heart model provided baseline data which gave confidence that the working heart provided a closer approximation of normal physiology than the Langendorff heart, as well as enabling the development of a formula to account for the contribution of variations in HR to functional indices. The initial findings from Langendorff studies of modest changes to diastolic function in response to QT prolongation alone did appear to be somewhat replicated using the working heart setup in the form of an increase in the time constant of relaxation, tau, although this occurred in the absence of any changes to LVEDP or dP/dtmin. Subsequent experiments, however, failed to replicate findings from Langendorff studies when looking at the impact of pharmacologically induced ventricular repolarisation abnormalities on diastolic function in the presence of sodium elevation and/or impaired SERCA activity. No strong associations between diastolic function and ventricular repolarisation abnormalities were demonstrated as a result of these studies, however, it was felt that it was important to explore this relationship in the failing heart where other pathologies may be present which contribute to this interaction.

The guinea pig DOCA-salt model was identified as a potentially suitable model for heart failure with diastolic dysfunction based on literature which proposed this to be a suitable model for HFpEF in the mouse.[147] This is a relatively novel model in the guinea pig and there is no existing functional data available on diastolic or systolic function in DOCA-salt guinea pig hearts, necessitating extensive characterisation before working heart studies to test the experimental hypothesis could be conducted. This was done using serial, combined blood pressure and ECG radiotelemetry recordings alongside cardiac ultrasound and anaesthetised ECG recordings. Cardiac gross anatomy on termination was also examined, alongside baseline function of working hearts, allowing for comparison of *in vivo* and *ex vivo* cardiac hypertrophy and functional measurements. Findings

revealed the guinea pig DOCA-salt model to demonstrate diastolic dysfunction alongside preserved systolic function *in vivo*, with QT prolongation also present in anaesthetised QTc recordings and elevated heart rate and blood pressure in conscious animals. LA and LV hypertrophy were also present and, despite *in vivo* measurements revealing no systolic dysfunction using clinically accepted measures, *ex vivo* measurements in working DOCA-salt hearts revealed systolic dysfunction under baseline conditions. NMR studies confirmed the presence of elevated intracellular sodium in failing DOCA hearts, while western blotting revealed reduced SERCA expression and increased NCX expression commonly reported in HF. Overall, characterisation data demonstrates the guinea pig DOCA-salt model to be a very suitable model for exploring the role of ventricular repolarisation abnormalities in diastolic dysfunction in HF. The experimental hypothesis was then tested by pharmacologically prolonging ventricular repolarisation in isolated working DOCA-salt and sham hearts. Data revealed that diastolic function was not further impaired in failing hearts in response to QT prolongation, indicating that ventricular repolarisation abnormalities are likely not the major cause of diastolic dysfunction seen in failing human hearts presenting with QT interval abnormalities in the clinic. Possible reasons for this, alongside other contributing mechanisms, will be discussed below.

6.2 Guinea Pig DOCA-Salt Model

The present study aimed to address whether the abnormalities of ventricular repolarisation commonly seen in patients presenting to the clinic with HF may causally contribute to diastolic dysfunction in HFpEF. In order to properly investigate this, it was necessary to develop an animal model of HFpEF which displayed key clinical criteria, giving confidence that it mirrored the human condition as closely as possible. Therefore, when considering the findings of the study, it is relevant to ask whether the guinea pig DOCA-salt model meets the criteria to be defined as a model of HFpEF. There are four diagnostic steps, according to the European Society of Cardiology (ESC)[208], which must be followed in order for a confident diagnosis of HFpEF to be given, detailed in Table 6.1.

Table 6.1 HFA-PEFF Algorithm for the Diagnosis of HFpEF

Recommended steps to confirm a clinical diagnosis of HFpEF, according to the Heart Failure Association (HFA) of the European Society of Cardiology (ESC).[208] Additional column summarises characterisation data from the guinea pig DOCA-salt model in the context of this algorithm.

Step	*Diagnostic Approach*	*Guinea Pig DOCA-Salt Model*
P: Pretest Assessment	Assessment of the presence of any risk factors associated with HF as well as signs and/or symptoms of HF.	Elevated HR, tachycardia, reduced weight gain.
E: Echocardiographic and Natriuretic Peptide Score	Comprehensive echocardiographic assessment and measurement of serum levels of natriuretic peptides.	Preserved EF, LA enlargement, LV hypertrophy w/o LV dilation.
F1: Functional Testing in Case of Uncertainty	Exercise stress echocardiography and invasive haemodynamic measurements. To be conducted in case of uncertainty following the previous steps.	Elevated filling pressures (LVEDP) from *ex vivo* pressure-volume measurements.
F2: Final Aetiology	Further tests to determine disease aetiology e.g. cardiovascular magnetic resonance, cardiac or non-cardiac biopsies, genetic testing etc.	Decreased SERCA and increased NCX expression, elevated intracellular sodium.

The guinea pig DOCA-salt model demonstrates substantial arterial hypertension alongside elevated resting heart rate and reduced weight gain, thereby satisfying the initial criteria for step ‘P’. Arterial hypertension is listed as a risk factor for HF, while tachycardia and loss of appetite/weight loss/tissue wasting are listed as signs and symptoms of HF according to ESC guidelines.[209] Step ‘E’ involves echocardiographic

assessment of diastolic function and measurement of serum natriuretic peptides, after which a score can be assigned to patients according to the presence of major and minor criteria based on perturbations to particular functional variables and serum levels of natriuretic peptides. Although this scoring system cannot be applied directly, since normal values of cardiac functional parameters are not the same in guinea pigs and not all echocardiographic variables were measured, DOCA-salt guinea pigs clearly demonstrate preserved EF, LA enlargement and LV hypertrophy in the absence of left ventricular dilation. Alone, these findings are sufficient for a diagnosis of HFpEF, according to the authors of the algorithm, if echocardiography is carried out as part of step 'P'.[208] Natriuretic peptide levels were not measured in DOCA-salt guinea pigs but are not required for a diagnosis of HFpEF because a substantial proportion of patients with HFpEF, diagnosed by invasive techniques, do not have elevated natriuretic peptide levels. This is believed to be due to the fact that the main driver for elevated natriuretic peptide levels is increased LV wall stress, which may be absent in HFpEF patients due to the characteristic LVH in the absence of LV dilation.[208, 210, 211] Step 'F1' is only required in case of uncertainty in the previous steps, which does not appear to be the case with the DOCA-salt guinea pig model. However, if *ex vivo* LV pressure-volume studies are interpreted in a similar light to invasive haemodynamic measurements in patients, then the elevated filling pressures demonstrated by elevated LVEDP in DOCA hearts can be taken as proof of the presence of HFpEF, according to the algorithm. Step 'F2' concerns further testing to identify any specific diseases or underlying pathologies which may be the cause of HFpEF in individual patients and is suggested to aid the provision of more targeted therapies. This is not especially relevant to an animal model of disease, but further characterisation data from DOCA-salt guinea pigs did reveal abnormalities in calcium handling proteins and elevated intracellular sodium in DOCA hearts, both of which are characteristic of HF.[53-56, 58, 59, 110-112, 143, 194-197] Taken together, characterisation data from the present study suggests that the guinea pig DOCA-salt model meets clinical criteria, set out by the ESC, to be defined as a model of HFpEF.

Having established that the guinea pig DOCA-salt model presents with HFpEF that meets clinical diagnostic criteria, it is useful to consider the advantages afforded by this model over other rodent models of diastolic dysfunction and HF. Some of these advantages have

been discussed previously and relate to the increased similarity of cardiac physiology between guinea pigs and humans when compared to murine species. Guinea pigs have a plateaued ventricular AP expressing many of the same ion currents as humans, which differs significantly from the triangular AP seen in rats and mice, as is necessitated by the very high heart rate in these species.[22, 108, 109] Ventricular intracellular calcium handling in guinea pigs is also more similar to humans, with SERCA and NCX contributions to cytosolic calcium clearance falling at around 70% and 30% respectively, compared to around 97% SERCA contribution in rats and mice.[49] All of these factors make the guinea pig a very suitable species of choice for studies involving cardiac electrophysiology and calcium handling and may allow more parallels to be drawn to human conditions. The DOCA-salt model also offers several advantages over other common animal models of HF. This model offers a more rapid onset of disease and cardiac remodelling than pressure overload models such as transverse aortic constriction, with this approach in the guinea pig reported to take 150 days to induce decompensated HF.[63] The surgical skill and training required to perform unilateral nephrectomy and pellet implantation compared to transverse aortic constriction is also significantly less, and there is no requirement to ventilate. The simpler surgical procedure also translates into improved animal survival and recovery. Combined with the close similarities to clinical HFpEF demonstrated by the present study, these advantages make the guinea pig DOCA-salt model a valuable research tool in order to improve our understanding of the mechanisms involved in HFpEF.

The possible mechanism for the contribution of repolarisation abnormalities to diastolic dysfunction in HF has been extensively discussed (Sections 1.2.3 & 1.2.4). However, other mechanisms may be involved in the development of impaired ventricular relaxation and, based on data from the present study, are likely to be the driving force behind onset in the guinea pig DOCA-salt model. This model acts in the same manner as hyperaldosteronism and, combined with high salt intake, results in elevated circulating blood volume due to increased sodium and chloride retention alongside increased potassium excretion, both of which act to increase water retention. The resultant hypertension is likely exacerbated by increased sympathetic tone and altered neurohumoral pressor baroreflexes as a result of increased mineralocorticoid receptor

activation and sodium retention.[151, 212] The increase in afterload due to arterial hypertension is a direct driving force for cardiac remodelling with progression to cardiac dysfunction and failure.[213] However, there is evidence to suggest that DOCA treatment may also elicit direct effects on the heart, with studies reporting the expression of mineralocorticoid receptors in myocardial tissue which bind aldosterone and may act to induce cardiac remodelling.[214] Chronic administration of aldosterone has been shown to induce cardiac fibrosis in rats, associated with increased expression of collagen type I and III.[215] Studies have also demonstrated that this induction of cardiac fibrosis in response to type I mineralocorticoid receptor occupancy is independent of increases in blood pressure.[216] One proposed mechanism by which binding of aldosterone to mineralocorticoid receptors brings about fibrosis is by increasing levels of free intracellular calcium. Indeed, it has been shown that administration of calcium channel blockers alongside chronic infusion of aldosterone acts to reduce collagen deposition at sites of cardiac fibrosis.[215] The authors proposed that calcium acts to regulate the process of fibrosis in such models by altering the collagen turnover and growth of myofibroblasts. Therefore, the administration of DOCA, a mineralocorticoid agonist, may act to bring about cardiac remodelling independently of hypertension, which could contribute to some of the changes in cardiac function observed in this study. Indeed, if activation of mineralocorticoid receptors does exert its effects on cardiac fibrosis via elevated levels of intracellular free calcium, this could also have a profound and direct effect on diastolic function and result in elevated LV filling pressures (e.g. LVEDP) and delayed/slowed ventricular relaxation. Western blotting data from the present study reveals that the DOCA-salt guinea pig hearts demonstrate altered expression levels of intracellular calcium handling proteins SERCA and NCX, which could also lead to elevated diastolic calcium levels due to an impaired ability to clear cytosolic calcium. This would be compounded by the elevated intracellular sodium levels identified using ^{23}Na NMR, which would decrease the driving force for calcium extrusion by NCX. Elevated diastolic calcium levels, as a consequence of various potential mechanisms, are therefore a very possible contributor to impaired ventricular diastolic function in this model.

There may also be a role for the sarcomeric protein titin the guinea pig DOCA-salt model of HFpEF. Cardiac titin possesses an extensible region, giving the protein an elastic

property and allowing for the generation of passive tension upon stretching of the sarcomere.[217] This is important for cardiac function as it contributes to diastolic wall tension and determination of ventricular filling during diastole.[218] It has been reported that alterations to the relative expression of the N2B/N2BA titin isoforms, or the degree of phosphorylation of titin, may contribute to the pathogenesis of heart disease. One protein kinase which is capable of phosphorylating titin is PKCα, with phosphorylation by this kinase resulting in increased passive tension muscle strips and cardiomyocytes from several species.[219, 220] This isoform of PKC has been shown to demonstrate increased activity and/or expression in models of cardiac hypertrophy and failure and could therefore contribute to diastolic dysfunction via increased phosphorylation of titin.[221-223] PKCα and can also undergo pathological activation and cleavage to a more active fragment by calpains in the calcium-overloaded heart.[224] Therefore, titin dysregulation represents a potential mechanism which may contribute to the impairment of diastolic function in the guinea pig DOCA-salt model of HFpEF.

There is evidence that oxidative stress may also play a role in the pathogenesis of cardiac dysfunction in DOCA-salt rodent models.[225] Studies have previously implicated aldosterone-mediated activation of a Nox2-containing NADPH oxidase in the upregulation of fibrotic activity in mineralocorticoid-dependent hypertension.[226] It has also been shown that expression of nNOS is increased in diseased hearts, and it is proposed that increased production of nitric oxide may negatively impact on cardiac contractility.[227] Indeed, this role for oxidative stress in disease progression would only increase the suitability of the DOCA-salt guinea pig as a model of HFpEF, according to a novel paradigm for this condition which has recently been proposed.[228] In this review, the authors propose that a systemic proinflammatory state arises due to comorbidities associated with HFpEF, causing endothelial cells in the coronary microvasculature to produce reactive oxygen species. This is proposed to limit nitric oxide in adjacent cardiomyocytes, thereby decreasing the activity of PKG, and result in pro-hypertrophic environment with reduced phosphorylation of titin and a stiffened myocardium. Aldosterone has been shown to bring about superoxide production by NADPH oxidase in endothelial cells via mineralocorticoid receptor activation, which may act to replicate this microvascular oxidative stress in DOCA-salt animals.[229]

Therefore, there are many contributing mechanisms to diastolic function in the normal ventricular myocardium, both active and passive. These interactions should not be over-simplified, and it is likely that pathological changes to a combination of these factors contribute to the impairment of ventricular relaxation in any given model of diastolic dysfunction, with the DOCA-salt guinea pig being no exception.

6.3 Role of Repolarisation in Diastolic Dysfunction in Heart Failure

The experiments conducted as part of this study set out to address the experimental hypothesis concerning a potential role for abnormal ventricular repolarisation in HF as a contributor to diastolic dysfunction. The mechanisms via which this could act to impair normal diastolic function have been extensively discussed, however, data from the studies did not support the hypothesis. This was true in both healthy isolated working hearts, those in which pathological characteristics of HF had been replicated pharmacologically and in failing hearts. As already discussed, the guinea pig DOCA-salt model represents an excellent novel model of HFpEF, demonstrating many of the key characteristics of HF as reported in other models and clinically, including repolarisation abnormalities *in vivo*. Therefore, the model in which the hypothesis was tested was highly suitable. This leaves the question of whether the experimental approach used was able to fully address the hypothesis. In order to understand this, it is useful to look at the literature on this subject.

There is a growing interest in the use of ranolazine, a $I_{Na,late}$ blocker currently licensed for the treatment of angina, as a treatment for diastolic dysfunction in HF and LQTS. One such study examined the effect of ranolazine on contractility and relaxation in isometrically contracting muscle strips from failing human hearts.[230] Results demonstrated no significant impairment of systolic function (measured by twitch force amplitude and SR calcium loading), while frequency-dependent onset of diastolic impairment (measured by diastolic tension) was ameliorated by 30% following ranolazine treatment. Further investigations in isolated rabbit ventricular myocytes led the authors to suggest that this was due to ranolazine acting to reduce intracellular sodium concentration and subsequent diastolic calcium loading. Another study conducted a small randomised, double-blind and placebo-controlled trial to determine whether ranolazine may provide a suitable therapy for patients with HFpEF.[231] Ranolazine was given

intravenously for 24hr, at the start of which invasive haemodynamic measurements were taken, and then given orally for 13 days with echocardiography performed at the start and end of this period. Some evidence of diastolic improvement with ranolazine infusion was observed, with a decrease in LVEDP. However, this occurred alongside a decrease in cardiac output and no evidence of improved active relaxation was observed, with tau and dP/dt_{min} remaining unchanged. Similarly, echocardiography revealed no improvement in diastolic function at either time point. A third patient study looked at the effect of three months of ranolazine treatment on diastolic function in patients with angina.[232] Echocardiography revealed improved diastolic function in the ranolazine treatment group with improvements in functional parameters including E/A ratio and IVRT. This study did not report the effects of ranolazine on QT interval in these patients, however, the previous study demonstrated an increase in QT interval following ranolazine treatment which was particularly marked at the end of the infusion protocol. Whilst listed as non-significant, this increase was present in raw QT values as well as when two separate correction formulas were applied and was not present in the control group.[231] This is a very unexpected result given that one would expect inhibition of the late sodium current to shorten APD, since this current contributes to the plateau phase of the AP, and particularly in light of the fact that ranolazine has been suggested as a suitable therapy for patients with LQTS. Indeed, one study looked at the effect of therapeutic doses of ranolazine (delivered during an 8-hour intravenous infusion) in patients with LQT3 on diastolic function using echocardiography.[233] These patients have a mutation which results in a sustained inward sodium current, thus prolonging cardiac repolarisation. Ranolazine infusion resulted in a 26ms shortening of QTc interval in LQTS patients and an improvement in diastolic function as evidenced by reduced IVRT, increased E wave velocity and decreased E wave deceleration time. Interestingly, this corresponds to the 24- or 27ms increase in QTc interval (depending on correction used) reported following ranolazine infusion in HFpEF patients.[231]

Clearly the literature surrounding the effects of ranolazine on ventricular repolarisation and diastolic function is not straightforward. The picture is complicated by the use of ranolazine in patients with a variety of underlying health conditions. There is also a question as to whether ranolazine mediates all of its effects via its action on the late

sodium current. One study examined the effects of ranolazine treatment on diastolic function in DOCA-salt mice, based on the hypothesis that these animals may demonstrate increased $I_{Na,late}$ due to oxidative stress,[234] with resultant delayed calcium removal from the cytosol.[235] Echocardiography revealed diastolic dysfunction which was partially ameliorated by ranolazine treatment, however, the DOCA-salt mice displayed no difference in $I_{Na,late}$ or calcium transient dynamics. Further investigation revealed that the effects of ranolazine were in fact due to increased calcium sensitivity in the myofilaments which was reversed by ranolazine treatment. Overall, whilst ranolazine may exert some positive effects on diastolic function, it seems likely that these effects are not mediated directly via alterations to cardiac repolarisation or APD. Rather, these effects likely occur due to the influence of ranolazine on intracellular sodium concentration and/or intracellular calcium handling, be this via direct or indirect mechanisms. This could have short-term effects on parameters such as LVEDP if diastolic calcium levels were reduced but may also have long-term implications on factors such as cardiac fibrosis given that calcium is an important intracellular signalling molecule. If this is indeed the case, interventions which alter repolarisation without affecting intracellular sodium concentration, and therefore calcium transient dynamics, are unlikely to influence diastolic function in the acute setting. This is in agreement with the present findings, where ^{23}Na NMR revealed no effect of QT prolongation by I_{Kr} and I_{Ks} blockade on intracellular sodium concentration. Therefore, the experimental approach used achieved its aim of isolating the role for ventricular repolarisation abnormalities in diastolic function, but perhaps does not provide full insight into the bigger picture of how this may interact with underlying calcium transient dynamics and signalling.

6.4 Determination of Relaxation *In Vivo*

One significant conclusion from the present study is that prolonging the intracellular calcium transient by QT prolongation has no appreciable impact on diastolic function in healthy or failing hearts. This suggests that the recovery of the calcium transient is not a key determinant of myocardial relaxation *in vivo.* It has been proposed that there are four principle determinants of relaxation.[134] These are: i) rate of calcium removal from the cytosol, ii) myofilament crossbridge kinetics, iii) the elastic properties of the myocardium

and within cardiomyocytes and iv) afterload. It is likely that these factors may have different contributions to myocardial relaxation in different settings i.e. isolated cells vs intact hearts *in vivo.* This would explain the findings of studies which have indicated the importance of the calcium transient decay or diastolic calcium levels in determining rates of relaxation in *ex vivo* tissue or isolated cell preparations.[43, 45, 236] Such studies have reported that slowing of the intracellular calcium transient recovery impacts negatively on relaxation or cell shortening (used as a surrogate for relaxation in isolated cell work). One important caveat that applies to many of these studies is that such work is often carried out at unphysiological pacing rates or temperatures and under conditions where preload, afterload, tissue elastance and three-dimensional geometry are all markedly different to the intact heart. This means that caution must be used when extrapolating findings to an *in vivo*, whole-heart setting. Indeed, other studies have demonstrated that dissociation of calcium from troponin C occurs before the onset of relaxation during isometric contraction, implying that other factors predominate in determining the rate of myocardial relaxation.[133]

However, there are also studies which indicate that calcium may not be the primary determinant of myocardial relaxation, even in diseased hearts. One such study examined relaxation and calcium transient dynamics in human myocardial strip preparations and revealed findings which could be interpreted to support calcium not being a major determinant of myocardial relaxation.[237] Studies were performed at physiological pacing rates and allowed for the simultaneous measurement of force and free intracellular calcium, with data revealing that a sudden increase in pacing rate (from 60 to 180bpm) resulted in proportional increases in diastolic calcium in tissue from both control and failing myocardial strips (taken from patients with hypertensive heart disease or hypertensive heart disease combined with HFpEF). Interestingly, this increase in diastolic calcium only resulted in increased diastolic force in the diseased muscle strips. This may be indicative of elevated resting calcium levels prior to rate increase in diseased myocardium (since the technique used was not quantitative), however, elemental analysis revealed that resting calcium concentration was only significantly increased in muscle strips from patients who had HFpEF in combination with hypertensive heart disease, relative to control. This suggests that elevated calcium levels alone are not sufficient to

explain the increased diastolic tension in diseased myocardium at higher heart rates. Another study used isolated, Langendorff-perfused rabbit and rat hearts loaded with aequorin to determine whether diastolic dysfunction brought about by low-flow ischemia was worsened by further elevation of intracellular calcium by delivery of calcium bolus.[238] Ischemia resulted in elevated diastolic calcium levels and slowed calcium transient decline, alongside elevated diastolic pressure (measured by intraventricular balloon). Interestingly, further increasing intracellular calcium concentration by calcium bolus resulted in no further increase in diastolic pressure or worsening of the delay in the decline of the calcium transient. This led the authors to conclude that diastolic dysfunction due to ischemia does not occur as a direct result of elevated diastolic calcium levels.

If it is to be accepted that the calcium transient recovery is not a major determinant of ventricular relaxation then the question remains, which factors do represent key mechanisms of ventricular relaxation in healthy and diseased hearts? As mentioned above, elastance within the myocardium and individual cardiomyocytes likely plays an important role in determining the rate of relaxation. Titin is a major contributor to myocardial elastance at the cellular level in both healthy and diseased hearts (Section 6.2), with collagen likely becoming a more significant determinant in the diseased, fibrotic myocardium. In recent years, there has also been increasing interest in the role of the mechanical control of relaxation in the myocardium.[239] There is evidence that myocardial strain rate (i.e. the speed of myocardial lengthening) may interact with myofilament crossbridge kinetics and contribute to determining the subsequent rate of myocardial relaxation. It has been observed that there is a period of strain (lengthening) in healthy hearts during the portion of the cardiac cycle termed the ‘proto-diastolic phase’ by Wiggers, and it is proposed that this brief lengthening which occurs at the end of systole will aid the rapid closure of the aortic valve.[240] Indeed, work using load-clamping techniques in isolated trabeculae from various species has demonstrated that this end-systolic strain rate is a determinant of relaxation rate, and that this occurs as a result of detachment of actin-myosin cross-bridges due to this partial re-lengthening of the myocardium during end systole.[241] This is proposed to come about because sarcomere lengthening acts to reduce the duration of crossbridge formation. Thus, as the myocardium lengthens at end systole, sarcomeric shortening favours this state of

shortened crossbridge duration which facilitates subsequent relaxation as calcium is removed from the cytosol and actin-myosin binding becomes inhibited.[239, 241] Interestingly, this period of peak strain rate at end systole has been shown to be lost in some diseased hearts, including those with diastolic dysfunction.[242, 243] Given the findings related to the regulatory role of end systolic strain rate and myocardial relaxation rate, it is possible that this could contribute to impaired diastolic function in diseased hearts in a manner that is independent of both CaTD and APD.[241]

Therefore, although regulation of intracellular calcium is undoubtedly fundamental to the process of EC coupling, diastolic calcium concentration and/or the rate of decay of the calcium transient may not be the key determinant of myocardial relaxation in intact healthy or diseased hearts *in vivo*. It is likely that there are a multitude of contributing mechanisms to normal myocardial relaxation ranging from passive elastic properties, conferred by factors such as titin isoform expression and phosphorylation state, to mechanical and biomolecular factors such as myocardial strain and myofilament crossbridge kinetics and calcium sensitivity. This interaction is likely to become much more complex in the diseased heart, where varying pathologies could alter the normal contributions of all of the above factors to myocardial relaxation.

6.5 Further Work

The overt diastolic dysfunction observed in the novel guinea pig DOCA-salt model of HFpEF characterised in the present study, coupled with the lack of obvious connection to repolarisation abnormalities as postulated in the experimental hypothesis, leave questions surrounding the cause of dysfunction in this model. As the model itself appears to be a valuable contribution to the armoury of techniques available for exploring the mechanism of diastolic dysfunction in HFpEF, it would be of interest to better understand the pathogenesis of disease even in the absence of a direct role for repolarisation abnormalities. There are several approaches which could be used in other to elucidate this.

One obvious point of interest in improving understanding of this model would be the characterisation of the intracellular calcium transient in failing DOCA-salt hearts.

Comparison of calcium transient dynamics using whole heart optical mapping would be one method of approaching this and could provide information about any changes to CaTD or rate of decay relative to healthy hearts. It would also allow any different effects of QT prolongation on calcium handling in failing vs healthy hearts to be determined. The assessment of calcium transient dynamics in isolated ventricular myocytes may be of interest. This would allow for additional characterisation of calcium transient dynamics to that described above, with the possibility of determining SERCA and NCX activity and contribution to cytosolic calcium clearance using techniques such as caffeine application. However, any data obtained from isolated cardiomyocytes should be treated with some caution as it may not mirror the underlying pathophysiology in an intact heart. Indeed, the present study has already highlighted differences between *in vivo* and *ex vivo* cardiac function from the same model, and it is likely that differences would be greater still in isolated cells.

Isolated cell work would also allow for the possible mechanism behind the QT prolongation in failing guinea pig DOCA-salt hearts to be examined. If it could be identified which ion currents may be responsible for these alterations to ventricular repolarisation, it may help to determine whether the pharmacological methods of QT prolongation used in the present study provided an approximation of the changes seen *in vivo*, or whether a different approach may be more informative in future studies.

Histological examination of ventricular tissue from DOCA-salt hearts to determine the level of fibrosis present would also be a useful addition to the characterisation data for this model. This could be coupled with additional western blotting studies to look at titin isoform expression and phosphorylation status. Together, these data would help to inform about the contribution of passive mechanisms to diastolic dysfunction in the guinea pig DOCA-salt model of HFpEF.

Finally, the possible contribution of sympathetic tone to repolarisation abnormalities in the model was discussed in detail in Section 5.4.1. Performing functional studies in isolated working hearts necessitates that any influence of increased sympathetic tone is lost, and indeed, QT prolongation was not present in isolated DOCA-salt hearts. It may therefore be relevant to replicate such studies in an *in vivo* setting, with the administration

of QT-altering drugs prior to/during cardiac ultrasound or invasive cardiac catheterisation. This could help to determine whether this may be a significant factor in the lack of effect on diastolic function in this setting. Alternative methods of altering cardiac repolarisation may also have more far-reaching effects, as seen with ranolazine in LQT3 patients. In order better understand this, one approach would be to first determine a pharmacological means of prolonging or shortening the AP which does affect intracellular sodium concentration, and then look at the effects of chronic administration on diastolic function *in vivo* in the guinea pig DOCA-salt model.

6.6 Concluding Remarks

The present study set out to understand the role of ventricular repolarisation abnormalities in diastolic dysfunction in HF. This was addressed using isolated working heart preparations with pharmacological manipulation of ventricular repolarisation to replicate the changes in QT interval observed in the clinic. These studies culminated in the development and characterisation of a novel guinea pig model of HFpEF, which met clinical criteria for the diagnosis of HFpEF and displayed many of the same pathological changes. These included repolarisation abnormalities comparable to those seen in patients, giving confidence in the DOCA-salt guinea pig as a suitable model in which to test the experimental hypothesis. QT prolongation in failing guinea pig DOCA-salt hearts had no discernible impact on the level of diastolic dysfunction in these hearts. This was in agreement with initial studies in healthy isolated hearts, indicating that there was no fundamental role for repolarisation abnormalities and diastolic dysfunction in an acute setting.

To conclude, the present study has succeeded in isolating repolarisation abnormalities as a single factor in a myriad of contributing factors to diastolic dysfunction in HF and scrutinising their contribution to the impairment of diastolic function. Results demonstrate that, alone, ventricular repolarisation abnormalities are not sufficient to induce or exacerbate diastolic dysfunction in the isolated working heart.

REFERENCE LIST

1. Ponikowski P, Anker SD, AlHabib KF, Cowie MR, Force TL, Hu S, Jaarsma T, Krum H, Rastogi V, Rohde LE, Samal UC, Shimokawa H, Budi Siswanto B, Sliwa K, Filippatos G. Heart failure: Preventing disease and death worldwide. *ESC Heart Failure*. 2014;1:4-25.

2. Conrad N, Judge A, Tran J, Mohseni H, Hedgecott D, Crespillo AP, Allison M, Hemingway H, Cleland JG, McMurray JJV, Rahimi K. Temporal trends and patterns in heart failure incidence: A population-based study of 4 million individuals. *The Lancet*. 2018;391:572-580.

3. Lenzen MJ, Scholte op Reimer, W J M, Boersma E, Vantrimpont, P J M J, Follath F, Swedberg K, Cleland J, Komajda M. Differences between patients with a preserved and a depressed left ventricular function: A report from the EuroHeart failure survey. *eurheartj*. 2004;25:1214-1220.

4. Owan TE, Hodge DO, Herges RM, Jacobsen SJ, Roger VL, Redfield MM. Trends in prevalence and outcome of heart failure with preserved ejection fraction. *N Engl J Med*. 2006;355:251-259.

5. Savarese G, Lund LH. Global public health burden of heart failure. *Cardiac failure review*. 2017;3:7-11.

6. Authors/Task FM, McMurray JJV, Adamopoulos S, Anker SD, Auricchio A, Böhm M, Dickstein K, Falk V, Filippatos G, Fonseca C, Gomez-Sanchez M, Jaarsma T, Køber

L, Lip GYH, Maggioni AP, Parkhomenko A, Pieske BM, Popescu BA, Rønnevik PK, Rutten FH, Schwitter J, Seferovic P, Stepinska J, Trindade PT, Voors AA, Zannad F, Zeiher A, ESC Committee for Practice Guidelines, (CPG), Bax JJ, Baumgartner H, Ceconi C, Dean V, Deaton C, Fagard R, Funck-Brentano C, Hasdai D, Hoes A, Kirchhof P, Knuuti J, Kolh P, McDonagh T, Moulin C, Popescu BA, Reiner Ž, Sechtem U, Sirnes PA, Tendera M, Torbicki A, Vahanian A, Windecker S, Reviewers D, McDonagh T, Sechtem U, Bonet LA, Avraamides P, Ben Lamin HA, Brignole M, Coca A, Cowburn P, Dargie H, Elliott P, Flachskampf FA, Guida GF, Hardman S, Iung B, Merkely B, Mueller C, Nanas JN, Nielsen OW, Ørn S, Parissis JT, Ponikowski P. ESC guidelines for the diagnosis and treatment of acute and chronic heart failure 2012. *European Journal of Heart Failure*. 2012;14:803-869.

7. Zile MR, Baicu CF, Gaasch WH. Diastolic heart failure — abnormalities in active relaxation and passive stiffness of the left ventricle. *N Engl J Med*. 2004;350:1953-1959.

8. Shah SJ, Gheorghiade M. Heart failure with preserved ejection fraction: Treat now by treating comorbidities. *JAMA*. 2008;300:431-433.

9. van Heerebeek L, Borbély A, Niessen HWM, Bronzwaer JGF, van der Velden J, Stienen GJM, Linke WA, Laarman GJ, Paulus WJ. Myocardial structure and function differ in systolic and diastolic heart failure. *Circulation*. 2006;113:1966-1973.

10. Martos R, Baugh J, Ledwidge M, O'Loughlin C, Conlon C, Patle A, Donnelly SC, McDonald K. Diastolic heart failure: Evidence of increased myocardial collagen turnover linked to diastolic dysfunction. *Circulation*. 2007;115:888-895.

11. Shah SJ, Katz DH, Deo RC. Phenotypic spectrum of heart failure with preserved ejection fraction. *Heart failure clinics*. 2014;10:407-418.

12. Shah SJ, Katz DH, Selvaraj S, Burke MA, Yancy CW, Gheorghiade M, Bonow RO, Huang C, Deo RC. Phenomapping for novel classification of heart failure with preserved ejection fraction. *Circulation*. 2015;131:269-279.

13. Pitt B, Pfeffer MA, Assmann SF, Boineau R, Anand IS, Claggett B, Clausell N, Desai AS, Diaz R, Fleg JL, Gordeev I, Harty B, Heitner JF, Kenwood CT, Lewis EF, O'Meara E, Probstfield JL, Shaburishvili T, Shah SJ, Solomon SD, Sweitzer NK, Yang S, McKinlay SM. Spironolactone for heart failure with preserved ejection fraction. *N Engl J Med*. 2014;370:1383-1392.

14. Massie BM, Carson PE, McMurray JJ, Komajda M, McKelvie R, Zile MR, Anderson S, Donovan M, Iverson E, Staiger C, Ptaszynska A. Irbesartan in patients with heart failure and preserved ejection fraction. *N Engl J Med*. 2008;359:2456-2467.

15. Redfield MM, Chen HH, Borlaug BA, Semigran MJ, Lee KL, Lewis G, LeWinter MM, Rouleau JL, Bull DA, Mann DL, Deswal A, Stevenson LW, Givertz MM, Ofili EO, O'Connor CM, Felker GM, Goldsmith SR, Bart BA, McNulty SE, Ibarra JC, Lin G, Oh JK, Patel MR, Kim RJ, Tracy RP, Velazquez EJ, Anstrom KJ, Hernandez AF, Mascette AM, Braunwald E, RELAX Trial ft. Effect of phosphodiesterase-5 inhibition on exercise capacity and clinical status in heart failure with preserved ejection fraction: A randomized clinical trial. *JAMA*. 2013;309:1268-1277.

16. MacLeod K. *An Essential Introduction to Cardiac Electrophysiology.* Imperial College Press; 2014.

17. Szentadrassy N, Banyasz T, Biro T, Szabo G, Toth BI, Magyar J, Lazar J, Varro A, Kovacs L, Nanasi PP. Apico–basal inhomogeneity in distribution of ion channels in canine and human ventricular myocardium. *cardiovascres*. 2005;65:851-860.

18. Clark RB, Bouchard RA, Salinas-Stefanon E, Sanchez-Chapula J, Giles WR. Heterogeneity of action potential waveforms and potassium currents in rat ventricle. *cardiovascres*. 1993;27:1795-1799.

19. Fabiato A. Time and calcium dependence of activation and inactivation of calcium-induced release of calcium from the sarcoplasmic reticulum of a skinned canine cardiac purkinje cell. *The Journal of General Physiology*. 1985;85:247-289.

20. Linz KW, Meyer R. Profile and kinetics of L-type calcium current during the cardiac ventricular action potential compared in guinea-pigs, rats and rabbits. *Pflügers Archiv*. 2000;439:588-599.

21. Linz KW, Meyer R. Control of L-type calcium current during the action potential of guinea-pig ventricular myocytes. *J Physiol (Lond)*. 1998;513:425-442.

22. Kiyosue T, Arita M. Late sodium current and its contribution to action potential configuration in guinea pig ventricular myocytes. *Circ Res*. 1989;64:389.

23. Egan TM, Noble D, Noble SJ, Powell T, Spindler AJ, Twist VW. Sodium-calcium exchange during the action potential in guinea-pig ventricular cells. *J Physiol (Lond)*. 1989;411:639-661.

24. Sato D, Bartos D, Ginsburg K, Bers D. Depolarization of cardiac membrane potential synchronizes calcium sparks and waves in tissue. *Biophysical Journal*. 2014;107:1313-1317.

25. Sanguinetti MC. HERG1 channelopathies. *Pflügers Archiv. - European Journal of Physiology*. 2010;460:265-276.

26. Ibarra J, Morley GE, Delmar M. Dynamics of the inward rectifier K+ current during the action potential of guinea pig ventricular myocytes. *Biophysical Journal*. 1991;60:1534-1539.

27. Virág L, Iost N, Opincariu M, Szolnoky J, Szécsi J, Bogáts G, Szenohradszky P, Varró A, Papp JG. The slow component of the delayed rectifier potassium current in undiseased human ventricular myocytes. *cardiovascres*. 2001;49:790-797.

28. Jost N, Papp JG, Varró A. Slow delayed rectifier potassium current (IKs) and the repolarization reserve. *Annals of Noninvasive Electrocardiology*. 2007;12:64-78.

29. Sanguinetti MC, Jurkiewicz NK, Scott A, Siegl PK. Isoproterenol antagonizes prolongation of refractory period by the class III antiarrhythmic agent E-4031 in guinea pig myocytes. mechanism of action. *Circ Res*. 1991;68:77-84.

30. Stengl M, Volders PGA, Thomsen MB, Spätjens, Roel L H M G, Sipido KR, Vos MA. Accumulation of slowly activating delayed rectifier potassium current (IKs) in canine ventricular myocytes. *J Physiol (Lond)*. 2003;551:777-786.

31. Varró A, Baláti B, Iost N, Takács J, Virág L, Lathrop DA, Csaba L, Tálosi L, Papp JG. The role of the delayed rectifier component IKs in dog ventricular muscle and purkinje fibre repolarization. *J Physiol (Lond)*. 2000;523:67-81.

32. Aronsen JM, Swift F, Sejersted OM. Cardiac sodium transport and excitation–contraction coupling. *Journal of Molecular and Cellular Cardiology*. 2013;61:11-19.

33. Ohtsuki I, Morimoto S. Troponin: Regulatory function and disorders. *Biochem Biophys Res Commun*. 2008;369:62-73.

34. Bers DM. Species differences and the role of sodium-calcium exchange in cardiac muscle relaxation. *Ann N Y Acad Sci*. 1991;639:375-385.

35. Balke CW, Egan TM, Wier WG. Processes that remove calcium from the cytoplasm during excitation-contraction coupling in intact rat heart cells. *J Physiol (Lond)*. 1994;474:447-462.

36. Eisner DA, Diaz ME, Li Y, O'Neill SC, Trafford AW. Stability and instability of regulation of intracellular calcium. *Exp Physiol*. 2005;90:3-12.

37. Catterall WA. Structure and regulation of voltage-gated Ca^{2+} channels. *Annu Rev Cell Dev Biol*. 2000;16:521-555.

38. Anderson ME, Braun AP, Schulman H, Premack BA. Multifunctional Ca^{2+}/calmodulin-dependent protein kinase mediates Ca^{2+}-induced enhancement of the L-type Ca2+ current in rabbit ventricular myocytes. *Circ Res*. 1994;75:854-861.

39. Bers DM. Cardiac excitation-contraction coupling. *Nature*. 2002;415:198-205.

40. Simmerman HKB, Jones LR. Phospholamban: Protein structure, mechanism of action, and role in cardiac function. *Physiol Rev*. 1998;78:921-947.

41. Gui-Rong Li, Yang B, Feng J, Bosch RF, Carrier M, Nattel S. Transmembrane I_{Ca} contributes to rate-dependent changes of action potentials in human ventricular myocytes. *American Journal of Physiology-Heart and Circulatory Physiology*. 1991;276:H98-H106.

42. Carmeliet E. Intracellular Ca^{2+} concentration and rate adaptation of the cardiac action potential. *Cell Calcium*. 2004;35:557-573.

43. Bouchard RA, Clark RB, Giles WR. Effects of action potential duration on excitation-contraction coupling in rat ventricular myocytes: Action potential voltage-clamp measurements. *Circulation Research*. 1995;76:790-801.

44. Grossman W, McLaurin LP, Rolett EL. Alterations in left ventricular relaxation and diastolic compliance in congestive cardiomyopathy. *Cardiovasc Res*. 1979;13:514-522.

45. Gwathmey JK, Copelas L, MacKinnon R, Schoen FJ, Feldman MD, Grossman W, Morgan JP. Abnormal intracellular calcium handling in myocardium from patients with end-stage heart failure. *Circulation Research*. 1987;61:70-76.

46. Beuckelmann DJ, Nãubauer M, Erdmann E. Intracellular calcium handling in isolated ventricular myocytes from patients with terminal heart failure. *Circulation*. 1992;85:1046-1055.

47. Zile MR, Baicu CF, Gaasch WH. Diastolic heart failure — abnormalities in active relaxation and passive stiffness of the left ventricle. *N Engl J Med*. 2004;350:1953-1959.

48. Frank FK, Bölck B, Brixius K, Kranias GE, Schwinger GR. Modulation of SERCA: Implications for the failing human heart. *Basic Res Cardiol*. 2002;97:I72-I78.

49. Bers DM. Calcium fluxes involved in control of cardiac myocyte contraction. *Circ Res*. 2000;87:275.

50. Bassani JW, Bassani RA, Bers DM. Relaxation in rabbit and rat cardiac cells: Species-dependent differences in cellular mechanisms. *J Physiol (Lond)*. 1994;476:279-293.

51. Bers DM, Bridge JH, Spitzer KW. Intracellular Ca^{2+} transients during rapid cooling contractures in guinea-pig ventricular myocytes. *J Physiol (Lond)*. 1989;417:537-553.

52. He H, Giordano FJ, Hilal-Dandan R, Choi DJ, Rockman HA, McDonough PM, Bluhm WF, Meyer M, Sayen MR, Swanson E, Dillmann WH. Overexpression of the rat sarcoplasmic reticulum Ca^{2+} ATPase gene in the heart of transgenic mice accelerates calcium transients and cardiac relaxation. *J Clin Invest*. 1997;100:380-389.

53. Despa S, Islam MA, Weber CR, Pogwizd SM, Bers DM. Intracellular Na^{+} concentration is elevated in heart failure but Na/K pump function is unchanged. *Circulation*. 2002;105:2543.

54. Baartscheer A, Schumacher CA, Belterman CNW, Coronel R, Fiolet JWT. $[Na^+]_i$ and the driving force of the Na^+/Ca^{2+}-exchanger in heart failure. *Cardiovasc Res*. 2003;57:986-995.

55. Baartscheer A, Schumacher CA, van Borren, M M G J, Belterman CNW, Coronel R, Fiolet JWT. Increased Na^+/H^+-exchange activity is the cause of increased $[Na^+]_i$ and underlies disturbed calcium handling in the rabbit pressure and volume overload heart failure model. *Cardiovasc Res*. 2003;57:1015-1024.

56. Gray RP, McIntyre H, Sheridan DS, Fry CH. Intracellular sodium and contractile function in hypertrophied human and guinea-pig myocardium. *Pflügers Archiv*. 2001;442:117-123.

57. Pieske B, Maier LS, Piacentino V, Weisser J, Hasenfuss G, Houser S. Rate dependence of $[Na^+]_i$ and contractility in nonfailing and failing human myocardium. *Circulation*. 2002;106:447.

58. Mercadier JJ, Lomprã AM, Duc P, Boheler KR, Fraysse JB, Wisnewsky C, Allen PD, Komajda M, Schwartz K. Altered sarcoplasmic reticulum Ca^{2+}-ATPase gene expression in the human ventricle during end-stage heart failure. *J Clin Invest*. 1990;85:305-309.

59. Hasenfuss G, Reinecke H, Studer R, Meyer M, Pieske B, Holtz J, Holubarsch C, Posival H, Just H, Drexler H. Relation between myocardial function and expression of sarcoplasmic reticulum Ca^{2+}-ATPase in failing and nonfailing human myocardium. *Circ Res*. 1994;75:434.

60. McDonough AA, Velotta JB, Schwinger RHG, Philipson KD, Farley RA. The cardiac sodium pump: Structure and function. *Basic Res Cardiol*. 2002;97:I19-I24.

61. Ove Semb S, Lunde PK, Holt E, Tãnnessen T, Christensen G, Sejersted OM. Reduced myocardial Na^+, K^+-pump capacity in congestive heart failure following myocardial infarction in rats. *J Mol Cell Cardiol*. 1998;30:1311-1328.

62. Sweadner KJ, Herrera VL, Amato S, Moellmann A, Gibbons DK, Repke KR. Immunologic identification of Na^+,K^+-ATPase isoforms in myocardium. isoform change in deoxycorticosterone acetate-salt hypertension. *Circ Res*. 1994;74:669-678.

63. Ke H-, Yang H-, Francis AJ, Collins TP, Surendran H, Alvarez-Laviada A, Firth JM, MacLeod KT. Changes in cellular Ca^{2+} and Na^+ regulation during the progression towards heart failure in the guinea pig. *J Physiol*. 2020;598:1339-1359.

64. Verdonck F, Volders PGA, Vos MA, Sipido KR. Intracellular Na^+ and altered Na^+ transport mechanisms in cardiac hypertrophy and failure. *Journal of Molecular and Cellular Cardiology*. 2003;35:5-25.

65. Hurst JW. Naming of the waves in the ECG, with a brief account of their genesis. *Circulation*. 1998;98:1937-1942.

66. Zhu TG, Patel C, Martin S, Quan X, Wu Y, Burke JF, Chernick M, Kowey PR, Yan G. Ventricular transmural repolarization sequence: Its relationship with ventricular relaxation and role in ventricular diastolic function. *Eur Heart J*. 2009.

67. Noble D, Cohen I. The interpretation of the T wave of the electrocardiogram. *Cardiovasc Res*. 1978;12:13-27.

68. Volders PGA, Sipido KR, Carmeliet E, Spätjens, Roel L H M G, Wellens HJJ, Vos MA. Repolarizing K^+ currents I_{TO1} and I_{ks} are larger in right than left canine ventricular midmyocardium. *Circulation*. 1999;99:206.

69. Yan G, Shimizu W, Antzelevitch C. Characteristics and distribution of M cells in arterially perfused canine left ventricular wedge preparations. *Circulation*. 1998;98:1921-1927.

70. Liu D, Antzelevitch C. Characteristics of the delayed rectifier current (I_{Kr} and I_{Ks}) in canine ventricular epicardial, midmyocardial, and endocardial myocytes : A weaker I_{Ks} contributes to the longer action potential of the M cell. *Circulation Research*. 1995;76:351-365.

71. Zygmunt AC, Eddlestone GT, Thomas GP, Nesterenko VV, Antzelevitch C. Larger late sodium conductance in M cells contributes to electrical heterogeneity in canine ventricle. *American Journal of Physiology - Heart and Circulatory Physiology*. 2001;281:H689-H697.

72. Conrath CE, Wilders R, Coronel R, de Bakker, Jacques M T, Taggart P, de Groot J, Opthof T. Intercellular coupling through gap junctions masks M cells in the human heart. *Cardiovasc Res*. 2004;62:407-414.

73. McIntosh MA, Cobbe SM, Smith GL. Heterogeneous changes in action potential and intracellular Ca^{2+} in left ventricular myocyte sub-types from rabbits with heart failure. *Cardiovasc Res*. 2000;45:397-409.

74. Lou Q, Fedorov VV, Glukhov AV, Moazami N, Fast VG, Efimov IR. Transmural heterogeneity and remodeling of ventricular excitation-contraction coupling in human heart failure. Clinical Perspective. *Circulation*. 2011;123:1881-1890.

75. Ramakers C, Vos MA, Doevendans PA, Schoenmakers M, Wu YS, Scicchitano S, Iodice A, Thomas GP, Antzelevitch C, Dumaine R. Coordinated down-regulation of KCNQ1 and KCNE1 expression contributes to reduction of I_{Ks} in canine hypertrophied hearts. *Cardiovasc Res*. 2003;57:486-496.

76. Furukawa T, Bassett AL, Furukawa N, Kimura S, Myerburg RJ. The ionic mechanism of reperfusion-induced early afterdepolarizations in feline left ventricular hypertrophy. *J Clin Invest*. 1993;91:1521-1531.

77. Marionneau Céline, Sylvain B, Flagg Thomas P, Pilgram Thomas K, Sophie D, Nerbonne Jeanne M. Distinct cellular and molecular mechanisms underlie functional remodeling of repolarizing K^+ currents with left ventricular hypertrophy. *Circ Res*. 2008;102:1406-1415.

78. Tsuji Y, Opthof T, Kamiya K, Yasui K, Liu W, Lu Z, Kodama I. Pacing-induced heart failure causes a reduction of delayed rectifier potassium currents along with decreases in calcium and transient outward currents in rabbit ventricle. *Cardiovasc Res*. 2000;48:300-309.

79. Ryder KO, Bryant SM, Hart G. Membrane current changes in left ventricular myocytes isolated from guinea pigs after abdominal aortic coarctation. *Cardiovasc Res*. 1993;27:1278-1287.

80. Brooksby P, Levi AJ, Jones JV. The electrophysiological characteristics of hypertrophied ventricular myocytes from the spontaneously hypertensive rat. *J Hypertens*. 1993;11.

81. Näbauer M, Kääb S. Potassium channel down-regulation in heart failure. *Cardiovasc Res*. 1998;37:324-334.

82. Furukawa T, Kurokawa J. Potassium channel remodeling in cardiac hypertrophy. *J Mol Cell Cardiol*. 2006;41:753-761.

83. Wettwer E, Amos GJ, Posival H, Ravens U. Transient outward current in human ventricular myocytes of subepicardial and subendocardial origin. *Circ Res*. 1994;75:473-482.

84. Beuckelmann DJ, Näbauer M, Erdmann E. Alterations of K^+ currents in isolated human ventricular myocytes from patients with terminal heart failure. *Circulation Research*. 1993;73:379-385.

85. Kääb S, Dixon J, Duc J, Ashen D, Näbauer M, Beuckelmann DJ, Steinbeck G, McKinnon D, Tomaselli GF. Molecular basis of transient outward potassium current downregulation in human heart failure. *Circulation*. 1998;98:1383-1393.

86. Wilcox JE, Rosenberg J, Vallakati A, Gheorghiade M, Shah SJ. Usefulness of electrocardiographic QT interval to predict left ventricular diastolic dysfunction. *Am J Cardiol*. 2016;108:1760-1766.

87. Sauer A, Wilcox JE, Andrei A, Passman R, Goldberger JJ, Shah SJ. Diastolic electromechanical coupling: Association of the ECG T-peak to T-end interval with echocardiographic markers of diastolic dysfunction. *Circulation: Arrhythmia and Electrophysiology*. 2012;5:537-543.

88. Gemici K, Baran İ, Güllülü S, Kazazoğlu AR, Cordan J, Özer Z. Evaluation of diastolic dysfunction and repolarization dispersion in behcet's disease. *Int J Cardiol*. 2000;73:143-148.

89. Fu G, Meissner A, Simon R. Repolarization dispersion and sudden cardiac death in patients with impaired left ventricular function. *Eur Heart J*. 1997;18:281-289.

90. Lubinski A, Lewicka-Nowak E, Kempa M, Baczynska AM, Romanowska I, Swiatecka G. New insight into repolarization abnormalities in patients with congenital long QT syndrome: The increased transmural dispersion of repolarization. *Pacing and Clinical Electrophysiology*. 1998;21:172-175.

91. Haugaa KH, Edvardsen T, Leren TP, Gran JM, Smiseth OA, Amlie JP. Left ventricular mechanical dispersion by tissue doppler imaging: A novel approach for identifying high-risk individuals with long QT syndrome. *Eur Heart J*. 2009;30:330-337.

92. Nador F, Beria G, De Ferrari GM, Stramba-Badiale M, Locati EH, Lotto A, Schwartz PJ. Unsuspected echocardiographic abnormality in the long QT syndrome. Diagnostic, prognostic, and pathogenetic implications. *Circulation*. 1991;84:1530-1542.

93. Nakayama K, Yamanari H, Otsuka F, Fukushima K, Saito H, Fujimoto Y, Emori T, Matsubara H, Uchida S, Ohe T. Dispersion of regional wall motion abnormality in patients with long QT syndrome. *Heart*. 1998;80:245-250.

94. Savoye C, Klug D, Denjoy I, Ennezat PV, Le Tourneau T, Guicheney P, Kacet S. Tissue doppler echocardiography in patients with long QT syndrome. *European Heart Journal - Cardiovascular Imaging*. 2003;4:209-213.

95. Alessandrini RS, McPherson DD, Kadish AH, Kane BJ, Goldberger JJ. Cardiac memory: A mechanical and electrical phenomenon. *Am J Physiol*. 1997;272:H1952-9.

96. Van Der Velden, Huub M W, Van Der Zee L, Wijffels, Maurits C E F, Van Leuven C, Dorland R, Vos MA, Jongsma HJ, Allessie MA. Atrial fibrillation in the goat induces changes in monophasic action potential and mRNA expression of ion channels involved in repolarization. *J Cardiovasc Electrophysiol*. 2000;11:1262-1269.

97. Kääb S, Nuss HB, Chiamvimonvat N, O'Rourke B, Pak PH, Kass DA, Marban E, Tomaselli GF. Ionic mechanism of action potential prolongation in ventricular myocytes from dogs with pacing-induced heart failure. *Circulation Research*. 1996;78:262-273.

98. Greenstein JL, Wu R, Po S, Tomaselli GF, Winslow RL. Role of the calcium-independent transient outward current I_{to1} in shaping action potential morphology and duration. *Circulation Research*. 2000;87:1026-1033.

99. Hondeghem LM, Carlsson L, Duker G. Instability and triangulation of the action potential predict serious proarrhythmia, but action potential duration prolongation is antiarrhythmic. *Circulation*. 2001;103:2004-2013.

100. Eykyn TR, Aksentijević D, Aughton KL, Southworth R, Fuller W, Shattock MJ. Multiple quantum filtered ^{23}Na NMR in the langendorff perfused mouse heart: Ratio of triple/double quantum filtered signals correlates with $[Na]_i$. *J Mol Cell Cardiol*. 2015;86:95-101.

101. Sidell RJ, Cole MA, Draper NJ, Desrois M, Buckingham RE, Clarke K. Thiazolidinedione treatment normalizes insulin resistance and ischemic injury in the zucker fatty rat heart. *Diabetes*. 2002;51:1110.

102. Fuller W, Howie J, McLatchie LM, Weber RJ, Hastie CJ, Burness K, Pavlovic D, Shattock MJ. FXYD1 phosphorylation in vitro and in adult rat cardiac myocytes: Threonine 69 is a novel substrate for protein kinase C. *American journal of physiology. Cell physiology*. 2009;296:C1346-C1355.

103. Skrzypiec-Spring M, Grotthus B, Szeląg A, Schulz R. Isolated heart perfusion according to Langendorff—Still viable in the new millennium. *Journal of Pharmacological and Toxicological Methods*. 2007;55:113-126.

104. Bell RM, Mocanu MM, Yellon DM. Retrograde heart perfusion: The langendorff technique of isolated heart perfusion. *Journal of Molecular and Cellular Cardiology*. 2011;50:940-950.

105. Guo D, Zhao X, Wu Y, Liu T, Kowey PR, Yan G. L-type calcium current reactivation contributes to arrhythmogenesis associated with action potential triangulation. *J Cardiovasc Electrophysiol*. 2007;18:196-203.

106. Guo L, Dong Z, Guthrie H. Validation of a guinea pig langendorff heart model for assessing potential cardiovascular liability of drug candidates. *Journal of Pharmacological and Toxicological Methods*. 2007;60:130-151.

107. Nygren A, Baczkó I, Giles WR. Measurements of electrophysiological effects of components of acute ischemia in langendorff-perfused rat hearts using voltage-sensitive dye mapping. *J Cardiovasc Electrophysiol*. 2006;17:S113-S123.

108. Heath BM, Terrar DA. Separation of the components of the delayed rectifier potassium current using selective blockers of I_{Kr} and I_{Ks} in guinea-pig isolated ventricular myocytes. *Exp Physiol*. 1996;81:587-603.

109. Varró A, Lathrop DA, Hester SB, Nánási PP, Papp JGY. Ionic currents and action potentials in rabbit, rat, and guinea pig ventricular myocytes. *Basic Res Cardiol*. 1993;88:93-102.

110. Weisser-Thomas J, Piacentino I, Gaughan JP, Margulies K, Houser SR. Calcium entry via Na/Ca exchange during the action potential directly contributes to contraction of failing human ventricular myocytes. *Cardiovasc Res*. 2003;57:974-985.

111. Sande J, Sjaastad I, Hoen IB, Bãkenes J, Tãnnessen T, Holt E, Lunde PK, Christensen G. Reduced level of serine16 phosphorylated phospholamban in the failing

rat myocardium: A major contributor to reduced SERCA2 activity. *Cardiovasc Res*. 2002;53:382-391.

112. Schwinger RHG, Münch G, Bölck B, Karczewski P, Krause E, Erdmann E. Reduced Ca^{2+}-sensitivity of SERCA2a in failing human myocardium due to reduced serin-16 phospholamban phosphorylation. *Journal of Molecular and Cellular Cardiology*. 1999;31:479-491.

113. Kovács M, Tóth J, Hetényi C, Málnási-Csizmadia A, Sellers JR. Mechanism of blebbistatin inhibition of myosin II. *Journal of Biological Chemistry*. 2004;279:35557-35563.

114. Camm AJ, Lau C. Electrophysiological effects of a single intravenous administration of ivabradine (S 16257) in adult patients with normal baseline electrophysiology. *Drugs in R & D*. 2003;4:83-89.

115. Olsson RA, Bünger R. Metabolic control of coronary blood flow. *Progress in Cardiovascular Diseases*. 1987;29:369-387.

116. Uzelac I, Ji YC, Hornung D, Schröder-Scheteling J, Luther S, Gray RA, Cherry EM, Fenton FH. Simultaneous quantification of spatially discordant alternans in voltage and intracellular calcium in langendorff-perfused rabbit hearts and inconsistencies with models of cardiac action potentials and ca transients. *Frontiers in Physiology*. 2017;8:819.

117. Terrar DA, White E, Noble D. Changes in cytosolic calcium monitored by inward currents during action potentials in guinea-pig ventricular cells. *Proceedings of the Royal Society of London B Biological Sciences*. 1989;238:171-188.

118. White E, Le Guennec J, Nigretto JM, Gannier F, Argibay JA, Garnier D. The effects of increasing cell length on auxotonic contractions; membrane potential and intracellular calcium transients in single guinea-pig ventricular myocytes. *Exp Physiol*. 1993;78:65-78.

119. Brandes R, Bers DM. Simultaneous measurements of mitochondrial NADH and Ca^{2+} during increased work in intact rat heart trabeculae. *Biophys J*. 2002;83:587-604.

120. Trollinger DR, Cascio WE, Lemasters JJ. Mitochondrial calcium transients in adult rabbit cardiac myocytes: Inhibition by ruthenium red and artifacts caused by lysosomal loading of Ca^{2+}-indicating fluorophores. *Biophys J*. 2000;79:39-50.

121. Nido PJD, Glynn P, Buenaventura P, Salama G, Koretsky AP. Fluorescence measurement of calcium transients in perfused rabbit heart using rhod 2. *American Journal of Physiology-Heart and Circulatory Physiology*. 1998;274:H728-H741.

122. Choi B, Salama G. Simultaneous maps of optical action potentials and calcium transients in guinea-pig hearts: Mechanisms underlying concordant alternans. *J Physiol (Lond)*. 2000;529:171-188.

123. Laurita KR, Singal A. Mapping action potentials and calcium transients simultaneously from the intact heart. *American Journal of Physiology-Heart and Circulatory Physiology*. 2001;280:H2053-H2060.

124. Wang DW, Kiyosue T, Sato T, Arita M. Comparison of the effects of class I anti-arrhythmic drugs, cibenzoline, mexiletine and flecainide, on the delayed rectifier K^+ current of guinea-pig ventricular myocytes. *J Mol Cell Cardiol*. 1996;28:893-903.

125. Hoey A, Harrison SM, Boyett MR, Ravens U. Effects of the anemonia sulcata toxin (ATX II) on intracellular sodium and contractility in rat and guinea-pig myocardium. *Pharmacol Toxicol*. 1994;75:356-365.

126. Neely, Liebermeister H, Battersby E, Morgan H. Effect of pressure development on oxygen consumption by isolated rat heart. *American Journal of Physiology-Legacy Content*. 1967;212:804-814.

127. Flynn SB, Gristwood RW, Owen DA. An isolated guinea-pig working heart: Preliminary studies with histamine and noradrenaline [proceedings]. *Br J Pharmacol*. 1977;59:530P.

128. Barr RL, Lopaschuk GD. Direct measurement of energy metabolism in the isolated working rat heart. *Journal of Pharmacological and Toxicological Methods*. 1997;38:11-17.

129. Flynn SB, Gristwood RW, Owen DA. Differentiation of the roles of histamine H1- and H2-receptors in the mediation of the effects of histamine in the isolated working heart of the guinea-pig. *Br J Pharmacol*. 1979;65:127-137.

130. Langer SFJ, Schmidt HD. Different left ventricular relaxation parameters in isolated working rat and guinea pig hearts influence of preload, afterload, temperature, and isoprenaline. *The International Journal of Cardiac Imaging*. 1998;14:229-240.

131. Ferron M, Prat V, Roul D, Cadiet j, Gauthier C, Rozec B, Lauzier B. Study of intrinsic cardiac dysfunction in septic shock conditions by isolated working heart: A primary approach before new therapeutic proposals? *SM Emergency Medicine and Critical Care*. 2017;1.

132. Sutherland FJ, Shattock MJ, Baker KE, Hearse DJ. Mouse isolated perfused heart: Characteristics and cautions. *Clinical and Experimental Pharmacology and Physiology*. 2003;30:867-878.

133. Peterson JN, Hunter WC, Berman MR. Estimated time course of Ca^{2+} bound to troponin C during relaxation in isolated cardiac muscle. *Am J Physiol Heart Circ Physiol*. 1991;260:H1013.

134. Shattock MJ, Cave AC. What are the cellular mechanisms of impaired myocardial relaxation and diastolic dysfunction? *Dialogues in Cardiovascular Medicine*. 1999;4:201-209.

135. Bers DM. Ca transport during contraction and relaxation in mammalian ventricular muscle. *Alterations of Excitation-Contraction Coupling in the Failing Human Heart.* Heidelberg: Steinkopff; 1998:1-16.

136. Clark JE, Marber MS. Advancements in pressure–volume catheter technology – stress remodelling after infarction. *Exp Physiol*. 2013;98:614-621.

137. Borlaug BA, Kass DA. Invasive hemodynamic assessment in heart failure. *Heart failure clinics*. 2009;5:217-228.

138. Grieve DJ, Cave AC, Byrne JA, Layland J, Shah AM. Analysis of *ex vivo* left ventricular pressure–volume relations in the isolated murine ejecting heart. *Exp Physiol*. 2004;89:573-582.

139. Bünger R, Sommer O, Walter G, Stiegler H, Gerlach E. Functional and metabolic features of an isolated perfused guinea pig heart performing pressure-volume work. *Pflügers Archiv*. 1979;380:259-266.

140. Schwinger RHG, Brixius K, Bavendiek U, Hoischen S, Mãller-Ehmsen J, Bälck B, Erdmann E. Effect of cyclopiazonic acid on the force-frequency relationship in human nonfailing myocardium. *J Pharmacol Exp Ther*. 1997;283:286.

141. Takahashi S, Kato Y, Adachi M, Agata N, Tanaka H, Shigenobu K. Effects of cyclopiazonic acid on rat myocardium: Inhibition of calcium uptake into sarcoplasmic reticulum. *J Pharmacol Exp Ther*. 1995;272:1095.

142. Pery-Man N, Chemla D, Coirault C, Suard I, Riou B, Lecarpentier Y. A comparison of cyclopiazonic acid and ryanodine effects on cardiac muscle relaxation. *American Journal of Physiology-Heart and Circulatory Physiology*. 1993;265:H1364-H1372.

143. Studer R, Reinecke H, Bilger J, Eschenhagen T, Bãhm M, Hasenfuss G, Just H, Holtz J, Drexler H. Gene expression of the cardiac Na^{+}-Ca^{2+} exchanger in end-stage human heart failure. *Circ Res*. 1994;75:443.

144. Ahmmed GU, Dong PH, Song G, Ball NA, Xu Y, Walsh RA, Chiamvimonvat N. Changes in Ca^{2+} cycling proteins underlie cardiac action potential prolongation in a

pressure-overloaded guinea pig model with cardiac hypertrophy and failure. *Circ Res*. 2000;86:558.

145. Madamanchi A. Beta-adrenergic receptor signaling in cardiac function and heart failure. *McGill journal of medicine : MJM : an international forum for the advancement of medical sciences by students*. 2007;10:99-104.

146. Port JD, Bristow MR. Altered beta-adrenergic receptor gene regulation and signalling in chronic heart failure. *Journal of Molecular and Cellular Cardiology*. 2001;33:887-905.

147. Silberman GA, Fan TM, Liu H, Jiao Z, Xiao HD, Lovelock JD, Boulden BM, Widder J, Fredd S, Bernstein KE, Wolska BM, Dikalov S, Harrison DG, Dudley SC. Uncoupled cardiac nitric oxide synthase mediates diastolic dysfunction. *Circulation*. 2010;121:519-528.

148. Tiritilli A. DOCA-salts induce heart failure in the guinea pig. *European Journal of Heart Failure*. 2001;3:545-551.

149. Tiritilli A. RF. Induction of hypertension and cardiac hypertrophy in guinea pig DOCA-salt. *Meth Find Exp Clin Pharmacol*. 1994;16(6):391-6.

150. Schnelle M, Catibog N, Zhang M, Nabeebaccus AA, Anderson G, Richards DA, Sawyer G, Zhang X, Toischer K, Hasenfuss G, Monaghan MJ, Shah AM. Echocardiographic evaluation of diastolic function in mouse models of heart disease. *J Mol Cell Cardiol*. 2018;114:20-28.

151. Schenk J, McNeill JH. The pathogenesis of DOCA-salt hypertension. *Journal of Pharmacological and Toxicological Methods*. 1992;27:161-170.

152. Hutchison RB, Shapiro JI. Measurement of intracellular sodium with NMR methods. *Concepts Magn Reson*. 1991;3:215-236.

153. Schepkin VD, Choy IO, Budinger TF, Obayashi DY, Taylor SE, Decampli WM, Amartur SC, Young JN. Sodium TQF NMR and intracellular sodium in isolated crystalloid perfused rat heart. *Magn Reson Med*. 1998;39:557-563.

154. Alam M, Wardell J, Andersson E, Samad BA, Nordlander R. Effects of first myocardial infarction on left ventricular systolic and diastolic function with the use of mitral annular velocity determined by pulsed wave doppler tissue imaging. *Journal of the American Society of Echocardiography*. 2000;13:343-352.

155. Myreng Y, Smiseth OA. Assessment of left ventricular relaxation by doppler echocardiography. comparison of isovolumic relaxation time and transmitral flow velocities with time constant of isovolumic relaxation. *Circulation*. 1990;81:260-266.

156. Ochi H, Ikuma I, Toda H, Shimada T, Morioka S, Morioka K. Isovolumic relaxation period as an index of left ventricular relaxation under different afterload conditions: Comparison with the time constant of left ventricular pressure decay in the dog. *Jpn Circ J*. 1989;53:1521-1529.

157. Thomas JD, Flachskampf FA, Chen C, Guererro JL, Picard MH, Levine RA, Weyman AE. Isovolumic relaxation time varies predictably with its time constant and

aortic and left atrial pressures: Implications for the noninvasive evaluation of ventricular relaxation. *Am Heart J*. 1992;124:1305-1313.

158. Appleton CP, Galloway JM, Gonzalez MS, Gaballa M, Basnight MA. Estimation of left ventricular filling pressures using two-dimensional and doppler echocardiography in adult patients with cardiac disease: Additional value of analyzing left atrial size, left atrial ejection fraction and the difference in duration of pulmonary venous and mitral flow velocity at atrial contraction. *J Am Coll Cardiol*. 1993;22:1972-1982.

159. Park J, Marwick TH. Use and limitations of E/e' to assess left ventricular filling pressure by echocardiography. *Journal of cardiovascular ultrasound*. 2011;19:169-173.

160. Kadappu KK, Thomas L. Tissue doppler imaging in echocardiography: Value and limitations. *Heart, Lung and Circulation*. 2015;24:224-233.

161. Ommen SR, Nishimura RA, Appleton CP, Miller FA, Oh JK, Redfield MM, Tajik AJ. Clinical utility of doppler echocardiography and tissue doppler imaging in the estimation of left ventricular filling pressures. *Circulation*. 2000;102:1788-1794.

162. Kadappu KK, Thomas L. Tissue doppler imaging in echocardiography: Value and limitations. *Heart, Lung and Circulation*. 2015;24:224-233.

163. Schirmer H, Lunde P, Rasmussen K. Mitral flow derived doppler indices of left ventricular diastolic function in a general population. The Tromsø study. *Eur Heart J*. 2000;21:1376-1386.

164. Santas E, García-Blas S, Miñana G, Sanchis J, Bodí V, Escribano D, Muñoz J, Chorro FJ, Núñez J. Prognostic implications of tissue doppler Imaging–Derived E/Ea ratio in acute heart failure patients. *Echocardiography*. 2015;32:213-220.

165. Pucci ML, Miller KB, Dick LB, Guan H, Lin L, Nasjletti A. Vascular responsiveness to nitric oxide synthesis inhibition in hypertensive rats. *Hypertension*. 199423:744-751.

166. Kramer F, Sandner P, Klein M, Krahn T. Plasma concentrations of matrix metalloproteinase-2, tissue inhibitor of metalloproteinase-1 and osteopontin reflect severity of heart failure in DOCA-salt hypertensive rat. *Biomarkers*. 2008;13:270-281.

167. Muthalif Mubarack M, Benter Ibrahim F, Zinat K, Lillian G, Anne E, Suzanna M, Parmentier Jean-Hugues, Veeraswamy M, Malik Kafait U. Contribution of ras GTPase/MAP kinase and cytochrome P450 metabolites to deoxycorticosterone-Saltâ€“Induced hypertension. *Hypertension*. 2000;35:457-463.

168. Hall CE, Hungerford S. Prevention of DOCA-salt hypertension with the calcium blocker nitrendipine. *Clinical and Experimental Hypertension Part A: Theory and Practice*. 1983;5:721-728.

169. Hofbauer KG, Mah SC, Baum HP, Hãnni H, Wood JM, Kraetz J. Endocrine control of salt and water excretion: The role of vasopressin in DOCA-salt hypertension. *J Cardiovasc Pharmacol*. 1984;6 Suppl 1:S184-91.

170. Hess P, Rey M, Wanner D. Measurements of blood pressure and electrocardiogram in conscious freely moving guineapigs: A model for screening QT interval prolongation effects. *Lab Anim*. 2007;41:470-480.

171. Brown JN, Thorne PR, Nuttall AL. Blood pressure and other physiological responses in awake and anesthetized guinea pigs. *Lab Anim Sci*. 1989;39:142-148.

172. Hasking GJ, Esler MD, Jennings GL, Burton D, Johns JA, Korner PI. Norepinephrine spillover to plasma in patients with congestive heart failure: Evidence of increased overall and cardiorenal sympathetic nervous activity. *Circulation*. 1986;73:615-621.

173. Wang W, Ma R. Cardiac sympathetic afferent reflexes in heart failure. *Heart Fail Rev*. 2000;5:57-71.

174. Ferguson DW, Berg WJ, Sanders JS, Kempf JS. Clinical and hemodynamic correlates of sympathetic nerve activity in normal humans and patients with heart failure: Evidence from direct micronenrographic recordings. *J Am Coll Cardiol*. 1990;16:1125.

175. Moe GW, Stopps TP, Angus C, Forster C, De Bold AJ, Armstrong PW. Alterations in serum sodium in relation to atrial natriuretic factor and other neuroendocrine variables in experimental pacing-induced heart failure. *J Am Coll Cardiol*. 1989;13:173-179.

176. Abhayaratna WP, Seward JB, Appleton CP, Douglas PS, Oh JK, Tajik AJ, Tsang TSM. Left atrial size: Physiologic determinants and clinical applications. *J Am Coll Cardiol*. 2006;47:2357-2363.

177. Nagueh SF, Smiseth OA, Appleton CP, Byrd BF, Dokainish H, Edvardsen T, Flachskampf FA, Gillebert TC, Klein AL, Lancellotti P, Marino P, Oh JK, Popescu BA, Waggoner AD. Recommendations for the evaluation of left ventricular diastolic function by echocardiography: An update from the American society of echocardiography and the

European association of Cardiovascular imaging. *Journal of the American Society of Echocardiography*. 2016;29:277-314.

178. Tsang TSM, Barnes ME, Gersh BJ, Bailey KR, Seward JB. Left atrial volume as a morphophysiologic expression of left ventricular diastolic dysfunction and relation to cardiovascular risk burden. *Am J Cardiol*. 2002;90:1284-1289.

179. Pritchett AM, Mahoney DW, Jacobsen SJ, Rodeheffer RJ, Karon BL, Redfield MM. Diastolic dysfunction and left atrial volume. *J Am Coll Cardiol*. 2005;45:87.

180. Douglas PS. The left atrium. *J Am Coll Cardiol*. 2003;42:1206.

181. Gibson DG, Francis DP. Clinical assessment of left ventricular diastolic function. *Heart*. 2003;89:231.

182. Paulus WJ, Tschãpe C, Sanderson JE, Rusconi C, Flachskampf FA, Rademakers FE, Marino P, Smiseth OA, De Keulenaer G, Leite-Moreira A, Borbãly A, Ãdes I, Handoko ML, Heymans S, Pezzali N, Pieske B, Dickstein K, Fraser AG, Brutsaert DL. How to diagnose diastolic heart failure: A consensus statement on the diagnosis of heart failure with normal left ventricular ejection fraction by the heart failure and echocardiography associations of the european society of cardiology. *Eur Heart J*. 2007;28:2539-2550.

183. Ogilvie LM, Edgett BA, Huber JS, Platt MJ, Eberl HJ, Lutchmedial S, Brunt KR, Simpson JA. Hemodynamic assessment of diastolic function for experimental models. *American Journal of Physiology-Heart and Circulatory Physiology*. 2020;318:H1139-H1158.

184. Alderman EL, Glantz SA. Acute hemodynamic interventions shift the diastolic pressure-volume curve in man. *Circulation*. 1976;54:662-671.

185. Weiss JL, Frederiksen JW, Weisfeldt ML. Hemodynamic determinants of the time-course of fall in canine left ventricular pressure. *J Clin Invest*. 1976;58:751-760.

186. Weisfeldt M, Scully H, Frederiksen J, Rubenstein J, Pohost G, Beierholm E, Bello A, Daggett W. Hemodynamic determinants of maximum negative dP-dt and periods of diastole. *American Journal of Physiology-Legacy Content*. 1974;227:613-621.

187. Karliner JS, Lewinter MM, Mahler F, Engler R, O'Rourke RA. Pharmacologic and hemodynamic influences on the rate of isovolumic left ventricular relaxation in the normal conscious dog. *J Clin Invest*. 1977;60:511-521.

188. Stengl M, Ramakers C, Donker DW, Nabar A, Rybin AV, Spãtjens, Roel L H M G, van der Nagel T, Wodzig, Will K W H, Sipido KR, Antoons G, Moorman AFM, Vos MA, Volders PGA. Temporal patterns of electrical remodelling in canine ventricular hypertrophy: Focus on I_{Ks} downregulation and blunted beta2-adrenergic activation. *Cardiovasc Res*. 2006;72:90-100.

189. Volders, Paul G A, Sipido Karin R, Vos Marc A, Spãtjens Roel L H M G, Leunissen Jet D M, Edward C, Wellens Hein J J. Downregulation of delayed rectifier K^+ currents in dogs with chronic complete atrioventricular block and acquired torsades de pointes. *Circulation*. 1999;100:2455-2461.

190. Kanda VA, Purtell K, Abbott GW. Protein kinase C downregulates I_{Ks} by stimulating KCNQ1-KCNE1 potassium channel endocytosis. *Heart Rhythm*. 2011;8:1641-1647.

191. Zhang ZJ, Jurkiewicz NK, Folander K, Lazarides E, Salata JJ, Swanson R. K^+ currents expressed from the guinea pig cardiac I_{Ks} protein are enhanced by activators of protein kinase C. *Proc Natl Acad Sci USA*. 1994;91:1766.

192. Wang H, Huang T, Wang Z, Ge N, Ke Y. Effect of down-regulation of IKs repolarization-reserve on ventricular arrhythmogenesis in a guinea pig model of cardiac hypertrophy. *Journal of Central South University Medical sciences*. 2018;43:428-433.

193. Varró A, Baláti B, Iost N, Takács J, Virág L, Lathrop DA, Csaba L, Tálosi L, Papp JG. The role of the delayed rectifier component I_{Ks} in dog ventricular muscle and purkinje fibre repolarization. *J Physiol (Lond)*. 2000;523:67-81.

194. Wei X, Yanli T, Deborah D, Tomaselli Gordon F. Transmural heterogeneity of Na^+-Ca^{2+} exchange. *Circ Res*. 2005;97:207-209.

195. Mishra S, Sabbah HN, Rastogi S, Imai M, Gupta RC. Reduced sarcoplasmic reticulum Ca^{2+} uptake and increased Na^+-Ca^{2+} exchanger expression in left ventricle myocardium of dogs with progression of heart failure. *Heart Vessels*. 2005;20:23-32.

196. Kenta I, Xinhua Y, Minori T, Zhi S, Barry William H, Lorell Beverly H. Contractile reserve and intracellular calcium regulation in mouse myocytes from normal and hypertrophied failing hearts. *Circ Res*. 2000;87:588-595.

197. Leszek P, Szperl M, Klisiewicz A, Janas J, Biederman A, Rywik T, Piotrowski W, Kopacz M, Korewicki J. Alteration of myocardial sarcoplasmic reticulum Ca2+-ATPase and Na^+-Ca^{2+} exchanger expression in human left ventricular volume overload. *European Journal of Heart Failure*. 2007;9:579-586.

198. Schwinger Robert H G, Jiangnan W, Konrad F, Mãller-Ehmsen Jochen, Klara B, McDonough Alicia A, Erland E. Reduced sodium pump α_1, α_3, and β_1-isoform protein levels and Na^+,K^+-ATPase activity but unchanged Na^+-Ca^{2+} exchanger protein levels in human heart failure. *Circulation*. 1999;99:2105-2112.

199. Allen PD, Schmidt TA, Marsh JD, Kjeldsen K. Na,K-ATPase expression in normal and failing human left ventricle. *Basic Res Cardiol.* 1992:87-94.

200. Trouve P, François Carre, Belikova I, Leclercq C, Dakhli T, Soufir L, Coquard I, Juan Ramirez-Gil, Danièle Charlemagne. Na^+-K^+-ATPase α_2-isoform expression in guinea pig hearts during transition from compensation to decompensation. *American Journal of Physiology-Heart and Circulatory Physiology*. 2000;279:H1972-H1981.

201. Fuller W, Tulloch LB, Shattock MJ, Calaghan SC, Howie J, Wypijewski KJ. Regulation of the cardiac sodium pump. *Cellular and molecular life sciences: CMLS*. 2013;70:1357-1380.

202. Berry RG, Despa S, Fuller W, Bers DM, Shattock MJ. Differential distribution and regulation of mouse cardiac Na^+/K^+-ATPase alpha1 and alpha2 subunits in T-tubule and surface sarcolemmal membranes. *Cardiovasc Res*. 2007;73:92-100.

203. Yuen GK, Galice S, Bers DM. Subcellular localization of Na/K-ATPase isoforms in ventricular myocytes. *J Mol Cell Cardiol*. 2017;108:158-169.

204. James PF, Grupp IL, Grupp G, Woo AL, Askew GR, Croyle ML, Walsh RA, Lingrel JB. Identification of a specific role for the Na,K-ATPase alpha2 isoform as a regulator of calcium in the heart. *Mol Cell*. 1999;3:555-563.

205. Juhaszova M, Blaustein MP. Na^+ pump low and high ouabain affinity alpha subunit isoforms are differently distributed in cells. *Proc Natl Acad Sci USA*. 1997;94:1800.

206. Despa S, Lingrel JB, Bers DM. Na^+/K^+-ATPase alpha2-isoform preferentially modulates Ca^{2+} transients and sarcoplasmic reticulum Ca^{2+} release in cardiac myocytes. *Cardiovasc Res*. 2012;95:480-486.

207. Frank JS, Mottino G, Reid D, Molday RS, Philipson KD. Distribution of the Na^+-Ca^{2+} exchange protein in mammalian cardiac myocytes: An immunofluorescence and immunocolloidal gold-labelling study. *J Cell Biol*. 19992;117:337-345.

208. Pieske B, Tschöpe C, de Boer R, Fraser AG, Anker SD, Donal E, Edelmann F, Fu M, Guazzi M, Lam CSP, Lancellotti P, Melenovsky V, Morris DA, Nagel E, Pieske-Kraigher E, Ponikowski P, Solomon SD, Vasan RS, Rutten FH, Voors AA, Ruschitzka F, Paulus WJ, Seferovic P, Filippatos G. How to diagnose heart failure with preserved ejection fraction: The HFA–PEFF diagnostic algorithm: A consensus recommendation from the heart failure association (HFA) of the European society of cardiology (ESC). *Eur Heart J*. 2019;40:3297-3317.

209. Ponikowski P, Voors AA, Anker SD, Bueno H, Cleland JGF, Coats AJS, Falk V, González-Juanatey JR, Harjola V, Jankowska EA, Jessup M, Linde C, Nihoyannopoulos P, Parissis JT, Pieske B, Riley JP, Rosano GMC, Ruilope LM, Ruschitzka F, Rutten FH, van der Meer P, ESC Scientific DG. 2016 ESC guidelines for the diagnosis and treatment of acute and chronic heart failure: The task force for the diagnosis and treatment of acute and chronic heart failure of the European society of cardiology (ESC) developed with the

special contribution of the heart failure association (HFA) of the ESC. *Eur Heart J*. 2016;37:2129-2200.

210. Meijers WC, Hoekstra T, Jaarsma T, van Veldhuisen DJ, de Boer RA. Patients with heart failure with preserved ejection fraction and low levels of natriuretic peptides; 26940695. *Netherlands Heart Journal.* 2016;24:287-295.

211. Anjan VY, Loftus TM, Burke MA, Akhter N, Fonarow GC, Gheorghiade M, Shah SJ. Prevalence, clinical phenotype, and outcomes associated with normal B-type natriuretic peptide levels in heart failure with preserved ejection fraction. *The American Journal of Cardiology*. 2012;110:870-876.

212. Tomaschitz A, Pilz S FAU - Ritz, Eberhard, Ritz E FAU - Obermayer-Pietsch, Barbara, Obermayer-Pietsch B FAU - Pieber, Thomas, Pieber TR. Aldosterone and arterial hypertension. *Nature Reviews. Endocrinology.* 2010;6:83-93.

213. Kenchaiah S, Pfeffer MA. Cardiac remodelling in systemic hypertension. *Med Clin North Am*. 2004;88:115-130.

214. Lombès M, Alfaidy N, Eugene E, Lessana A, Farman N, Bonvalet J. Prerequisite for cardiac aldosterone action: Mineralocorticoid receptor and 11ß-hydroxysteroid dehydrogenase in the human heart. *Circulation*. 1995;92:175-182.

215. Ramires FJA, Sun Y, Weber KT. Myocardial fibrosis associated with aldosterone or angiotensin II administration: Attenuation by calcium channel blockade. *J Mol Cell Cardiol*. 1998;30:475-483.

216. Young M, Fullerton M, Dilley R, Funder J. Mineralocorticoids, hypertension, and cardiac fibrosis. *J Clin Invest*. 1994;93:2578-2583.

217. Helmes M, Trombitás K, Centner T, Kellermayer M, Labeit S, Linke WA, Granzier H. Mechanically driven contour-length adjustment in rat cardiac titin's unique N2B sequence: Titin is an adjustable spring. *Circulation Research*. 1999;84:1339-1352.

218. Granzier HL, Irving TC. Passive tension in cardiac muscle: Contribution of collagen, titin, microtubules, and intermediate filaments. *Biophys J*. 1995;68:1027-1044.

219. Silvia R, Bos Denielli da, Silva Goncalves, Louis HM, Nico W, Ger S, Coen O, Max G, Dorfmüller Peter, Christophe G, Marc H, Bogaard Harm-Jan, Remedios Cd, Chandra S, Hidalgo Carlos G, Granzier Henk L, Vonk-Noordegraaf Anton, van der VJ, de Man Frances S. Protein changes contributing to right ventricular cardiomyocyte diastolic dysfunction in pulmonary arterial hypertension. *Journal of the American Heart Association*. 2004;3:e000716.

220. Carlos H, Bryan H, Julius B, Yi Z, Brian A, Marion G, Siegfried L, Henk G. PKC phosphorylation of titin's PEVK element. *Circ Res*. 2009;105:631-638.

221. Bowling N, G, Walsh RA FAU - Song, Song G FAU - Estridge, T, Estridge T FAU - Sandusky, L, Sandusky GE FAU - Fouts, K, Fouts RL FAU - Mintze, Mintze K FAU - Pickard, T, Pickard T FAU - Roden, R, Roden R FAU - Bristow, N, Bristow MR FAU - Sabbah, L, Sabbah HN FAU - Mizrahi, G, Mizrahi JL FAU - Gromo, Gromo G FAU - King, J, King GL FAU - Vlahos, Vlahos CJ. Increased protein kinase C activity and

expression of Ca^{2+}-sensitive isoforms in the failing human heart. *Circulation.* 1999;99:384-391.

222. Koide Y, Tamura K, Suzuki A, Kitamura K, Yokoyama K, Hashimoto T, Hirawa N, Kihara M, Ohno, S, Umemura S. Differential induction of protein kinase C isoforms at the cardiac hypertrophy stage and congestive heart failure stage in dahl salt-sensitive rats. *Hypertension Research*. 2003;26:421-426.

223. Bayer AL, Heidkamp MC, Patel N, Porter M, Engman S, Samarel AM. Alterations in protein kinase C isoenzyme expression and autophosphorylation during the progression of pressure overload-induced left ventricular hypertrophy. In: Kardami E, Hryshko L, Mesaeli N, eds. *Cardiac Cell Biology.* 2003:145-152.

224. Kang MY, Zhang Y FAU - Matkovich, Scot, Abhinav, Matkovich SJ FAU - Diwan, Diwan A FAU - Chishti, Athar, 2nd, Chishti AH FAU - Dorn, 2nd DG. Receptor-independent cardiac protein kinase C alpha activation by calpain-mediated truncation of regulatory domains. *Circulation research.* 2010;107:903-912.

225. Iyer A, Chan V, Brown L. The DOCA-salt hypertensive rat as a model of cardiovascular oxidative and inflammatory stress. *Current cardiology reviews*. 2010;6:291-297.

226. Johar S, Cave AC, Narayanapanicker A, Grieve DJ, Shah AM. Aldosterone mediates angiotensin II-induced interstitial cardiac fibrosis via a Nox2-containing NADPH oxidase. *The FASEB Journal*. 2006;20:1546-1548.

227. Damy T, Ratajczak P, Shah AM, Camors E, Marty I, Hasenfuss G, Marotte F, Samuel J, Heymes C. Increased neuronal nitric oxide synthase-derived NO production in the failing human heart. *The Lancet*. 2004;363:1365-1367.

228. Paulus WJ, Tschöpe C. A novel paradigm for heart failure with preserved ejection fraction. *J Am Coll Cardiol*. 2013;62:263.

229. Iwashima F, Yoshimoto T FAU - Minami, Isao, Minami I FAU - Sakurada, Maya, Sakurada M FAU - Hirono, Yuki, Hirono Y FAU - Hirata, Yukio, Hirata Y. Aldosterone induces superoxide generation via Rac1 activation in endothelial cells. *Endocrinology.* 2008;149(3):1009-1014.

230. Sossalla S, Wagner S, Rasenack ECL, Ruff H, Weber SL, Schãndube FA, Tirilomis T, Tenderich G, Hasenfuss G, Belardinelli L, Maier LS. Ranolazine improves diastolic dysfunction in isolated myocardium from failing human hearts: the role of late sodium current and intracellular ion accumulation. *J Mol Cell Cardiol*. 2008;45:32-43.

231. Maier LS, Layug B, Karwatowska-Prokopczuk E, Belardinelli L, Lee S, Sander J, Lang C, Wachter R, Edelmann F, Hasenfuss G, Jacobshagen C. RAnoLazIne for the treatment of diastolic heart failure in patients with Preserved Ejection Fraction: The RALI-DHF proof-of-concept study. *JACC: Heart Failure*. 2013;1:115-122.

232. Babalis D, Tritakis VF, Floros GF, Mouzarou AF, Kafkas NF, Bampali KF, Mertzanos G. Effects of ranolazine on left ventricular diastolic and systolic function in patients with chronic coronary disease and stable angina. *Hellenic journal of cardiology.* 2015;56:237-241.

233. Moss AJ, Zareba W, Schwarz KQ, Rosero S, McNitt S, Robinson Jl. Ranolazine shortens repolarization in patients with sustained inward sodium current due to type-3 long-QT syndrome. *J Cardiovasc Electrophysiol*. 2008;19:1289-1293.

234. Song Y, Shryock JC, Wagner S, Maier LS, Belardinelli L. Blocking late sodium current reduces hydrogen peroxide-induced arrhythmogenic activity and contractile dysfunction. *J Pharmacol Exp Ther*. 2006;318:214.

235. Lovelock JD, Monasky MM, Jeong E, Lardin HA, Liu H, Patel BG, Taglieri DM, Gu L, Kumar P, Pokhrel N, Zeng D, Belardinelli L, Sorescu D, Solaro RJ, Dudley SC. Ranolazine improves cardiac diastolic dysfunction through modulation of myofilament calcium sensitivity. *Circ Res*. 2012;110:841-850.

236. Morgan JP, Erny RE, Allen PD, Grossman W, Gwathmey JK. Abnormal intracellular calcium handling, a major cause of systolic and diastolic dysfunction in ventricular myocardium from patients with heart failure. *Circulation*. 1990;81:21-32.

237. Elisabeth RK, Bell Stephen P, Selby Donald E, Häußler Tim N, Takamuru A, LeWinter Martin M, Palmer Bradley M, Markus M. Relaxation and the role of calcium in isolated contracting myocardium from patients with hypertensive heart disease and heart failure with preserved ejection fraction. *Circulation: Heart Failure*. 2017;10:e004311.

238. Eberli Franz R, Strömer Hinrik, Ferrell Margaret A, Niraj V, Morgan James P, Stefan N, Apstein Carl S. Lack of direct role for calcium in ischemic diastolic dysfunction in isolated hearts. *Circulation*. 2002;102:2643-2649.

239. Chung CS. How myofilament strain and strain rate lead the dance of the cardiac cycle. *Arch Biochem Biophys*. 2019;664:62-67.

240. Karamanoglu M, Feneley MP. Late systolic pressure augmentation: Role of left ventricular outflow patterns. *American Journal of Physiology-Heart and Circulatory Physiology*. 1999;277:H481-H487.

241. Chung CS, Hoopes CW, Campbell KS. Myocardial relaxation is accelerated by fast stretch, not reduced afterload. *J Mol Cell Cardiol*. 2017;103:65-73.

242. Pacileo G, Baldini L, Limongelli G, Di Salvo G, Iacomino M, Capogrosso C, Rea A, D'Andrea A, Russo MG, Calabrò R. Prolonged left ventricular twist in cardiomyopathies: A potential link between systolic and diastolic dysfunction. *Eur J Echocardiogr*. 2011;12:841-849.

243. Saito M, Okayama H, Yoshii T, Hiasa G, Sumimoto T, Inaba S, Nishimura K, Inoue K, Ogimoto A, Ohtsuka T, Funada J, Shigematsu Y, Higaki J. The differences in left ventricular torsional behavior between patients with hypertrophic cardiomyopathy and hypertensive heart disease. *Int J Cardiol*. 2011;150:301-306.